4. SITE 1050[1]

Shipboard Scientific Party[2]

HOLE 1050A

Position: 30°05.9977′N, 76°14.1011′W

Date occupied: 0130 hr, 17 January 1997

Spud hole: 0715 hr, 17 January 1997

Date departed: 0015 hr, 20 January 1997

Time on hole: 70.75 hr (2 day, 22 hr, 45 min)

Seafloor (drill pipe measurement from rig floor, mbrf): 2311.0

Distance between rig floor and sea level (m): 11.2

Water depth (drill pipe measurement from sea level, m): 2299.8

Total depth (drill pipe measurement from rig floor, mbrf): 2630.9

Penetration (m): 319.9

Number of cores (including cores having no recovery): 36

Total core recovered (m): 293.70

Core recovery (%): 91.8

Oldest sediment cored:
Depth (mbsf): 319.9
Lithology: nannofossil chalk
Age: late Paleocene

HOLE 1050B

Position: 30°05.9981′N, 76°14.0958′W

Date occupied: 0015 hr, 20 January 1997

Spud hole: 0200 hr, 20 January 1997

Date departed: 1730 hr, 21 January 1997

Time on hole: 41.25 hr (1 day, 17 hr, 15 min)

Seafloor (drill pipe measurement from rig floor, mbrf): 2311.0

Distance between rig floor and sea level (m): 11.2

Water depth (drill pipe measurement from sea level, m): 2299.8

Total depth (drill pipe measurement from rig floor, mbrf): 2551.0

Penetration (m): 240.0

Number of cores (including cores having no recovery): 27

Total core recovered (m): 219.44

Core recovery (%): 91.4

Oldest sediment cored:
Depth (mbsf): 240.0
Lithology: nannofossil chalk
Age: early Eocene

HOLE 1050C

Position: 30°5.9953′N, 76°14.0997′W

Date occupied: 1930 hr, 8 February 1997

Spud hole: 0045 hr, 9 February 1997

Date departed: 0600 hr, 13 February 1997

Time on hole: 106.5 hr (4 day, 10 hr, 30 min)

Seafloor (drill pipe measurement from rig floor, mbrf): 2308.0

Distance between rig floor and sea level (m): 11.5

Water depth (drill pipe measurement from sea level, m): 2296.5

Total depth (drill pipe measurement from rig floor, mbrf): 2914.0

Penetration (m): 606.0

Number of cores (including cores having no recovery): 31

Total core recovered (m): 200.19

Core recovery (%): 69.4

Oldest sediment cored:
Depth (mbsf): 606.0
Lithology: nannofossil claystone
Age: late Albian

Comments: Drilled from 0.0 to 317.5 mbsf.

Principal results: Site 1050 was drilled in 2300 m of water on the Blake Nose, 10 km upslope from Site 1049. Two advanced hydraulic piston corer/extended core barrel (APC/XCB) holes were drilled (1050A and 1050B), which produced extremely high (up to 95%) recovery throughout the section, except for two minor intervals. Hole 1050C was drilled with the rotary core barrel (RCB) and is described in this summary after the results for Holes 1050A and 1050B. Although Site 1050 is a short distance from Site 1049, the middle Eocene and upper Paleocene intervals are much more expanded at Site 1050 than at Site 1049. The sediments that contain well-preserved calcareous microfossils will be used to reconstruct the deep-water mass characteristics in the Eocene through the correlation of stable isotope data, lithostratigraphy, and benthic fauna between sites at different water depths on the Blake Nose. The record of Eocene sediments recovered during Leg 171B will document how depth shifts of the boundary between deep waters and intermediate waters occurred as the climate switched from the early Eocene warm period to Antarctic glaciation in the late middle to late Eocene. Site 1050 was also chosen to identify the ages of several strong seismic reflectors that can be traced along nearly the entire length of the Leg 171B depth transect.

The lithostratigraphy is remarkably uniform through most of the Eocene and Paleocene and consists of green to pale yellow siliceous nannofossil ooze and chalk, with minor amounts of chert and diatomaceous nannofossil chalk. We divided the section into three lithologic units based on color and microfossil content. Lithologic Unit I contains an upper layer that comprises manganese nodules and probably represents the present seafloor (lithologic Subunit IA) and a lower section (~38 m) of yellow middle Eocene siliceous nannofossil ooze, with varying amounts of foraminifers and clay (lithologic Subunit IB). A distinctive 5-cm-thick vitric ash bed occurs in the upper portion of lithologic Subunit IB. A sharp color

[1]Norris, R.D., Kroon, D., Klaus, A., et al., 1998. *Proc. ODP, Init. Repts.*, 171B: College Station, TX (Ocean Drilling Program).

[2]Shipboard Scientific Party is given in the list preceding the Table of Contents.

change from yellow to green at ~40 mbsf was used to divide lithologic Unit I from Unit II, but it should be noted that there is no apparent change in sediment composition across the contact. The color change from yellow to green does not appear to represent a primary depositional feature and may represent differences in redox conditions within the sediment cover of the Blake Nose. Lithologic Unit II (~276 m thick; middle Eocene to late Paleocene in age) is composed of light grayish green nannofossil ooze to siliceous nannofossil ooze that grades downhole to a light grayish green siliceous nannofossil chalk and nannofossil chalk, with varying contents of radiolarians, sponge spicules, and diatoms. The transition from ooze to chalk occurs at a depth of ~90 mbsf. The contact between Subunits IIA and IIB is placed at the top of a manganese hardground at ~154 mbsf that occurs within an interval with common, thin chert layers and corresponds to a decrease in carbonate content. At least 10 vitric ash layers occur in Unit II. The ash layers, together with the color reflectance, magnetic susceptibility, and gamma-ray attenuation porosity evaluator (GRAPE) bulk density data, make it possible to produce a detailed correlation between the two holes at this site. The ash layers are composed largely of clear glass shards. Several ash layers also contain euhedral biotite and feldspar grains that may provide an absolute chronology for the section. Most ash layers are about 1 cm thick, but many thinner laminae have probably been destroyed by bioturbation or drilling disturbance, as we have found that many of the gray wisps in the chalk contain volcanic glass shards. Peaks in abundance of siliceous microfossils were observed at 140–155 mbsf and 180–220 mbsf in both holes. Sediments containing the latest Paleocene benthic foraminifer extinction were recovered in Hole 1050B, but not in Hole 1050A because this interval consists of hard chalk or chert that jammed in the core barrel. However, the lowermost Eocene and upper Paleocene sediments adjacent to this interval of extremely low recovery are biostratigraphically and biomagnetostratigraphically complete; this suggests that the interval of poor recovery does not contain a major hiatus. Lithologic Unit III (14.8 m thick; late early Paleocene to early late Paleocene in age) is a diatomaceous nannofossil chalk to nannofossil diatomite. It is distinguishable from the overlying unit by a color shift to grayish olive and an increase in diatom abundance.

A combination of biomagnetostratigraphy and biostratigraphy provides a preliminary chronostratigraphic framework for the sedimentary sequences in Holes 1050A and 1050B. Shipboard magnetostratigraphy within the middle Eocene interval was not well defined, but discrete samples produced a well-defined polarity scale from Chron C21n to C19r during post-cruise research. The upper Paleocene to lower Eocene section displays a complete, well-defined biomagnetostratigraphy from Chrons C26r through lower C22n. The deepest part of Hole 1050A was dated within the lowest Selandian (lower Chron C26r). Shore-based refinement of the biomagnetostratigraphy will make Site 1050 a reference site for calibration of the Paleogene biostratigraphy to magnetic polarity chrons.

The preservation of the calcareous nannofossils and planktonic foraminifers is good in the middle Eocene section and moderate to good in the lower Eocene and Paleocene. The exception is the interval straddling the Paleocene/Eocene boundary, where all calcareous microfossils show poor preservation because of extensive overgrowth and calcite cementation. The radiolarian faunas are generally well preserved. The youngest Eocene deposits correspond to calcareous nannofossil Zone CP14a and planktonic foraminifer Zone P12, and the oldest sediments recovered belong to calcareous nannofossil Zone CP3 and the earliest part of planktonic foraminifer Zone P3a. The apparent absence of calcareous nannofossil Zones CP12a and CP10 suggests the presence of two hiatuses in the Eocene, each between 1.5 and 2 m.y in duration.

Bulk density increases gradually in the upper 140 m of both holes and shows an abrupt increase, followed by an equally sharp decrease at 150 mbsf, where the first chert stringers were encountered. Below this, bulk density increases steadily to a high value near 200 mbsf, and bulk density remains high through the upper Paleocene section. The transition from nannofossil chalk to diatomaceous nannofossil chalk at 300 mbsf corresponds to an abrupt drop in bulk density and *P*-wave velocity. *P*-wave velocity increases significantly at about 90 mbsf, corresponding to the transition from ooze to chalk and to the depth at which we were forced to switch from APC to XCB coring. Pelagic carbonates in Neogene sequences typically show a transition from ooze to chalk at about 160–200 mbsf. Hence, the relatively shallow depth of this lithologic and physical properties transition at Site 1050 suggests that at least part of the sedimentary sequence has been eroded. Estimates of the amount of sediment removed, based on measured shear strength and bulk density, suggest that as much as 147 m of section may have been eroded from the top of the Blake Nose at this site.

Interstitial-water chemistry shows significant changes with depth. Strontium, lithium, potassium, magnesium, calcium, and alkalinity all display marked gradients, particularly between about 80 and 220 mbsf. Major cation changes are consistent with seawater interactions with the volcaniclastic sediments (such as the volcanic ashes found throughout the Eocene section) and/or the underlying Jurassic–Cretaceous carbonate platform. Strontium concentrations and strontium/calcium ratios are both consistent with recrystallization of biogenic carbonates and pervasive calcite overgrowth and cements in the lower Eocene and upper Paleocene sequence. Carbonate content is about 70%–75% in the upper 150 m. Marked decreases in carbonate content occur between 150 and 160 mbsf and again at 300 mbsf, where carbonate drops first to 50% and then to 30%. Both decreases in carbonate content are associated with increases in biogenic silica.

Organic carbon content is extremely low throughout the section and averages about 0.05 wt% in the upper 200 m. Other than a few spikes of <0.3 wt%, total organic carbon (TOC) is essentially zero below 225 mbsf. Methane decreases upsection, probably as a result of increases in methane consumption by aerobic bacteria in the shallow sediments.

Hole 1050C was drilled at the deep end of the Blake Nose as an addendum to Holes 1050A and 1050B in order to obtain an equivalent sequence of the Cretaceous section recovered at the shallow-water Site 1052 transect. We drilled through the top 317 m with the RCB system without coring and started recovering lower Paleocene sediments at the depth where we had stopped drilling in Hole 1050B. The dominant lithology in the lower Paleocene is a clayey siliceous chalk with nannofossils. Color varies from light greenish gray to greenish gray, with the darker lithology more clay rich. The lithology changes to an interval dominated by claystone and nannofossil chalk at 340 mbsf. This unit extends to 463 mbsf (upper Paleocene to upper Maastrichtian). A complete polarity record from Chron C30 through lower C26r is present.

The K/T boundary was found at 405.93 mbsf. In contrast to Site 1049, no impact ejecta are preserved, although the K/T boundary is biostratigraphically complete: the topmost Maastrichtian *Micula prinsii* Zone is present as well as the early Paleocene Pα Zone, represented by greenish gray claystone with nannofossils and nannofossil claystone and fragments of dark gray clay in a drilling breccia between drilling biscuits. The K/T boundary is influenced only slightly by slumping, but in view of the extensive slumping above and below the K/T boundary, it is conceivable that the ejecta layer has been slumped away from this site.

Moderately to heavily bioturbated nannofossil chalk to nannofossil claystone was found in the interval from 463 to 491 mbsf (upper Maastrichtian to upper Campanian). There are subtle meter-scale alternations between lighter and darker intervals. Wavy laminae, microfaults, soft-sediment deformation, and chaotic bedding typify much of this unit, and probably most of this interval has been slumped. A series of hardgrounds of varying character spanning 15.5 m.y. that formed during the Late Cretaceous was recovered in the interval from 491 to 501 mbsf. The hardgrounds differ in character from reddened, weakly bioturbated chalk to a hard, heavily bored phosphate/iron crust more than 1 cm thick, and they mark a distinct change in sediment deposition in the area from the late (but not latest) Cenomanian to the late Campanian. The underlying sediment, although chaotically bedded, still bears evidence of its original character as rhythmic alternations of white, heavily bioturbated chalk and laminated black shale. Laminated sediment virtually does not recur above the hardgrounds. The oldest hardground represents the Cenomanian/Turonian boundary.

The interval from 501 to 605 mbsf (upper Cenomanian to upper Albian) includes hemipelagic sediment, with the amount of terrigenous components increasing downhole. The color changes from light greenish gray to almost black at the bottom of Hole 1050C. The top of this interval is placed at the last downhole occurrence of the hardgrounds. This unit comprises light to medium greenish gray nannofossil chalk or limestone and dark to very dark claystone, including some black shale intervals. Soft-sediment deformation with slumping and possible sediment-creep folding are common throughout the top of this interval. In addition, the sediment is cut by numerous normal faults that range in orientation from subvertical to subhorizontal. Although most subvertical faults are slickensided, many subhorizontal faults display millimeter-scale clay seams, and it is difficult to discern some of the latter from drilling-induced core fractures that were sealed with slurry.

Despite the black color of most of the Cenomanian–Albian sequence, these rocks generally contain <1% TOC, which is rich in humic matter. The black shales recovered in Hole 1050C represent a deep-water equivalent of the green laminated claystones recovered updip at Site 1052, which were also dominated by humic debris. Laminated claystones at both sites contain exquisitely preserved calcareous microfossils. Hole 1050C was successfully logged from the bottom of the hole to 110 mbsf with the usual string of tools such as the triple-combo, Formation MicroScanner (FMS), and geological high-sensitivity magnetic tool (GHMT).

BACKGROUND AND OBJECTIVES

Site 1050 is located at a water depth of 2300 m below sea level (mbsl), which is about 370 m shallower than Site 1049. The MCS line suggests that the middle Eocene and upper Paleocene intervals are much more expanded at Site 1050 than at Site 1049. Paleogene sediments at Site 1050 were deposited near their present water depth. These sediments will be used to reconstruct the water-mass characteristics of deep waters in the Eocene through the correlation of isotope data, lithostratigraphy, and benthic fauna among sites at different water depths on the Blake Nose. The excellent record of Eocene sediments recovered during Leg 171B will document how the boundary between deep waters and intermediate waters changed as the climate switched from the early Eocene warm period to the onset of Antarctic glaciation in the late Eocene. Site 1050 was also chosen to identify the ages of several strong seismic reflectors that can be traced along nearly the entire length of the Leg 171B depth transect. Information on the ages and depths of these reflectors was used to predict the stratigraphic sequence of the remaining Blake Nose sites to be drilled and to refine the coring program for the leg.

We also expected to recover a thicker Cretaceous sequence than is present at Site 1049. This would enable us to determine the lithologic and faunal characteristics of the down-dip equivalents of the Cretaceous rocks at Site 1052. We particularly wished to obtain a depth transect across the K/T boundary, the mid-Maastrichtian, and the Albian–Cenomanian sections.

OPERATIONS

Site 1050

After a 1-hr transit from Site 1049, we deployed a beacon at Site 1050 at 0130 hr on 17 January 1997. After adding a new APC/XCB bit (RBI C-3) to the bottom-hole assembly (BHA), the drill string was run in to 2263 m below rig floor (mbrf), the top drive was picked up, and the bit was gently lowered to establish the mudline depth. The driller observed a reduction in drill-string weight at 2311.0 mbrf, which was only 1.4 m shallower than the precision depth recorder (PDR) measured depth of 2312.4 mbrf. Because of the possibility of damaging hardware in attempting an APC mudline core through the manganese nodules and sand cover (as occurred in Hole 1049A), we spudded Hole 1050A with the XCB at 0715 hr on 17 January. We rotated 15 min, coring from 0 to 10.1 mbsf, and recovered 6.9 m of nannofossil ooze with some manganese nodules. APC coring commenced with Core 171B-1050A-2H (Table 1) and continued to 95.6 mbsf. Core 10H could not be extracted from the formation with 100,000 lb of overpull, and we had to free it by slowly drilling over the stuck barrel.

We then switched to XCB coring, which provided excellent core recovery, albeit with slow and ever-decreasing rates of penetration (ROPs). The high clay content of the sediments was apparently adhering to the cutting structure of the bit, thereby reducing the penetrating ability and making it difficult to advance into the formation. The weight on bit, pump pressure, and rotary speed were varied in an attempt to increase the ROP, with negative results. The average ROP on 19 January had decreased to 4.7 m/hr.

We considered the possibility of dropping a free-fall funnel so that we could trip the pipe to change the rotary core bit to one more suited for this formation (e.g., $10^1/_8$-in polycrystalline diamond compact [PDC] fixed-cutter bit). However, after reviewing the conditions of microfossil preservation, slow ROP, and time/risk to round trip for a PDC XCB bit, we decided to terminate Hole 1050A at 319.9 mbsf. We decided to increase the penetration in Hole 1050B to ~240 mbsf and to not drill a third hole at this site as originally planned. The time saved would be used to achieve primary scientific objectives at another site. We pulled the drill string up to 100 mbsf and displaced the hole with 40 bbl of 10.5 lb/gal mud. Hole 1050A ended at 0015 hr on 20 January when the drill string was pulled above the seafloor.

Hole 1050B

We offset the vessel 10 m to the east and spent 1 hr to accomplish the routine task of cutting and slipping 115 ft of drilling line. After the driller verified that the seafloor depth was the same as in Hole 1050A (2311.0 mbrf; based on an observed reduction in drill-string weight), we spudded Hole 1050B with the XCB at 0200 hr on 20 January. XCB Core 171B-1050B-1X was cut from 0 to 7.0 mbsf. We then took APC Cores 2H through 9H to 83.0 mbsf. We wanted to switch to the XCB at this depth because this was just above the depth where we had to drill over the stuck APC core barrel in Hole 1050A. XCB coring continued to a total depth of 240.0 mbsf. After the last core was retrieved (1325 hr, 21 January) we started pulling the drill string out of the hole. As soon as the drill bit was a safe distance above the seafloor, the beacon was recovered, and, while the drill pipe was being retrieved, the vessel was slowly offset toward the next site.

Hole 1050C

After the 16.5-nmi transit to return to Site 1050, we deployed a beacon at 1930 hr on 8 February 1997. We wanted to reoccupy Site 1050 to core the deep objectives that were not attained earlier in the leg when the XCB coring system could not penetrate to the desired depth of at least 500 mbsf in Hole 1050A. We decided to use the RCB coring system to core deeper than the penetration depth in Hole 1050A until the remaining operational time for the leg expired.

Hole 1050C was spudded at 0045 hr on 9 February at a depth of 2308.0 m. We used an RCB BHA with a mechanical bit release and new bit (RBI C-3). We drilled without coring to 317.5 mbsf and then started RCB coring at 1545 hr on 9 February. Rotary coring advanced without incident to a depth of 606.0 mbsf, coring 288.5 m and recovering 200.19 m of core (69.4% recovery; see expanded version of Table 1 on CD-ROM, back pocket, this volume). Operations were terminated at 2130 hr on 11 February after the operational time for this leg expired. The average ROP for the cored segment of this hole was 11.2 m/hr.

Table 1. Site 1050 coring summary.

Core	Date (January 1997)	Time (UTC)	Depth (mbsf)	Length cored (m)	Length recovered (m)	Recovery (%)
171B-1050A-						
1X	17	1315	0.0-10.1	10.1	6.88	68.1
2H	17	1400	10.1-19.6	9.5	10.11	106.4
3H	17	1515	19.6-29.1	9.5	10.04	105.7
4H	17	1640	29.1-38.6	9.5	9.64	101.0
5H	17	1725	38.6-48.1	9.5	9.75	102.0
6H	17	1820	48.1-57.6	9.5	9.76	103.0
7H	17	1910	57.6-67.1	9.5	9.93	104.0
8H	17	2005	67.1-76.6	9.5	9.59	101.0
9H	17	2055	76.6-86.1	9.5	9.74	102.0
10H	17	2240	86.1-95.6	9.5	9.85	103.0
11X	17	2350	95.6-105.2	9.6	8.84	92.1
12X	18	0035	105.2-114.8	9.6	1.34	13.9
13X	18	0125	114.8-124.4	9.6	7.69	80.1
14X	18	0215	124.4-134.0	9.6	8.34	86.9
15X	18	0305	134.0-143.6	9.6	7.83	81.5
16X	18	0400	143.6-153.2	9.6	9.80	102.0
17X	18	0545	153.2-162.8	9.6	4.79	49.9
18X	18	0745	162.8-172.4	9.6	6.15	64.0
19X	18	1000	172.4-182.0	9.6	9.79	102.0
20X	18	1200	182.0-189.6	7.6	9.84	129.0
21X	18	1430	189.6-199.2	9.6	9.71	101.0
22X	18	1740	199.2-208.8	9.6	9.80	102.0
23X	18	1935	208.8-218.4	9.6	9.92	103.0
24X	18	2125	218.4-228.0	9.6	9.84	102.0
25X	19	0000	228.0-237.7	9.7	0.30	3.1
26X	19	0145	237.7-241.7	4.0	4.33	108.0
27X	19	0340	241.7-247.3	5.6	7.45	133.0
28X	19	0615	247.3-256.9	9.6	8.11	84.5
29X	19	0900	256.9-266.5	9.6	9.94	103.0
30X	19	1200	266.5-276.1	9.6	9.64	100.0
31X	19	1600	276.1-285.7	9.6	9.88	103.0
32X	19	1800	285.7-288.9	3.2	6.06	189.0
33X	19	2000	288.9-295.3	6.4	9.23	144.0
34X	19	2300	295.3-304.9	9.6	4.81	50.1
35X	20	0150	304.9-314.5	9.6	9.74	101.0
36X	20	0330	314.5-319.9	5.4	5.24	97.0
Coring totals:				319.9	293.70	91.8
171B-1050B-						
1X	20	0810	0.0-7.0	7.0	7.65	109.0
2H	20	0920	7.0-16.5	9.5	9.46	99.6
3H	20	1030	16.5-26.0	9.5	9.84	103.0
4H	20	1115	26.0-35.5	9.5	9.78	103.0
5H	20	1205	35.5-45.0	9.5	9.81	103.0
6H	20	1305	45.0-54.5	9.5	10.01	105.3
7H	20	1350	54.5-64.0	9.5	9.61	101.0
8H	20	1435	64.0-73.5	9.5	9.86	104.0
9H	20	1530	73.5-83.0	9.5	9.89	104.0
10X	20	1700	83.0-90.6	7.6	9.11	120.0
11X	20	1745	90.6-100.2	9.6	9.22	96.0
12X	20	1830	100.2-109.8	9.6	9.67	101.0
13X	20	1925	109.8-119.4	9.6	8.65	90.1
14X	20	2000	119.4-129.0	9.6	8.02	83.5
15X	20	2100	129.0-138.6	9.6	8.28	86.2
16X	20	2200	138.6-148.2	9.6	6.58	68.5
17X	21	0005	148.2-154.7	6.5	7.98	123.0
18X	21	0105	154.7-157.8	3.1	4.15	134.0
19X	21	0225	157.8-167.4	9.6	1.65	17.2
20X	21	0330	167.4-177.0	9.6	9.77	102.0
21X	21	0440	177.0-186.6	9.6	9.89	103.0
22X	21	0625	186.6-196.2	9.6	9.39	97.8
23X	21	0800	196.2-205.8	9.6	9.83	102.0
24X	21	1015	205.8-215.5	9.7	9.84	101.0
25X	21	1315	215.5-225.1	9.6	9.90	103.0
26X	21	1610	225.1-230.4	5.3	0.31	3.2
27X	21	1825	230.4-240.0	9.6	1.29	13.4
Coring totals:				240.0	219.44	91.4
171B-1050C-						
1R	09	1630	317.50-327.10	9.6	0.00	0.00
2R	09	1800	327.10-336.70	9.6	9.89	103.00
3R	09	1955	336.70-346.30	9.6	6.78	70.60
4R	09	2200	346.30-355.90	9.6	8.13	84.70
5R	10	0025	355.90-365.50	9.6	8.22	85.60
6R	10	0210	365.50-375.20	9.7	9.84	101.40
7R	10	0350	375.20-384.90	9.7	5.18	53.40
8R	10	0535	384.90-394.50	9.6	4.79	49.90
9R	10	0655	394.50-404.10	9.6	6.90	71.90
10R	10	0810	404.10-408.70	4.6	2.33	50.70
11R	10	0935	408.70-413.70	5.0	4.28	85.60
12R	10	1105	413.70-423.30	9.6	0.20	2.10
13R	10	1230	423.30-433.00	9.7	9.92	102.30
14R	10	1355	433.00-442.60	9.6	0.00	0.00
15R	10	1520	442.60-452.20	9.6	9.94	103.50
16R	10	1650	452.20-461.80	9.6	4.12	42.90
17R	10	1800	461.80-471.40	9.6	8.93	93.00
18R	10	1905	471.40-481.00	9.6	7.50	78.10
19R	10	2005	481.00-490.60	9.6	3.58	37.30
20R	10	2125	490.60-500.20	9.6	6.38	66.50
21R	10	2300	500.20-509.80	9.6	9.95	103.60
22R	11	0035	509.80-519.40	9.6	0.77	8.00
23R	11	0335	519.40-529.10	9.7	9.88	101.90
24R	11	0530	529.10-538.70	9.6	3.07	32.00
25R	11	0755	538.70-548.40	9.7	5.39	55.60
26R	11	0930	548.40-558.00	9.6	7.22	75.20
27R	11	1210	558.00-567.60	9.6	9.67	100.70
28R	11	1435	567.60-577.20	9.6	9.78	101.90
29R	11	1710	577.20-586.80	9.6	9.51	99.10
30R	11	1915	586.80-596.40	9.6	9.03	94.10
31R	11	2130	596.40-606.00	9.6	9.01	93.90
Cored totals:				288.5	200.19	69.39
Drilled:				317.50		
Total:				606.00		

Note: An expanded version of this coring summary table that includes lengths and depths of sections and comments on sampling is included on CD-ROM (back pocket, this volume).

After a 20-bbl, high-viscosity mud flush was circulated, a wiper trip (105–606 mbsf) was conducted to prepare the hole for logging. The region from 586 to 606 mbsf had to be washed and reamed. The bit was then released with the wireline at the bottom of the hole, and the hole was displaced with 155 bbl of sepiolite mud. The end of the drill string was pulled up to the logging depth of 105 mbsf.

At 0245 hr on 12 February, the Schlumberger equipment was rigged up and the triple-combo was run in the hole. All data collected are of high quality. No problems were experienced during the run. The hole appeared to be in good condition, with an average diameter of 10 in. By 0900 hr on 21 February, the triple-combo was retrieved and rigged down.

At 0910 hr, the second logging string (FMS-sonic digital logging tool [SDT] array–natural-gamma spectrometry tool [NGT]) was run in the hole. All data collected are of high quality. No problems were experienced during the run, except for some noise on the analog sonic curves. The digital data appear to be good, however. The FMS calipers indicate that the hole was slightly oval and that it was washed out to 14 in just below the bottom of the drill pipe. The maximum hole deviation was 1.5°. Although two full passes were planned, the second logging pass was canceled. When the tool reached the oval sections while approaching the drill pipe, it became apparent that the "track" left in the borehole by the caliper of the tool used on the first logging run could be seen in the image of the second run. Consequently, the second pass was shortened.

At 1500 hr, the second logging tool string was rigged down, and the third and final logging suite was made up. At 1515 hr, the third log for magnetic susceptibility (GHMT-NGT) was run in the hole. All data collected are of high quality. All three logging tools reached the bottom of the hole. Only the upper 40 m of the hole (105–145 mbsf) suffered significant washout. The hole was successfully logged between 103 and 606 mbsf. Sea conditions were mild, with swells <1.5 m.

After the logging equipment was rigged down, the hole was displaced with 35 bbl of 10.5 lb/gal mud. The pipe was pulled out of the hole, and the BHA was disassembled into individual drill collars and laid down. The main and backup beacons were retrieved, and the drilling equipment was secured by 0600 hr on 13 February.

LITHOSTRATIGRAPHY

Description of Lithologic Units

Holes 1050A and 1050B were drilled in 2299.8 m of water, and Hole 1050C was drilled in 2296.5 m water depth on the Blake Nose, 10 km upslope from Site 1049 (see "Operations" section, this chap-

Table 2. Summary of lithologic units from Holes 1050A and 1050B.

Lithologic unit/subunit	Hole 1050A	Hole 1050B	Age	Lithologies
IA	Interval 1X-1, 0-3 cm, thickness unknown	Interval 1X-1, 0-5 cm, thickness unknown	Pleistocene to Holocene	Mn nodules and phosphatic sand
IB	Interval 1X-1, 4 cm, to 4H-CC, 36 cm 0.03-38.71 mbsf 38.7 m	1X-1, 5 cm, to 5H-2, 79 cm 0.05-37.79 mbsf 37.8 m	middle Eocene	Yellow siliceous nannofossil ooze
IC	Interval 4H-5, 0 cm, to 16X-7, 42 cm 38.7-153.05 mbsf 114.35 m	5H-2, 79 cm, to 17X-6, 23 cm 37.8-155.4 mbsf 117. 6 m	middle Eocene to early Eocene	Green siliceous nannofossil ooze and nannofossil chalk with siliceous microfossils
ID	Interval 16X-7, 43 cm, to 34X-CC, 49 cm 153.06-300.1 mbsf 147.04 m	Interval 17X-6, 24 cm, to 27X-CC, 47 cm 155.24-240.0 84.76+ m base not recovered	early Eocene to late Paleocene	Green siliceous nannofossil chalk
II	Interval 35X-1, 0 cm, to 36X-CC, 15 cm 304.9-319.7 mbsf 14.8 m	Not recovered	late Paleocene	Diatomaceous nannofossil chalk and diatomite with nannofossils

ter). Although Site 1050 is a short distance from Site 1049, the lower to middle Paleogene section is much thicker than at the previous site, as predicted by seismic data. We divided the section into six lithologic units based on color and microfossil content (Table 2; Fig. 1). The upper two units were recovered in Holes 1050A and 1050B; the lower three units were recovered in Hole 1050C. The uppermost unit consists of four subunits, which include an upper layer containing manganese nodules that probably represents the present seafloor (lithologic Subunit IA). Lithologic Subunit IB is an ~38-m-thick interval of yellow middle Eocene siliceous nannofossil ooze, with varying amounts of foraminifers and clay (lithologic Subunit IB). A distinctive 5-cm-thick vitric ash bed occurs in the upper portion of lithologic Subunit IB. A sharp color change from yellow to green at ~38 mbsf was used to divide lithologic Subunit IB from Subunit IC. There is no apparent change in sediment composition across the contact. Lithologic Subunit ID (~276 m thick; middle Eocene to late Paleocene in age) is composed of light grayish green nannofossil chalk with varying amounts of radiolarians, sponge spicules, and diatoms (see Section 5 on CD-ROM, back pocket, this volume). The transition from ooze to chalk at a depth of ~90 mbsf corresponds to an increase in bulk density (see "Physical Properties" section, this chapter). The contact between Subunits IC and ID is placed at the top of a hardground at ~154 mbsf that occurs within an interval with common, thin chert layers and corresponds to a decrease in carbonate content (see "Organic Geochemistry" section, this chapter). At least 11 vitric ash layers occur in Unit I and correlate well between Holes 1050A and 1050B (Fig. 2). Peaks in abundance of siliceous microfossils were observed at 140–155 and 180–220 mbsf in both holes, as well. Lithologic Unit II (>14.8 m thick; late early Paleocene to early late Paleocene in age) is a diatomaceous nannofossil chalk to nannofossil diatomite. It is distinguished from the overlying unit based on a color shift to grayish olive and an increase in diatom abundance.

The section in Hole 1050C (Fig. 3; Table 3) begins with lithologic Unit III, a rhythmically alternating clay-rich, clay-poor siliceous chalk with a few cherty horizons. Lithologic Unit IV lacks a significant siliceous microfossil component and comprises alternations of calcareous-rich chalks and clay-rich claystones. Much of the sediment in this unit bears contorted bedding. In a relatively undeformed interval, we recovered a biostratigraphically complete, but drilling-disturbed, K/T boundary. Lithologic Unit V comprises a remarkable series of hardgrounds that took over 17 m.y. to form during the mid- to Late Cretaceous. Lithologic Unit VI is a Lower Cretaceous sequence of alternating chalk and terrigenous component-rich clay and siltstone, all deformed by syn- and postdepositional deformation, forming visually stunning patterns of black-and-white folded sediment. A few intervals contain strong lamination, and we interpret these as black shales.

The Site 1050 Paleocene–Eocene composite section is 399.3 m thick, compared with the 87-m-thick section for equivalent-aged strata at Site 1049 (Fig. 4). Manganese-nodule-rich Subunit IA at Site 1050 almost certainly correlates directly with the similar Subunit IA at Site 1049. However, correspondence between other lithologic boundaries is difficult to assess. The top and bottom of lithologic Subunits IC and ID at Site 1050 are defined by color changes that were not observed at Site 1049. At Site 1049, Unit II is defined as a chert-rich interval (53–73 mbsf), whereas at Site 1050 chert is restricted to three thin layers at the contact between lithologic Subunits IC and ID (138–154 mbsf) and to a few horizons in lithologic Unit III. Lithologic Unit II at Site 1049 and lithologic Subunit ID consist of light grayish green, silica-rich nannofossil chalk of early to middle Eocene age. No equivalent to Site 1050's lithologic Unit II was found at Site 1049, perhaps because of low recovery of equivalent-aged sediment at the latter site. Furthermore, the K/T boundary is more lithified at Site 1050 than at Site 1049.

The Cretaceous section is thicker at Site 1050 than at Site 1049, and it differs in character. The absence of much of the Upper Cretaceous section at Site 1049 is reflected in the series of hardgrounds recovered as lithologic Unit V at Site 1050. The Lower Cretaceous section at Site 1050 shows considerable deformation and is younger than any Albian strata encountered at Site 1049.

Unit I

Description: Mn oxide nodules and nannofossil ooze to siliceous nannofossil ooze
Intervals: 171B-1050A-1X-1, 0 cm, to 34X-CC, 49 cm; 171B-1050B-1X-1, 0 cm, to 27X-CC, 47 cm
Depth: 0–300.1 mbsf, Hole 1050A; 0–240.0 mbsf, Hole 1050B (base not recovered)
Thickness: 300.1 m, Hole 1050A; 240.0 m, Hole 1050B
Age: Pleistocene to late Paleocene

Lithologic Unit I is divided into four subunits. The upper Subunit IA is a 3- to 5-cm-thick layer, with manganese nodules similar to those described as lithologic Subunit IA at Site 1049. Below this, Subunit IB is ~38 m thick and is composed of yellowish middle Eocene siliceous nannofossil ooze, with varying amounts of foraminifers and clay (on CD-ROM, back pocket, this volume). At ~38 mbsf, there is a sharp, even color change from pale yellow to grayish green. This color boundary is used to divide the yellow lithologic Subunit IB from the green Subunit IC. There is no detectable compositional change across this boundary, and we believe it represents some sort of diachronous diagenetic front through Eocene sediment across the Blake Nose (see discussions in "Lithostratigraphy" section, "Site 1051" and "Site 1053" chapters, this volume). Lithologic Subunit ID is similar to Subunit IC in composition: a siliceous nannofossil ooze to chalk. These two subunits are separated at a hardground with biogenic chert above and below the hardground.

Subunit IA

Description: Mn oxide nodules

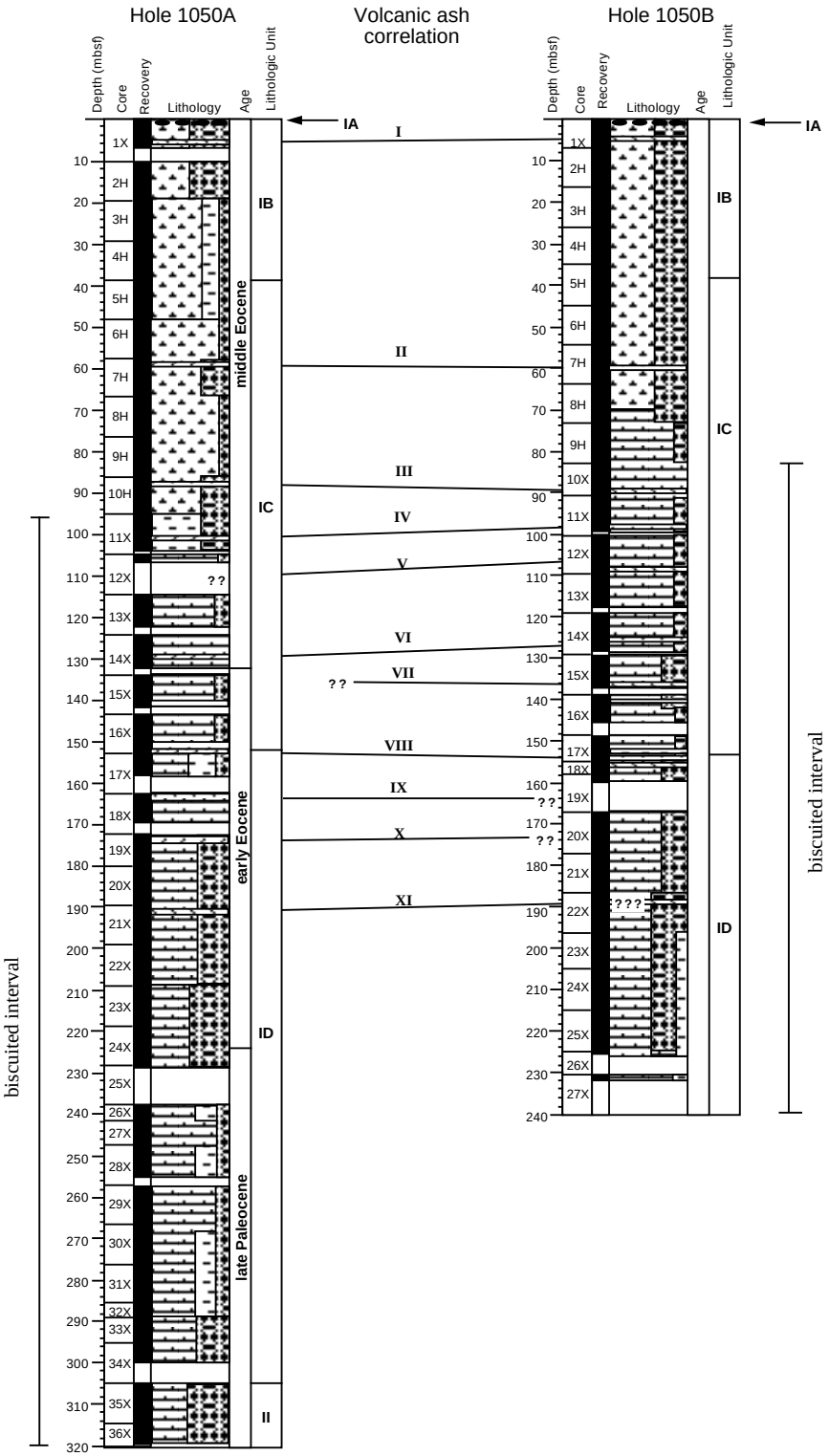

Figure 1. Summary of lithology, core recovery, and age for sediment recovered from Holes 1050A and 1050B. Symbols are the same as those used in Figure 1, "Site 1049" chapter (this volume).

Intervals: 171B-1050A-1X-1, 0–3 cm; 171B-1050B-1X-1, 0–5 cm
Depth: 0–0.03 mbsf, Hole 1050A; 0–0.05 mbsf, Hole 1050B
Thickness: 0.03 m, Hole 1050A; 0.05 m, Hole 1050B
Age: ?Pleistocene

Mn flecks were recovered in the upper 3 cm of Core 171B-1050A-1X, and a single Mn nodule was recovered at the top of Core 171B-1050B-1X. This Mn-rich interval most likely corresponds to the Mn oxide layer recovered at the top of Site 1049, where it was also designated lithologic Subunit IA. A Mn/phosphate crust or layer of nodules was also recovered at Sites 1051, 1052, and 1053.

Subunit IB

Description: Nannofossil ooze to siliceous nannofossil ooze
Intervals: 171B-1050A-1X-1, 3 cm, through 4H-CC; 171B-1050B-1X-1, 5 cm, to 5H-2, 79 cm
Depth: 0.03–38.7 mbsf, Hole 1050A; 0.05–37.79 mbsf, Hole 1050B
Thickness: 38.7 m, Hole 1050A; 37.8 m, Hole 1050B

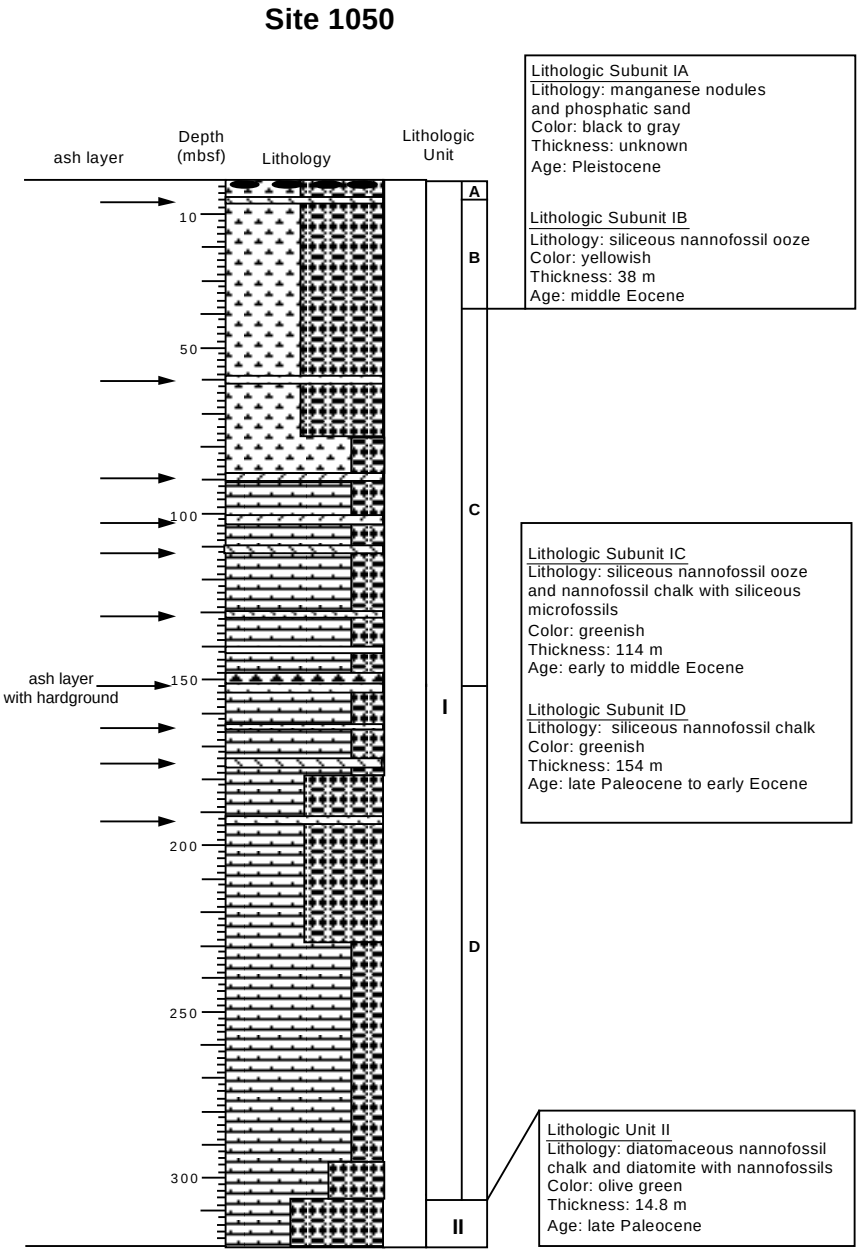

Figure 2. Composite section from Holes 1050A and 1050B with correlation of the ash layers between the holes. Symbols are the same as those used in Figure 1, "Site 1049" chapter (this volume).

Age: middle Eocene

Lithologic Subunit IB is middle Eocene ooze dominated by calcareous nannofossils with varying amounts of siliceous microfossils. The base of lithologic Subunit IB is defined by a sharp change in color from pale yellow (5Y 8/2) to light grayish green (10G 7/1–8/1). Bedding is poorly defined, and the sediment is homogeneous. This fabric appears thoroughly bioturbated in intervals, although scattered, burrow-mottled intervals can be recognized (Fig. 5). Rare mollusk fragments may represent the remains of some of the burrowing organisms. Pyrite flecks are disseminated throughout the unit. An ash layer is present in both holes at Sections 171B-1050A-1X-5, 11–16 cm (6.11–6.16 mbsf), and 171B-1050B-1X-5, 97–99 cm (6.97–6.99 mbsf; Fig. 6). The sediments of lithologic Subunit IB were slightly disturbed by drilling in both holes.

Subunit IC

Description: Siliceous nannofossil ooze to nannofossil chalk with siliceous microfossils

Intervals: 171B-1050A-4H-5, 0 cm, to 16X-7, 42 cm; 171B-1050B-5H-2, 79 cm, to 17X-6, 23 cm
Depth: 38.7–153.1 mbsf, Hole 1050A; 37.8–155.4 mbsf, Hole 1050B
Thickness: 114.4 m, Hole 1050A; 117.6 m, Hole 1050B
Age: late early Eocene to middle Eocene

The top of lithologic Subunit IC is placed at the color change from pale yellow (5Y 8/2) in the overlying Subunit IB to light grayish green (10GY 8/1). Within lithologic Subunit IC, the color varies from light grayish green (10GY 8/1) to grayish green (5G 6/1). The dominant lithology in Subunit IC is a siliceous nannofossil ooze that grades into a siliceous nannofossil chalk in Cores 171B-1050A-10H and 171B-1050B-8H. Drilling-induced biscuiting of the cores occurs throughout the interval drilled by XCB (from Sections 171B-1050A-11X and 171B-1050B-10X) and increases in intensity downhole. Siliceous microfossils identified in this interval include radiolarians, sponge spicules, and diatoms (on CD-ROM, back pocket, this volume). Distinct bioturbation includes *Zoophycos* spreiten (Fig. 7). A chert layer was recovered in intervals 171B-1050A-15X-4, 127–150

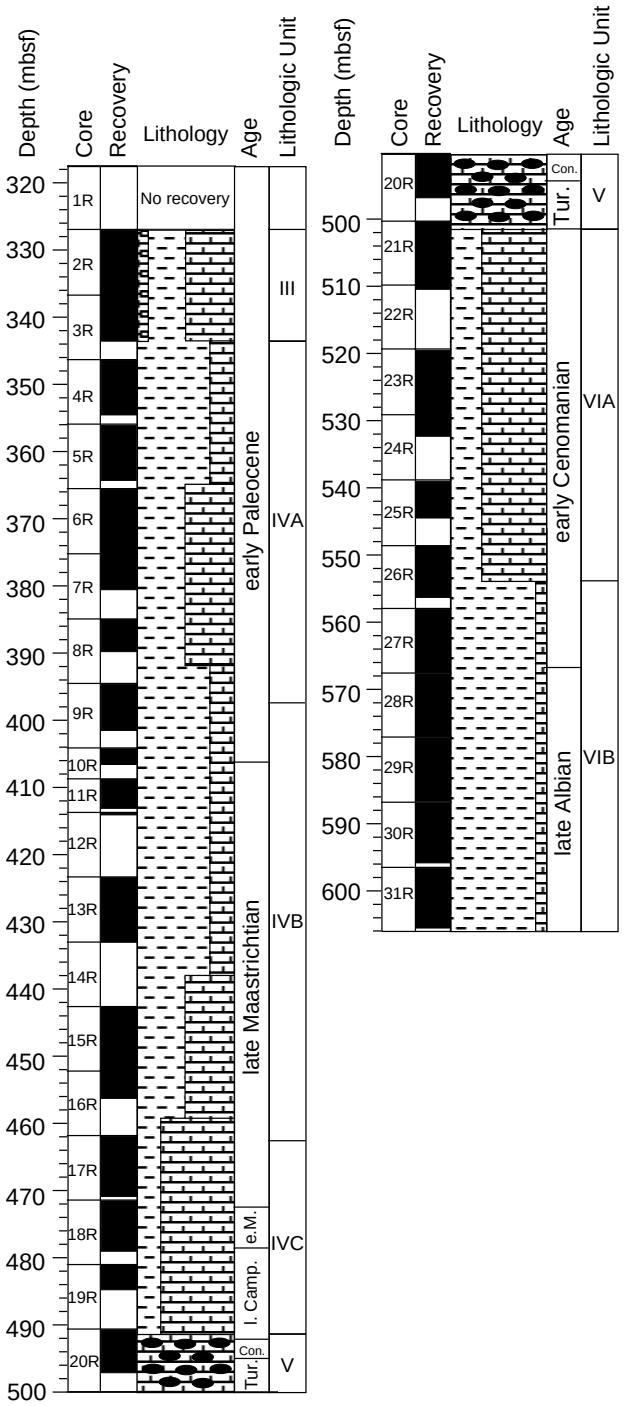

Figure 3. Summary of lithology, core recovery, and age for sediment recovered from Hole 1050C. Symbols are the same as those used in Figure 1, "Site 1049" chapter (this volume).

cm (139.8–140.0 mbsf), and 171B-1050B-16X-1, 80–100 cm (144.4–144.6 mbsf).

Subunit ID

Description: Siliceous nannofossil chalk to nannofossil chalk with siliceous microfossils
Intervals: 171B-1050A-16X-7, 42 cm, to 34X-CC, 49 cm; 171B-1050B-17X-6, 23 cm, to 27X-CC, 47 cm
Depth: 153.1–300.1 mbsf, Hole 1050A; 155.2–240.0 mbsf, Hole 1050B
Thickness: 147.0 m, Hole 1050A; 84.8 m, Hole 1050B
Age: late early Eocene to late Paleocene

A hardground found in Sections 171B-1050A-16X-7, 42 cm (153.0 mbsf), and 171B-1050B-17X-6, 23 cm (155.4 mbsf), separates lithologic Subunits IC and ID (Fig. 8). The surface of the hardground is characterized by borings and other bioerosion features. The resulting cavities are filled with the lighter colored overlying sediment. Below the hardground is a thin (<0.3 cm) greenish layer (iron oxide rich) with high abundances of volcanic glass that grades into a brownish gray (5YR 7/2) layer (6 cm). Above and below the hardground are two intervals of bioturbated chert (Fig. 9). Within lithologic Subunit ID, the color varies from light grayish green (10GY 8/1) to grayish green (5G 6/1). The dominant lithology in Subunit ID is a siliceous nannofossil chalk, or nannofossil chalk, with siliceous nannofossils similar to that of the overlying subunit.

Unit II

Description: Diatomaceous nannofossil chalk and nannofossil diatomite
Interval: 171B-1050A-35X-1, 0 cm, to 36X-CC, 15 cm
Depth: 304.9–319.9 mbsf
Thickness: 14.8 m
Age: early late Paleocene to late early Paleocene

Lithologic Unit II is a diatomaceous nannofossil chalk to nannofossil diatomite. It is distinguished from lithologic Unit I by a higher proportion of diatoms (as much as 55%), burrow replacement by pyrite, and abundant dark pyrite specks, as well as a shift from light grayish green (10GY 8/1) to olive green color. Bioturbation and drilling-induced biscuiting occur throughout this unit. The lower contact was not recovered.

Unit III

Description: Clayey siliceous chalk with nannofossils and chert
Interval: 171B-1050C-2R-1, 0 cm, to 3R-CC, 2 cm
Depth: 327.1–343.5 mbsf, Hole 1050C
Thickness: 16.4 m, Hole 1050C
Age: early Paleocene

The contact between Units II and III was not recovered. Unit III was recovered only in Hole 1050C. The dominant lithology in Unit III is a clayey siliceous chalk with nannofossils. Color varies from light greenish gray (5GY 6/1) to greenish gray (2.5GY 5/1), with the darker lithology the more clay rich. Light–dark color banding is apparent throughout the unit, on a scale of ~1 m in Core 171B-1050C-2R, and thin glauconitic laminae occur intermittently throughout the unit. Minor drilling-induced biscuiting and moderate fracturing of the cores occur throughout Unit III. Core disturbance is particularly pervasive in Sections 171B-1050C-3R-3 through 3R-5 and corresponds to the presence of chert, which is restricted to this interval in this unit. Bioturbation is moderate to intense in Unit III, with *Zoophycos*, *Chondrites*, and numerous unidentified burrows. The base of Unit III is placed at the last downhole occurrence of siliceous microfossil-rich sediments.

Unit IV

Description: Calcareous claystone with nannofossils, claystone with nannofossils, limestone with nannofossils, nannofossil claystone, nannofossil chalk with clay, calcareous nannofossil claystone, nannofossil chalk with clay, and nannofossil foraminifer chalk at the K/T boundary interval
Interval: 171B-1050C-4R-1, 0 cm, to 20R-1, 79 cm
Depth: 343.5–491.4 mbsf, Hole 1050C
Thickness: 147.9 m, Hole 1050C
Age: early Paleocene to late Campanian

Table 3. Summary of lithologic units from Hole 1050C.

Lithologic unit/subunit	Hole 1050C	Age	Lithologies
IA	Drilled without coring	Pleistocene to Holocene	Not recovered
IB	Drilled without coring	middle Eocene	Not recovered
IC	Drilled without coring	middle Eocene to early Eocene	Not recovered
ID	Drilled without coring	early Eocene to late Paleocene	Not recovered
II	Drilled without coring	late Paleocene	Not recovered
III	Interval 2R-1, 0 cm, to 3R-CC, 2 cm	early Paleocene 327.10-343.48 mbsf 16.38 m	Clayey siliceous chalk with nannofossils, chert
IV	Interval 4R-1, 0 cm, to 9R-1, 43 cm	early Paleocene 343.48-394.93 mbsf 51.45 m	Claystone with variable amounts of nannofossil, nannofossil chalk with variable amounts of clay
IV	Interval 9R-1, 43 cm, to 17R-2, 42 cm	late Maastrichtian 394.93-462.72 mbsf 67.79 m	Nannofossil claystone, calcareous claystone, nannofossil foraminifer chalk
IV	Interval 17R-2, 42 cm, to 20R-1, 79 cm	late Maastrichtian to late Campanian 462.72-491.39 mbsf 28.67 m	Nannofossil claystone, nannofossil chalk, clayey nannofossil chalk, nannofossil chalk with foraminifers
V	Interval 20R-1, 79 cm, to 21R-2, 0 cm	late Campanian to Turonian 491.39-501.70 mbsf 10.31 m	Hardgrounds of varying character and sediments on which they formed
VI	Interval 21R-2, 0 cm, to 26R-4, 104 cm	early Cenomanian 501.70-553.94 mbsf 52.24 m	Nannofossil chalk or limestone with variable amounts of clay, claystone with variable amounts of nannofossils
VI	Interval 26R-4, 104 cm, to 31R-CC, 27 cm	early Cenomanian to late Albian 553.94-605.41 mbsf 51.47 m	Nannofossil claystone, claystone with nannofossils, calcareous claystone with nannofossils and foraminifers, nannofossil claystone with organic debris and feldspar

The top of Unit IV is defined by the last downhole occurrence of siliceous microfossil-rich sediments. This unit is divided into three subunits based primarily on color and variations in clay content. The boundary between Subunits IVB and IVC is based on the top of an interval of prevalent slumping. RCB drilling introduced slight disturbance with limited fragmentation and biscuiting.

Subunit IVA

Description: Claystone with variable amounts of nannofossils and nannofossil chalk with variable amounts of clay
Interval: 171B-1050C-4R-1, 0 cm, to 171B-1050C-9R-1, 43 cm
Depth: 343.5–394.9 mbsf, Hole 1050C
Thickness: 51.4 m, Hole 1050C
Age: early Paleocene

Subunit IVA consists of various shades of greenish gray (10GY 5/1) to light greenish gray (10GY 8/1) clayey nannofossil lithologies, except for Core 171B-1050C-7R, which contains some light brownish gray (2.5 6/1) intervals. Most contacts between shades of greenish gray are gradual, except for a few sharp color contacts, with color alternations varying from centimeters to meters. Darker intervals are usually more clay rich, and lighter intervals are more carbonate rich. Bioturbation is moderate to heavy, with burrow mottling throughout the unit; *Chondrites*, *Planolites*, and *Zoophycos* are abundant. Burrows are usually outlined or completely infilled with black framboidal pyrite. The upper contact of this subunit is defined as the last downhole occurrence of sediments rich in siliceous microfossils, and the lower contact is placed at the color change from grayish green (10GY 5/1) nannofossil claystone to light greenish gray (10Y 7/1) calcareous nannofossil claystone at the top of Subunit IVB.

Subunit IVB

Description: Nannofossil claystone, calcareous nannofossil claystone, and nannofossil foraminifer chalk
Interval: 171B-1050C-9R-1, 43 cm, to 171B-1050C-17R-2, 42 cm
Depth: 394.9–462.7 mbsf, Hole 1050C
Thickness: 67.8 m, Hole 1050C
Age: early Paleocene to late Maastrichtian

The top of Subunit IVB is placed at the color change from grayish green (10GY 5/1) nannofossil claystone in Subunit IVA to light greenish gray (10Y 7/1) calcareous nannofossil claystone at the top of Subunit IVB. Bioturbation is moderate throughout Subunit IVB. Burrows are particularly visible in Cores 171B-1050C-15R and 16R in the darker intervals. Core 171B-1050C-15R displays a few spectacular, complete *Zoophycos* burrows in Sections 171B-1050C-15R-2 and 15R-4 (Fig. 10). Slumping probably has affected most of Subunit IVB, with the exception of the interval from 171B-1050C-15R-1, 45 cm, to 17R-2, 40 cm.

The K/T boundary occurs at 171B-1050C-10R-2, 36 cm (405.93 mbsf; Fig. 11). In contrast to Site 1049, no impact ejecta are preserved, although the K/T boundary is biostratigraphically complete: the topmost Maastrichtian *Micula prinsii* Zone is present, as well as the basal Paleocene Pα Zone (see "Biostratigraphy" section, this chapter), represented by fragments of dark gray clay in a drilling breccia between drilling biscuits. The K/T boundary is influenced only slightly by slumping, but in view of the extensive slumping above and below the K/T boundary, it is conceivable that the ejecta were slumped away from this site.

Subunit IVC

Description: Nannofossil claystone, nannofossil chalk, clayey nannofossil chalk, and nannofossil chalk with foraminifers
Interval: 171B-1050C-17R-2, 42 cm, to 20R-1, 79 cm
Depth: 462.7–491.4 mbsf, Hole 1050C
Thickness: 28.7 m, Hole 1050C
Age: late Maastrichtian to late Campanian

Subunit IVC is characterized by various shades of greenish gray, (primarily 5GY 8/1 to 6/1) moderately to heavily bioturbated nannofossil chalk to nannofossil claystone. There are subtle meter-scale alternations between lighter and darker intervals. Wavy laminae, microfaults, soft-sediment deformation, and chaotic bedding typify much of Subunit IVC and probably constitute a slumped interval. Subunit IVC is more clay rich than the overlying Subunit IVB. The upper boundary of Subunit IVC marks the top of an interval of prevalent slumping; a similar slumped interval was recovered at Site 1052. The lower boundary is placed at a phosphate/iron hardground at Section 171B-1050C-20R-1, 79 cm. Overlying this hardground (i.e., the lowermost part of Subunit IVC) is ~80 cm of light brownish gray (2Y 6/2) to pale brown (10YR 6/3) nannofossil chalk with foraminifers.

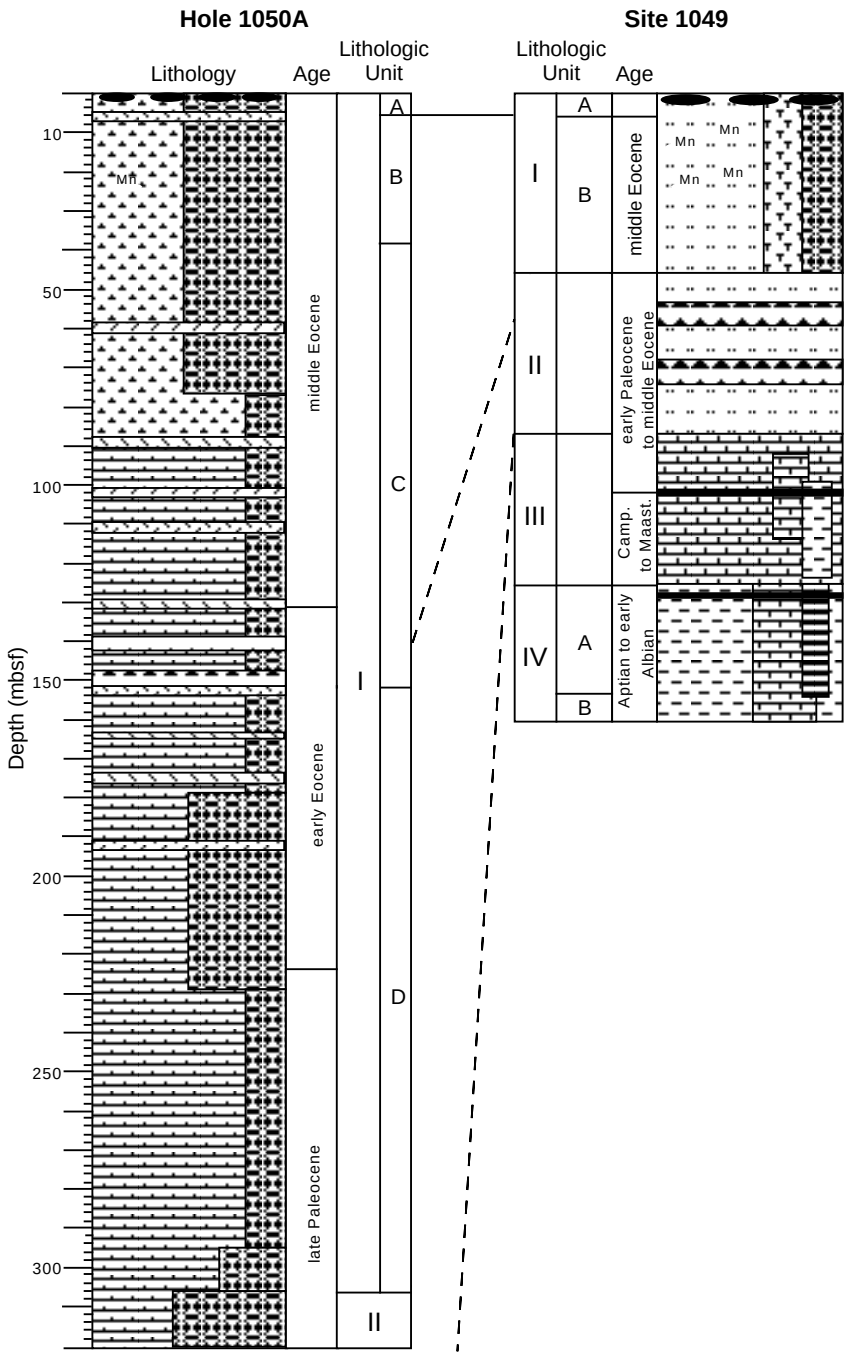

Figure 4. Correlation of Hole 1050A and Site 1049 lithologic units. Symbols are the same as those used in Figure 1, "Site 1049" chapter (this volume).

Unit V

Description: A series of hardgrounds of varying character and the sediment on which they formed
Interval: 171B-1050C-20R-1, 79 cm, to 21R-1, 77 cm
Depth: 491.4–501.7 mbsf, Hole 1050C
Thickness: 10.3 m, Hole 1050C
Age: late Turonian to late Campanian

Lithologic Unit V includes a series of hardgrounds and the sediment they formed on over an ~17.5-m.y. period during the Late Cretaceous (Figs. 12, 13; also see "Biostratigraphy" section, this chapter). The various hardgrounds differ in character from reddened, weakly bioturbated chalk to a hard, heavily bored phosphate/iron crust more than 1 cm thick, and they mark a distinct change in sedimentation style in the area from the late (but not latest) Cenomanian to the late Campanian. The underlying sediment, lithologic Unit VI, although chaotically bedded, still bears evidence of its original character as rhythmic alternations of white, heavily bioturbated chalk and laminated black shale. Laminated sediment does not recur above the hardgrounds.

Because hardgrounds occur on top of sediment, we discuss this unit from the bottom upward. The oldest hardground represents the Cenomanian/Turonian boundary (see "Biostratigraphy" section, this chapter). It occurs over interval 171B-1050C-21R-1, 77–85 cm (~501 mbsf), and is the reddened, upper part of Cenomanian foraminifer nannofossil chalk (Fig. 14). The chalk reddens upward over a 15-cm-thick interval and is heavily bioturbated. Overlying this hardground are a few centimeters of white nannofossil chalk that bears a

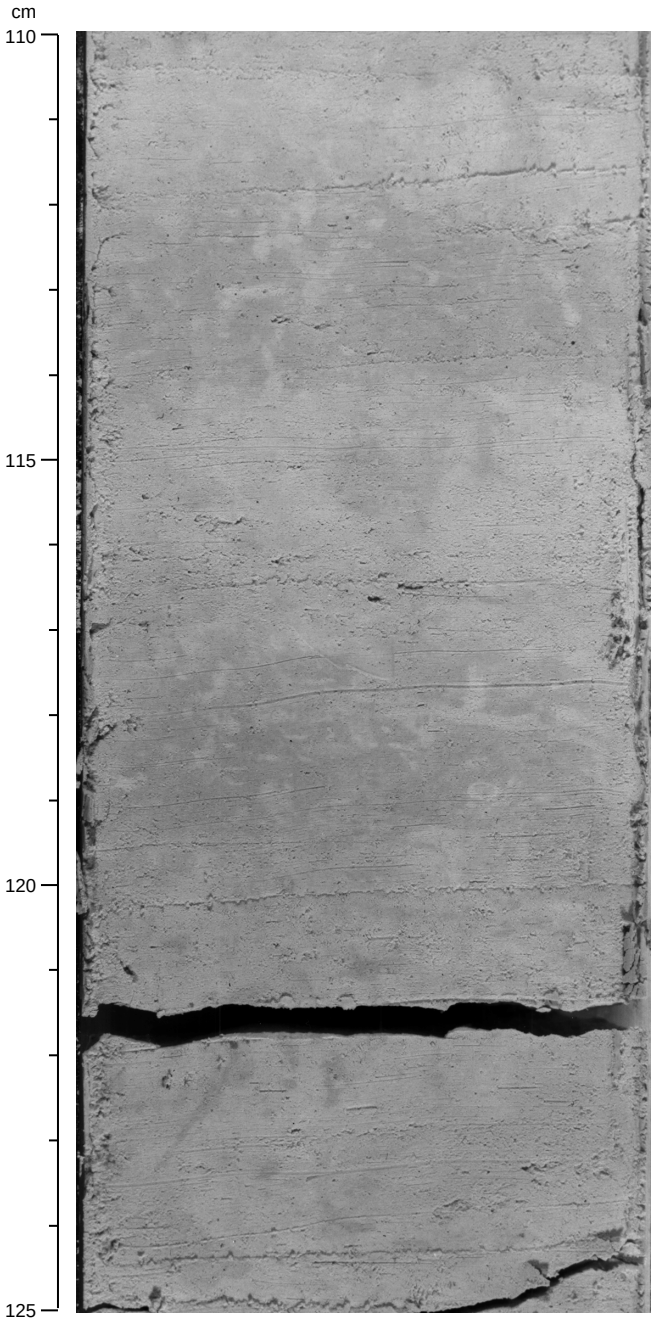

Figure 5. Interval 171B-1050B-3H-1, 110–125 cm (17.6–17.75 mbsf). Moderately bioturbated light–dark alterations in siliceous nannofossil ooze of lithologic Subunit IB.

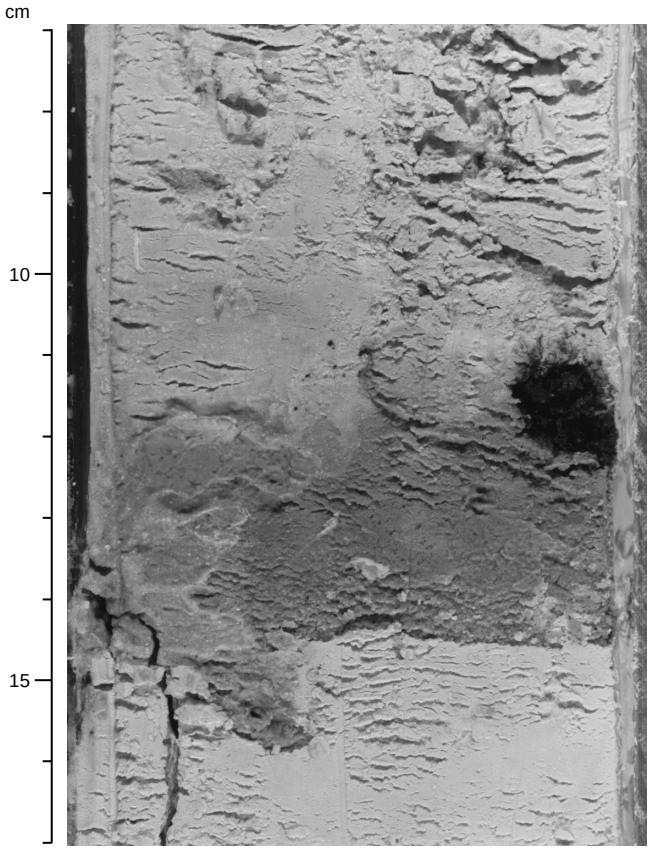

Figure 6. Interval 171B-1050A-1X-5, 7–17 cm (6.07–6.17 mbsf). Vitric ash in lithologic Subunit IB.

black claystone clast, 2 cm across. The chalk is capped by an 8-cm-thick clay-clast conglomerate. The clasts in this interval form a squeezed jumble of varying colors, ranging from a vivid pink to green, to black, to varying shades of tan. One of the larger clasts, 3 cm long, is deep black—similar to black sediment in underlying lithologic Unit VI—and contains green clasts within it, indicating that it has experienced at least two generations of erosion and redeposition (Fig. 14). The clay clasts have been compacted, presumably by deposition of the overlying sediment, and appear to flow into one another. The high concentration of clasts, their varying sizes, and their lack of grading or bedding indicates that they were deposited by a debris flow. Above this deposit, 1 cm of reddish brown chalk is overlain by a 3-cm-thick massive reddish brown claystone. The slick feel of the claystone is reminiscent of bentonite. An additional 2 cm of upper Turonian reddish brown chalk is subsequently overlain by sediment that continues into the overlying section at Section 171B-1050C-20R-3, 122 cm (Fig. 12). The Turonian sediment is 2.8 m thick and is a foraminifer nannofossil chalk. This sediment is purplish red, a color unique to this interval. The Turonian strata are generally heavily bioturbated and burrow mottled throughout. Interval 171B-1050C-20R-4, 102–150 cm, is an exception and consists of three beds of chalk, each ~15 cm thick, which are massive and burrow mottled at the base and laminated at the top (Fig. 12). Within the laminated beds, the color changes from deep purplish red at the base to a lighter shade of red upward, and culminates with a few centimeters of dusky yellowish green submillimeter-thick laminae. The laminated sequence suggests the development of anoxic water conditions over each interval. Oxygenated water probably contributed to the deep red color of the sediment and helped to support the bioturbating fauna. As anoxic conditions developed, the red tone became less developed, or it was postdepositionally altered. The green color and lamination of the top of these beds probably results from anoxic conditions that reduced (or at least did not allow the oxidation of) iron in the sediment and also eliminated benthic infauna. These were the youngest laminated sediments deposited at Site 1050.

The Turonian section is capped by another hardground at Section 171B-1050C-20R-3, 122 cm (Figs. 12, 15). The sediment character above and below this interval is quite different, and the interval is clearly burrowed and perhaps bored. A thin layer of the overlying white Coniacian nannofossil chalk (see “Biostratigraphy” section, this chapter) has been worked downward into the red Turonian chalk

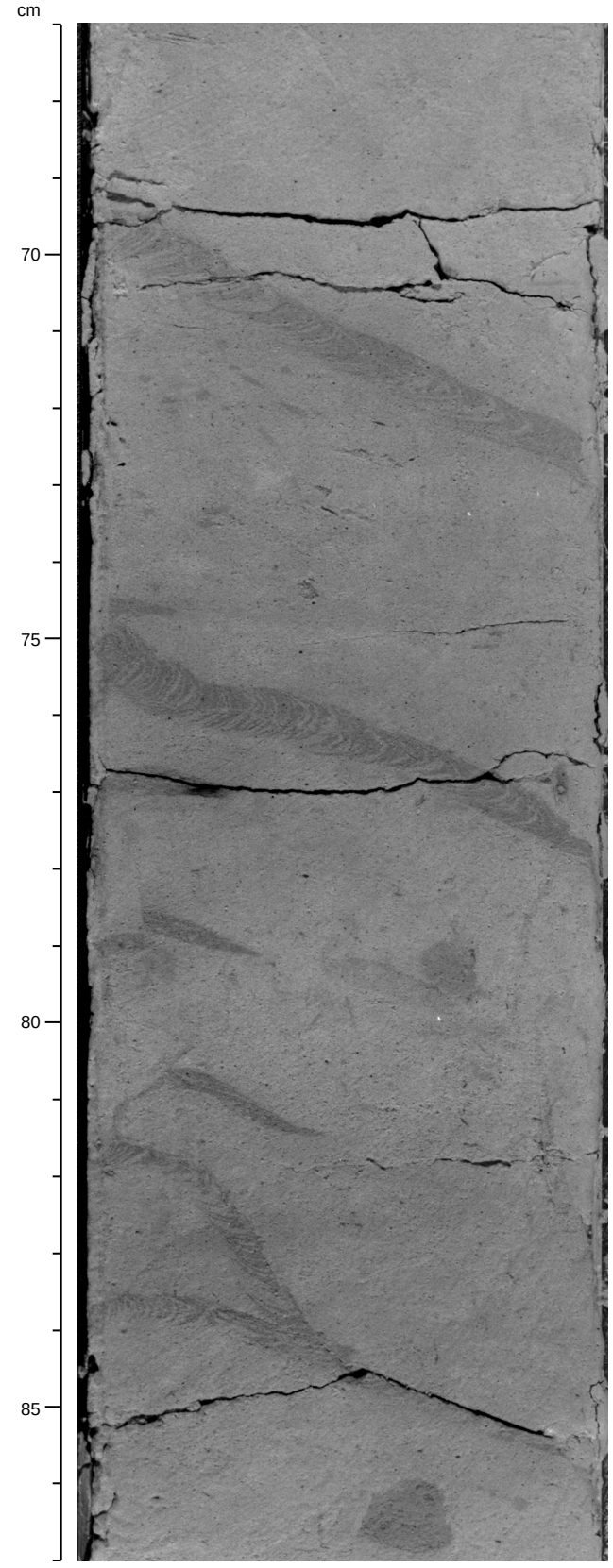

Figure 7. Interval 171B-1050A-9H-6, 67–87 cm (84.37–84.57 mbsf). *Zoophycos* burrow in lithologic Subunit IC.

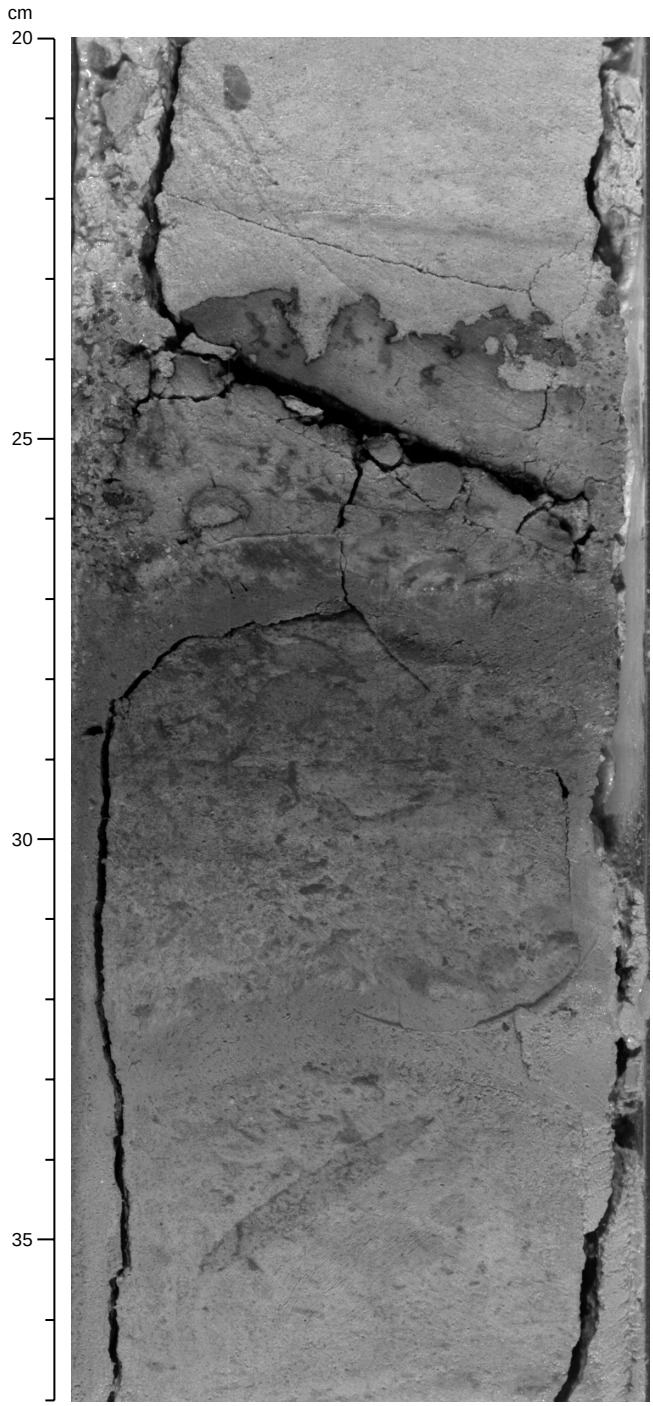

Figure 8. Interval 171B-1050B-17X-6, 20–37 cm (155.40–155.57 mbsf). Vitric ash layer with iron oxide–rich hardground (23–24 cm) representing the contact between the siliceous nannofossil chalks of lithologic Subunits IC and ID (23 cm).

and has caused a faint reduction halo into the older chalk (Fig. 15). Although the Coniacian sediment overlying the hardground is highly variable, it is dominantly a foraminifer nannofossil chalk with clay rip-up clasts. At its base just above the hardground, large clasts of black claystone, similar to sediment observed in the underlying lithologic Unit VI, and reddish clasts, similar to the underlying Turonian

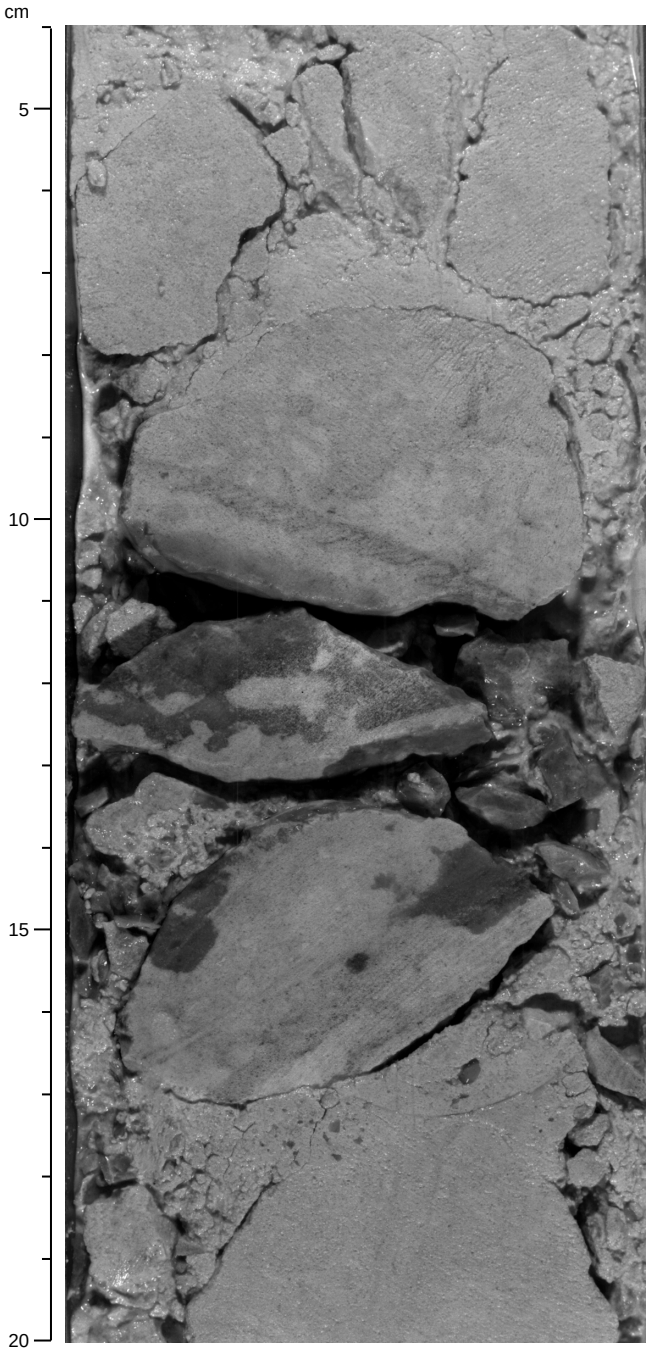

Figure 9. Interval 171B-1050B-17X-6, 4–20 cm (155.24–155.40 mbsf). Bioturbated chert with *Zoophycos* burrow in lithologic Subunit ID.

sediment, occur floating in the chalk matrix (Fig. 15). Angular to subrounded smaller clasts, mostly submillimeter to a few millimeter in diameter, are common throughout what is an evidently heavily bioturbated interval (Fig. 15). Two larger reddish clasts have green rims of apparent alteration halos (Fig. 15; 106–108 cm). The halos suggest that the clasts were ripped up from red sediment, transported to a reducing environment, and subsequently ripped up again to be deposited with this sediment, which is mottled white and faint brown.

Overlying the interval with large clay rip-up clasts, in intervals 171B-1050C-20R-3, 76–88 cm, and 93–100 cm, are two heavily bioturbated levels with high concentrations of clay clasts, most of which are as much as 5 mm in diameter, but with a few as much as 2 cm in diameter (Fig. 12). These are apparently clay-clast conglomerates or diamictons, which were subsequently spread about the chalk matrix by burrowing organisms. Above this interval through the next 75 cm, the sediment is Coniacian chalk that is rich in clay rip-up clasts, heavily bioturbated, and alternates from a pale tan to a deep brown color (Fig. 12). Beneath the heavy overprint of bioturbation, the sediment appears to have originally been alternations of lighter, more nannofossil-rich sediment and browner, more foraminifer-rich sediment, with frequent input of granule-sized clay clasts either as traction load or debris flows.

In interval 171B-1050C-20R-2, 136–146 cm, is a layer of laminated nannofossil siltstone with iron oxide. Foraminifers, lined or filled with pyrite, rare quartz grains, and unpyritized foraminifers give this sediment a salt-and-pepper appearance (Fig. 16). Black clay and tan chalk clasts occur throughout. A surprising component is rare, slightly altered volcanic glass. The upper 2 cm appears to be cross-laminated. Above this ashy layer is another 30 cm of foraminifer chalk with clay rip-up clasts capped by a sharp, uneven contact with the overlying sediment. This sediment is also Coniacian in age (see "Biostratigraphy" section, this chapter) but differs from the underlying meter of sediment by having only rare clay clasts. It is composed of heavily bioturbated, pale tan foraminifer nannofossil chalk (Fig. 12). Three beds overlying interval 171B-1050C-20R-2, 38–104 cm, have a higher concentration of granule- to sand-sized clay clasts, some of which are concentrated in burrows (Fig. 17). These intervals are heavily bioturbated and appear to be a mix of background sediment and a layer of clay clasts deposited near 38, 82, and 93 cm in Section 171B-1050C-20R-2 (Fig. 12).

Above this interval is rather normal-looking Coniacian chalk, with *Zoophycos* burrows over the lower 20 cm of Section 171B-1050C-20R-1 (Fig. 12). The chalk continues upward with increasing amounts of clay clasts and heavy bioturbation for another 25 cm, alternating darker and lighter brown, to interval 171B-1050C-20R-1, 107–110 cm. This 3-cm-thick interval is a nearly pure white, Santonian nannofossil chalk, occurring only as burrow fill (Fig. 18). These chalk-filled burrows represent the only Santonian-aged sediment recovered to date on the Blake Nose (see "Biostratigraphy" section, this chapter).

Above the Santonian white burrows is a dark red layer with a submillimeter-thick coating of a black mineral (Fig. 18; 100 cm). The mineral coating and bioturbation of the overlying light brown sediment into the dark red layer indicates another hardground. This sediment is a nannofossil chalk with foraminifers and contains large clasts of black, hard, bored sediment (Fig. 18; 95–100 cm). These clasts are identical in appearance to a bored hardground that occurs a few centimeters above them at interval 171B-1050C-20R-1, 79–80 cm (Fig. 19). These are assumed to be pieces of a hardground that was ripped up and distributed through the sediment by bioturbating organisms or currents. The hard black material gives no reaction to hydroxylamine HCl, which indicates that it is not composed of Mn oxide. In the hydroxylamine HCl solution, the material began to fall apart into brown and black clay-sized material. The brown color is similar to that of the phosphate/Mn nodules we recovered at every Leg 171B site as lithologic Unit IA (see "Lithostratigraphy" section, "Site 1049" chapter, this volume). The pieces of hardground produced a strong signal in the cryomagnetometer, suggesting a high iron content (see "Magnetostratigraphy" section, this chapter). Between the pieces of ripped-up hardground and the in situ hardground is highly bioturbated tan and white chalk (Fig. 19; 80–86 cm). Above the final hardground in this unit is late Campanian sediment (see "Biostratigraphy" section, this chapter) of lithologic Unit IV. The

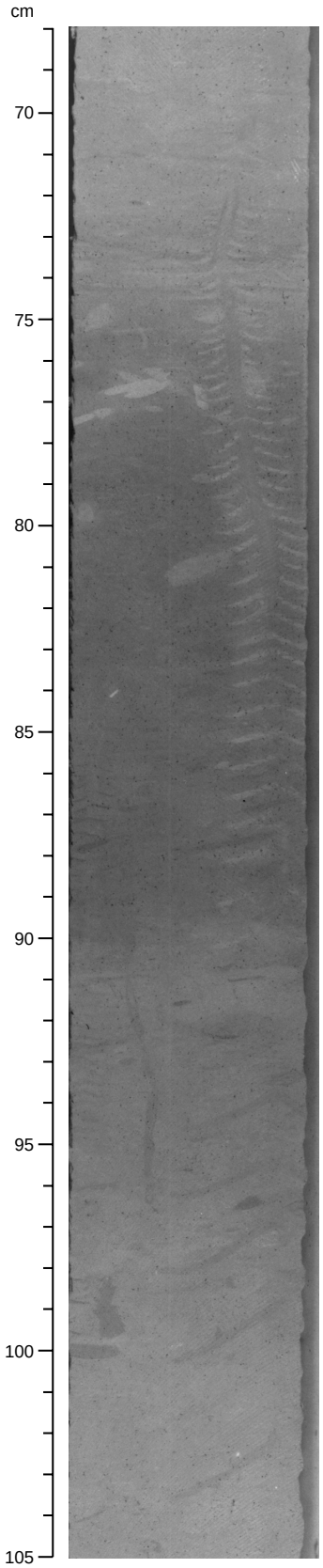

Figure 10. Interval 171B-1050C-15R-2, 68–105 cm. A complete *Zoophycos* burrow penetrates nannofossil claystone of lithologic Subunit IVB (68–103 cm).

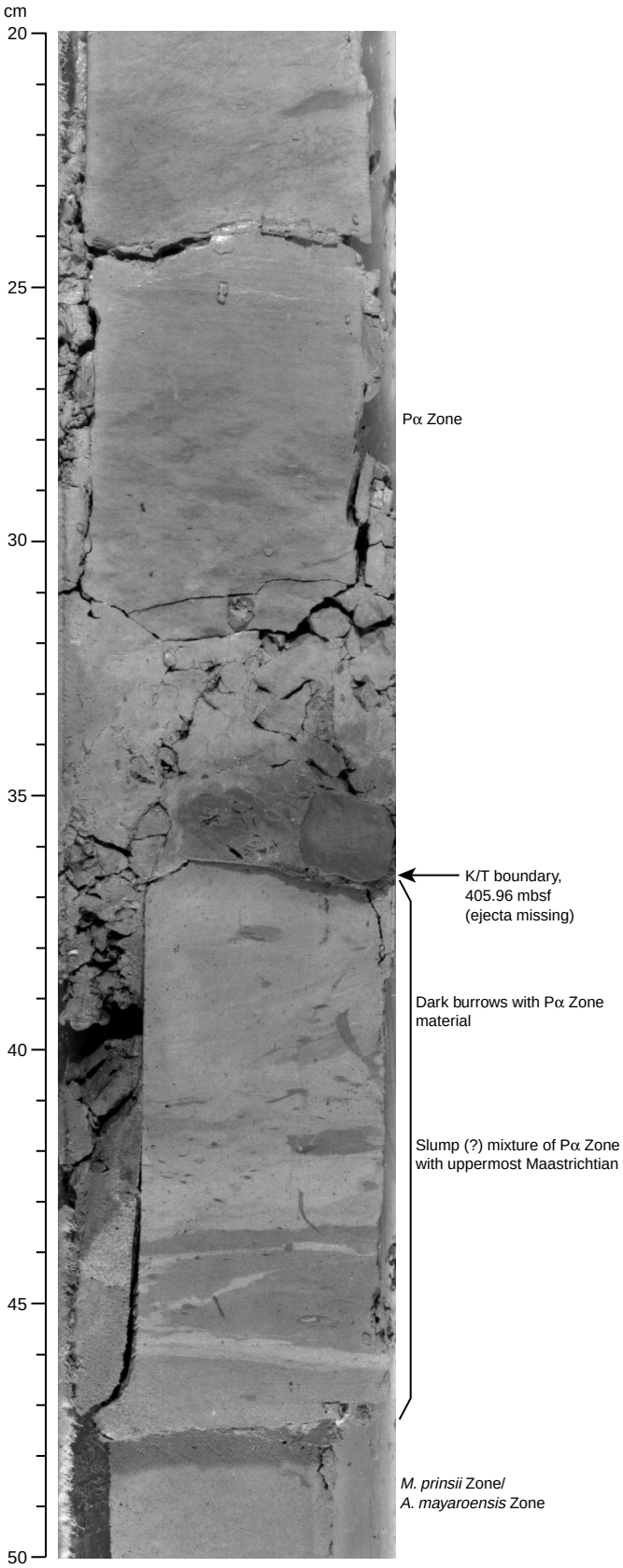

Figure 11. Interval 171B-1050C-10R-2, 20–50 cm. The K/T boundary (405.96 mbsf) is represented by fragments of dark gray clay in a drilling breccia.

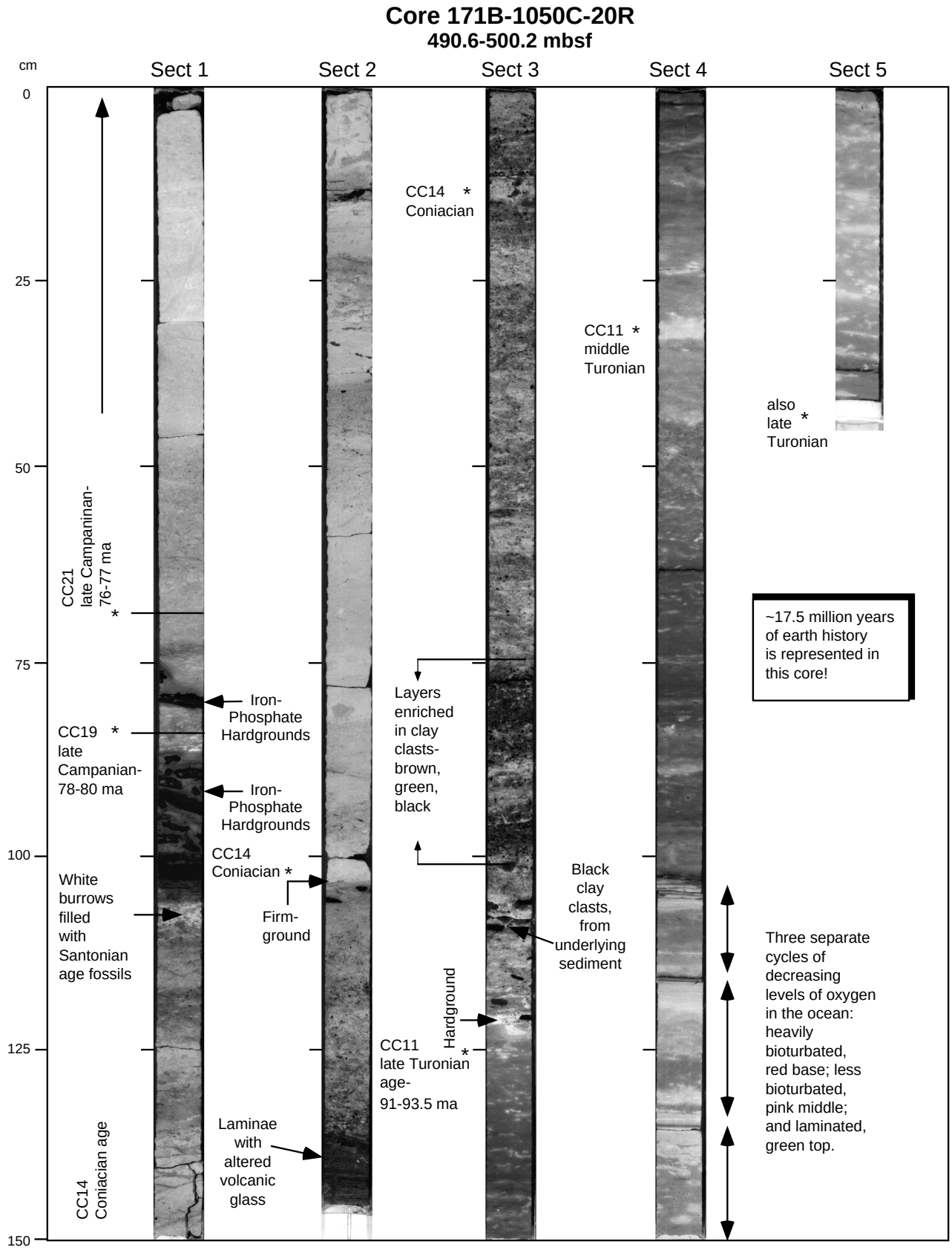

Figure 12. Summary of the hardgrounds and sediments of lithologic Unit V in Core 171B-1050C-20R. * = location of samples taken to establish bio-stratigraphic ages.

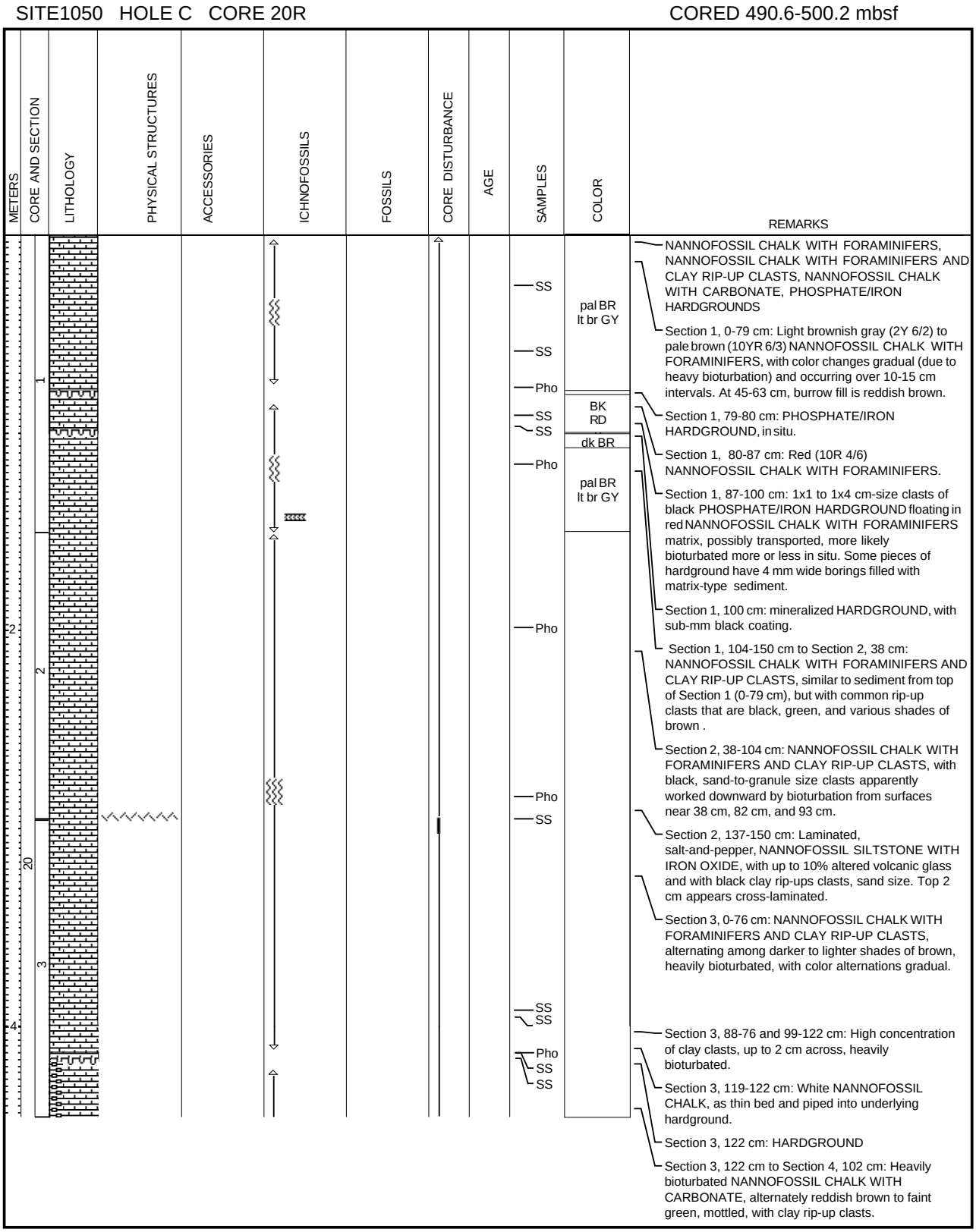

Figure 13. Barrel sheets of Core 171B-1050C-20R and Section 171B-1050C-21R-1 illustrating the distribution of hard- and firmgrounds that form lithologic Unit V.

SITE1050 HOLE C CORE 20R CORED 490.6-500.2 mbsf

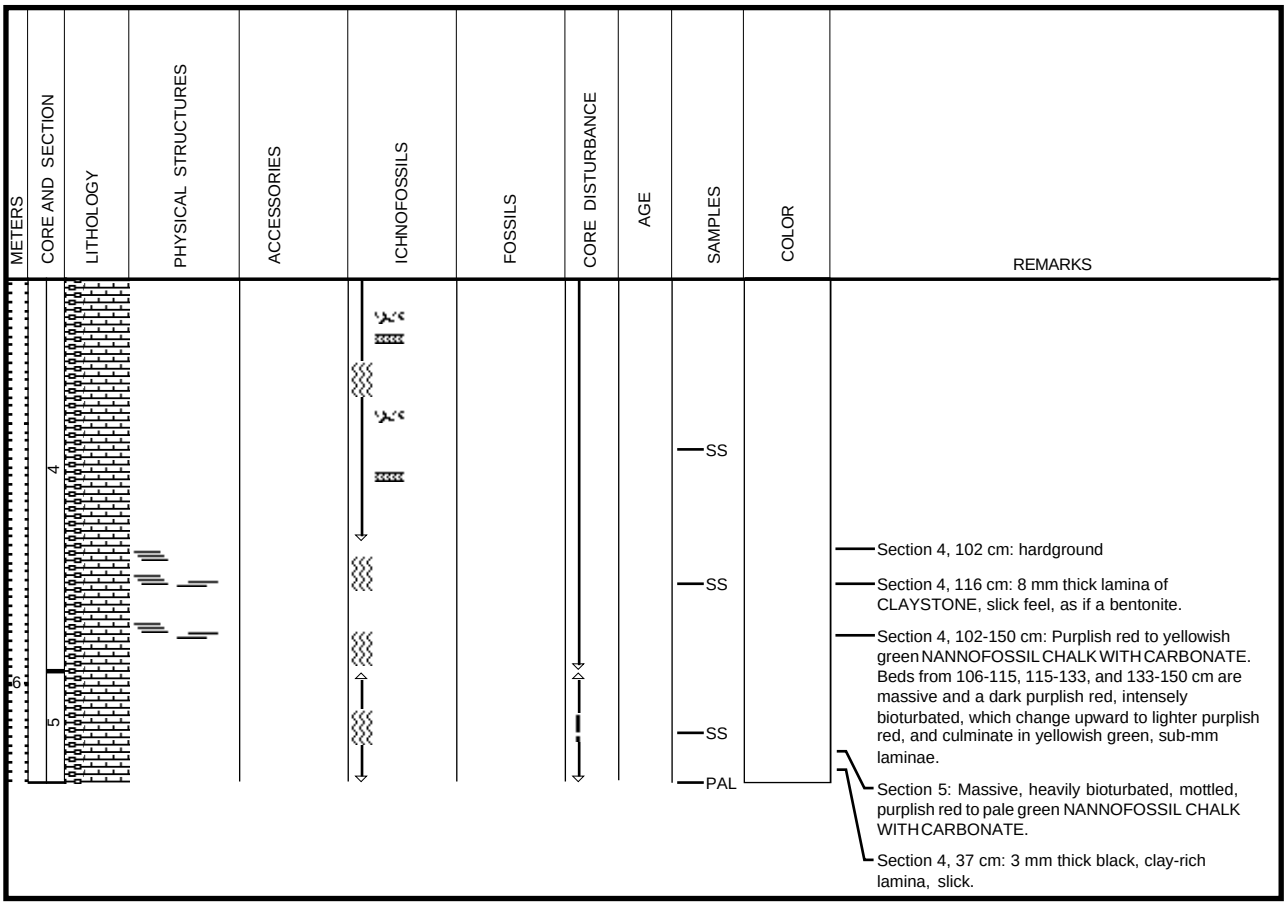

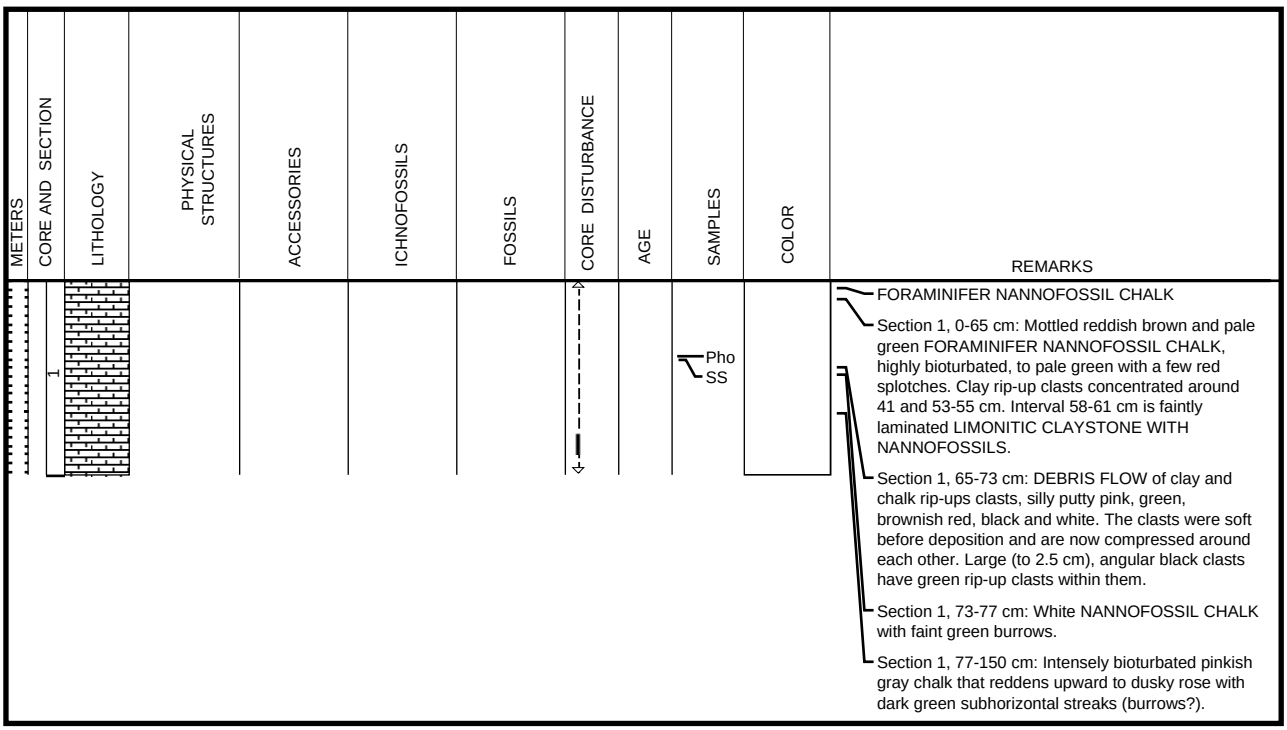

Figure 13 (continued).

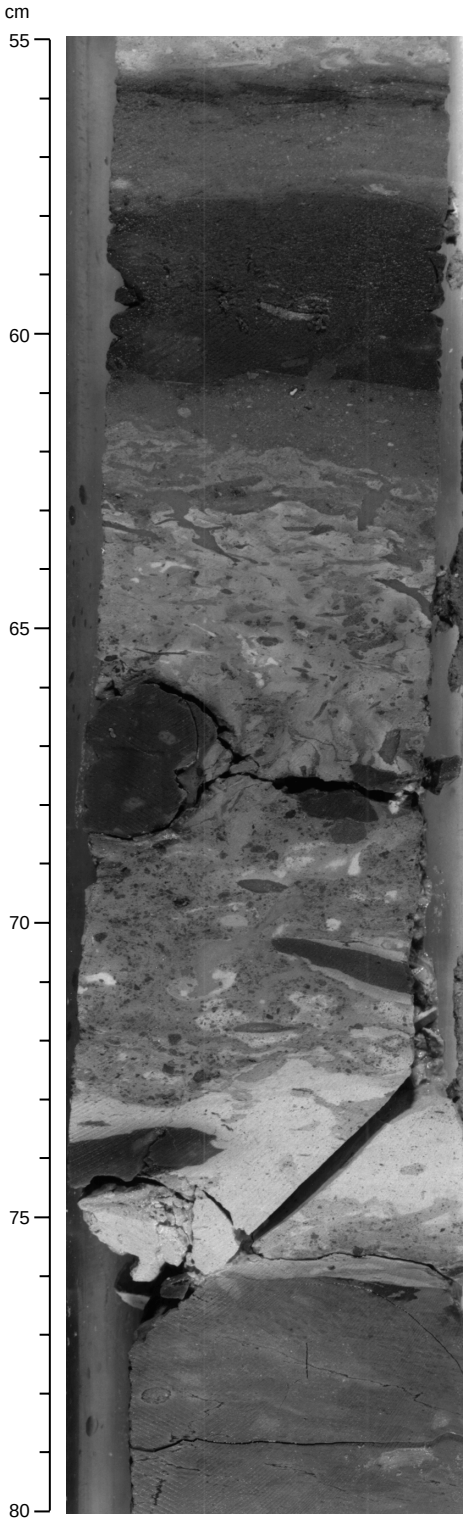

Figure 14. Interval 171B-1050C-21R-1, 55–80 cm. Cenomanian/Turonian boundary and the base of lithologic Unit V. From 76 to 80 cm is the reddened, burrowed top of Cenomanian chalk, and from 73 to 76 cm is white Turonian nannofossil chalk with a large black clay clast. A clay-clast conglomerate deposited from a debris flow occurs from 63 to 73 cm. Clasts are pink, green, and black. The large black clay clast from 66 to 68 cm includes green clasts within it. The dark red claystone from 58 to 61 cm is slick to the touch and may be bentonite.

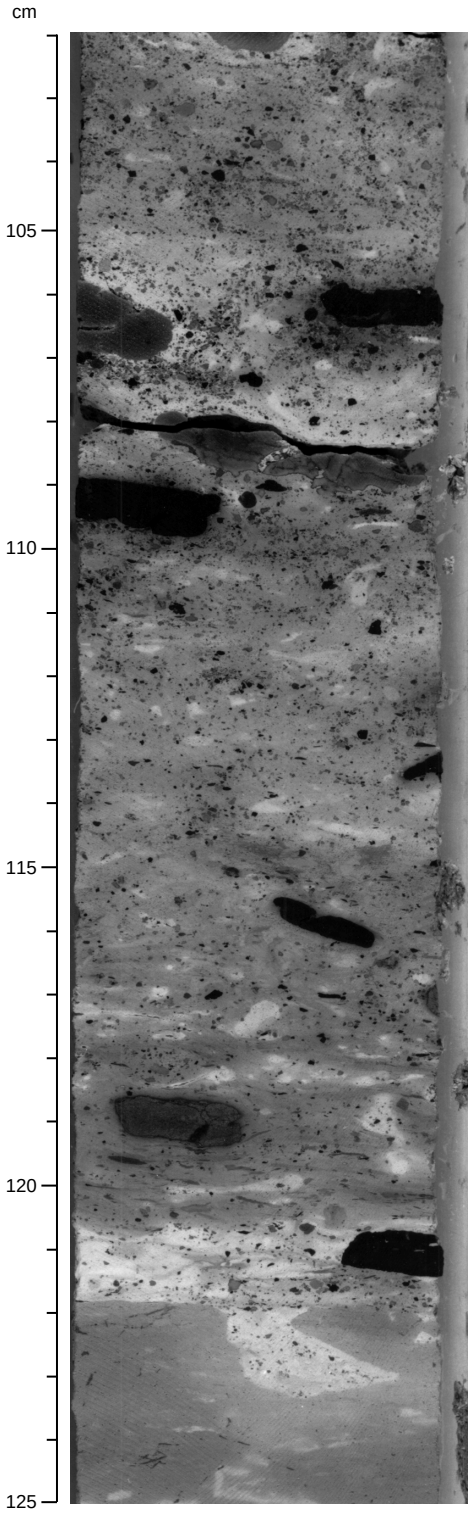

Figure 15. Interval 171B-1050C-20R-3, 102–125 cm. The burrowed hardground at 122 cm is the Turonian/Coniacian boundary. This marks the change in depositional style at Site 1050 from dominantly interbedded massive chalk and laminated claystones (lithologic Unit VI) to dominantly chalk (lithologic Unit IV and younger). The hiatus associated with this disconformity is ~1 m.y. Above the hardground, the Coniacian chalk is enriched by black claystone clasts and, to a lesser extent, by red and brown chalk clasts. Extensive bioturbation has probably distributed these clasts throughout the chalk matrix.

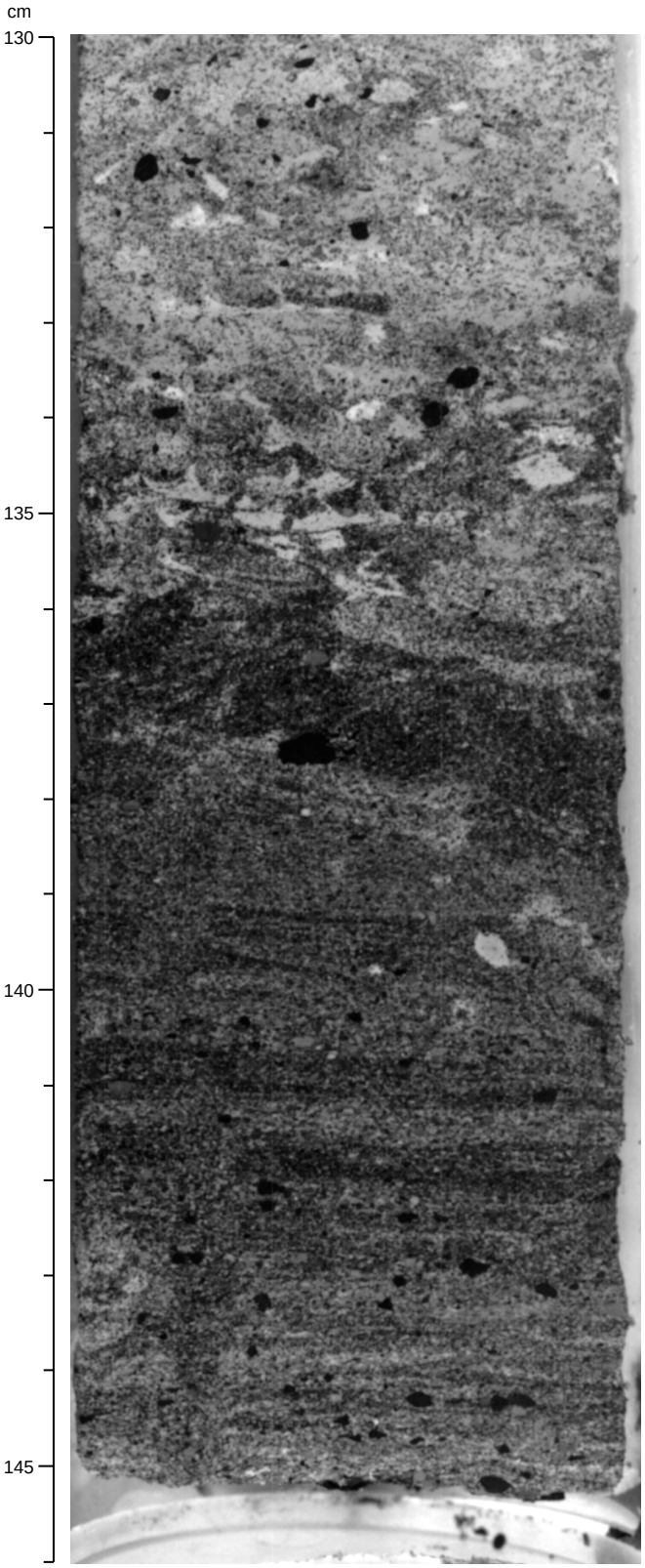

Figure 16. Interval 171B-1050C-20R-2, 130–146 cm. Laminated nannofossil siltstone with iron oxide of lithologic Unit V has rare, somewhat altered volcanic glass fragments. The salt-and-pepper appearance arises from black pyrite lining and/or filling foraminifers. Granule-sized clay clasts are distributed throughout. The remains of cross-lamination appear at 136–137 cm. The upper part of this bed is intensively bioturbated.

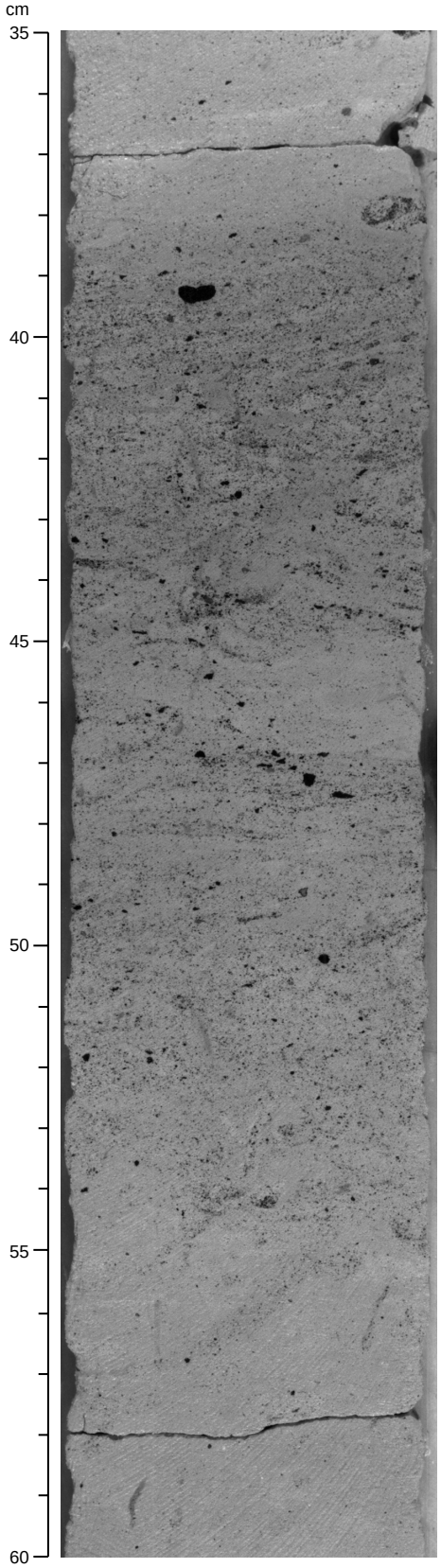

Figure 17. Interval 171B-1050C-20R-2, 35–60 cm. The enrichment of clay clasts in the Coniacian foraminifer nannofossil chalk of lithologic Unit V over relatively narrow intervals suggests that near this level, high-energy processes deposited sand and pebble-sized grains, which subsequently bioturbated into the underlying sediment.

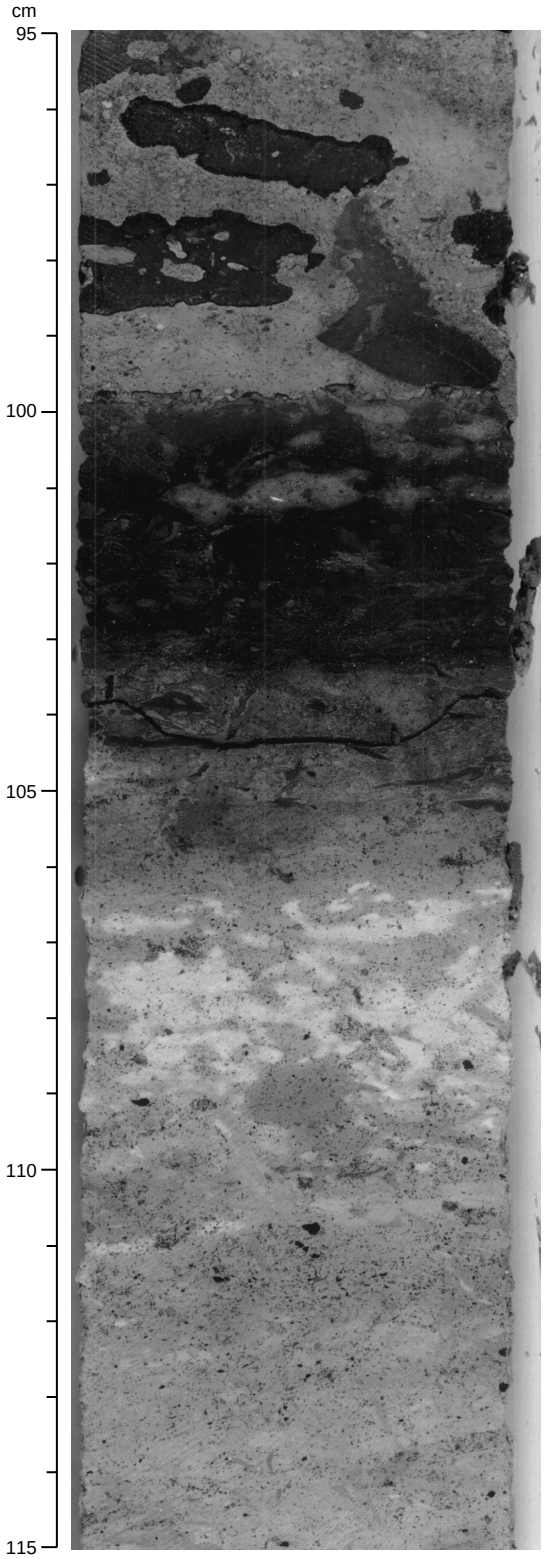

Figure 18. Interval 171B-1050C-20R-1, 95–115 cm. White burrows overlying Coniacian chalk from 107 to 110 cm contain nannofossils that indicate a Santonian age, all of lithologic Unit V. These burrows represent the entire recovery of Santonian sediment during Leg 171B. At 100 cm is a bored hardground with a submillimeter-thick mineral coating. Large clasts of phosphate/iron hardground float in upper Campanian sediment from 96 to 100 cm.

sediment above and below the phosphate/Fe hardground differs in age by 5 m.y. (see "Biostratigraphy" section, this chapter).

Unit VI

Description: Nannofossil chalk or limestone with variable amounts of clay and claystone with variable amounts of nannofossils
Interval: 1050C-21R-1, 77 cm, to 31R-CC, 27 cm
Depth: 501.0–606.0 mbsf, Hole 1050C
Thickness: 104.4 m, Hole 1050C
Age: late Cenomanian to late Albian

Lithologic Unit VI includes hemipelagic sediment with the amount of terrigenous components increasing downhole. The color changes from light greenish gray tones to almost black at the bottom of Hole 1050C. The top of Unit VI is placed at the last downhole occurrence of hardgrounds. The bottom of the unit was not reached, as the hole was terminated for time constraints. This unit comprises light to medium greenish gray nannofossil chalk or limestone with variable amounts of clay in lithologic Subunit VIA, and dark to very dark claystone with variable amounts of nannofossils, including some black shale intervals, in Subunit VIB. Soft-sediment deformation with convolute bedding and, possibly, sediment-creep folding is common throughout Subunit VIA (Fig. 20). In addition, the sediment is cut by numerous faults that range in orientation from subvertical (Fig. 21) to subhorizontal (Fig. 22). Most subvertical faults are slickensided, whereas many subhorizontal faults display millimeter-scale clay seams, and it is difficult to tell some of the latter from drilling-induced core fractures that were sealed with slurry. Slickensided, unsealed faults are much more common in Subunit VIA than they are in Subunit VIB, which may explain the variable, sometimes poor, recovery in Subunit VIB.

Subunit VIA

Description: Nannofossil chalk or limestone with variable amounts of clay and claystone with variable amounts of nannofossils
Interval: 171B-1050C-21R-2, 0 cm, to 26R-4, 104 cm
Depth: 501.0–553.9 mbsf, Hole 1050C
Thickness: 53.0 m, Hole 1050C
Age: late to early Cenomanian

The dominant lithology in Subunit VIA is variably indurated calcareous nannofossil-rich chalk and limestone with fluctuating, but generally downhole-increasing, amounts of clay and silt. The upper boundary of Subunit VIA is defined at the top of a 15-cm interval of reddened foraminifer nannofossil chalk in Section 171B-1050C-21R-1, 77–85 cm (~501 mbsf), that is capped by a hardground. Sediment below that boundary is characterized by colors less vivid than the varicolored sediments in Unit V and by its mixed clayey and pelagic grain composition. The base of Subunit VIA is placed in Section 171B-1050C-26R-4, 104 cm (553.94 mbsf), with the first downhole occurrence of gray to black nannofossil claystone (without the greenish tinge) that is characteristic of most sediment in Subunit VIA (Fig. 23). The color varies gradually from light to medium greenish gray, and there is a tendency toward darker colors downhole. A remarkable exception to these pale colors occurs toward the base of Subunit VIA in Sections 171B-1050C-26R-2 through 26R-4, where brownish, reddish, and yellowish colors occur. The red, pink, and white sediments of this interval are completely burrow mottled (Fig. 24), whereas lamination is preserved in the intervening greenish layers. Sediment composition in this interval is not significantly different from the overlying nannofossil claystone and clayey nannofossil chalk, except for the presence of common iron oxide grains in the red intervals. Bioturbation is mostly intense but sporadically interrupted in Subunit VIA, and lamination is preserved. A longer interval with reduced bioturbation and faint, wispy laminae occurs in Core 171B-1050C-24R.

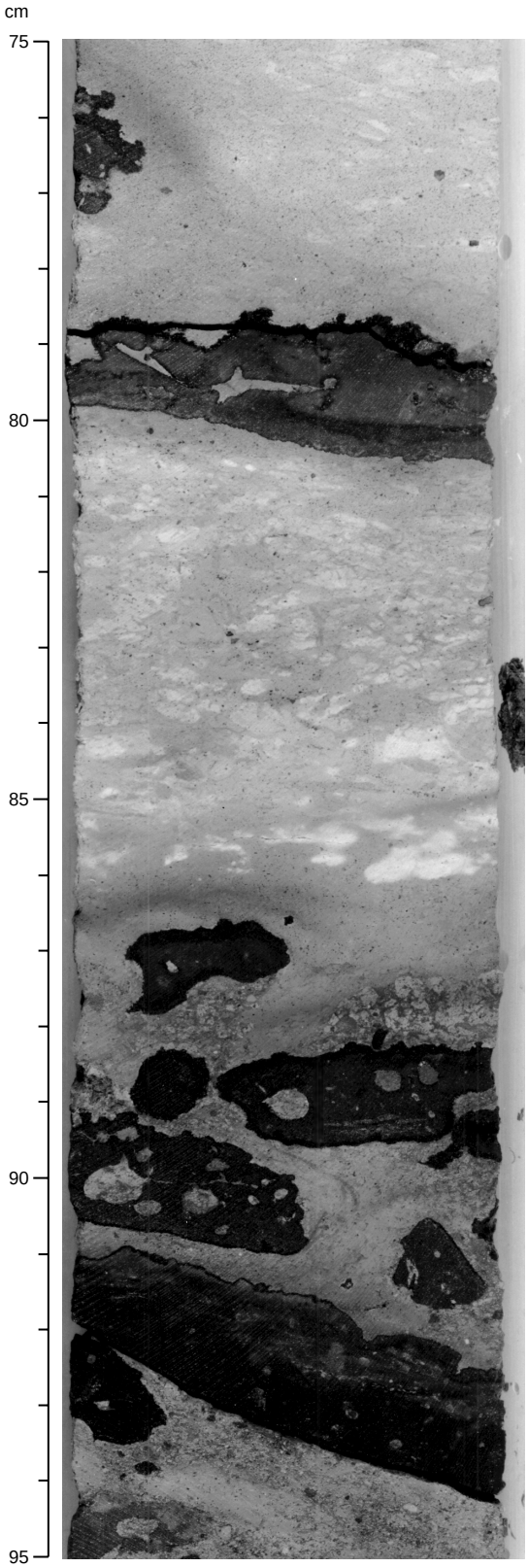

Figure 19. Interval 171B-1050C-20R-1, 75–95 cm. A thin bed of chalk with white burrows separates an interval of pieces of hardground probably from an in situ hardground at 79–80 cm, the top of lithologic Unit V. The borings are filled with red chalk similar in color and composition to the matrix from 87–95 cm.

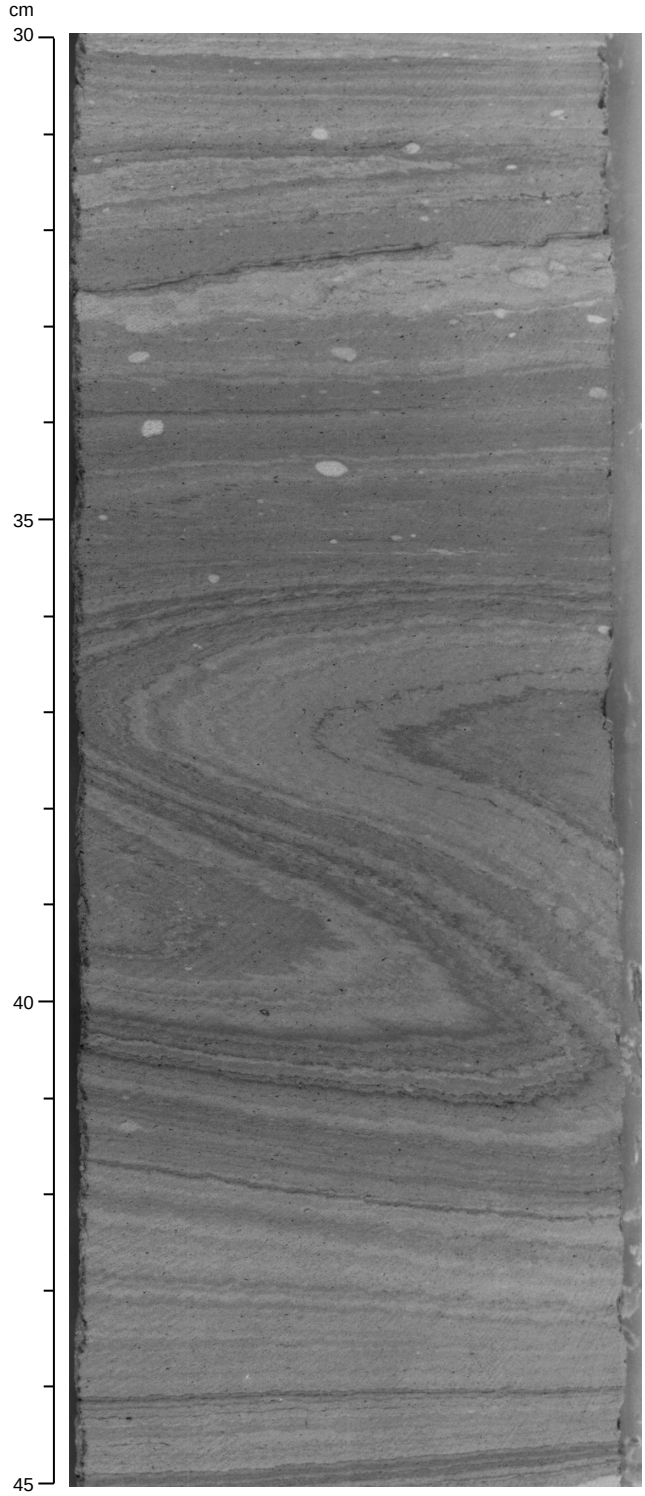

Figure 20. Interval 171B-1050C-23R-2, 30–45 cm. Slump fold with parasitic folds and microfaults along the bent laminae of alternating clayey nannofossil chalk and nannofossil chalk with clay of lithologic Subunit VIA.

Subunit VIB

Description: Claystone with variable amounts of nannofossils and foraminifers and silty claystone with organic debris and feldspar
Interval: 171B-1050C-26R-4, 104 cm, to 31R-CC, 27 cm
Depth: 553.9 to 606.0 mbsf, Hole 1050C
Thickness: 51.5 m, Hole 1050C
Age: late Albian to early Cenomanian

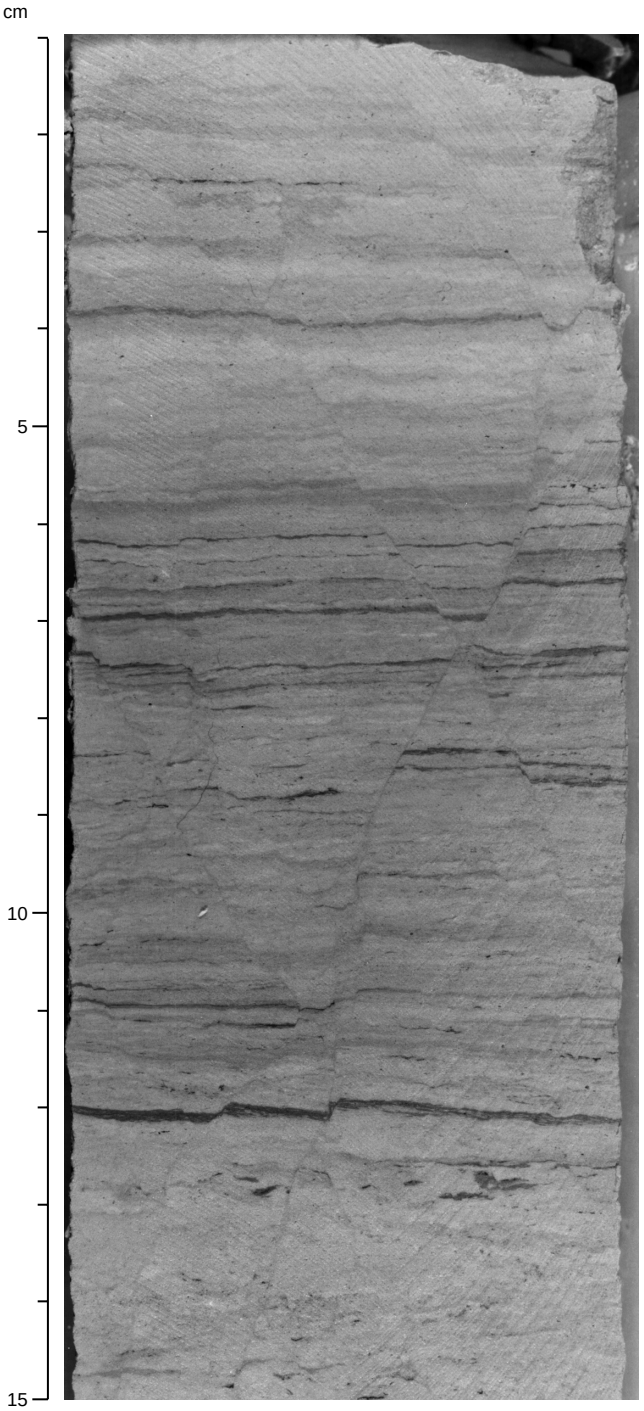

Figure 21. Interval 171B-1050C-23R-2, 1–15 cm. Set of conjugate faults in limestone with clay of lithologic Subunit VIA. Faults of this type were usually observed with open, slickensided surfaces.

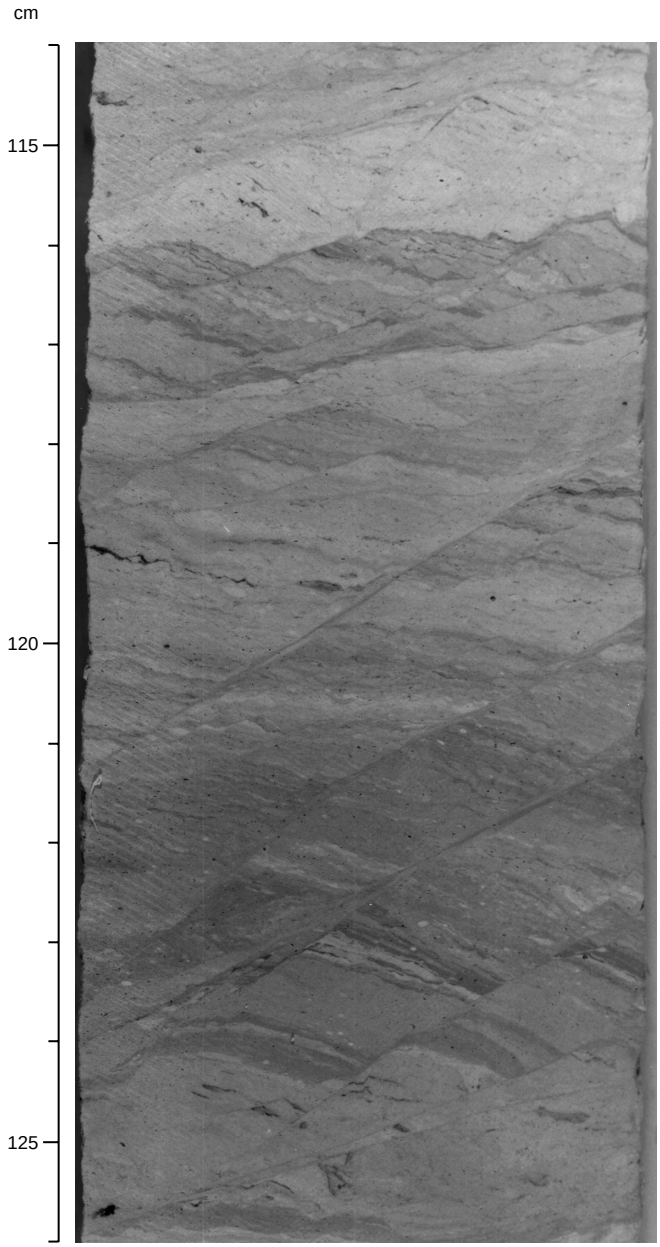

Figure 22. Interval 171B-1050C-23R-4, 114–126 cm. Set of subparallel faults with clay seams on their surfaces from lithologic Subunit VIA. These faults may have formed when the sediment was already stiff as a result of the shear exerted by an overlying slump deposit, such as the one that occurs in Section 23R-3 of this core.

Subunit VIB is a 51-m-thick upper Albian to lowermost Cenomanian sequence of olive-gray claystone alternating with laminated dark claystones (referred to as "black shale"; see "Lithostratigraphy" section, "Site 1052" chapter, this volume). The claystones contain variable amounts of pelagic calcareous microfossils, neritic shell debris, and siliciclastic components (mainly quartz, feldspar, and mica). Laminated black shales are rich in pyrite and contain clay with varying amounts of calcareous nannofossils, silt-sized quartz and feldspar, fish remains, and organic debris. Light gray calcareous chalks with calcispheres occur as a minor lithology in Core 171B-1050C-29R (Fig. 25). The color varies from light olive gray in lightly laminated, nannofossil-rich intervals to dark olive gray in the black shales. Drilling disturbance is slight to moderate, and recovery was high. The upper boundary of lithologic Subunit VIB is defined by the first downhole occurrence of gray to black nannofossil claystone in a severely slumped interval in Section 171B-1050C-26R-4, 104 cm (553.94 mbsf; Fig. 23). The lower boundary was not recovered. Quartz, feldspar, mica, and heavy minerals, such as tourmaline and apatite, occur throughout. Bioturbation is slight to strong throughout Subunit VIB (e.g., *Chondrites* and *Planolites*). There is no bioturbation in the laminated intervals, except for rare *Chondrites.* Well-pre-

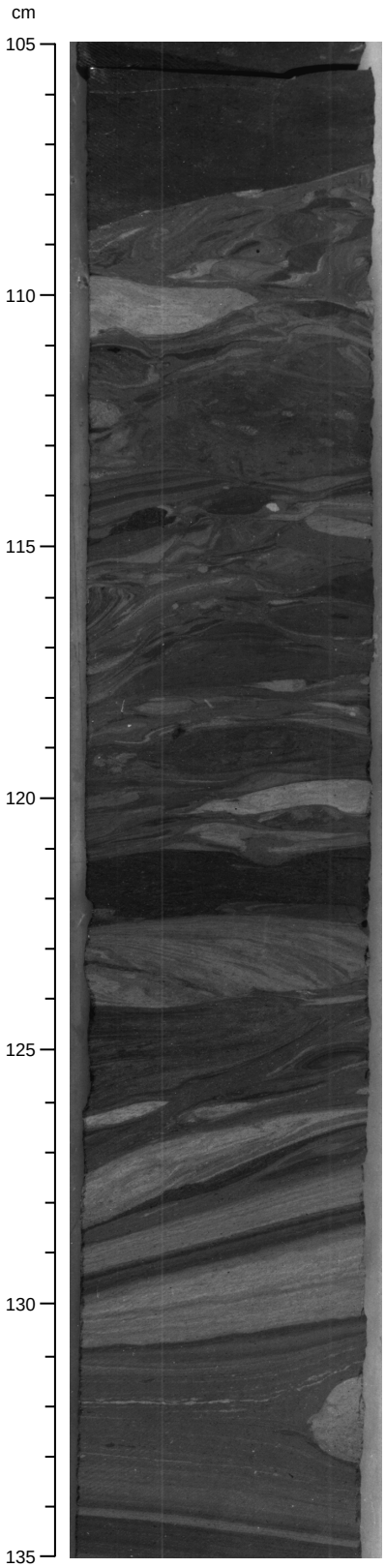

Figure 23. Interval 171B-1050C-26R-4, 105–135 cm. Examples of soft-sediment deformation and mass movement from the top of lithologic Subunit VIB. Below 121 cm, the sediment is sheared but not completely disrupted and possibly forms part of a slump deposit. The interval from 107 to 121 cm contains deformed mud clasts engulfed in a matrix. This interval probably formed as part of a debris-flow deposit.

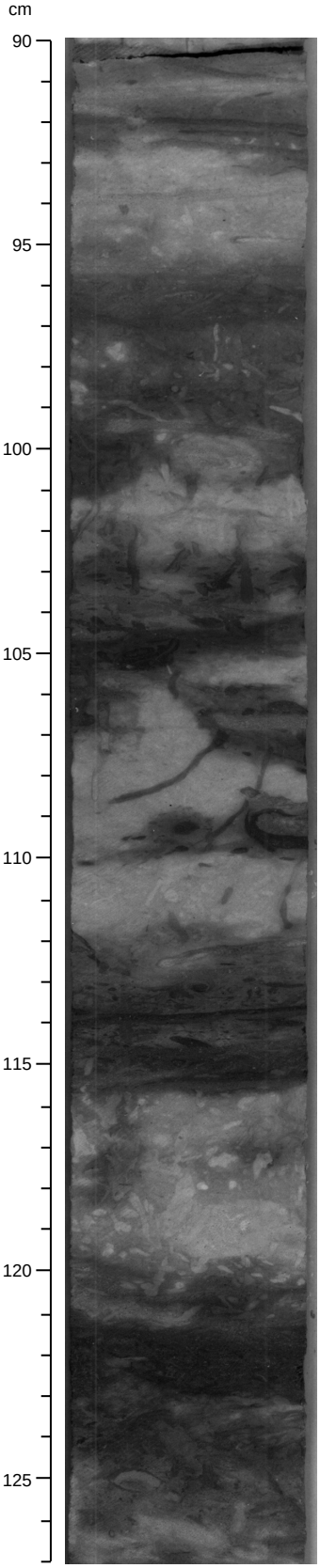

Figure 24. Interval 171B-1050C-26R-3, 90–127 cm. Alternation of reddish and light greenish gray burrow-mottled clayey nannofossil chalk with foraminifers and Fe oxide in lithologic Subunit VIB.

served ammonites and bivalves (pyritized or aragonitic) are present in Cores 171B-1050C-29R through 31R.

Slumping structures (Fig. 23), convolute bedding (Fig. 20), mud-pebble layers, current-induced lamination, and cross-lamination (Fig. 26) are common throughout lithologic Subunit VIB (Fig. 27). However, lamination that is probably related not only to current activity was observed in Section 171B-1050C-26R-4, 104 cm, through Core 31R and is increasingly well defined downhole (Cores 171B-1050C-29R through 31R). Section 171B-1050C-29R-1 reveals the finest laminated black shale interval, consisting of quartz- and feldspar-rich silty claystone (Fig. 27; 30–40 cm).

Discussion

In comparison with Lower Cretaceous sediment recovered from lithologic Subunit VB in Hole 1052E, sediment from lithologic Subunit VIB in Hole 1050C lacks coarse-grained intervals of siliciclastic and carbonate material. Here, very fine-grained, faintly to distinctly laminated intervals dominate the sediment. This difference could be explained either by the greater distance between Site 1050 and the platform or by some heterogeneity in source regions. Another striking phenomenon of the upper Albian sediments recovered in Hole 1050C is the predominance of structures indicative of mass movement (slump folds and microfaulting). Significant relief during the late Albian is implied, which is consistent with the position of Site 1050 at the lower part of the Blake Nose. The more distal position of Site 1050 is also supported by the occurrence of thin layers of light-colored calcareous chalk with calcispheres.

Dark laminated sediment (black shale) in Subunit VIB contains common detrital material including terrestrial organic debris. Sedimentation probably took place within a dysoxic zone of the water column, as indicated by the lack of macrobenthic fossils such as bivalves or most trace fossils, except for the occurrence of *Chondrites* within the black shales (compare to "Lithostratigraphy" section, "Site 1052" chapter, this volume). The rare occurrence of *Chondrites* can be interpreted as short oxygenation events within anoxic periods.

Lithologic Subunit VIA was deposited in a hemipelagic environment with a fine-grained terrigenous input comprising quartz and feldspar silt, clay, mica flakes, and heavy minerals. The abundance of slump structures and evidence for multiple reworking of sediment testifies to an unstable depositional site upslope of Site 1050, such as possibly at Site 1052, where more proximal equivalents of the Subunit VIA sedimentary facies occur.

Some 17.5 m.y. passed between the deposition of upper Cenomanian chalk at the base of lithologic Unit V and upper Campanian chalk at the top of this 10.3-m-thick interval. The reddened hardground at the top of the Cenomanian sediment (Fig. 14) indicates that, beginning with a period of oxidizing seafloor conditions during or after the late Cenomanian, the seafloor at Site 1050 experienced debris flows of chalk and clay-rich sediment, deposition of volcanic ash layers, and probably significant currents that eroded black Albian to Cenomanian sediment and worked it into layers and laminae amidst a background of sparse nannofossil and foraminifer deposition. The foraminifer enrichment of the sediment over this interval is evidence for winnowing by currents. Oxic bottom conditions allowed an active benthic community to work the clay rip-up clasts into the accumulating calcareous matrix. The last vestiges of anoxic conditions at Site 1050 are recorded by thin, millimeter-scale, green laminae of late Turonian age. Oxic conditions with currents affecting winnowing persisted from the late Turonian to the late Campanian, culminating with strong winnowing by bottom currents during the Santonian–Campanian that allowed the formation of a phosphate/iron-rich hardground (Fig. 12). Although these Upper Cretaceous sediments give only a hint of conditions on the Blake Nose for a 17.5-m.y. period, they provide the only evidence for that time period, as equivalent-aged sediment was not recovered elsewhere during Leg 171B.

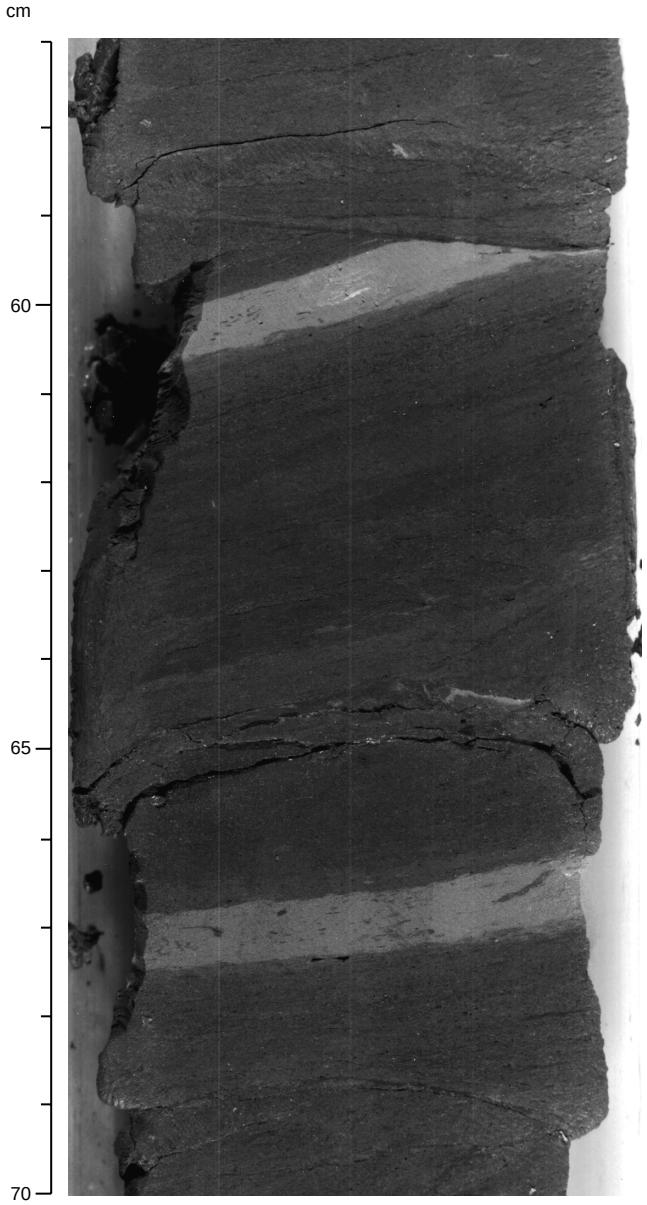

Figure 25. Interval 171B-1050C-29R-2, 57–70 cm. Two layers of light gray calcareous chalk with calcispheres are intercalated with darker claystone with carbonate in lithologic Subunit VIB. The chalk contains few terrigenous components.

Lower Maastrichtian sections similar to those in Unit IV at Site 1050 were recovered at Sites 1049, 1050, and 1052, with slumped intervals at the tops of those sections (see "Site 1049," "Site 1050," and Site 1052" chapters, this volume). Sediments below the slumped intervals are light colored and carbonate rich. Upper Maastrichtian sediments are clay rich and heavily bioturbated above the slumped intervals, yet the sediment color differs significantly at the three sites. This color variation may reflect a circulation change from a uniform

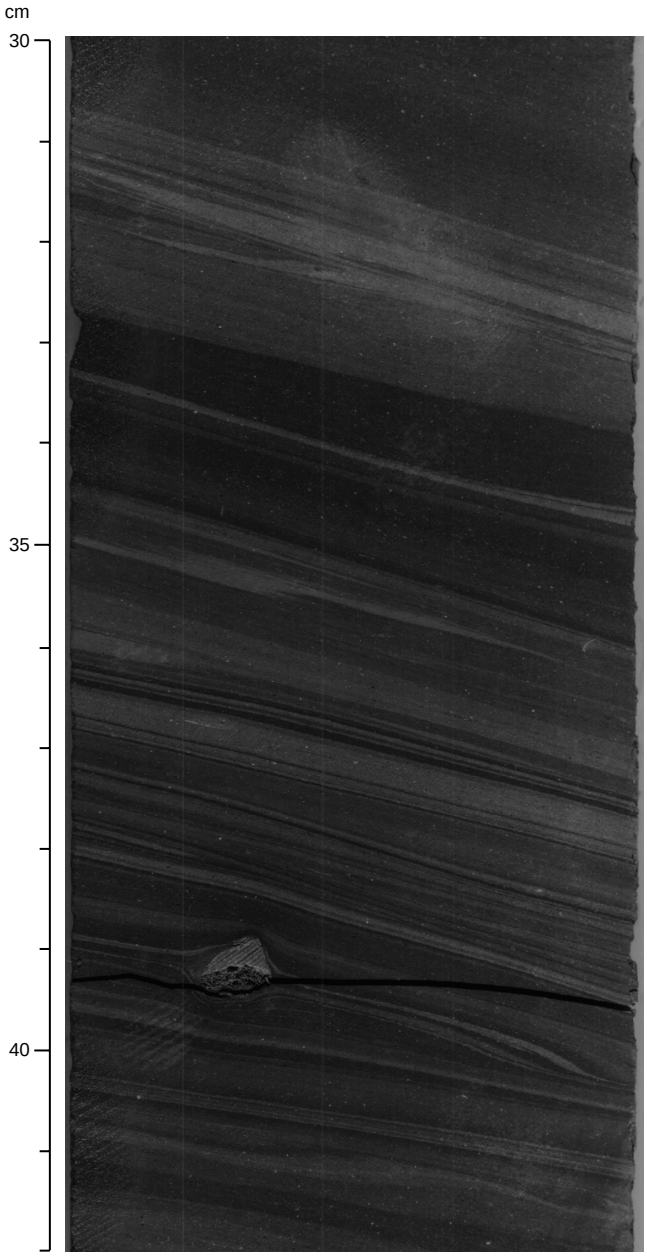

Figure 26. Interval 171B-1050C-27R-2, 30–42 cm. Laminae in this interval of lithologic Subunit VIB are partly truncated or pinch out against one another. This suggests that current activity, rather than in situ changes in oxygenation, is responsible for the lamination. A pyrite nodule at Section 171B-1050C-27R-2, 39 cm, has displaced the sediment around it. Subsequent compaction led to bending of the laminae around the nodule.

early Maastrichtian deep-water mass to a late Maastrichtian depth stratification (see “Lithostratigraphy” section, “Site 1052” chapter, this volume, for discussion of the alternative possibilities).

The K/T boundary at Site 1050 appears to be biostratigraphically complete (see “Biostratigraphy” section, this chapter). Unfortunately, recovery was poor, and the dark gray boundary clay is partly broken up and mixed with drilling-induced slurry. Above and below the clay are nannofossil carbonate claystone and clayey nannofossil chalk, respectively. Fossil preservation in this sediment is good and promises fruitful future study.

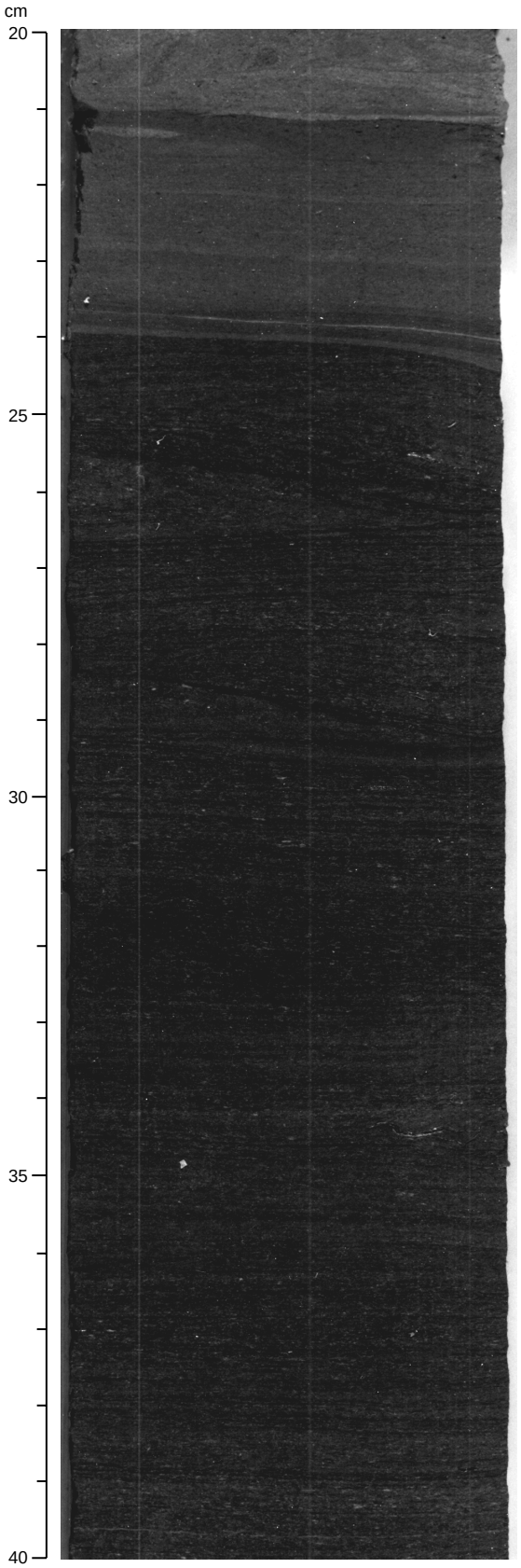

Figure 27. Interval 171B-1050C-29R-1, 20–40 cm. Top of black shale interval of lithologic Subunit VIB. Cross-lamination and/or folding occurs between 24 and 29 cm.

Siliceous biogenic input began during the early Paleocene and persisted during deposition of lithologic Units I through III at Site 1050, but siliceous microfossils (radiolarians, diatoms, and sponge spicules) are particularly abundant throughout lithologic Unit II, in lithologic Subunit ID from 172 to 228 mbsf, and in Subunit IC from 38 to 72 mbsf. Intervals with abundant biogenic opal may reflect periods of increased productivity in the surface waters or enhanced preservation of biogenic silica in the sediment column.

Ash layers occurring in the Eocene section provided excellent tie points between Holes 1050A and 1050B (Fig. 2). In addition, they may also allow us to augment and constrain biostratigraphic and paleomagnetic datums with radiometric model ages, determined from analyses of micas and/or feldspars. The origin and geologic significance of the ash layers, though, is less apparent. Von Rad and Kreuzer (1987) described a middle to lower middle Eocene vitric ash layer of rhyolitic composition at Sites 605 and 613 (Deep Sea Drilling Project [DSDP] Legs 93 and 95) from the continental rise off New Jersey. They proposed that the ash represented a major subaerial eruption of the Bermuda volcano. The ash layer off New Jersey is comparable in scale and composition to those we observed and may have had the same source. The presence of 11 ash layers at Site 1050, as opposed to a single layer at Sites 605 and 613, is not particularly problematic because Site 1050 is both closer to Bermuda and in a logical downwind direction (southeast) for the Northern Hemisphere trade winds belt. We have not attempted to use the number and thicknesses of ash layers as a proxy for the episodicity and/or intensity of volcanism in the source region because (1) local, contemporary weather patterns would have had a strong influence on the delivery of ash to the site; (2) variation in thickness among the ashes is not great; (3) the ashes were smeared by bioturbation; (4) many thin ash layers may have been obscured by bioturbation because rare glass and biotite occurred in many smear slides removed from unrecognized ashes; and (5) the ash layers were usually disturbed by drilling.

Nondeposition or erosion of any sediment has persisted from the late middle Eocene to the present. A Mn oxide sand and nodule layer <1 m thick formed between the late middle Eocene and/or the Pleistocene.

Table 4. Calcareous nannofossil datums for Holes 1050A and 1050B.

Datum	Species	Zone	Age (Ma)	Core, section	Depth (mbsf)	Error depth (mbsf)
				171B-1050A-		
B	*R. umbilicus*	b CP14a	43.7	4X-CC	38.72	48.34
T	*N. fulgens*		43.1	13X-CC	122.49	106.54
B	*C. gigas*	b CP13b	46.1	14X-5	131.08	132.72
B	*N. fulgens*	b CP13a	47.3	15X-1	134.65	136.12
B	*R. inflata*	b CP12b	48.5	15X-CC	141.8	153.37
B	*D. sublodoensis*	b CP12	49.7	17X-CC	157.95	168.92
B	*T. crassus*	b CP11	51.5	21X-3	193.24	194.7
B	*D. lodoensis*	b CP10	52.85	21X-3	193.24	194.7
B	*T. orthostylus*	b CP9b	53.64	22X-6	207.39	208.97
T	*F. tympaniformis*		55.33	26X-1	237.71	228.3
B	*C. eodela*	(b CP8a)	55.5	28X-3	250.92	255.38
B	*D. multiradiatus*	b CP8a	56.2	28X-3	250.92	255.38
B	*D. mohleri*	b CP6	57.5	30X-5	273.17	274.65
B	*S. anarrhopus*		58.4	30X-6	274.65	276.11
B	*H. kleinpelli*	b CP5	58.4	30X-CC	276.11	284.61
B	*T. tympaniformis*	b CP4	59.7	34X-3	298.92	300.08
B	*C. consuetus*		59.7	34X-3	298.92	300.08
B	*F. ulii*		59.9	34X-CC	300.08	314.61
B	*C. bidens*		60.7	34X-CC	300.08	314.61
B	*S. primus*		60.6	35X-CC	314.61	319.72
B	*E. macellus*	b CP3	62.2	36X-CC	319.72	Bottom
				171B-1050B-		
B	*N. fulgens*		43.1	8H-CC	73.86	64.11
B	*R. umbilicus*	b CP14a	43.7	9H-CC	83.37	92.08
T	*C. gigas*	t CP13b	44.5	13X-CC	118.45	109.87
B	*C. gigas*	b CP13b	46.1	14X-CC	127.41	137.27
B	*R. inflata*	b CP12b	48.5	17X-6	155.6	156.17
B	*D. sublodoensis*	b CP12a	49.7	17X-6	155.6	156.17
B	*D. lodoensis*	b CP10	52.85	22X-CC	195.48	205.66
B	*T. orthostylus*	b CP9b	53.64	24X-CC	215.25	225.27
T	*T. bramlettei*		53.89	25X-CC	225.27	215.64
B	*T. contortus*		54.37	25X-CC	225.38	231.67
B	*R. bramlettei*	b CP9a	55	26X-CC	225.25	231.67

Notes: Bases of age and biozonal datums are represented by B and b; tops of age and biozonal datums are represented by T and t. Error depths refer to depth to next sample studied above or below a datum level. Parentheses around zones refer to species used to approximate zonal boundaries. These data reflect post-cruise modifications and are, thus, more up to date than data presented in the range charts and in the biostratigraphy and sedimentation rate figures (this chapter).

BIOSTRATIGRAPHY

Calcareous Nannofossils

Hole 1050A was sampled and examined for calcareous nannofossil content to establish the biostratigraphic framework. Sample spacing was approximately one sample per section (every 1.5 m) and included the core catchers. Critical boundaries were sampled at closer intervals. A list of chronostratigraphically significant biohorizons is presented in Table 4. Mainly core-catcher material was examined from Hole 1050B. Nannofossil biostratigraphy for the two holes is presented in Figure 28.

The calcareous nannofossil biostratigraphy in Hole 1050C is based on examination of core-catcher material. Additional smear-slide samples were examined to determine placement of critical boundaries or to refine the biostratigraphy (Fig. 29). Calcareous nannofossil datums and their depths are listed in Table 5. Calcareous nannofossil preservation ranged from moderate to well preserved, with the exception of the Paleocene/Eocene boundary interval, where preservation was poor.

Preservation of calcareous nannofossil assemblages is moderate in the lower Paleocene, good throughout the Maastrichtian and Campanian, and moderate to good from the Coniacian to the Albian. Soft-sediment deformation and slumping of this material occurred occasionally in the Paleocene and with greater frequency during the Maastrichtian and the late Albian through mid-Cenomanian. However, the lack of significant reworking either of calcareous nannofossils or planktonic foraminifers argue that large-scale sediment mixing did not occur during deformation.

The basal upper middle Eocene Subzone CP14b is represented by only one sample in Hole 1050A (Sample 171B-1050A-1H-1, 0–1 cm), based on the presence of *Dictyococcites bisecta* and the absence of *Chiasmolithus solitus*. One sample farther downcore (Sample 171B-1050A-1H-1, 57–58 cm) is placed in middle to basal Subzone CP14a, based on the presence of *Reticulofenestra umbilica* and the absence of *Cribrocentrum reticulatum.*

The middle Eocene Subzone CP14a is represented by an interval ranging from Sample 171B-1050A-1H-1, 57–58 cm, through Section 4H-CC. Reworking of older Eocene material has occurred, making the placement of the basal boundary for this subzone questionable. In addition, we disagree with Berggren et al. (1995) in placing the first occurrence (FO) of *Reticulofenestra umbilica* (the marker species for this subzone) at 43.7 Ma and instead follow Wei and Wise (1989) in placing the boundary in the upper part of magnetozone Chron 20n at 42.7 Ma. Subzone CP14a rests conformably on Subzone CP13c, based on the absence of both *R. umbilica* and *Chiasmolithus gigas.* The marker species for Subzone CP13b, *C. gigas*, occurs from Section 171B-1050A-10H-CC through Sample 171B-1050A-14X-5, 68–72 cm. Subzone CP13b represents only ~2 m.y. of deposition; however, increased sedimentation rates throughout this section suggest that this subzone is somewhat expanded (Fig. 30). Additionally, the sporadic occurrence of *C. gigas* in the upper part of its range at this site strongly suggests that it has been reworked. Therefore, age determinations based on planktonic foraminifer datums for this interval provide a more accurate biostratigraphic interpretation.

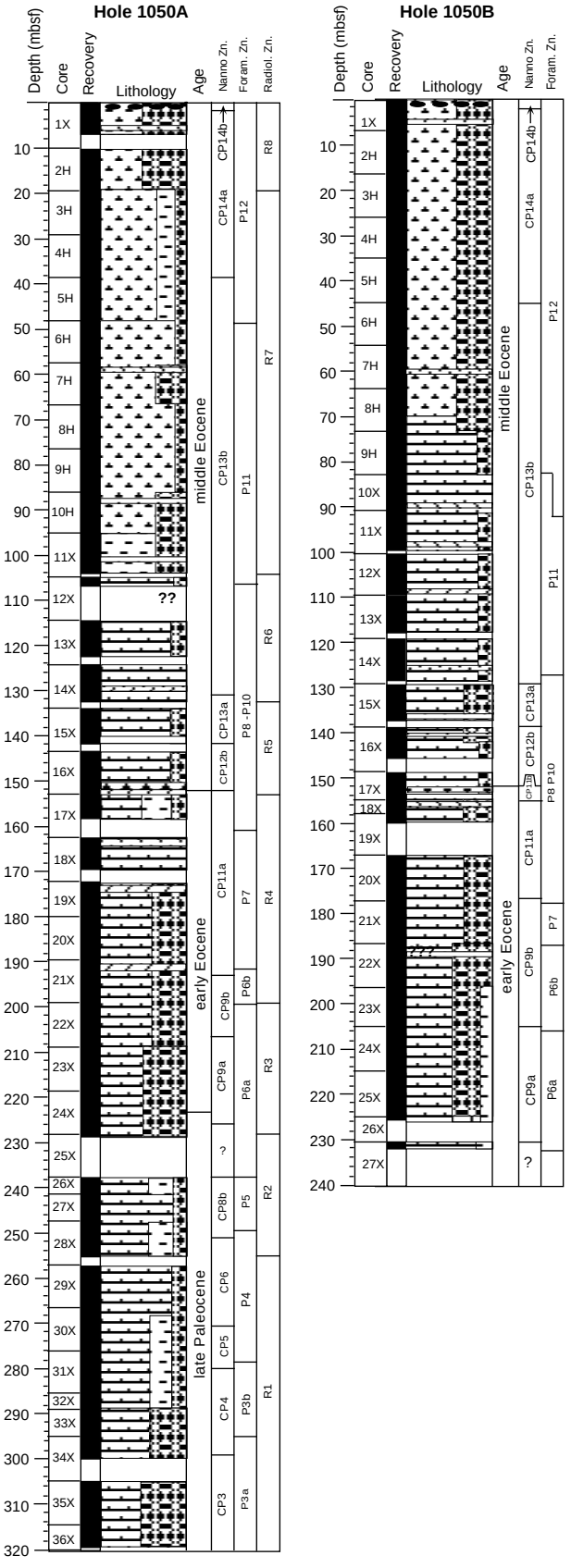

Figure 28. Biostratigraphic summary for Site 1050. See Figure 1, "Site 1049" chapter (this volume) for an explanation of lithologic symbols. Refer to the nannofossil and foraminifer datum tables (this chapter) for biostratigraphic data that reflect post-cruise additions and modifications to range data.

Subzone CP13a is very thin in this hole and is basically confined to the interval between core-catcher Samples 171B-1050A-14X-CC and 15X-CC. It conformably overlies the *Rhabdosphaera inflata* Subzone (CP12b), which occurs in the interval ranging from Sections 171B-1050A-15X-CC through 16X-6. Despite trace amounts of older reworked Eocene material that is present throughout this interval, correlation of the nannofossil and planktonic foraminifer biozones is good (Fig. 28).

The lower Eocene at this site is only partially complete. Zone CP10 and Subzone CP12a are missing, whereas the lower portion of Zone CP11 and a largely complete section of Zone CP9 are present. This is best represented in Figures 28 and 30. The lower section of Zone CP11 is overlain unconformably by Subzone CP12b and ranges from Sections 171B-1050A-16X-CC through 21X-3. Only the lower portion of Zone CP11 is represented based on the co-occurrence of *Tribrachiatus orthostylus* and *Toweius crassus* throughout this interval. Zone CP11 rests unconformably on Subzone CP9b, which occurs in Sections 171B-1050A-21X-4 through 22X-6. The basal Eocene, which was found in Sections 171B-1050A-22X-CC through 24X-7, is nearly complete. Both *Rhomboaster contortus* (FO in middle upper Subzone CP9a; last occurrence [LO] at top of Subzone CP9a) and *Tribrachiatus digitalis* (overlaps briefly with *R. contortus* near middle of Subzone CP9a [Aubry, 1996]) occur in Section 171B-1050A-22X-CC. *Rhomboaster contortus* is absent from Sections 171B-1050A-23X-7 through 24X-7, suggesting that these samples belong to the earliest part of Subzone CP9a or older. Comparison of the calcareous nannofossil floral assemblage to the planktonic foraminifer assemblage suggests that a nearly complete Paleocene/Eocene boundary section is present in Hole 1050A. Preservation decreases downcore throughout Subzone CP9a until species identification in Sample 171B-1050A-24X-CC becomes impossible. Core-catcher Sample 171B-1050A-25X-CC contains a latest Paleocene Subzone CP8b assemblage.

A nearly complete upper Paleocene sequence was recovered at this site, spanning Zone CP3 in Sample 171B-1050A-36X-CC to Subzone CP8b in Sample 171B-1050A-25X-CC. Closely spaced sampling intervals in Core 28X indicate that upper Paleocene Subzone CP8a and Zone CP7 were not recovered at this site. Correlation with planktonic foraminifer biozones is very good, with minor differences being largely a result of higher resolution sampling for calcareous nannofossils. Magnetostratigraphic evidence suggests that the upper Paleocene continues downward into Core 171B-1050C-2R, where the top of Chron 20N marks the Danian/Selandian boundary (see "Paleomagnetism" section, this chapter).

The lower Danian Zone CP2 appears to be relatively thick at this site, compared with the corresponding section at Site 1052. This apparent thickness may be partially because of the difficulty in placing the Zone CP2/CP3 boundary. The zonal boundary marker *Ellipsolithus macellus* is sporadic near its FO. As a result, placement of this boundary may change with further examination.

A biostratigraphically complete K/T boundary section was recovered in Sample 171B-1050C-10R-2, 35–37 cm. Calcareous nannofossil assemblages from Samples 171B-1050C-10R-1, 95 cm, through 10R-1, 126 cm, are indicative of the lower Danian (Subzone CP1a), based on the presence of *Neobiscutum parvulum, N. romenii*, abundant *Thoracosphaera*, and the absence of the large morphotype of *Cruciplacolithus primus*. Preservation throughout this interval is moderate, and abundances decrease downcore toward the boundary event. Sample 171B-1050C-10R-2, 33 cm, contains rare *Thoracosphaera* and only occasional *C. primus* (small morphotype). The absence of *N. parvulum* strongly suggests that this sample is representative of an earliest post-event flora. Sediment immediately below the boundary horizon at Sample 171B-1050C-10R-2, 38 cm, contains an abundant, well-preserved flora indicative of late Maastrichtian

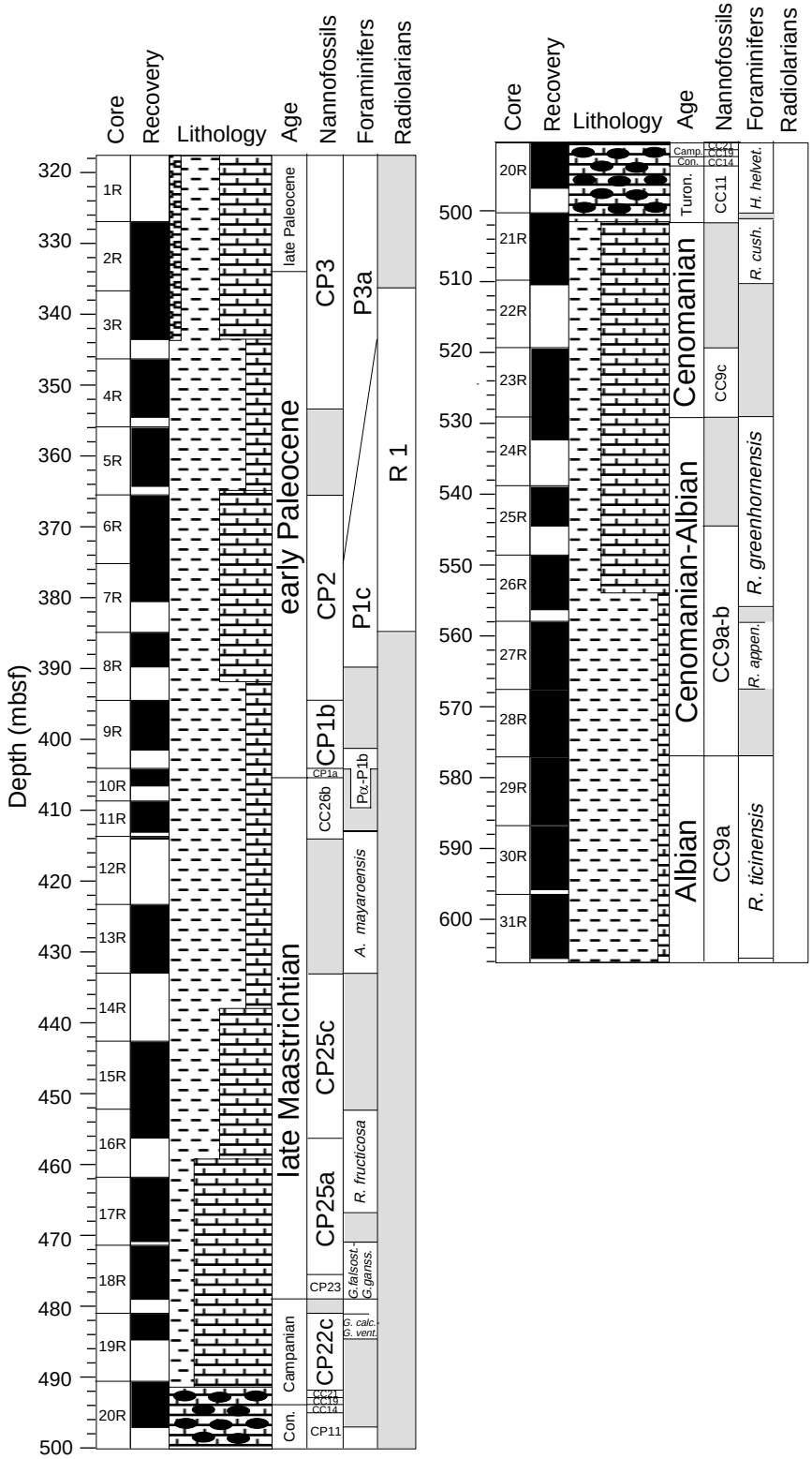

Figure 29. Age assignments for Hole 1050C.

Subzone CC26b, based on the presence of *Micula prinsii*, *M. murus*, and *Ceratolithoides kamptneri*.

Although the late Maastrichtian is well represented at this site, calcareous nannofossil assemblages differ significantly from those at Sites 1049 and 1052. Transitional forms between *Micula murus* and *M. prinsii* make identification of the CC26a/CC26b subzonal boundary difficult. Differentiation of the CC25/CC26 boundary also is difficult because of the absence of *Nephrolithus frequens* and the paucity of *Ceratolithoides kamptneri*, a species used as a proxy marker in the absence of *N. frequens. Ceratolithoides kamptneri* is common at both Sites 1052 and 1049, but it is rare at Site 1050. The apparent absence of *C. kamptnerii* and the presence of *M. murus* in Samples

Table 5. Calcareous nannofossil datums for Hole 1050C.

Datum	Species	Zone	Age (Ma)	Core, section, interval (cm)	Error depth (mbsf)
				171B-1050C-	
B	*E. macellus*	b CP3	62.2	4R-6, 61-63	354.40-364.10
B	*C. danicus*	b CP2	63.8	8R-CC	389.70-401.40
B	*C. tenuis*	b CP1b	64.5	9R-CC	401.30-401.40
B	*C. primus*		64.8	10R-2, 32-33	401.30-401.40
T	*E. turriseiffellii*	t Cretaceous	65.0	10R-2, 37	405.60-406.40
B	*M. prinsii*	b CC26b	66.0	12R-1, 18-20	413.90-433.20
B	*M. murus*	b CC25c	68.5	15R-CC	452.50-470.70
T	*R. levis*		69.4	18R-5, 77-78	475.20-478.20
T	*T. phacelosus*	t CC23	71.6	18R-5, 77-78	475.20-478.20
T	*A. parcus*	t CC23a	74.6	18R-CC	478.20-478.90
T	*E. eximius*	t CC22	75.0	19R-1, 126-127	478.90-482.30
B	*Q. sissinghii*	b CC22	77.1	20R-1, 70-71	491.30-491.40
B	*C. aculeus*	b CC20	78.5	20R-1, 70-71	491.30-491.40
B	*A. parcus parcus*	b CC18	82.5	20R-1, 84-85	491.40-493.10
B	*A. parcus constrictus*	t CC18a	83.5	20R-1, 84-85	491.40-493.10
T	*L. septinarius*		84.9	20R-2, 103-104	491.40-493.10
B	*M. decussata*	b CC14	87.2	20R-3, 13-14	493.70-495.40
B	*E. eximius*		91.0	20R-3, 13-14	493.10-493.70
B	*Q. gartnerii*	b CC11	93.5	21R-1, 30-31	500.50-500.70
T	*C. kennedyi*		93.9	21R-1, 30-31	500.50-500.70
B	*C. kennedyi*	b CC9c	97.4	23R-CC	529.30-544.10
T	*R. irregularis*	t CC9a	99.0	29R-CC	577.40-586.70

Notes: Bases of age and biozonal datums are represented by B and b; tops of age and biozonal datums are represented by T and t. Error depths refer to depth to next sample studied above or below a datum level. These data reflect post-cruise modifications and are, thus, more up to date than data presented in the range charts and in the biostratigraphy and sedimentation rate figures (this chapter).

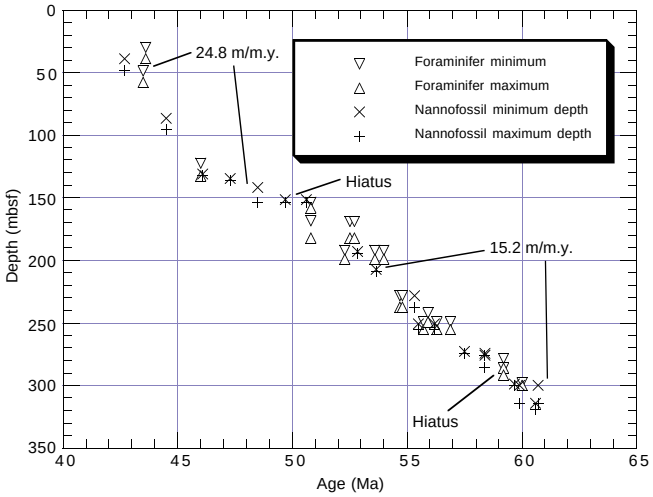

Figure 30. Sediment accumulation rate for Hole 1050A based on the calcareous nannoplankton and planktonic foraminifer datums listed in Tables 4 and 6, respectively.

171B-1050C-18R-3, 80–81 cm, through 13R-CC place this material in Subzone CC25c. Further examination of this sequence may result in a different placement of the subzonal boundary.

Well-preserved and abundant calcareous nannofossil assemblages of late Campanian age occur in a thin interval (~13 m; Samples 171B-1050C-18R-5, 77–78 cm, through 20R-1, 84 cm) that nevertheless contains at least four calcareous nannofossil zones representing 6 m.y. Sample 171B-1050C-18R-5, 77–78 cm, occurs within Zone CC23 and is latest Campanian in age. Placement within this zone is based on the presence of both *Tranolithus phacelosus* and *Reinhardtites levis*. Sporadic occurrences of *Aspidolithus parcus constrictus* are considered to be reworked. Calcareous nannofossil Zone CC22 is identified from Samples 171B-1050C-19R-1, 126–127 cm, and 19R-2, 141–142 cm, based on the occurrence of *Reinhardtites levis* with *R. anthophorous* and common *Eiffelithus eximius*. This thin interval is underlain disconformably by sediments of Zone CC21, defined by the presence of rare *Quadrum sissinghii* and the absence of *Q. trifidum*. Species from the genus *Quadrum* are typically thought to be representative of warmer water temperatures, which makes their scarcity in this assemblage surprising.

The sequence of biostratigraphic events recorded in interval 171B-1050C-20R-1, 30–31 cm, is impressive. Sample 171B-1050C-20R-1, 84 cm, is mid-Campanian in age (Zone CC19), based on the absence of both *Marthasterites furcatus* and *Ceratolithoides aculeus*, the latter of which is recorded consistently throughout the late Campanian and Maastrichtian of this hole. This zone is underlain disconformably by upper Coniacian Zone CC14 in Samples 171B-1050C-20R-2, 103–104 cm, and 20R-3, 13–14 cm. The disconformity is marked by a complex of bioeroded black mudstone clasts with phosphate and represents a hiatus spanning at least 5 m.y. Zone CC14, in turn, disconformably overlies mid-Turonian (Zone CC11) varicolored chalk. *Quadrum gartneri*, the marker species for Zone CC11, is common in Samples 171B-1050C-20R-4, 32–33 cm, through 21R-1, 30–31 cm, and common *Q. intermedium* is dominated by forms with five rays. These two facts suggest that this interval is in the upper part of Zone CC11. Minor reworking of Cenomanian nannofossils into the Turonian is evident. *Corollithion kennedyi*, a species whose range defines Subzones CC9c through CC10b and should not overlap with *Q. gartneri*, is present in Sample 171B-1050C-21R-1, 30–31 cm. Placement of this sample in the planktonic foraminifer *Helvetoglobotruncana helvetica* Zone corroborates a mid-Turonian age.

This incredible package of sediments consists of a series of spectacular hardgrounds separated by thin layers of sedimentary oozes. Currently, sediments dated as Turonian, Coniacian, possible Santonian, and Campanian are all present in this complex of <10-m thickness. However, further detailed analysis of the material between the hardgrounds could reveal that more time is represented in this condensed section than is currently recorded.

The middle Turonian lies directly on sediments of middle Cenomanian age, suggesting a hiatus of at least 2 m.y. The upper Cenomanian Zone CC10 (as well as the partly correlative *Whiteinella archaeocretacea* foraminifer zone) is missing. The sharp nature of the contact between adjacent drilling biscuits suggests that any transitional hardground or disconformity surface was removed by drilling. The lower and lower middle Cenomanian (Subzones CC9b and CC9c) is present in Samples 171B-1050C-21R-7, 0–1 cm, through 26R-CC. *Corollithion kennedyi*, whose presence marks the base of Subzone CC9c, is present from Samples 171B-1050C-23R-CC to 21R-7, 0–1 cm.

Coring at this site reached the upper Albian (Zone CC9a) in Samples 171B-1050C-27R-CC through 31R-CC. Identification of this zone was difficult because of the paucity of both *Hayesites albiensis* and *Rucinolithus irregularis*. As at Site 1052, these species were rare, and their LOs were significantly below the supposedly correlative FO of *Rotalipora greenhornensis*. Sediments throughout this interval consisted of alternating black shales and laminated claystones. Soft-sediment deformation was prevalent, although little evidence for reworking can be seen from the calcareous nannofossil assemblages. Preservation was moderate to good, and abundances of specimens were typically common to abundant.

Planktonic Foraminifers

Planktonic foraminifer biostratigraphy for Holes 1050A and 1050B was based almost entirely on core-catcher samples. Zonal assignments are summarized in Figure 28 and Table 6, and distribution charts for the two holes are presented in Tables 7 and 8. Planktonic foraminifer Subzone P3a through Zone P12 (upper Paleocene–middle Eocene) were identified in Hole 1050A, and Subzone P6b through Zone P12 (lower–middle Eocene) were identified in Hole

1050B. Planktonic foraminifers are abundant in most middle Eocene samples and are rare to abundant in upper Paleocene and lower Eocene samples primarily because of variations in dilution by radiolarians. Preservation is very good in the middle Eocene and moderate to good in the lower Eocene and Paleocene. Reworking of several Maastrichtian planktonic foraminifer species was observed in a number of lower and middle Eocene samples from both holes.

The K/T and Cenomanian/Turonian boundaries were examined at closely spaced sample intervals. Zonal assignments are summarized in Figure 29 and Table 9, and a distribution chart is presented in Table 10. A list of foraminifer datums used to calculate the sediment accumulation rate is included in Table 9.

The base of Zone P12 of the middle Eocene was identified on the LO of *Morozovella aragonensis*, which co-occurs with *M. lehneri* at both holes.This is contrary to the relative order of appearance and datum ages used by Berggren et al. (1995), who observed that the LO of *M. aragonensis* occurs below the FO of *M. lehneri.* The base of Zone P11 was identified by the FO of the marker species *Turborotalia possagnoensis.* Near the top of this zone is the FO of *Hantkenina dumblei.* Although rare, this distinctive species occurs in all samples spanning its range and may prove to be a valuable middle Eocene biomarker.

The boundaries for Zones P10–P8 could not be distinguished at any of the holes using the Berggren et al. (1995) zonal scheme because of the absence of the zonal markers *Hantkenina nuttali* and *Planorotalites palmerae.* However, we used the biostratigraphic overlap of *Acarinina broedermanni, Morozovella lensiformis,* and *M. caucasica* to identify the stratigraphic interval represented by Zone P8, as suggested by Toumarkine and Luterbacher (1985). Within the lower part of Zones P9–P10 is the distinctive FO of *Guembelitrioides higginsi.* This bioevent may prove to be useful for correlation within this broadly zoned interval. The base of Zone P8 was recognized by the LOs of *M. formosa* and *A. pentacamerata.*

The FO of *Morozovella aragonensis* occurs within one core below the LO of *M. formosa* in both holes and was used to define the base of Zone P7. The base of Subzone P6b was identified from the co-occurring FOs of *M. formosa* and *M. lensiformis* in Hole 1050A. Only the FO of *M. lensiformis* was used to identify the base of Subzone P6b in Hole 1050B because the FO of *M. formosa* was not determined. Zone P6a comprises a longer stratigraphic interval in both holes at Site 1050 than does Subzone P6b. This is the reverse of the Berggren et al. (1995) zonal scheme, suggesting that part of Subzone P6b may be missing. The Subzone P6a assemblage is characterized by the relatively common occurrences of *M. marginodentata, M. gracilis,* and *M. subbotinae;* rare occurrence of *Chiloguembelina wilcoxensis,* and consistent occurrence of *Pseudohastigerina wilcoxensis* in the fine-sized fraction.

Zones P5 through P3 were identified in Hole 1050A. The top of Zone P5, which is used to define the Paleocene/Eocene boundary, was determined at the LO of *Morozovella velascoensis* in Sample 171B-1050A-26X-1, 8–10 cm. A typical Zone P4 assemblage, including *Globanomalina pseudomenardii, M. velascoensis, M. acuta, Acarinina mackannai,* and *A. nitida,* was recognized in Samples 171B-1050A-27X-CC and 31X-3, 61–62 cm. The base of Subzone P3b coincides with the FOs of *M. velascoensis* and *Igorina albeari,* which occurred in Sample 171B-1050-33X-CC. Species identified within this interval include *M. angulata, M. acuta, M. conicotruncata,* and *A. mackannai.* The deepest core from Hole 1050A yielded a Subzone P3a assemblage, including abundant *M. conicotruncata* and relatively common *I. pusilla* and *G. chapmani.*

The 288-m sequence drilled at Site 1050C ranges from late Paleocene (Subzone P3a) to late Albian *(Rotalipora ticinensis* Zone) in age (Fig. 28). Foraminifers are common to rare and moderately to poorly preserved in the Paleocene nannofossil claystone samples from Subzones P1b through P3a, and they are very well preserved in the calcareous nannofossil claystone from Subzones Pα through P1a. Nearly all Cretaceous foraminifers are abundant to common and well preserved. Particularly well-preserved assemblages occur in the soft, finely laminated claystones of Albian age and in the Turonian nannofossil chalk. The extraordinary preservation of assemblages from these intervals will afford detailed analysis of foraminifer wall ultrastructure and will test morphology for evolutionary and taxonomic studies, thereby providing new insight into the evolution of mid-Cretaceous planktonic foraminifers.

Upper Paleocene Subzone P3a is identified in Sections 171B-1050C-2R-CC and 3R-CC based on the presence of *Morozovella angulata* and *M. conicotruncata.* Subzones P1c–P3a are undifferentiated in Cores 171B-1050C-4R through 6R. *Globanomalina compressa* is present, but the absence of biomarkers for Subzone P3a and Zone P2 may be an artifact of poor sample preservation.

Sample 171B-1050C-10R-1, 0–1 cm, yields a well-preserved assemblage with abundant *Guembelitria cretacea;* few *Woodringina claytonensis, W. hornerstownensis,* and *Chiloguembelina midwayensis*; and very rare *Praemurica taurica* and *Parasubbotina pseudobulloides*. The presence of the latter two species and the absence of *Parvulorugoblobigerina eugubina* and *Subbotina triloculinoides* indicate that this is a Subzone P1a assemblage; however, the abundance of *G. cretacea* and other minute foraminifers in a package of sediments that show evidence of slumping causes some uncertainty in this zonal assignment. Subzone Pα is identified in Sample 171B-1050C-10R-2, 32–33 cm, based on the co-occurrence of abundant *P. eugubina* with *G. cretacea,* and *Globanomalina archeocompressa.* No samples were analyzed from immediately below and above the K/T boundary, which is placed in Sample 171B-1050C-10R-2, 36 cm (405.93 mbsf), on the basis of nannofossil evidence.

Table 6. Planktonic foraminifer datums for Holes 1050A and 1050B.

Datum	Species	Zone	Age (Ma)	Core, section, interval (cm)	Depth (mbsf)	Error depth (mbsf)
				171B-1050A-		
T	*M. aragonensis*	b P12	43.60	4H-CC	38.72	29.61
B	*M. lehneri*		43.50	6H-CC	57.83	48.34
B	*T. possagnoensis*	b P11	46.00	13X-CC	122.47	132.72
T	*M. formosa*	b P8	50.80	19X-CC	182.16	168.95
T	*M. lensiformis*		52.70	19X-CC	182.19	168.95
B	*M. aragonensis*	b P7	52.30	20X-CC	191.82	199.29
T	*M. marginodentata*		52.50	20X-CC	191.84	182.19
T	*M. aequa*		53.60	21X-CC	199.31	191.84
B	*M. lensiformis*	b P6b	54.00	21X-CC	199.31	191.84
B	*M. formosa*	b P6b	54.00	21X-CC	199.31	191.84
B	*M. marginodentata*	(b P6a)	54.80	25X-CC	228.28	237.7
T	*M. velascoensis*	b P6a	54.70	26X-1, 8-10	237.8	237.71
B	*M. subbotinae*	b P5	56.90	27X-CC	249.12	255.38
T	*G. pseudomenardii*	t P4	55.90	27X-CC	249.15	242.03
T	*M. acuta*		54.70	28X-CC	255.41	249.15
B	*M. acuta*		55.70	28X-CC	255.41	249.15
T	*A. mckannai*		56.30	28X-CC	255.41	249.15
B	*G. pseudomenardii*	b P4	59.20	31X-3, 61-62	278.57	285.95
T	*P. varianta*		59.20	32X-CC	291.76	285.98
B	*M. aequa*		56.50	33X-CC	298.11	300.08
B	*I. albeari*	b P3b	60.00	33X-CC	298.11	300.08
B	*M. velascoensis*	b P3b	60.00	33X-CC	298.11	300.08
				171B-1050B-		
T	*M. aragonensis*	b P12	43.60	6H-CC	54.99	45.28
B	*M. lehneri*		43.50	9H-CC	83.37	92.08
B	*T. possagnoensis*	b P11	46.00	14X-CC	127.41	137.27
T	*M. lensiformis*		52.70	19X-CC	159.45	158.85
T	*S. velascoensis*		53.50	20X-CC	177.17	159.45
T	*M. formosa*	b P8	50.80	20X-CC	177.17	159.45
B	*M. aragonensis*	b P7	52.30	21X-CC	186.88	195.97
T	*M. marginodentata*	(t P6b)	52.50	22X-CC	195.99	186.89
B	*M. lensiformis*	b P6b	54.00	23X-CC	206.01	215.62
T	*M. aequa*		53.60	25X-CC	225.40	225.27

Notes: Bases of age and biozonal datums are represented by B and b; tops of age and biozonal datums are represented by T and t. Error depths refer to depth to next sample studied above or below a datum level. Parentheses around zones refer to species used to approximate zonal boundaries. These data reflect post-cruise modifications and are, thus, more up to date than data presented in the range charts and in the biostratigraphy and sedimentation rate figures (this chapter).

Table 7. Distribution chart for planktonic foraminifers from Hole 1050A.

Age	Zone	Core, section, interval (cm)	Depth (mbsf)	Abundance	Preservation	*Chiloguembelina crinita*	*Chiloguembelina midwayensis*	*Chiloguembelina subtriangularis*	*Chiloguembelina virgata*	*Globanomalina chapmani*	*Globanomalina compressa*	*Globanomalina ehrenbergi*	*Globanomalina imitata*	*Igorina pusilla*	*Morozovella conicotruncata*	*Parasubbotina varianta*	*Zeauvigerina aegyptiaca*	*Acarinina mckannai*	*Acarinina nitida*	*Subbotina triangularis*	*Igorina albeari*	*Morozovella aequa*	*Morozovella angulata*	*Morozovella occlusa*	*Morozovella velascoensis*	*Morozovella acuta*	*Parasubbotina pseudobulloides*	*Subbotina trilocullinoides*	*Globanomalina pseudomenardii*	*Subbotina velascoensis*	*Acarinina primitiva*	*Acarinina soldadoensis*	*Morozovella subbotinae*	*Subbotina linaperta*	*Globanomalina planoconica*	*Chiloguembelina wilcoxensis*	*Subbotina cancellata*
		171B-1050A																																		
middle Eocene	P12	1X-CC	6.86		G																									R						
middle Eocene	P12-P11	2H-CC	20.18		G																															
middle Eocene	P12	3H-CC	29.61		G																															
middle Eocene	P12	4H-CC	38.72		G																															
middle Eocene	P11	5H-CC	48.34	C	G																															
middle Eocene	P11	6H-CC	57.83	A	G																															
middle Eocene	P11	7H-CC	67.5	C	G																												F			
middle Eocene	P11	8H-CC	76.66	C	M																												F			
middle Eocene	P11	9H-CC	86.32	C	M																												R			
middle Eocene	P11	11X-CC	104.42	A	G																												A			
middle Eocene	P11	12X-CC	106.52	C	G																												A			
middle Eocene	P11	13X-CC	122.47	A	G																												F			
early-middle Eocene	P10-P9	14X-CC	132.72	A	M																												A			
early-middle Eocene	P10-P9	15X-CC	141.8	A	M																												F			
early-middle Eocene	P10-P9	16X-CC	153.37		M																											R				
early-middle Eocene	P10-P9	17X-CC	157.95		M																											R				
early-middle Eocene	P8	18X-CC	168.92		M																											F				
early Eocene	P7	19X-CC	182.16	R	M																										R	F	R				
early Eocene	P7	20X-CC	191.82	F	G																										R	F	F	F			
early Eocene	P6b	21X-CC	199.29	C	G																	R									R	R	R	F		R	
early Eocene	P6a	22X-CC	208.97	C	G																											F	F	A	R		
early Eocene	P6a	23X-CC	218.69	C	G																												A	A	R	R	
early Eocene	P6a	24X-CC	228.22	F	P																												A	F	R		
early Eocene	P6a	25X-CC	228.28	C	M																											F	F	A	R		
late Paleocene	P5	26X-1, 8-10	237.78	A	M																				F							F	A	F		R	R
late Paleocene	P5	26X-CC	242.01	C	M					R															F							F	A		F		
late Paleocene	P4c	27X-CC	249.12	A	M																				F				F			F	A	A			
late Paleocene	P4	28X-CC	255.38	F	M													R	F						F	F		F	F								
late Paleocene	P4	29X-CC	266.82	F	G													P	F						F	F		F	F		R						
early Paleocene	P4	30X-CC	276.11	F	M													R							F	F		F	F		R						
late Paleocene	P4a	31X-3, 61-62	278.57	A	M									F	F						F				F	F		F	F	F							
early Paleocene	P3	31X-CC	285.95	F	M						R				F									R		F	F										
late Paleocene	P3b	32X-CC	291.73	A	M							F	R	R		F					F	R	R	F	R	F		F									
late Paleocene	P3b	33X-CC	298.11	C	M					R		R		R	R	F		R	R		F	F	R	A	F												
late Paleocene	P3a	34X-CC	300.08	F	P										A	F		F	R	F																	
late Paleocene	P3a	35X-CC	314.61	F	M		F			F		F		F	A	A																					
late Paleocene	P3a	36X-CC	319.72	C	G	F	F	R	R	R	R	F	R	F	A	A	R																				

Notes: Abundance: C = common; A = abundant; R = rare; F = few; P = present. Preservation: G = good; M = moderate; P = poor.

Table 7 (continued).

Age	Zone	Core, section, interval (cm)	Depth (mbsf)	Abundance	Preservation	*Subbotina hardingae*	*Subbotina hornibrooki*	*Acarinina coalingensis*	*Morozovella gracilis*	*Morozovella marginodentata*	*Pseudohastigerina wilcoxensis*	*Acarinina wilcoxensis*	*Acarinina quetra*	*Morozovella formosa*	*Morozovella lensiformis*	*Morozovella aragonensis*	*Acarinina bullbrooki*	*Morozovella caucasica*	*Subbotina frontosa*	*Globigerina senni*	*Globigerinatheka subconglobata*	*Guembelitrioides higginsi*	*Acarinina pentacamerata*	*Subbotina inaequispira*	*Acarinina cuneicamerata*	*Morozovella spinulosa*	*Pseudohastigerina micra*	*Chiloguembelina cubensis*	*Globigerinatheka senni*	*Turborotalia possagnoensis*	*Globigerinatheka mexicana*	*Acarinina collactea*	*Truncorotaloides topilensis*	*Hantkenina dumblei*	*Globigerinatheka index*	*Morozovella crassata*	*Acarinina topilensis*	*Hantkenina mexicana*	*Morozovella lehneri*	*Truncorotaloides rohri*
		171B-1050A																																					
middle Eocene	P12	1X-CC	6.86		G												F					R		R		R	R			F			F	F					
middle Eocene	P12-P11	2H-CC	20.18		G												F							F						R			P						
middle Eocene	P12	3H-CC	29.61		G												F			R				F						R			R				R	F	
middle Eocene	P12	4H-CC	38.72		G											R	F			P	F			F													R	F	
middle Eocene	P11	5H-CC	48.34	C	G											R	F					R		A		R	F				R		R	R	F			R		
middle Eocene	P11	6H-CC	57.83	A	G		R									R	F							F		R	A				F				F	R		R		
middle Eocene	P11	7H-CC	67.5	C	G			F									A							F		R	F				R			P	R					
middle Eocene	P11	8H-CC	76.66	C	M												F							F		R					R			P						
middle Eocene	P11	9H-CC	86.32	C	M			F								R	A					R		F		R	R		R		R									
middle Eocene	P11	11X-CC	104.42	A	G												F		R			R		F		F	P		R	R		R								
middle Eocene	P11	12X-CC	106.52	C	G			R									A		R			F		F		R	R			R	R									
middle Eocene	P11	13X-CC	122.47	A	G			F									A				R	R		F	R		R		R	R									
early-middle Eocene	P10-P9	14X-CC	132.72	A	M											R	A	R			R	F		F		R	F	R												
early-middle Eocene	P10-P9	15X-CC	141.8	A	M			F								F	A					R	R	F	R	R	R													
early-middle Eocene	P10-P9	16X-CC	153.37		M											R	F	R			R	P	R	F																
early-middle Eocene	P10-P9	17X-CC	157.95		M											F	R	R		R	P	P																		
early-middle Eocene	P8	18X-CC	168.92		M										R	F	F	F	P																					
early Eocene	P7	19X-CC	182.16	R	M									F	R	F																								
early Eocene	P7	20X-CC	191.82	F	G				R				F		R	R																								
early Eocene	P6b	21X-CC	199.29	C	G				F	R	R		F	R	F																									
early Eocene	P6a	22X-CC	208.97	C	G		R	R	A			F																											
early Eocene	P6a	23X-CC	218.69	C	G		F		A	F	F																												
early Eocene	P6a	24X-CC	228.22	F	P		F		A		R																												
early Eocene	P6a	25X-CC	228.28	C	M		R	F	A	F																													
late Paleocene	P5	26X-1, 8-10	237.78	A	M	R	R																																
late Paleocene	P5	26X-CC	242.01	C	M																																		
late Paleocene	P4c	27X-CC	249.12	A	M																																		
late Paleocene	P4	28X-CC	255.38	F	M																																		
late Paleocene	P4	29X-CC	266.82	F	G																																		
early Paleocene	P4	30X-CC	276.11	F	M																																		
late Paleocene	P4a	31X-3, 61-62	278.57	A	M																																		
early Paleocene	P3	31X-CC	285.95	F	M																																		
late Paleocene	P3b	32X-CC	291.73	A	M																																		
late Paleocene	P3b	33X-CC	298.11	C	M																																		
late Paleocene	P3a	34X-CC	300.08	F	P																																		
late Paleocene	P3a	35X-CC	314.61	F	M																																		
late Paleocene	P3a	36X-CC	319.72	C	G																																		

Table 8. Distribution chart for planktonic foraminifers from Hole 1050B.

Age	Zone	Core, section	Depth (mbsf)	Abundance	Preservation	*Morozovella quetra*	*Acarinina soldadoensis*	*Acarinina angulosa*	*Morozovella formosa*	*Morozovella marginodentata*	*Morozovella subbotinae*	*Subbotina linaperta*	*Acarinina nitida*	*Morozovella aequa*	*Morozovella gracilis*	*Subbotina triloculinoides*	*Acarinina broedermanni*	*Chiloguembelina wilcoxensis*	*Globanomalina chapmani*	*Pseudohastigerina wilcoxensis*	*Subbotina velascoensis*	*Morozovella lensiformis*	*Acarinina pentacamerata*	*Morozovella aragonensis*	*Morozovella caucasica*	*Acarinina coalingensis*	*Acarinina pseudotopilensis*	*Acarinina subsphaerica*	*Subbotina hardingae*	*Acarinina bullbrooki*
		171B-1050B-																												
middle Eocene	P12	1X-CC	7.62	A	G																									R
middle Eocene	P12-P11	2H-CC	16.43	C	G																									F
middle Eocene	P12	3H-CC	26.31	C	G																									F
middle Eocene	P12	4H-CC	35.76	A	G																									F
middle Eocene	P12	5H-CC	45.28	A	G																									F
middle Eocene	P12	6H-CC	54.99	A	G																			R						F
middle Eocene	P11	7H-CC	64.09	F	G																			R						
middle Eocene	P11	8H-CC	73.84	A	G																									R
middle Eocene	P11	9H-CC	83.37	A	G																									F
middle Eocene	P11	10X-CC	92.08	A	G							F												R						A
middle Eocene	P11	11X-CC	99.79	A	G							F												P						A
middle Eocene	P11	12X-CC	109.85	A	G																			R						A
middle Eocene	P11	13X-CC	118.44	A	G							A																		A
middle Eocene	P11	14X-CC	127.41	A	G							F												F		F	F			A
early-middle Eocene	P9-P10	15X-CC	137.27	A	G							F					R							F		R	R	R		A
early-middle Eocene	P9-P10	16X-CC	145.17	C	G							F					F							F		F	R	R		A
early-middle Eocene	P10-P9	17X-CC	156.17	C	M							A											R	R		R				F
early Eocene	P9	18X-CC	158.83	C	M		R					A					F						F	A	R		R			R
early Eocene	P8	19X-CC	159.44	C	M		F					F					R					F	F	A	F	F	R	R	R	
early Eocene	P7	20X-CC	177.16	C	M		A		F			A					R				R	F	F	R	R					
early Eocene	P7	21X-CC	186.88	C	G		F		R			F											R	R						
early Eocene	P6b	22X-CC	195.97	C	M	R		R		F	F	F	F		F							R								
early Eocene	P6b	23X-CC	206.01	C	M	R		R		F	F	A	R		F				R			R								
early Eocene	P6a	24X-CC	215.62	A	G	R				R	R	A			F	F				R										
early Eocene	P6a	25X-CC	225.38	A	G	F	F				F		R	R	F	F														
early Eocene	P6a	26X-CC	225.48	C	G	R			R	R	F	F	R		R	F	R	F	R	R										
early Eocene	P6a	27X-CC	231.67	R	M	R	F	R	F	R	F	F																		

Notes: Abundance: A = abundant; C = common; F = few; R = rare; P = present. Preservation: G = good; M = moderate.

Table 8 (continued).

Age	Zone	Core, section	Depth (mbsf)	Abundance	Preservation	*Acarinina cuneicamerata*	*Acarinina matthewsae*	*Pseudohastigerina micra*	*Globigerinatheka senni*	*Globigerinatheka subconglobata*	*Morozovella spinulosa*	*Subbotina inaequispira*	*Acarinina densa*	*Acarinina spinuloinflata*	*Guembelitrioides higginsi*	*Globigerina senni*	*Globigerinatheka mexicana*	*Turborotalia possagnoensis*	*Subbotina hagni*	*Hantkenina mexicana*	*Subbotina frontosa*	*Acarinina topilensis*	*Subbotina eocaena*	*Subbotina cryptomphala*	*Truncorotaloides rohri*	*Hantkenina dumblei*	*Morozovella lehneri*	*Globigerintheca subconglobata*	*Acarinina primitiva*	*Globigerinatheka index*
		171B-1050B-																												
middle Eocene	P12	1X-CC	7.62	A	G			R			F	F					F							R	F	R		R	F	
middle Eocene	P12-P11	2H-CC	16.43	C	G						F	R			R		F						F	F	R		R			
middle Eocene	P12	3H-CC	26.31	C	G						F	R			F	R	F						F	R	F	R	R			
middle Eocene	P12	4H-CC	35.76	A	G						R	R				R	F		F			R		F	F	R	R	R		
middle Eocene	P12	5H-CC	45.28	A	G							F			R		F		F		R	R	F	F	F	R	F	F		
middle Eocene	P12	6H-CC	54.99	A	G							F			R	R	F		F		P	R	F	F	R	R	R			
middle Eocene	P11	7H-CC	64.09	F	G							F			R	R	F		F		P	R		F	R	R				
middle Eocene	P11	8H-CC	73.84	A	G							F			R	R	F		F	R	P	R	F	F	R					
middle Eocene	P11	9H-CC	83.37	A	G							F			P	P	F		F			P	F	F	R					
middle Eocene	P11	10X-CC	92.08	A	G											R	F		F	P										
middle Eocene	P11	11X-CC	99.79	A	G			R				F			A	R	F	R		P	R										
middle Eocene	P11	12X-CC	109.85	A	G			P			R	A			A		F	F	F												
middle Eocene	P11	13X-CC	118.44	A	G	R		R				F			F	F	F	R													
middle Eocene	P11	14X-CC	127.41	A	G			R			R			F	F	F	R	R													
early-middle Eocene	P9-P10	15X-CC	137.27	A	G			R		R	R	R			F																
early-middle Eocene	P9-P10	16X-CC	145.17	C	G	R		F			R	F	R	R																	
early-middle Eocene	P10-P9	17X-CC	156.17	C	M		F	F	R	R	R	R																			
early Eocene	P9	18X-CC	158.83	C	M	R	F	F																							
early Eocene	P8	19X-CC	159.44	C	M																										
early Eocene	P7	20X-CC	177.16	C	M																										
early Eocene	P7	21X-CC	186.88	C	G																										
early Eocene	P6b	22X-CC	195.97	C	M																										
early Eocene	P6b	23X-CC	206.01	C	M																										
early Eocene	P6a	24X-CC	215.62	A	G																										
early Eocene	P6a	25X-CC	225.38	A	G																										
early Eocene	P6a	26X-CC	225.48	C	G																										
early Eocene	P6a	27X-CC	231.67	R	M																										

Table 9. Planktonic foraminifer datums for Hole 1050C.

Datum	Species	Zone	Age (Ma)	Core, section, interval (cm)	Error depth (mbsf)
				171B-1050C-	
B	*G. compressa*		63.0	7R-4, 66-68	380.36-389.68
B	*P. inconstans*	b P1c	63.0	8R-CC, 9-10	389.68-401.37
B	*S. triloculinoides*	b P1b	64.3	9R-CC, 4-7	401.37-405.92
B	*P. eugubina*	b Pa	65.0	10R-2, 32-33	405.92-412.96
B	*A. mayaroensis*	b *A. mayaroensis*	68.3	15R-6, 35-37	450.43-452.49
B	*R. fructicosa*	b *R. fructicosa*	69.6	16R-2, 38-42	454.08-456.29
B	*C. contusa*	b *C. contusa*	69.6	16R-1, 30-32	452.50-454.08
T	*H. helvetica*	t *H. helvetica*	90.8	20R-5, 41-43	484.58-496.98
B	*H. helvetica*	b *H. helvetica*	93.1	21R-1, 0-1	500.20-501.30
T	*R. cushmani*	t *R. cushmani*	93.9	21R-1, 110-113	500.21-501.33
B	*R. greenhornensis*	b *R. greenhornensis*	98.9	26R-CC, 12-14	555.60 -567.65
B	*R. appenninica*	b *R. appenninica*	100.4	27R-CC, 23-25	567.65-577.36

Notes: Bases of age and biozonal datums are represented by B and b; tops of age and biozonal datums are represented by T and t. Error depths refer to depth to next sample studied above or below a datum level. These data reflect post-cruise modifications and are, thus, more up to date than data presented in the range charts and in the biostratigraphy and sedimentation rate figures (this chapter).

The base of the *Abathomphalus mayaroensis* Zone is placed in Sample 171B-1050C-15R-6, 35–37 cm (450.45 mbsf), where *A. mayaroensis* occurs in very low abundance. The base of the *Racemiguembelina fructicosa* Zone is placed at the FO of the nominate species in Sample 171B-1050C-16R-2, 38–42 cm (454.08 mbsf). This taxon occurs consistently in low to moderate abundance throughout its range. The FO of *Contusotruncana contusa* (Section 171B-1050C-16R-1, 30–32 cm; 452.50 mbsf) occurs in the middle of the *R. fructicosa* Zone and near the same level as the LO of inoceramid prisms (Sample 171B-1050C-16R-3, 109–112 cm; 456.29 mbsf).

No specimens of *Gansserina gansseri* were found in samples from the *A. mayaroensis* Zone or *R. fructicosa* Zone. Hence, it is not clear that the absence of this species below the *R. fructicosa* Zone is because of its rarity at this site or because of a hiatus that spans the *G. gansseri* Zone. For this reason, the *G. gansseri* and *G. falsostuarti* Zones are not differentiated. This combined zonal interval extends from Sample 171B-1050C-16R-3, 109–111 cm (456.29 mbsf) through Section 18R-CC (478.8 mbsf), and includes well-preserved assemblages in the upper part and moderately preserved assemblages in the lower part. The *Radotruncana calcarata* Zone was not identified in Hole 1050C, but Section 171B-1050C-19R-CC (484.5 mbsf) is placed in the undifferentiated *R. calcarata* Zone and *Globotruncana ventricosa* Zone (mid-Campanian), based on the occurrence of *Globotruncanita atlantica.*

On the basis of calcareous nannofossil evidence, Core 171B-1050C-20R contains the Campanian, Santonian, and Coniacian stages bounded by hiatuses above the core catcher. Section 171B-1050C-20R-CC yields a pristinely preserved and diverse assemblage from the lower Turonian *Helvetotruncana helvetica* Zone. This zone extends through Sample 171B-1050C-21R-1, 0–1 cm, and yields common *H. helvetica, Dicarinella imbricata,* and *Whiteinella paradubia.* The ancestor to *H. helvetica, H. praehelvetica,* occurs in the lower part of this zone.

The Cenomanian/Turonian boundary is apparently incomplete in Hole 1050C, as foraminifers that mark the *Whiteinella archaeocretacea* Zone were not identified. The upper Cenomanian is represented by moderately to well-preserved foraminifers characteristic of the *Rotalipora cushmani* Zone. The base of this zone, which is determined from the FO of the nominate taxon, is placed in Sample 171B-1050C-22R-1, 50–51 cm (510.3 mbsf). A distinctive, but uncommon, morphotype, *Rotalipora deeckei,* ranges through most of this zone.

The FO of *Rotalipora brotzeni* and *R. greenhornensis* (primitive morphotypes) mark the base of the *R. greenhornensis* Zone, which spans from Samples 171B-1050C-23R-CC (529.2 mbsf) to 26R-CC (555.6 mbsf). A few specimens of *Costellagerina libyca* occur within this interval.

The Cenomanian/Albian boundary occurs within Core 171B-1050C-27R, as the core-catcher sample from this core yields a very well-preserved assemblage from the upper Albian *Rotalipora appenninica* Zone. Foraminifers from this zone include common *R. appenninica, R. ticinensis,* and *Biticinella breggiensis,* and numerous small, unidentified hedbergellids. Evidence for a significant hiatus spanning the lower *R. appenninica* Zone and upper *R. ticinensis* Zone is suggested by the absence of *Planomalina buxtorfi* and *P. praebuxtorfi,* which were observed in both zones at Site 1052.

The nannofossil claystone from Samples 171B-1050C-28R-CC, 15–17 cm (577.3 mbsf), to the bottom of the cored interval yields extraordinarily well-preserved foraminifers that are assigned to the upper Albian *Rotalipora ticinensis* Zone. In addition to common occurrences of the nominate taxon, assemblages from this zone are characterized by consistent occurrences of *Biticinella breggiensis, Ticinella roberti, T. praeticinensis, Planomalina* sp., *Hedbergella simplex,* and numerous small hedbergellids. It is noteworthy that *Schackoina cenomana, Hastigerinelloides alexanderi,* and *Guembelitria cenomana* occur in part to all of the *R. ticinensis* Zone. This is the first time these taxa have been recorded at such a low stratigraphic level.

Benthic Foraminifers

The preservation of benthic foraminifers is generally good to moderate throughout the middle Eocene to upper Paleocene interval cored in Hole 1050A, with the exception of Sample 171B-1050A-24X-CC, 37–39 cm, where preservation is poor (Table 11). Abundance of benthic foraminifers is low throughout, especially in samples of Eocene age (Table 11). The trace to few occurrences in the Eocene interval (planktonic foraminifer Zones P12–P6) are probably the result of high abundances of radiolarians diluting the benthic foraminifers. The abundance of benthic foraminifers is slightly higher in the late Paleocene, especially in Samples 171B-1050A-26X-CC, 22–24 cm, and 29X-CC, 38–40 cm, where benthic foraminifers are common. Paleodepth estimates based on the ubiquitous occurrence of *Nuttallides truempyi* and *Aragonia* spp. indicate lower bathyal depths (1000–2000 m) during late Paleocene through middle Eocene times at Site 1050.

After drilling without recovery through the Eocene, upper Paleocene to upper Albian sediments were recovered in the 605-m-deep Hole 1050C. Benthic foraminifer preservation improves downward in Hole 1050C, where it is moderate in Paleocene, moderate to good in the Upper Cretaceous (Maastrichtian to Campanian), and surprisingly good to very good in the Lower Cretaceous (Cenomanian to Albian; Table 12). The abundance of benthic foraminifers is generally high throughout Hole 1050C. They are abundant to few in the Paleocene and common and abundant in the Upper and Lower Cretaceous, respectively.

The middle–early Eocene fauna (between Core 171B-1050A-1H and Sample 171B-1050A-24X-6, 147–150 cm) is marked by typical post-Paleocene/Eocene benthic extinction taxa, including *Aragonia semireticulata, Bulimina* cf. *semicostata, B. macilenta, B. semicostata, B. thanetensis, Buliminella grata, Cibicidoides tuxpamensis, Gavelinella capitata, Karreriella chapapotensis, Osangularia mexicana,* and *Turrilina robertsi,* along with *Globocassidulina subglobosa* and *Quadrimorphina profunda.* An additional component of the Eocene fauna is represented by several taxa, ranging through the late Paleocene into the middle Eocene (i.e., pleurostomellids, *B. trinitatensis, Oridorsalis* spp., *Tritaxia* spp., and common *Nuttallides truempyi*).

Three samples of latest Paleocene to earliest Eocene age (i.e., Samples 171B-1050A-24X-CC, 37–39 cm, 171B-1050A-25X-CC, 12–14 cm, and 171B-1050A-25X-CC, 28–30 cm) have only traces of benthic foraminifers. The faunas in these samples are represented by a few poorly preserved, minute buliminids and *Nonion* spp., along with single specimens of two pre-Paleocene/Eocene benthic extinction taxa (*Osangularia velascoensis* and *Aragonia ouezzanensis*), in-

Table 10. Distribution chart for planktonic foraminifers from Hole 1050C.

Age	Zone	Core, section, interval (cm)	Depth (mbsf)	Abundance	Preservation	*Biticinella breggiensis*	*Hastigerinelloides* cf. *alexanderi*	*Hedbergella delrioensis*	*Hedbergella simplex*	*Rotalipora subticinensis*	*Rotalipora ticinensis*	*Schackoina cenomana*	*Ticinella praeticinensis*	*Ticinella roberti*	*Guembelitria cenomana*	*Praeglobotruncana delrioensis*	*Costellagerina libyca*	*Rotalipora appenninica*	*Ticinella raynaudi*	*Praeglobotruncana stephani*	*Rotalipora brotzeni*	*Rotalipora gandolfii*	*Rotalipora greenhornensis*	*Praeglobotruncana gibba*	*Rotalipora cushmani*	*Rotalipora deeckei*	*Rotalipora turonica*	*Whiteinella baltica*	*Heterohelix moremani*	*Dicarinella algeriana*	*Dicarinella imbricata*	*Helvetoglobotruncana helvetica*	*Helvetoglobotruncana praehelvetica*	*Heterohelix reussi*	*Schackoina bicornis*	*Whiteinella paradubia*	*Marginotruncana marianosi*	*Contusotruncana fornicata*	*Contusotruncana patelliformis*	*Globotruncana arca*	*Globotruncana linneiana*	*Globotruncana orientalis*	*Globotruncanita atlantica*	*Globotruncanita stuartiformis*	*Heterohelix globulosa*	*Globotruncana falsostuarti*	*Globotruncanella havanensis*	*Globotruncanella petaloidea*	*Planoglobulina acervulinoides*
		171B-1050C-																																												
late Paleocene	P3a	2R-CC, 20-22	336.97	C	M																																									
late Paleocene	P3a	3R-CC, 0-2	343.46	F	P																																									
late Paleocene	P3a-P1c	4R-6, 61-63	354.41	R	P																																									
late Paleocene	P3a-P1c	5R-CC, 25-27	364.10	R	P																																									
late Paleocene	P3a-P1c	6R-CC, 14-16	375.32	F	P																																									
early Paleocene	P1c	7R-4, 66-68	380.36	F	M																																									
early Paleocene	P1c	8R-CC, 9-10	389.68	R	P																																									
early Paleocene	P1b	9R-CC, 4-7	401.37	R	P																																									
early Paleocene	P1a	10R-1, 0-1	404.10	A	VG																																									
early Paleocene	Pα	10R-2, 32-33	405.92	C	VG																																								P	
Maastrichtian	*A. mayaroensis*	11R-CC, 11-13	412.96	C	M																																								P	
Maastrichtian	*A. mayaroensis*	12R-1, 18-20	413.88	A	G																																								P	
Maastrichtian	*A. mayaroensis*	13R-CC, 21-23	433.20	A	G																																									
Maastrichtian	*R. fructicosa*	15R-CC, 22-24	452.52	A	G																																									
Maastrichtian	*R. fructicosa*	16R-3, 109-112	456.29	A	G																																								
Campanian-Maastrichtian	*G. gansseri-G. falsostuarti*	17R-CC, 19-22	470.70	A	M																																								
Campanian-Maastrichtian	*G. gansseri-G. falsostuarti*	18R-CC, 0-4	478.86	A	G																																								
Campanian	*G. calcarata-G. ventricosa*	19R-CC, 15-17	484.56	A	G																																								
Turonian	*H. helvetica*	20R-5, 41-43	496.96	C	M															F				F																				
Turonian	*H. helvetica*	21R-1, 0-1	500.20	A	G															R	F			F				R	R	P	F	R	R	F	P	F								
Cenomanian	*R. cushmani*	21R-1, 110-113	501.30	C	G											F				R	F		F	P	R	P																		
Cenomanian	*R. cushmani*	21R-7, 0-1	508.30	C	M															R			R	R	R																			
Cenomanian	*R. cushmani*	21R-CC, 0-1	509.83	A	M											R		R		F	R		F	R	R	P			R															
Cenomanian	*R. cushmani*	21R-CC, 30-32	510.13	C	M			P										R		R	R		F	R	F		R		R														
Cenomanian	*R. cushmani*	22R-1, 50-51	510.30	A	G											R		R		A	F		R	A	F	R	R	R															
Cenomanian	*R. greenhornensis*	23R-CC, 18-21	529.25	C	G			P								F		R		F	F	P	F																				
Cenomanian	*R. greenhornensis*	24R-3, 69-71	532.15	A	G			R	R							R		R		R	F	P	F																				
Cenomanian	*R. greenhornensis*	25R-CC, 21-22	544.08	C	G			R								R		P		F	F	P	F	R																			
Cenomanian	*R. greenhornensis*	26R-CC, 12-14	555.60	A	G			R								R	F	P		R	F	P	F																				
Albian	*R. appenninica*	27R-CC, 23-25	567.65	A	VG	F			R		F			R	R		R	F	F																								
Albian	*R. ticinensis*	28R-CC, 15-17	577.36	A	G	F			R	F	F	P	F	R	R	R																											
Albian	*R. ticinensis*	29R-CC, 6-8	586.69	A	G	R		F	R	F	F			F	F																												
Albian	*R. ticinensis*	30R-CC, 20-22	595.81	A	VG	R		F	P	F	F	P	R	R	P																												
Albian	*R. ticinensis*	31R-CC, 25-27	605.39	A	VG	R	P	R	R	F	R	P	P	F																													

Notes: Abundance: C = common; F = few; R = rare; A = abundant; P = present. Preservation: M = moderate; P = poor; VG = very good; G = good.

Table 10 (continued).

Age	Zone	Core, section, interval (cm)	Depth (mbsf)	Abundance	Preservation	*Planoglobulina multicamerata*	*Pseudotextularia nuttalli*	*Favusella washitensis*	*Globotruncanita stuarti*	*Heterohelix navarroensis*	*Racemiguembelina fructicosa*	*Contusotruncana walfischensis*	*Abathomphalus mayaroensis*	*Contusotruncana contusa*	*Globotruncana dupeublei*	*Pseudoguembelina palpebra*	*Pseudotextularia elegans*	*Abathomphalus intermedius*	*Globotruncana aegyptiaca*	*Globotruncana esnehensis*	*Globotruncana rosetta*	*Rugoglobigerina hexacamerata*	*Rugoglobigerina rotundata*	*Rugoglobigerina rugosa*	*Trinitella scotti*	*Globanomalina archeocompressa*	*Globigerinelloides prairiehillensis*	*Guembelitria cretacea*	*Hedbergella monmouthensis*	*Parvularugoglobigerina alabamensis*	*Parvularugoglobigerina eugubina*	*Chiloguembelina midwayensis*	*Praemurica taurica*	*Woodringina claytonensis*	*Woodringina hornerstownensis*	*Parasubbotina pseudobulloides*	*Parvularugoglobigerina fringa*	*Subbotina triloculinoides*	*Morozovella trinidadensis*	*Praemurica inconstans*	*Globanomalina compressa*	*Morozovella praecursoria*	*Morozovella angulata*	*Morozovella conicotruncata*	*Parasubbotina varianta*	*Parasubbotina variospira*	*Subbotina cancellata*	*Chiloguembelina subtriangularis*	*Igorina pusilla*
		171B-1050C-																																													
late Paleocene	P3a	2R-CC, 20-22	336.97	C	M																										R																
late Paleocene	P3a	3R-CC, 0-2	343.46	F	P																										F																
late Paleocene	P3a-P1c	4R-6, 61-63	354.41	R	P																														R													
late Paleocene	P3a-P1c	5R-CC, 25-27	364.10	R	P																														R		P										
late Paleocene	P3a-P1c	6R-CC, 14-16	375.32	F	P																														R		R										
early Paleocene	P1c	7R-4, 66-68	380.36	F	M																														F		P	F	F								
early Paleocene	P1c	8R-CC, 9-10	389.68	R	P																														R		R	R	P								
early Paleocene	P1b	9R-CC, 4-7	401.37	R	P																														R	R	P										
early Paleocene	P1a	10R-1, 0-1	404.10	A	VG																							A	P	F		F	P	P	R											
early Paleocene	Pα	10R-2, 32-33	405.92	C	VG					R										P						R	P	R			A															
Maastrichtian	*A. mayaroensis*	11R-CC, 11-13	412.96	C	M				R		F			R	P		F		P		R	P	R	R	P																				
Maastrichtian	*A. mayaroensis*	12R-1, 18-20	413.88	A	G				R		F			R	P		F	P	P	P	R	P	R	R	P																				
Maastrichtian	*A. mayaroensis*	13R-CC, 21-23	433.20	A	G						F		P	R	R	R	R																												
Maastrichtian	*R. fructicosa*	15R-CC, 22-24	452.52	A	G				F		R	R																																	
Maastrichtian	*R. fructicosa*	16R-3, 109-112	456.29	A	G		R		R	A	R																																		
Campanian-Maastrichtian	*G. gansseri-G. falsostuarti*	17R-CC, 19-22	470.70	A	M			F																																				
Campanian-Maastrichtian	*G. gansseri-G. falsostuarti*	18R-CC, 0-4	478.86	A	G	R	R																																					
Campanian	*G. calcarata-G. ventricosa*	19R-CC, 15-17	484.56	A	G																																								
Turonian	*H. helvetica*	20R-5, 41-43	496.96	C	M																																							
Turonian	*H. helvetica*	21R-1, 0-1	500.20	A	G																																							
Cenomanian	*R. cushmani*	21R-1, 110-113	501.30	C	G																																							
Cenomanian	*R. cushmani*	21R-7, 0-1	508.30	C	M																																							
Cenomanian	*R. cushmani*	21R-CC, 0-1	509.83	A	M																																							
Cenomanian	*R. cushmani*	21R-CC, 30-32	510.13	C	M																																							
Cenomanian	*R. cushmani*	22R-1, 50-51	510.30	A	G																																							
Cenomanian	*R. greenhornensis*	23R-CC, 18-21	529.25	C	G																																							
Cenomanian	*R. greenhornensis*	24R-3, 69-71	532.15	A	G																																							
Cenomanian	*R. greenhornensis*	25R-CC, 21-22	544.08	C	G																																							
Cenomanian	*R. greenhornensis*	26R-CC, 12-14	555.60	A	G																																							
Albian	*R. appenninica*	27R-CC, 23-25	567.65	A	VG																																							
Albian	*R. ticinensis*	28R-CC, 15-17	577.36	A	G																																							
Albian	*R. ticinensis*	29R-CC, 6-8	586.69	A	G																																							
Albian	*R. ticinensis*	30R-CC, 20-22	595.81	A	VG																																							
Albian	*R. ticinensis*	31R-CC, 25-27	605.39	A	VG																																							

Table 11. Hole 1050A samples examined for benthic foraminifers.

Age	Core, section	Depth (mbsf)	Abundance	Preservation
	171B-1050A-			
middle Eocene	1X-CC	6.86	Few	Good
middle Eocene	4H-CC	38.72	Few	Good
middle Eocene	7H-CC	67.50	Rare	Good
middle Eocene	10H-CC	95.93	Few	Moderate
middle Eocene	13X-CC	122.47	Rare	Moderate
early Eocene	16X-CC	153.37	Few	Moderate
early Eocene	20X-CC	191.82	Few	Good
early Eocene	23X-CC	218.69	Rare	Good
early Eocene	24X-4	224.29	Rare	Good
early Eocene	24X-6	227.37	Rare	Good
early Eocene	24X-CC	228.00	Trace	Poor
early Eocene	25X-CC	228.12	Trace	Moderate
late Paleocene	25X-CC	228.28	Trace	Moderate
late Paleocene	26X-1	237.78	Rare	Moderate
late Paleocene	26X-2	239.32	Few	Moderate
late Paleocene	26X-3	240.84	Few	Moderate
late Paleocene	26X-CC	242.01	Common	Moderate
late Paleocene	29X-CC	266.82	Common	Good
late Paleocene	32X-CC	291.73	Few	Moderate
late Paleocene	35X-CC	314.61	Few	Moderate

Table 12. Hole 1050C samples examined for benthic foraminifers.

Age	Core, section, interval (cm)	Depth	Abundance	Preservation
	171B-1050C-			
late Paleocene	2R-CC	336.97	Abundant	Moderate
early Paleocene	7R-4, 66-68	380.36	Few	Moderate
late Maastrichtian	11R-CC	412.96	Abundant	Moderate
late Maastrichtian	13R-CC	433.20	Common	Good
middle Maastrichtian	16R-3, 109-112	456.29	Common	Good
late Campanian	18R-CC	478.86	Common	Good
late Campanian	19R-CC	484.56	Common	Good
Turonian	21R-1, 0-1	500.20	Common	Good
late Cenomanian	22R-1, 50-51	510.30	Abundant	Good
early Cenomanian	25R-CC	544.08	Abundant	Good
late Albian	27R-CC	567.65	Abundant	Very good
late Albian	29R-CC	586.69	Abundant	Very good

dicating that the Paleocene/Eocene benthic extinction event occurred in the unrecovered part of Core 171B-1050A-25X. The LO of *Gavelinella beccariiformis* is in Sample 171B-1050A-26X-2, 14–16 cm, and is somewhat later for *A. velascoensis* (in Sample 1050A-26X-1, 8–10 cm), whereas the LO for both *A. ouezzanensis* and *O. velascoensis* is in Sample 171B-1050A-25X-CC, 28–30 cm. This diachrony in LOs of certain pre-Paleocene/Eocene benthic extinction taxa may indicate that the Paleocene/Eocene benthic extinction was not necessarily an instantaneous event at the Blake Nose.

The upper Paleocene (Cores 171B-1050A-26X through 36X) is characterized by a number of taxa that were victimized by the Paleocene/Eocene benthic extinction (e.g., Tjalsma and Lohmann, 1983; Van Morkhoven et al., 1986) including *Aragonia velascoensis, A. ouezzanensis, Bolivinoides delicatulus, Bulimina spinea* (= *midwayensis*), *B. velascoensis, Cibicidoides dayi, C. hyphalus, Coryphostoma midwayensis, Gavelinella beccariiformis, Osangularia velascoensis, Paralabamina hillebrandti, Pullenia coryelli, Reussella szajnochae*, and *Pyrmidina rudita*.

The ratio of *G. beccariiformis* to *N. truempyi* at Site 1050 is similar to that at Site 1049 (see "Site 1049" chapter, this volume). This may indicate that the benthic foraminifer fauna at Site 1050 was influenced by low-oxygen, warm, saline, deep waters (i.e., similar deep-water conditions as in the deeper parts of the Blake Nose during Maastrichtian and Paleogene times [see "Site 1049" chapter, this volume]).

As at Site 1049, the nearby Hole 1050C paleodepth estimates, based on benthic foraminifers, suggest a deepening trend through time of middle bathyal depths (~800–1000 m) during Early Cretaceous times to lower bathyal depths (1000–2000 m) throughout the Late Cretaceous (Maastrichtian to Campanian) and the Paleocene.

Radiolarians

Radiolarians were recovered from nearly all core-catcher samples at Site 1050A. Diagnostic taxa indicate that the sequence spans the middle part of the Eocene to the mid-Paleocene. Time constraints prevented the processing of samples from Site 1050B. The faunas were generally well preserved throughout, although a few core-catcher samples had sparse faunas because of dissolution and dilution by high clay sedimentation. The zonal scheme for low-latitude faunas (Riedel and Sanfilippo, 1978) was used for a biostratigraphic framework. The abbreviations R1 through R16 are assigned to Riedel and Sanfilippo's (1978) Paleogene Zones (see "Explanatory Notes" chapter, this volume). Site 1050A contained radiolarian faunas assignable to Zones R1 through R8, shown in Figure 28. The biostratigraphically important markers, as well as the significant zone-to-zone faunal changes, are discussed below. Occurrence, abundance, and preservation of the radiolarian taxa in Hole 1050A are shown in Table 13. All core-catcher samples from Hole 1050C were processed and analyzed, but, unfortunately, few faunas were recovered. The preservation of the radiolarians was mostly poor, and the Hole 1050C faunas were difficult to study in transmitted-light view because of the large clay content and heavy recrystallization of their tests. Occurrence, abundance, and preservation of the radiolarian taxa are shown in Table 8.

Core-catcher samples 171B-1050A-1H-CC and 2H-CC contain a radiolarian assemblage that can be assigned to the middle Eocene *Podocyrtis ampla* Zone (Zone R8; Fig. 28; Table 13). The base of this zone is defined by the FO of *P. ampla* (evolutionary transition of *P. phyxis* to *P. ampl*a). *P. trachodes* makes its first appearance and *P. dorus* has its LO near the upper part of the zone. Samples 171B-1050A-3H-CC to 11H-CC contain a fauna assignable to the *Thyrsocyrtis triacantha* Zone (Zone R7), the base of which is defined by the first appearance of *Eusyringium lagena*. Rare, primitive morphotypes of *E. lagena* occur in Samples 171B-1050A-8H-CC to 11H-CC, whereas typical forms first appear in Sample 171B-1050A-9H-CC and range higher. *P. phyxis* is restricted to the uppermost part of the zone and was found in Samples 171B-1050A-3H-CC and 4H-CC. Another distinct long-ranging species, *Eusyringium fistuligerum*, first appears in Sample 171B-1050A-6H-CC.

Samples 171B-1050A-12H-CC through 14X-CC contain radiolarians assignable to the *Dictyopora mongolfieri* Zone (Zone R6), the base of which is defined by the FO of *D. mongolfieri*. Like *E. lagena, D. mongolfieri* exhibits a tremendous variation in morphology throughout its range, and several early morphotypes were observed in Sample 171B-1050A-14X-CC. The taxa *Lamptonium fabaeforme fabaeforme* and *Thecotyle cryptocephala* make their last appearance in the upper part of the zone. Sample 171B-1050A-15X-CC contains radiolarians indicative of the *T. cryptocephala* Zone (Zone R5). The base of this zone is defined by the evolutionary transition of *T. nigriniae* to *T. cryptocephala*, and the lower limit of the zone is synchronous with the final appearance of *Buryella clinata*. Unfortunately, Sample 171B-1050A-16X-CC contains only rare radiolarians, and the *T. cryptocephala* Zone could not be differentiated from the underlying early Eocene *Phormocyrtis striata striata* Zone.

The radiolarian faunas from Samples 171B-1050A-17X-CC through 20X-CC are characteristic of the *Phormocyrtis s. striata* Zone (Zone R4). The lower limit of this zone is synchronous with the first appearance of *P. striata striata* as well as the co-occurrence of the distinctive taxa *Lamptonium fabaeforme constrictum* and *Lychnocanoma bellum*. In Sample 171B-1050A-21X-CC, several primitive morphotypes of *P. striata striata* were found in addition to morphotypes of *Buryella tetradica*. The presence of *P. s. striata* is probably the result of contamination but could also reflect its evolutionary

Table 13. Radiolarian abundance and preservation at Hole 1050A.

Age	Zone	Core, section	Depth (mbsf)	Abundance	Preservation	*Amphisphaera minor*	*Astrosphaerin* sp. E	*Astrosphaerin* sp. F	*Bekoma campechensis*	*Buryella pentadica*	*Buryella tetradica*	*Clathrocyclomma parcum*	*Entapium regulare*	*Lamptonium pennatum*	*Phormocyrtis striata exquisita*	*Spongurus quadratus*	*Stylosphaera coranatus coranatus*	*Stylosphaera goruna*	*Dorcadospyris* sp. cf. *D. platycantha*	*Stylotrochus alveatus*	*Periphaena decora*	*Bathropyramis woodringi*	*Cromyomma riedeli*	*Lithomitra docilis*	*Lychnocanoma* sp. B	*Pterocodon ampla*	*Bekoma divaricata*	*Bekoma bidartensis*	*Bekoma* sp. aff. B. *campechensis*	*Theocorys phyzella*	*Pterocodon? anteclinata*	*Podocyrtis (Podocyrtis) papalis*	*Xiphosphaera circularis*	*Lithocyclia ocellus group*	*Buryella clinata*	*Theocotyle igriniae*	*Theocotylissa alpha*	*Thyrsocyrtis (Thyrsocyrtis) tarsipes*
		171B-1050A-																																			
middle Eocene	*P. ampla*	1X-CC	6.86	C	VG																											R		C			
middle Eocene	*P. ampla*	2H-CC	20.18	C	VG																C											C		C			
middle Eocene	*T. tricantha*	3H-CC	29.61	C	VG																C	R										C		A			
middle Eocene	*T. tricantha*	4H-CC	38.72	C	VG																											C		C			
middle Eocene	*T. tricantha*	5H-CC	48.34	C	VG																											F		C			
middle Eocene	*T. tricantha*	6H-CC	57.83	C	M																											C		C			
middle Eocene	*T. tricantha*	7H-CC	67.5	C	VG																											C		C			
middle Eocene	*T. tricantha*	8H-CC	76.66	C	VG																C											C		C			
middle Eocene	*T. tricantha*	9H-CC	86.32	A	VG												R				A	R										C		C		R	
middle Eocene	*T. tricantha*	10H-CC	95.93	C	VG																											C		F		F	
middle Eocene	*T. tricantha*	11X-CC	104.42	A	VG												C																			F	
middle Eocene	*D. mongolfieri*	12X-CC	106.52	A	VG												C															C		C		F	
middle Eocene	*D. mongolfieri*	13X-CC	122.47	A	VG												C															F				C	
middle Eocene	*D. mongolfieri*	14X-CC	132.72	C	VG												C															C		C		C	
middle Eocene	*T. cryptocephala*	15X-CC	141.8	C	VG																											C				F	
middle Eocene-early Eocene	*T. cryptocephala-P. striata striata*	16X-CC	153.37	R	P												R															R		A		A	
early Eocene	*P. striata striata*	17X-CC	157.95	A	VG												A															R		C	C	F	
early Eocene	*P. striata striata*	18X-CC	168.92	A	VG												A															C		C	F	C	
early Eocene	*P. striata striata*	19X-CC	182.16	C	VG												A															C		C	F	A	
early Eocene	*P. striata striata*	20X-CC	191.82	C	VG												C															C		C	F	C	
early Eocene	*B. clinata*	21X-CC	199.29	C	VG						C				C		C															C		F	F	C	
early Eocene	*B. clinata*	22X-CC	208.97	C	G						C				C	F	C											R					F	F	F	
early Eocene	*B. clinata*	23X-CC	218.69	C	G						C				C		C									R		F					F	F	F	F	R
early Eocene	*B. clinata*	24X-CC	228.22	R	P						F					F	F															F					
early Eocene	*B. bidartensis*	25X-CC	228.28	T	P						R					F															R						
late Paleocene-early Eocene	*B. bidartensis*	26X-CC	242.01	C	VG		C		F		C			C	F		C	F				R									R	F					
late Paleocene	*B. bidartensis*	27X-CC	249.12	C	VG				F		A		C		R	C	A	F		F							F			F						
late Paleocene-early Eocene	*B. bidartensis*	28X-CC	255.38	C	VG				R				C		F		A	F										F	R	C							
early Paleocene-late Paleocene	*B. campechensis*	29X-CC	266.82	C	G				F	F	C				C		A		F				C														
early Paleocene-late Paleocene	*B. campechensis*	30X-CC	276.11	R	M						F				R		C	F							R			R									
early Paleocene-late Paleocene	*B. campechensis*	31X-CC	285.95	C	G		C		F	F	C	F					A					F	C				R										
early Paleocene-late Paleocene	*B. campechensis*	32X-CC	291.73	C	G		C		F	F	C						A					R	C	F	F	F											
early Paleocene-late Paleocene	*B. campechensis*	33X-CC	298.11	C	VG		C	F	F	F	C				F	C	A	C		F	C																
early Paleocene-late Paleocene	*B. campechensis*	34X-CC	300.08	F	M		F		R	R	F						C																				
early Paleocene-late Paleocene	*B. campechensis*	35X-CC	314.61	C	G	A	C		F	F	C		R			F	F	F	R	C																	
early Paleocene-late Paleocene	*B. campechensis*	36X-CC	319.72	C	VG	R	F	F	F	F	C	A	F	C	F	F	C	C																			

Notes: Abundance: C = common; A = abundant; R = rare; T = trace; F = few. Preservation: VG = very good; M = moderate ; P = poor; G = good.

Table 13 (continued).

Age	Zone	Core, section	Depth (mbsf)	Abundance	Preservation	*Calocyclas hispida*	*Spongatractus balbis*	*Theocotylissa auctor*	*Calocycloma castum*	*Lamptonium fabaeforme fabaeforme*	*Periphaena decora*	*Phormocyrtis striata striata*	*Podocyrtis turgida*	*Spongatractus pachystylus*	*Thyrsocyrtis (Thyrsocyrtis) hirsuta*	*Thyrsocyrtis (Thyrsocyrtis) rhizodon*	*Lamptonium fabaeforme chaunothorax*	*Lamptonium sanfilippoae*	*Podocyrtis (Lampterium) acalles*	*Lamptonium fabaeforme constrictum*	*Theocotylissa ficus*	*Thyrsocyrtis (Pentalacorys) tensa*	*Lamptonium fabaeforme fabaeforme*	*Podocyrtis (Lampterium) sinuosa*	*Dictyoprora mongolfieri*	*Theocotyle cryptocephala*	*Podocyrtis (Podocyrtoges) dorus*	*Theocotyle venezuelensis*	*Thyrsocyrtis (Pentalacorys) triacantha*	*Podocyrtis (Podocyrtoges) diamesa*	*Eusyringium lagena*	*Lychnocanoma bellum*	*Theocotyle conica*	*Eusyringium fistuligerum*	*Podocyrtis (Lampterium) fasciolata*	*Podocyrtis tensa*	*Podocyrtis (Podocyrtoges) phyxis*	*Podocyrtis (Podocyrtoges) ampla*	*Podocyrtis (Lampterium) trachodes*
		171B-1050A-																																			
middle Eocene	*P. ampla*	1X-CC	6.86	C	VG	C					C	C			C	C								C	A			R	F								F
middle Eocene	*P. ampla*	2H-CC	20.18	C	VG	C						C		F		C								C	A			R	F							F	
middle Eocene	*T. tricantha*	3H-CC	29.61	C	VG	F						C		R	F	F								C	C				F		F	F					
middle Eocene	*T. tricantha*	4H-CC	38.72	C	VG	F					C	C		R	F	F								C	A			F	R		F	F					
middle Eocene	*T. tricantha*	5H-CC	48.34	C	VG	C					C	C		F	F	F				A				C	C			F	C		T	R	F	F			
middle Eocene	*T. tricantha*	6H-CC	57.83	C	M	C					C	C		C	F	C					F			C	A				R	F	F	F					
middle Eocene	*T. tricantha*	7H-CC	67.5	C	VG	F				R	C	A		R	C	F						R		C	A				F		F	R					
middle Eocene	*T. tricantha*	8H-CC	76.66	C	VG	C						C		C	F	C								C	A			R	R	R	R	F	R				
middle Eocene	*T. tricantha*	9H-CC	86.32	A	VG	C					C	C			F	C								C	A			F	R		F	R					
middle Eocene	*T. tricantha*	10H-CC	95.93	C	VG	C					C	C			R	F				R	F			C	A				F		R	F	F				
middle Eocene	*T. tricantha*	11X-CC	104.42	A	VG	F						C		F	F	F					F			C	A			R	F		R						
middle Eocene	*D. mongolfieri*	12X-CC	106.52	A	VG	F						C			F	F						R		C	A					R							
middle Eocene	*D. mongolfieri*	13X-CC	122.47	A	VG	F						C			C	C						R		C	A	F	R	F	P								
middle Eocene	*D. mongolfieri*	14X-CC	132.72	C	VG	F						C		F	C	F					R	R		C	C	F											
middle Eocene	*T. cryptocephala*	15X-CC	141.8	C	VG	F						C			F	C			F	F	F	F	R	F													
middle Eocene-early Eocene	*T. cryptocephala-P. striata striata*	16X-CC	153.37	R	P	R																R															
early Eocene	*P. striata striata*	17X-CC	157.95	A	VG					F		C			F	R	R		C		F	R															
early Eocene	*P. striata striata*	18X-CC	168.92	A	VG		F		F	F	C	C			F				C	R																	
early Eocene	*P. striata striata*	19X-CC	182.16	C	VG					F	C				F		F	R	C																		
early Eocene	*P. striata striata*	20X-CC	191.82	C	VG	F			F	F		C		A	F	F																					
early Eocene	*B. clinata*	21X-CC	199.29	C	VG	R	F		R	F	F	R	F																								
early Eocene	*B. clinata*	22X-CC	208.97	C	G	F	R	F																													
early Eocene	*B. clinata*	23X-CC	218.69	C	G																																
early Eocene	*B. clinata*	24X-CC	228.22	R	P																																
early Eocene	*B. bidartensis*	25X-CC	228.28	T	P																																
late Paleocene-early Eocene	*B. bidartensis*	26X-CC	242.01	C	VG																																
late Paleocene	*B. bidartensis*	27X-CC	249.12	C	VG																																
late Paleocene-early Eocene	*B. bidartensis*	28X-CC	255.38	C	VG																																
early Paleocene-late Paleocene	*B. campechensis*	29X-CC	266.82	C	G																																
early Paleocene-late Paleocene	*B. campechensis*	30X-CC	276.11	R	M																																
early Paleocene-late Paleocene	*B. campechensis*	31X-CC	285.95	C	G																																
early Paleocene-late Paleocene	*B. campechensis*	32X-CC	291.73	C	G																																
early Paleocene-late Paleocene	*B. campechensis*	33X-CC	298.11	C	VG																																
early Paleocene-late Paleocene	*B. campechensis*	34X-CC	300.08	F	M																																
early Paleocene-late Paleocene	*B. campechensis*	35X-CC	314.61	C	G																																
early Paleocene-late Paleocene	*B. campechensis*	36X-CC	319.72	C	VG																																

first appearance. The presence of the marker *B. tetradica* indicates that this sample probably belongs in the *B. clinata* Zone.

Samples from 171B-1050A-22X-CC through 23X-CC were assigned to the *Buryella clinata* Zone (Zone R3). The base of this zone is marked by the FO of *B. clinata* as well as *Lamptonium sanfilippoae* and *Spongatractis babis.* Other marker taxa that make their final appearance in the upper part of the zone are *Bekoma bitardensis* and *Buryella tetradica.*

Samples 171B-1050A-24X-CC and 25X-CC contain rare, poorly preserved radiolarian fragments. Sample 24X-CC contains both *Lithocyclia ocellus* and *Buryella tetradica,* indicating the *B. clinata* Zone. However, Sample 25X-CC contains *B. tetradica* and several forms that range down into the Paleocene, which tentatively indicate the underlying *Bekoma bitartensis* Zone.

Samples 171B-1050A-26X-CC to 28X-CC are assigned to the *Bekoma bidartensis* Zone (Zone R2), which ranges across the Paleocene/Eocene boundary (Table 13). The base of the zone is characterized by the FO of *B. bidartensis* and *Podocyrtis papalis,* and the taxa *Lamptonium f. fabaeforme* and *Calocyclomma castrum* first appear near the base of the zone. The taxa *Pterodon*? *anteclinata* is restricted to this zone, and other forms, such as *Stylosphaera coranatus coranatus* and *S. goruna,* range down into the Paleocene. The remainder of the samples from Site 1050A (Samples 171B-1050A-29X-CC through 36X-CC) are assigned to the mid- to late Paleocene *B. campechensis* Zone (Zone R1). This zone is defined by the FO of *B. campechensis* and contains the distinctive form *Buryella pentadica,* which ranges down into the unzoned Paleocene.

Many of the Paleocene taxa shown in Table 13 are not part of the low-latitude zonal scheme of Riedel and Sanfilippo (1978). However, both Blome (1992) and Nishimura (1992) have shown that many of these are biostratigraphically useful in the Paleocene part of the *Buryella bidartensis* Zone and all through the *B. campechensis* Zone. Examples include *Cromyomma riedeli, Stylosphaera goruna,* and *Stylotrochus alveatus*.

Samples 171B-1050C-2R-CC through 7R-CC all contained faunas assigned to the *Bekoma campechensis* Zone (Zone R1), which is shown in the biostratigraphic correlation (Fig. 28). This zone is defined by the first appearance of *B. campechensis* and contains the common form *Buryella tetradica,* which ranges through the Paleocene and early Eocene. Another *Buryella* species, *B. pentadica,* although generally rare, is also restricted to this zone and is found in Samples 171B-1050C-2R-CC, 4R-CC, and 6R-CC. Sample 171B-1050C-2R-CC contains the best-preserved fauna as well as marker taxa common to Zone R1. However, some of the taxa in Samples 171B-1050C-3R-CC through 7R-CC (Table 14) are not a part of the low-latitude zonal scheme of Riedel and Sanfilippo (1978). Blome (1992) and Nishimura (1992) both demonstrated that many of these taxa can be biostratigraphically useful in the lower part of *B. campechensis* Zone and into the unzoned Paleocene. Specific examples include *Bekoma*(?) *demissa robusta, Entapium chaenapium,* and *Stylotrochus nitidus*. Sample 171B-1050C-10R-2, 32–33 cm, collected immediately above the K/T boundary, surprisingly contained typical lower Paleocene radiolarians that included *Bekoma(?) demissa robusta,* and *Xiphosphaera circularis*. The sample also contained several downhole contaminants including the middle Eocene species *Eusyringium fistuligerum*.

All core-catcher samples from Sections 171B-1050C-11R-CC through 31R-CC were largely barren of identifiable radiolarians. One Late Cretaceous species, *Archaeospongoprunum* sp. cf. *A. rumseyensis,* was found in Sample 171B-1050C-13R-CC, and a relatively well-preserved form assignable to *Orbiculiforma* sp. was recovered in Sample 171B-1050C-28R-CC.

Sediment Accumulation Rate

Ages and sub-bottom depths for planktonic foraminifer and calcareous nannofossil datums used to estimate sedimentation accumulation rates for Hole 1050A are listed in Tables 4 and 6 and are plotted in Figure 30. The 320-m cored interval is estimated to range in age from ~43 to 61 Ma. Datums plotted from both fossil groups for this sequence indicate an average sediment accumulation rate of ~20 m/m.y., which is considerably higher than the sediment accumulation rate at Site 1049, despite their close proximity (~10 km). This difference may be the result of higher biosiliceous productivity over Site 1050, particularly during the middle Eocene. Hiatuses of ~1-m.y. duration occur within the lower Eocene at ~150–160 mbsf and ~280–290 mbsf.

Sediment accumulation rates for Hole 1050C were calculated based on the biostratigraphic datums listed in Tables 5 and 9. A line of correlation is proposed in Figure 31, based on those datums that are believed to be most reliable and tightly constrained.

Sediment accumulation rates for the upper part (327–400 mbsf) of Hole 1050C are relatively poorly constrained because of the generally moderate preservation of planktonic foraminifers and the lack of well-calibrated calcareous nannofossil biohorizons. Given the currently available biostratigraphic information, the sediment must have accumulated at a minimum rate of 20 m/m.y.

Sediment accumulation in the underlying upper Maastrichtian and Danian sequence appears to have been relatively continuous at an average rate of 17 m/m.y., although biostratigraphic control is not greatly refined within this interval. The Maastrichtian sequence lies atop a complex of hardgrounds that includes material of middle Turonian, late Coniacian, Santonian, and late Campanian age. Calculation of sediment accumulation rates for individual parts of this complex would be meaningless. On the whole, however, sediment accumulation for the entire complex was <1.5 m/m.y. The underlying upper Albian–lower Cenomanian sequence is complicated by slumping, which should increase the apparent sediment accumulation rate. However, a significant part of the upper Albian sequence, including the interval with *Planomalina buxtorfi* and *P. praebuxtorfi,* is absent. The resultant short *Rotalipora appeninica* Zone (consisting only of Core 171B-1050C-27R) artificially reduces the sediment accumulation rate for this interval to ~10 m/m.y.

PALEOMAGNETISM

The shipboard paleomagnetic measurements from Holes 1050A and 1050B display a high degree of noise because of weakly magnetized or coring-disturbed sediments, and the magnetostratigraphic interpretations are based largely on thermally demagnetized minicores. Portions from nearly all cores in Hole 1050C yielded high-quality magnetostratigraphic data, which were further enhanced by analysis of minicores. The combined holes resolve the full upper Maastrichtian through middle Eocene paleomagnetic polarity succession.

Laboratory Procedures and Interpretations

Measurements were made using the pass-through cryogenic magnetometer on archive halves of all cores >50 cm long. Most sections obtained in Holes 1050A and 1050B were measured at 5-cm intervals at natural remanent magnetization (NRM) and a single 15-mT alternating-field (AF) demagnetization step. It appears that higher (20-mT) AF demagnetization generally decreased the magnetization intensity (toward the background noise levels of the cryogenic magnetometer system, which were typically 1×10^{-2} mA/m) without significantly enhancing the capacity to determine polarity. Most sections of Hole 1050C were measured at 3-cm intervals at NRM and then either at a 15- or 20-mT AF demagnetization step, with multiple demagnetization steps used for some intervals.

Discrete samples were taken as oriented cylinders or plastic cubes from Holes 1050A and 1050C for post-cruise analysis, using progressive thermal and AF demagnetizations, respectively. A total of 370 cylinders (260 from Hole 1050A; 110 from Hole 1050C) underwent

Table 14. Radiolarian abundance and preservation in Hole 1050C.

Age	Zone	Core, section, interval (cm)	Depth (mbsf)	Abundance	Preservation	*Bekoma (?) demissa robusta*	*Xiphosphaera circularis*	*Dorcadospyris* sp. cf. *D. platycantha*	*Stylosphaera coranatus coranatus*	*Stylosphaera goruna*	*Stylotrochus nitidus*	*Buryella pentadica*	*Buryella tetradica*	*Entapium chaenapium*	*Amphymenium splendiarmatum*	*Bekoma campechensis*	*Entapium regulare*	*Phormocyrtis striata praexquisita*	*Tripocalpis cassidus*	*Lychnocanoma* sp. B	*Stylotrochus alveatus*
		171B-1050C-																			
Paleocene	*B. campechensis*	2R-CC, 20-22	336.97	F	M			R	F			F	F		R	R	F			R	R
Paleocene	*B. campechensis*	3R-CC, 0-2	343.46	F	P		R		F	F			R			R	R	R	R		
Paleocene	*B. campechensis*	4R-6, 61-63	354.41	R	P		R		F			F	R		R	R					
		5R-CC, 25-27	364.1	B																	
Paleocene	*B. campechensis*	6R-CC, 14-16	375.32	F	P		R		F			R	R	R							
Paleocene	*B. campechensis*	7R-4, 66-68	380.36	R	P		R	F	F	R	R										
		8R-CC, 9-10	389.68	B																	
Paleocene		10R-2, 32-33	405.92	T	P	R	R														
		11R-CC, 11-13	412.96	B																	
		12R-1, 18-20	413.88	B																	
		13R-CC, 21-23	433.2	B																	
		15R-CC, 22-24	452.52	B																	
		16R-3, 109-112	456.29	B																	
		17R-CC, 19-22	470.7	B																	
		18R-CC, 0-4	478.86	B																	
		19R-CC, 15-17	484.56	B																	
		20R-5, 41-43	496.96	B																	
		23R-CC, 18-21	529.25	B																	
		24R-3, 69-71	532.15	B																	
		25R-CC, 21-22	544.08	B																	
		26R-CC, 12-14	555.6	B																	
		27R-CC, 23-25	567.65	B																	
		28R-CC, 15-17	577.36	B																	
		29R-CC, 6-8	586.69	B																	
		30R-CC, 20-22	595.81	B																	
		31R-CC, 25-27	605.39	B																	

Notes: Abundance: F = few; R = rare; B = barren; T = trace. Preservation: M = moderate; P = poor.

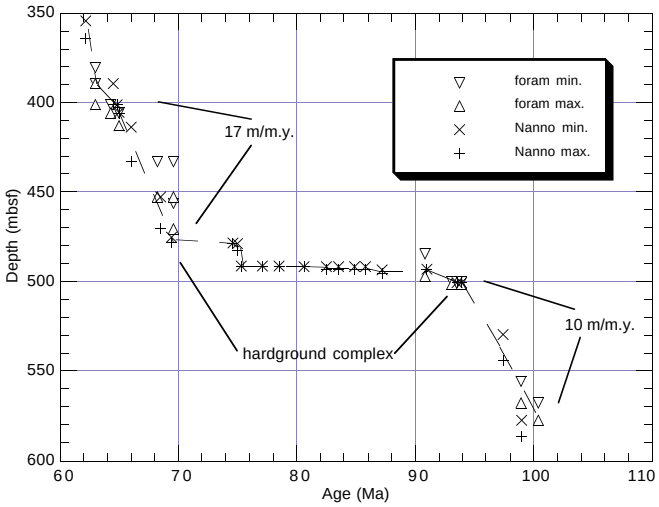

Figure 31. Age-depth relationship in Hole 1050C based on biohorizons presented in Tables 5 and 9.

progressive thermal demagnetization at the University of Oxford and the University of Michigan. These results and polarity interpretations played a key role in the interpretation of the magnetostratigraphy and are included in this *Initial Results* volume (Tables 15–18 [15, 17 in ASCII format; 16, 18 in PDF format] on CD-ROM, back pocket, this volume). Progressive thermal demagnetization steps were generally at 30°C increments from ~140° through 360°C, with continuation to higher thermal steps for the more stable samples.

In contrast to the magnetic behavior in the sediments recovered at Site 1049, the bioturbated firm oozes and chalks of Holes 1050A and 1050B do not exhibit a significant drilling-induced overprint. However, the older chalks and claystones of Hole 1050C exhibit such a drilling-induced overprint that is generally oriented steeply downward (high positive inclination) and radially inward (apparent preferential declination toward 0° or "north" when measuring the archive half of each split section). The same type of drilling-induced overprint has been described in the summary section in site chapters in Curry, Shackleton, Richter, et al. (1995).

The NRM of sediments recovered in Holes 1050A and 1050B exhibits common variable (and quasi-random) inclinations and declinations, and these patterns were improved only slightly by applying 15-mT AF demagnetization. In contrast, the secondary overprints on older Hole 1050C sediments were significantly removed by the 20-mT AF demagnetization step. In all holes, a thermal demagnetization step of 200°C was generally adequate to remove overprints. Most sediments from Holes 1050A and 1050B lost nearly all of their magnetization or became magnetically unstable at thermal steps exceeding 330°C.

Why are the Eocene intervals of Site 1050 less suitable for obtaining a magnetostratigraphy using the pass-through magnetometer than coeval sediments at Site 1049? We suggest three possible contributing factors. First, most of these nannofossil oozes and chalks, especially those with light green color, have weak magnetizations, and the magnetic carriers are probably diluted by biogenic components or are partially removed during diagenetic reactions. Second, the light yellow nannofossil oozes, constituting the upper 40 m at this site, may be discolored from long-term exposure to the overlying oxidizing bottom waters. Thus, the prevalent "normal-polarity" inclinations may represent a late-stage chemical remanent magnetic carrier (goe-

thite) that required removal by thermal demagnetization. Third, most XCB cores were rendered into alternations of 5- to 10-cm-thick drilling biscuits with equal thicknesses of homogenized slurry, and a new magnetization is imparted to this "drilling sediment" as it becomes firmer.

In contrast, polarity intervals in sediments from Hole 1050C were generally easy to distinguish using the shipboard pass-through magnetometer. Indeed, some polarity transitions could be resolved to 20-cm precision within intact blocks (e.g., the base of mid-Danian Chron 28r). The only portions of the section that yielded ambiguous shipboard paleomagnetic results are the Upper Cretaceous and Albian, which are affected by slumping, tectonic tilting, and fracturing of strata, and intervals recovered with biscuits or blocks in drilling slurry. However, even in these intervals, the polarity could generally be resolved even though the declinational data are distorted.

The demagnetized shipboard data were filtered before plotting by removing (1) the few measurements with inclinations >80° that were assumed to be dominated by a steep-downward drilling overprint; (2) data from the uppermost 20 cm of each core, where brecciation or downhole contamination are common; and (3) data within 5 cm of the ends of each section. We also omitted all samples with magnetizations $<5 \times 10^{-3}$ mA/m, presuming that these would contain an unacceptable high component of noise. A three-point moving average was applied to the inclination record within each core to smooth artifacts before plotting (Figs. 32–34).

Biomagnetostratigraphy

Polarity Zones and Chron Assignments

Recognition of polarity zones within the Eocene portion of Site 1050 relies heavily upon the extensive suite of thermally demagnetized minicores (Fig. 32), although a few of the polarity intervals can be recognized within the shipboard pass-through magnetometer data. Although the shipboard interpretations were generally reliable, the post-leg analysis of minicores enhanced the recognition of polarity zones within the Paleocene and Cretaceous portions of Site 1050. Assignment of polarity chrons to the polarity zones relies on the micropaleontology datums (especially nannofossil zones) and the chronostratigraphy of Berggren et al. (1995) and Gradstein et al. (1995).

Eocene

The uppermost 150 m of Site 1050 displays a relatively expanded section of middle Eocene. The major reversed-polarity Chron C20r of mid-Lutetian age provides a distinctive polarity feature that is assigned to the reversed-polarity zone (65–140 mbsf) coincident with nannofossil Zone CP13b (Fig. 35). Above Chron C20r is a trio of N-R-N polarity intervals within the minicore suite from Hole 1050A, and it is also recognized in the long-core measurements from Hole 1050B. This trio is tentatively assigned to Chrons C19n-C19r-C20n. Across a pronounced hardground at ~155 mbsf, the nannofossil biostratigraphy indicates the juxtaposition of Zone CP12b above Zone CP11. The magnetic polarity is normal on either side of this hardground, and the biomagnetostratigraphy implies that most of Chron C21n overlies a truncated Chron C22n—a hiatus of ~1.5 m.y. that encompasses nannofossil Zone CP12a and the lower portion of CP12b, according to the Berggren et al. (1995) time scale (Fig. 35). However, there is an apparent mismatch between the base of the overlying nannofossil Zone CP13a in these holes within the lower portion of a reversed-polarity zone (assigned as basal Chron C20r) and its placement in the Berggren et al. (1995) chronostratigraphy (in the middle of the earlier normal-polarity Chron C21n). This discrepancy may be a calibration uncertainty, an unrecognized minor hiatus, or a reflection of the need for improved biostratigraphy.

A second sedimentary discontinuity occurs at ~195 mbsf in Hole 1050A, where nannofossil Zone CP10 was not recognized. However, the apparent polarity pattern in Hole 1050A spanning this discontinuity seems to indicate a continuous succession from Chron C24r (earliest Eocene) through Chron C22r. Therefore, it is suggested that this sedimentary break is not as pronounced as was presumed from the shipboard paleontologic interpretation.

Paleocene

The polarity succession of Holes 1050A through 1050C represents a complete Paleocene magnetostratigraphy and can serve as a reference site for the calibration of biostratigraphic datums to polarity chrons.

The upper Paleocene magnetostratigraphy of Hole 1050A displays an apparently undistorted match to the late Paleocene polarity time scale of Chron C24r through Chron C26r. There remains a minor disagreement at ~260 mbsf (upper portion of Core 171B-1050A-29X), where the polarity pattern indicates the brief Chron C25n; however, the nannofossil biostratigraphy has not yet suggested the presence of Zones CP7 through CP8a, which encompass this chron.

The base of Chron C26r—hence, the base of the late Paleocene—is at ~333 mbsf (lower portion of Core 171B-1050C-2R). The polarity pattern of Hole 1050C downward to the K/T boundary, at ~405 mbsf, duplicates the scaling of Chrons C27r through C29r. The assignment of these chrons is within the uncertainty of the shipboard biostratigraphy. Therefore, it appears that the Danian stage has a constant sedimentation rate (20 m/m.y.) from the top of Chron C29r to the base of Chron C27n.

Maastrichtian and Campanian

The Maastrichtian chalks exhibit a dominance of normal polarity (Fig. 34). Weak magnetizations, coupled with coring gaps, preclude an elegant correlation to the magnetic polarity time scale. A reversed-polarity zone in Core 171B-1050C-15R is tentatively assigned to Chron C30r, thereby implying correlations of Chron C30n and Chron C31n to the adjacent normal-polarity intervals. The lower 7 m of polarity zone C31n is a major slump deposit (Sections 171B-1050C-17R-2 through 17R-7). The Maastrichtian strata below the slump are reversed in polarity, which must be a portion of Chron C31r. The basal Maastrichtian is normal in polarity and is assigned to Chron C32n.1n of the basal Maastrichtian. These assignments, coupled with the compact thickness of polarity zone C31r, imply that the removal of most of the lower Maastrichtian is associated with the major slump in Core 171B-1050C-17R.

The lowest recovered Maastrichtian white chalks have a sharp contact with the upper Campanian tan chalk near the top of Core 171B-1050C-19R. The Campanian overlies Coniacian strata above pronounced phosphatic and iron-manganese hardgrounds in Section 171B-1050C-20R-1. This thin slice of the upper Campanian has reversed polarity in Core 171B-1050C-19R and normal polarity in the underlying Core 20R. The associated nannofossil assemblages indicate an age range from near the middle of Zone CC23 through Zone CC21; therefore, we assign these polarity zones to lower Chron C32r and uppermost Chron C33n.

Coniacian Through Upper Albian

All Coniacian, Turonian, and lower Cenomanian through upper Albian cores yielded normal polarity within the Cretaceous Long Normal Chron C34n. Drilling did not penetrate the uppermost middle Albian to test the validity and accurately date the elusive reversed-polarity "M–3" subchron (e.g., Ryan et al., 1978; Gradstein et al., 1995). The discrete minicores yielded stable magnetic directions and will be used to derive a paleolatitude history during further post-cruise paleomagnetic studies.

CORE-CORE INTEGRATION

At Site 1050, magnetic susceptibility and GRAPE density data from the multisensor track (MST) and reflectance data from the

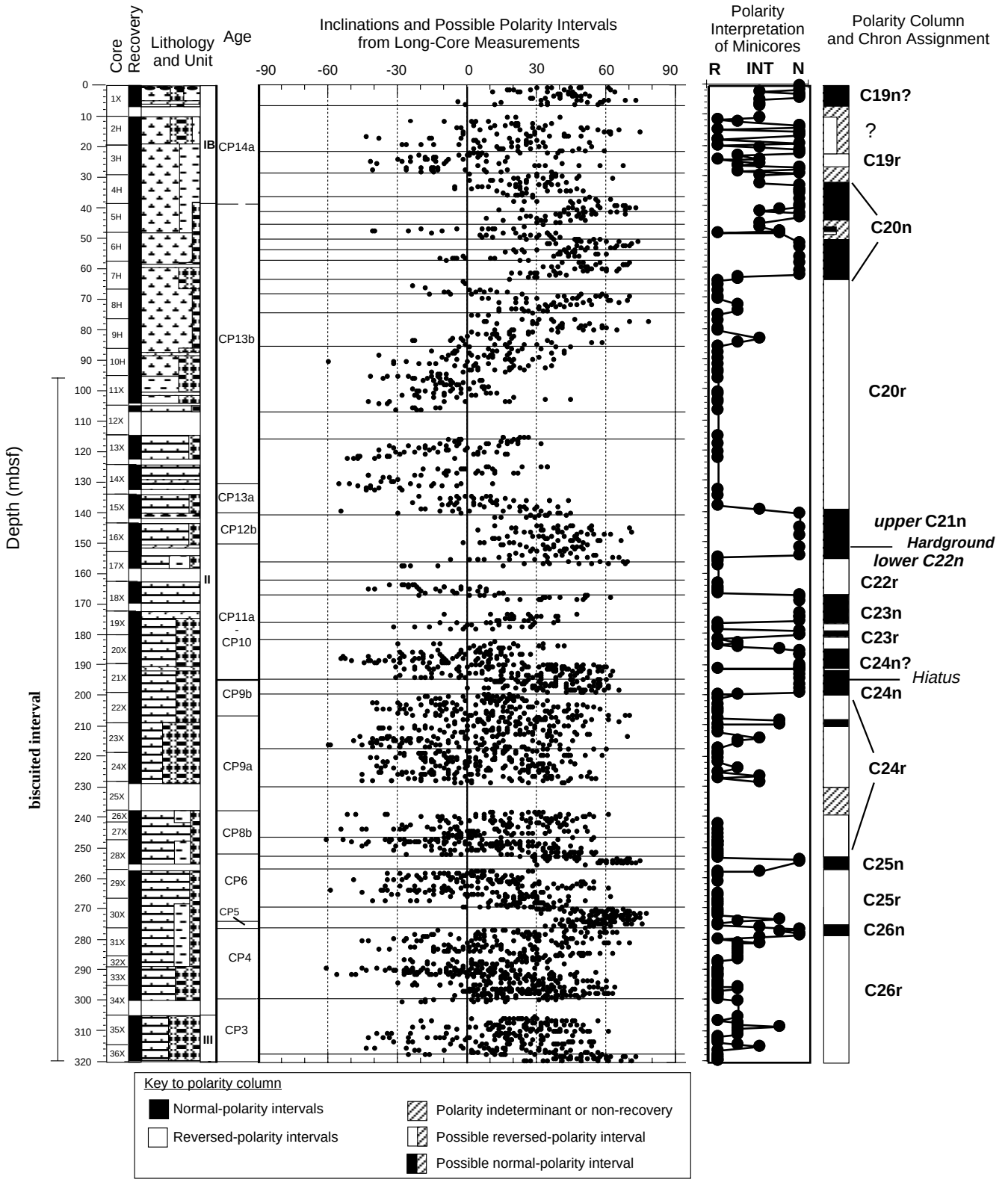

Figure 32. Magnetostratigraphy of Hole 1050A. Magnetic inclinations from long-core measurements are after AF demagnetization at 15, 20, or 25 mT and were filtered using a three-point moving average. Measurements from the uppermost 20 cm of each core and those having anomalously high or low magnetic intensities were removed. Horizontal lines delineate clusters of predominantly positive, negative, or equally mixed magnetic inclinations that were used for a preliminary shipboard polarity column. Polarity of discrete minicores are from interpretation of progressive thermal demagnetization and are assigned relative degrees of certainty. These polarity interpretations from discrete samples are given priority in the compilation of the summary polarity column. Polarity chron assignments are based upon the polarity zone pattern and nannofossil biostratigraphy.

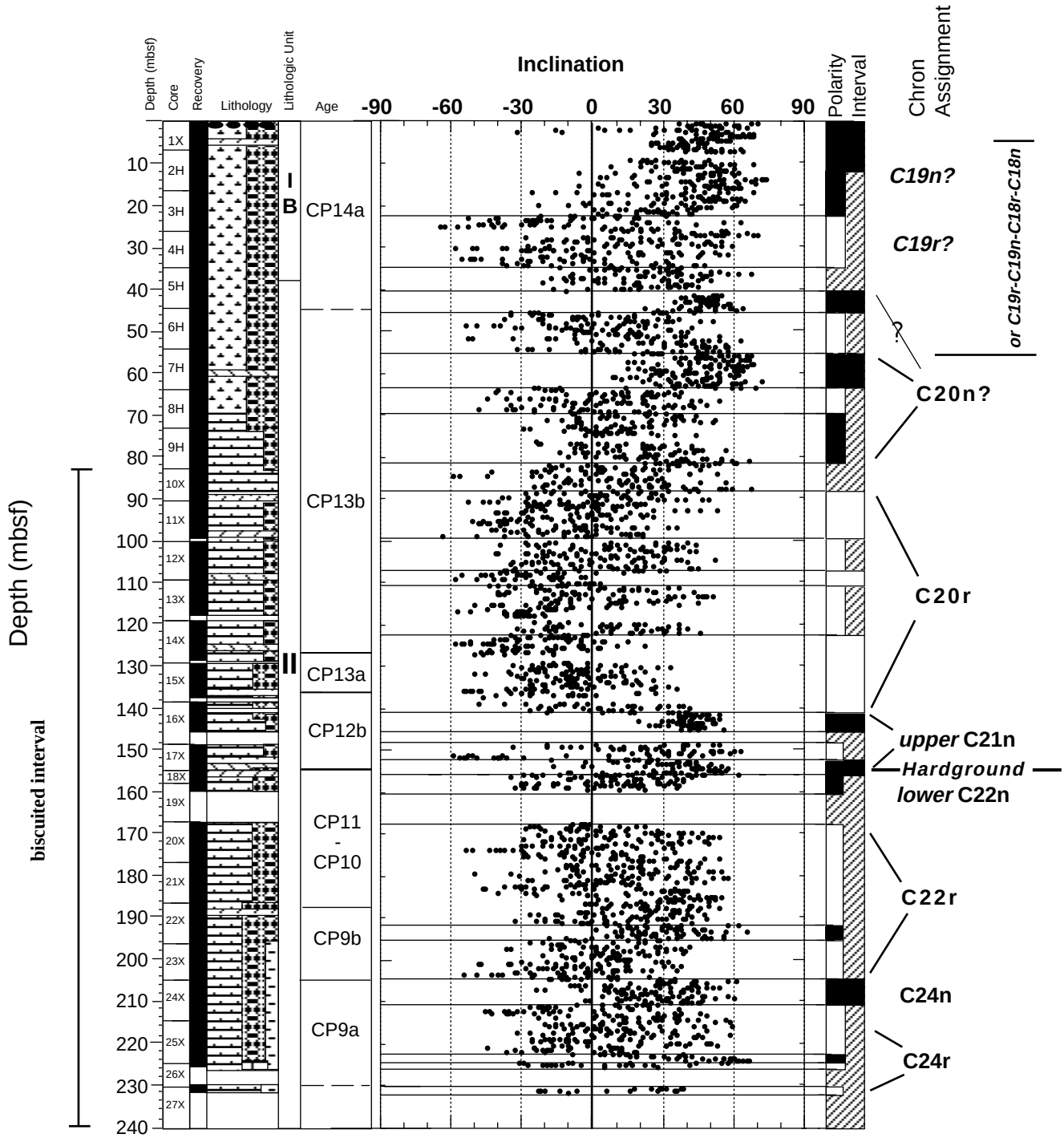

Figure 33. Magnetostratigraphy of Hole 1050B. Magnetic inclinations from long-core measurements are after AF demagnetization at 20 mT and were filtered using a three-point moving average. Measurements from the uppermost 20 cm of each core and those having anomalously high or low magnetic intensities were removed. Horizontal lines delineate clusters of predominantly positive, negative, or equally mixed magnetic inclinations that were used for a preliminary shipboard polarity column. Polarity chron assignments are based upon the polarity zone pattern and nannofossil biostratigraphy.

Minolta color scanner were available for attempting precise core-core integration. Only Holes 1050A and 1050B had significant overlap at Site 1050, which limited the potential for constructing a composite section. Several different types of output from the Minolta color scanner were examined: reflectance near the middle of the spectrum (480 nm), reflectance at the red end of the spectrum (700 nm), and the L*a*b lightness and chromaticity coordinates that are more suited to this work than the generally used Munsell color code (which uses a mixture of letters and figures). All data used are available in Tables 19–21 (CD-ROM, back pocket, this volume). Both the color and the lightness give a clear differentiation of the sediment in different intervals; lightness may be more useful where the chief characteristics of the record are light–dark changes, whereas the chromaticity coordinates are more appropriate where there are color changes within light sediment. If pure reflectance in a single wavelength channel is examined, the pattern of reflectance variability along a core is sim-

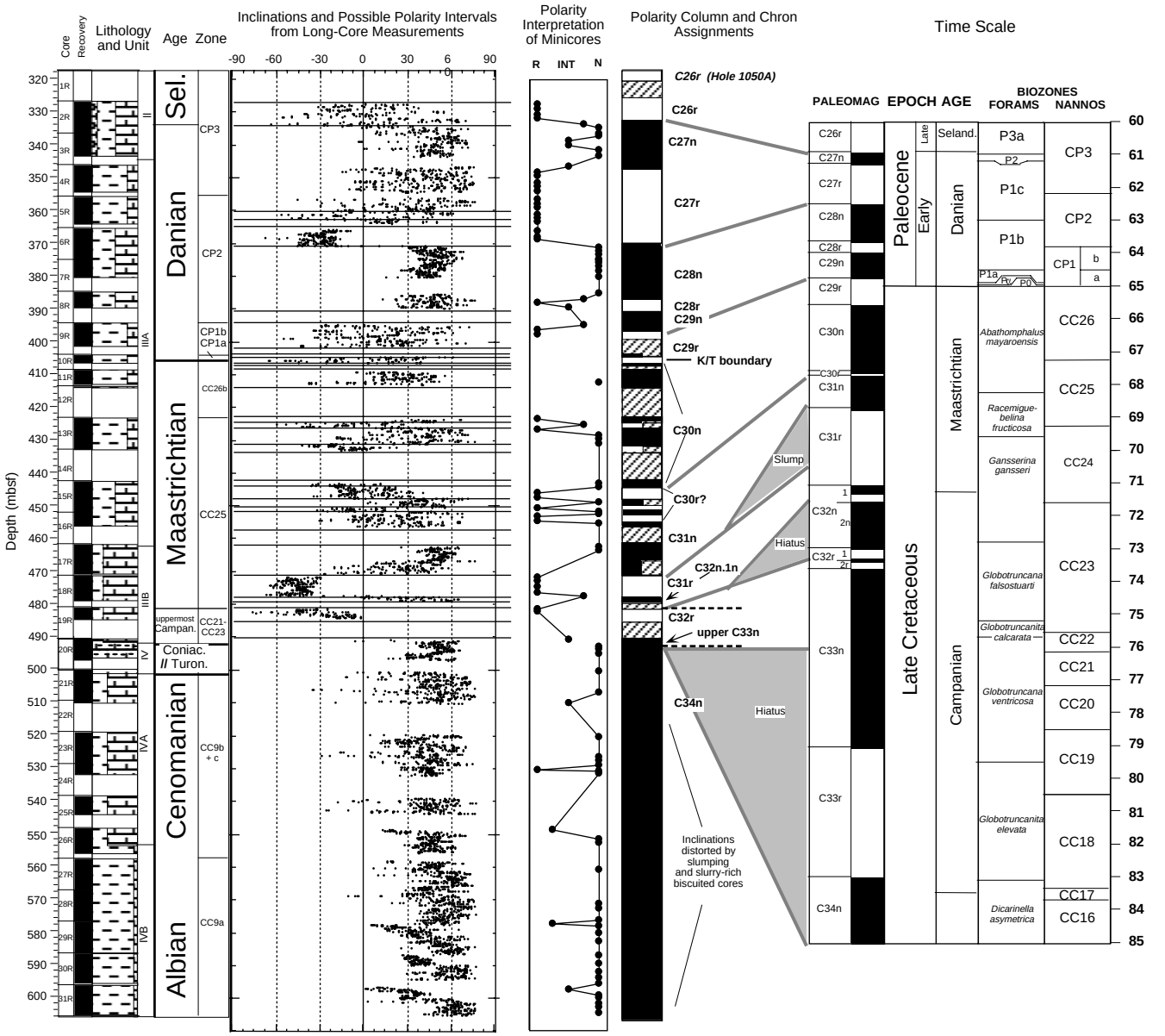

Figure 34. Magnetostratigraphy of Hole 1050C. Magnetic inclinations from long-core measurements are after AF demagnetization at 20 mT and were filtered using a three-point moving average. Measurements from the uppermost 20 cm of each core and those having anomalously high or low magnetic intensities were removed. Horizontal lines delineate clusters of predominantly positive, negative, or equally mixed magnetic inclinations that were used for a preliminary shipboard polarity column. Polarity of discrete minicores are from interpretation of progressive thermal demagnetization and are assigned relative degrees of certainty. These polarity interpretations from discrete samples are given priority in the compilation of the summary polarity column. Polarity chron assignments to the Paleogene and Cretaceous magnetic polarity time scale are based upon the polarity zone pattern and nannofossil biostratigraphy.

ilar over the whole spectrum, but the signal-to-noise ratio appears to be slightly higher at the red (long wavelength) end of the spectrum.

Figure 36 shows composite records of susceptibility, chromaticity coordinate a, and reflectance in the red band at Site 1050. The striking change in color from yellowish to greenish that was observed between Cores 171B-1050A-4H and 5H, and in Core 171B-1050B-5H at about 37.8 mbsf, it is clearly recorded as a change in chromaticity at 38.75 m composite depth (mcd). Elsewhere in the section, changes in color are evident. A comparison of Figures 36B (chromaticity a) and 36C (red reflectance, 700 nm) shows that even over intervals where the recorded reflectance values are noisy, the color value is relatively stable.

The magnetic susceptibility record of Site 1050 was difficult to use as a correlation tool for two reasons. First, the susceptibility values are low through most of the section (below 2×10^{-6} SI units over most of the upper 150 m, rising to 8×10^{-6} SI units at the bottom of the hole). At such low values, drift in value through each section measured becomes significant so that the observed quasi-cyclic variability with 1.5-m wavelength is an artifact. Second, the record is characterized by sporadic spikes to more than 100×10^{-6} SI units. A few of these spikes are caused by ash layers that are visible in the split section, but the majority are not. Furthermore, although some of the spikes appear to correlate between the holes, especially those associated with ash layers (e.g., evident at 61.3 mcd in Fig. 36A), others do not. Many of the spikes occur within intervals of generally higher susceptibility, and it is possible that they arise from pyrite nodules. In the Neogene sediments recovered during Leg 154, it was observed that pyrite nodules (and associated magnetic susceptibility spikes)

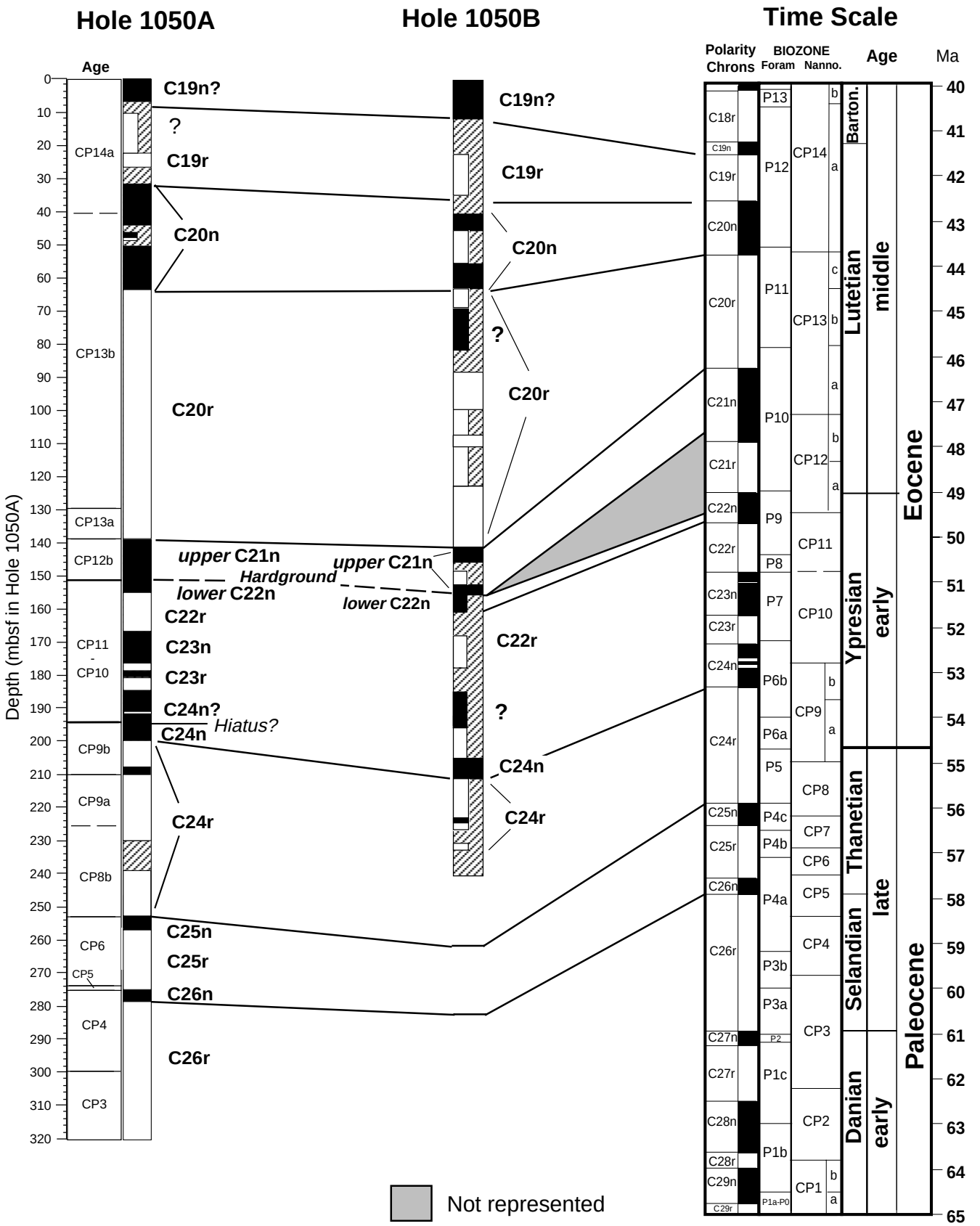

Figure 35. Comparison of polarity interpretations from Holes 1050A and 1050B with Paleogene chronostratigraphy. Polarity chron assignments are based upon the polarity zone pattern and nannofossil biostratigraphy. The polarity column from Hole 1050A is derived largely from post-cruise thermal demagnetization of 260 discrete minicores, whereas the column from Hole 1050B is an interpretation of shipboard long-core measurements. Therefore, Hole 1050A was used exclusively for assignment of polarity chrons.

were generally more common in intervals of higher background susceptibility. On the other hand, some spikes may reflect downhole contamination between the core and the core liner, some of which is removed as the core sections are split.

GRAPE density was seldom useful for correlation between holes at Site 1050. However, there is more potential for using GRAPE density than may be expected at a site where most of the recovery was with the XCB. In the rare intervals where the color shows clear cyclicity, the GRAPE output also shows cyclicity. The values cannot, of course, be equated with sediment density unless the core liner is completely filled; thus, in principle, the cyclicity could arise either from changes in the diameter of the recovered core (which might be controlled by lithologic change) or from variations in its density. Our observations at the MST suggest that, in general, the diameter of XCB core does not vary in a systematic manner and that where GRAPE values vary cyclically, the cause is probably true density variability.

A tentative composite section was constructed for Site 1050 (Table 22), but readers should be warned that many of the adjustments made are weakly justified. However, this composite section does allow the construction of spliced records for the site that does not entail jumps in absolute magnitude at each point where the splice makes a transition from one hole to the other. The spliced magnetic susceptibility record (Fig. 36A) was constructed to avoid (where a choice between holes was available) intervals containing spikes. On the other hand, the color splices (Fig. 36B,C) were constructed to make use of the less noisy data because a few cores yielded extremely noisy reflectance data for unknown reasons (possibly related to the core condition or its position in the liner).

Although two holes were cored, for which the links in the composite section are weakly justified, it is apparent that there are a number of gaps where no sediment was recovered in either hole. Nevertheless, the use of this composite section should assist in the selection of intervals for high-resolution sampling of the cores.

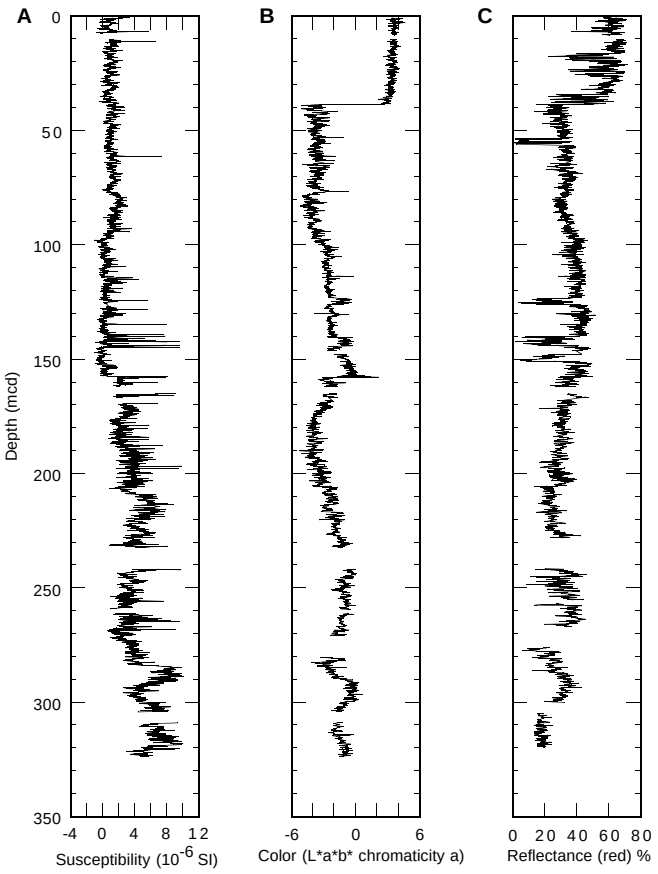

Figure 36. **A.** Spliced magnetic susceptibility record for Holes 1050A and 1050B vs. mcd. **B.** Spliced L*a*b chromaticity a color record for Holes 1050A and 1050B vs. mcd. See "Lithostratigraphy" section (this chapter) for descriptions of the colors in the sedimentary section. **C.** Spliced red-band reflectance record for Holes 1050A and 1050B vs. mcd. See "Lithostratigraphy" section (this chapter) for descriptions of the light–dark variations in the sedimentary section. See Tables 19 through 21 (CD-ROM, back pocket, this volume) for all data used for core-core integration.

ORGANIC GEOCHEMISTRY

Hole 1050A

Gas Analyses

In Hole 1050A, gas chromatographic analyses of headspace samples detected methane (C_1), with a trace of ethane (C_2) and ethylene (C_2=) below 260 mbsf (Table 23). Samples were also analyzed for total organic carbon, total carbon, carbonate, nitrogen, and sulfur (Table 24). C_1/C_2 ratios below 261 mbsf were within the potentially hazardous range of <100 (Fig. 37). No action was taken because the gas content remained below 0.1 vol% C_1. Because no hazardous levels of gas were detected in Hole 1050A, gases were not measured in Hole 1050B.

The headspace gas analyses were grouped into five gas zones based on the average methane content remaining in the sediment after coring. The gas zones appear to be related to changes in lithostratigraphy. The surface gas zone, which averages 46-ppm C_1 (Table 23), occurs within lithologic Subunit IB, a yellowish siliceous nannofossil chalk from 2 to 40 mbsf (Fig. 37). The middle gas zone, which averages 125 ppm C_1, occurs within lithologic Subunit IC, a greenish siliceous nannofossil ooze. The deep I gas zone, which averages 225-ppm C_1, occurs in the upper portion of Subunit ID, a greenish siliceous nannofossil chalk. The transition from Subunit IC to Subunit ID is also marked by a decrease in carbonate content from an average of 75 wt% in Subunit IC to 57 wt% in Subunit ID (Fig. 38; Table 24).

The deep II and deep III gas zones are characterized by the presence of ethane and increased methane contents. The deep II gas zone, which averages 366 ppm methane, occurs in the lower portion of lithologic Subunit ID.

The deep III gas zone, which averages 896 ppm methane, occurs within lithologic Unit II, an olive green diatomaceous nannofossil chalk. The transition from lithologic Subunit ID to lithologic Unit II is also accompanied by a decrease in carbonate content to an average of 36 wt% (Fig. 38; Table 24).

Hole 1050C

Gas Analyses

In Hole 1050C, gas chromatographic analyses of headspace samples detected small quantities of methane (C_1), with traces of ethane (C_2) and propane (C_3) (Table 25). Throughout most of the hole, the $C_1/(C_2 + C_3)$ ratio was in the potentially hazardous range of <100 (Table 25; Fig. 39). No restriction on drilling activities was required because the total gas content remained below 0.01 vol% C_1.

Five gas zones with varying amounts of average gas content were recognized in Hole 1050C (Fig. 39). These gas zones are distinguished from those identified in Hole 1050A by the suffix "C." The middle IC gas zone is in lithologic Unit III and has a relatively high C_1 content, averaging 25 ppm C_1. The transition from lithologic Unit III to Subunit IVA forms the upper boundary of the deep IC gas zone, which is marked by a sharp drop in C_1 content from 26 to 6 ppm and a lower C_1 content, averaging 14 ppm. After the sharp drop, the C_1 content generally increases again, reaching a peak of 20 ppm near the bottom of the deep IC gas zone at 462 mbsf (Fig. 39). The transition from lithologic Subunit IVB to Subunit IVC forms the upper boundary of the deep IIC gas zone, which contains the peak C_1 content in

Table 22. Offsets applied to individual cores at Site 1050 to create an approximate composite section.

Core	Offset (m)
171B-1050A-	
1X	0.84
2H	0.19
3H	0.16
4H	0.02
5H	0.02
6H	1.89
7H	2.41
8H	3.49
9H	4.07
10H	5.21
11X	4.65
13X	3.96
14X	4.36
15X	4.36
16X	4.36
17X	4.36
18X	5.36
19X	3.42
20X	2.74
21X	3.71
22X	3.71
23X	2.97
24X	4.15
26X	4.15
27X	4.15
28X	4.15
29X	4.15
30X	4.15
31X	4.15
32X	4.15
33X	4.15
34X	4.15
35X	4.15
36X	4.15
171B-1050B-	
1X	0.00
2H	0.00
3H	0.12
4H	0.12
5H	0.95
6H	0.95
7H	1.94
8H	1.54
9H	5.34
10X	4.00
11X	4.74
12X	4.74
13X	4.74
14X	4.74
15X	3.48
16X	4.38
17X	2.22
18X	3.98
19X	7.28
20X	1.82
21X	1.82
22X	–0.39
23X	2.95
24X	3.53
25X	3.45
27X	5.99

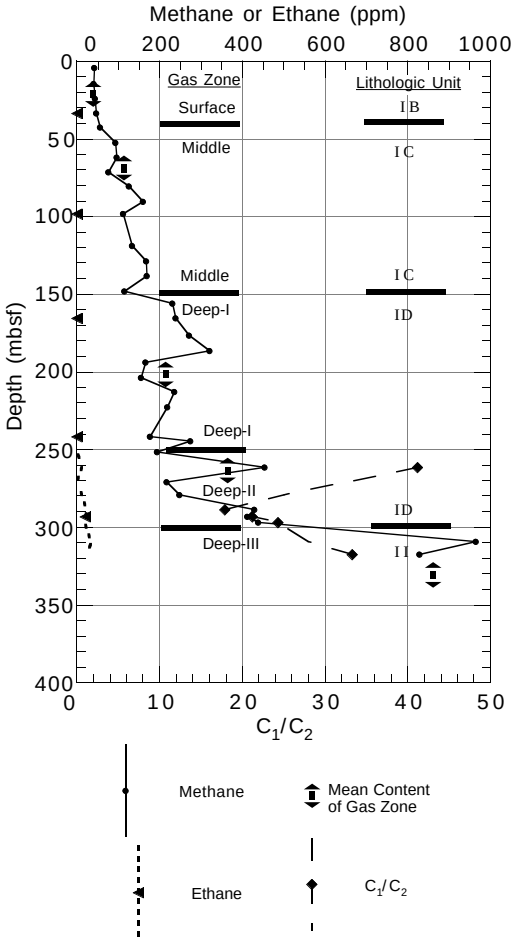

Figure 37. Methane (C_1) and ethane (C_2) contents and C_1/C_2 vs. depth in Hole 1050A. Lithologic units are described in the "Lithostratigraphy" section (this chapter).

the hole at 32 ppm and also has a high average gas content of 25 ppm. The deep IIC gas zone is entirely within lithologic Subunits IVC and Unit V. The transition from lithologic Unit V to Subunit VIA is marked by a decrease in gas content from 27 ppm in the deep IIC zone to 13 ppm in the middle of the deep IIIC zone. The deep IIIC gas zone, contained within lithologic Subunit VIA, is marked by a relatively low C_1 content, averaging 15 ppm. The deep IVC gas zone is within lithologic Subunit VIB and extends to the bottom of the hole at 606 mbsf (Fig. 39). This gas zone has an average gas content of 15 ppm, which is similar to that found in the deep IIIC gas zone but is distinguished by an abruptly changing gas content with depth.

Elemental Analyses

Three samples were taken from each core for carbon, carbonate, and total carbon, hydrogen, nitrogen, and sulfur (CHNS) analyses. In addition, scientists could select samples from other intervals in the core. We analyzed 49 samples over the 289-m section at Hole 1050C (Table 26; Fig. 40). Carbonate content generally increases from 34 wt% at the transition from lithologic Unit III to Subunit IVA to a peak of 94 wt% in lithologic Subunit IVC (Fig. 40). From the peak in lithologic Unit IVC, carbonate content shows a variable but generally decreasing trend from 80 wt% at the top of lithologic Subunit VIA to 32 wt% near the base of lithologic Subunit VIB. At the contact of lithologic Subunit VIA with Subunit VIB, carbonate content shows a sharp drop from a peak of 90 wt% to an average of about 40 wt% in lithologic Subunit VIB. The change in carbonate content correlates well with the lithologic change from Subunits VIA to VIB (Fig. 40).

TOC content is low, averaging 0.2 wt% and ranging from below the detection limit to 1.2 wt% (Table 25; Fig. 40). Overall, the average TOC content is comparable to the values measured in equivalent-aged strata at Sites 1051 and 1052. Like the lower Cenomanian to upper Albian claystones at Site 1052, these claystone-rich beds tend to have a higher TOC content.

Sulfur occurs only sporadically in the sediments (Fig. 41), and its occurrence is restricted to the claystones of Units VIA and VIB. The sulfur content averages only 0.03 wt% and ranges from 0 to 0.48 wt% (Table 25). The sulfur-bearing samples also tend to have an increased TOC content (Fig. 41). The variation of the occurrence and amount of sulfur may represent the sporadic deposition or preservation of marine kerogen, which carries much of the sulfur contained in the sediments.

Hydrogen content is also low, averaging 0.34 wt% and ranging from 0.04 to 0.78 wt%. Hydrogen is present in all samples (Fig. 41)

Table 23. Headspace gas composition from Hole 1050A.

Depth (mbsf)	Gas zone	C_1	C_2	C_2=	C_1/C_2	Comments
4.5	Surface	42.3				No significant gas voids
14.6	Surface	40.6				No significant gas voids
24.1	Surface	42.89				No significant gas voids
33.6	Surface	47.49				No significant gas voids
43.1	Surface	54.98				No significant gas voids
52.6	Middle	92.31				No significant gas voids
62.1	Middle	96.4				No significant gas voids
71.6	Middle	76.4				Minor gas voids in core; 3-5 mm gaps
80.7	Middle	125.5				Minor gas voids in core; 3-5 mm gaps
90.6	Middle	159.2				No significant gas voids
98.6	Middle	110.6				No significant gas voids
119.3	Middle	133.7				No significant gas voids
128.9	Middle	167.7				No significant gas voids
138.5	Middle	169.3				No significant gas voids
148.1	Middle	114.9				No significant gas voids
156.2	Deep I	230.7				No significant gas voids
165.8	Deep I	238.9				No significant gas voids
176.9	Deep I	271.3				No significant gas voids
186.5	Deep I	319.6				No significant gas voids
194.1	Deep I	165.5				No significant gas voids
203.7	Deep I	154.2				No significant gas voids
213.3	Deep I	236.2				No significant gas voids
222.9	Deep I	219.2				No significant gas voids
241.7	Deep I	176.1				No significant gas voids
244.7	Deep I	273.5				No significant gas voids
251.8	Deep I	192.8				No significant gas voids
261.4	Deep II	452.7	11		41.15	No significant gas voids
271	Deep II	217.5				No significant gas voids
279.5	Deep II	247.5	9.9		25.00	No significant gas voids
288.7	Deep II	428.4	24		17.85	No significant gas voids
293.4	Deep II	411.8	19.4		21.23	No significant gas voids
296.8	Deep II	437.3	18		24.29	No significant gas voids
309.4	Deep III	963.8	34.5		27.94	No significant gas voids
317.5	Deep III	827.5	24.9	9.2	33.23	No significant gas voids

Notes: In all cases, the injected sample size was 5 cm^3. Concentration of gas is in parts per million by volume. Where no values are reported, concentrations are below detection limits.

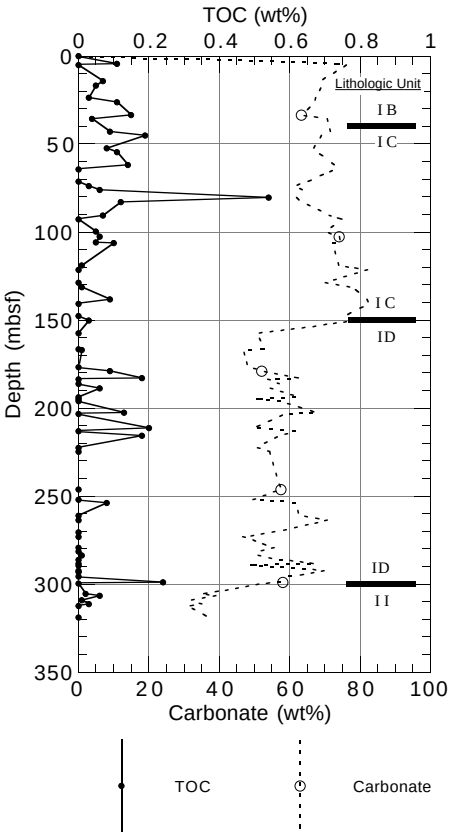

Figure 38. TOC and $CaCO_3$ contents vs. depth in Hole 1050A. Except for the value of 0.54 wt% at 80.5 mbsf, the TOC content is essentially below the detection limit of the difference method. Lithologic units are described in the "Lithostratigraphy" section (this chapter).

and tends to increase as TOC increases. This sympathetic relationship may represent a constant low background level of kerogen deposition, which carries much of TOC and hydrogen contained in the sediments.

Nitrogen occurs only sporadically in the sediments (Fig. 41). The nitrogen content is low, averaging 0.02 wt% and ranging from 0.0 to 0.17 wt%. The variation of nitrogen content may also represent the sporadic deposition or preservation of marine kerogen, which carries much of the nitrogen content in sediments.

Discussion

The strata in Hole 1050C are moderately to heavily bioturbated (see "Lithostratigraphy" section, this chapter). This suggests that the low quantities of TOC, S, N, and H measured in these sediments are the result of bioturbation and oxidation during early diagenesis (see "Organic Geochemistry" section, "Site 1050" and "Site 1052" chapters, this volume). The low level of hydrogen in these sediments suggests that what kerogen remains is a low-hydrogen type III or a type IV similar to that found at Site 1052.

The small quantities of methane measured in Hole 1050C are also consistent with the small amounts of TOC found in the sediments here, as well as those at nearby sites drilled during Leg 171B. The thick claystone beds near the bottom of Hole 1050C may limit the upward migration of hydrocarbons generated from deeper sources.

INORGANIC GEOCHEMISTRY

Analytical Results

Interstitial-water samples were taken from 25 core samples in Holes 1050A and 1050C. Shipboard interstitial-water data from Site 1050 are presented in Table 27. Most pore-water salinities at Site 1050 are within a narrow range similar to that recorded in Hole 1049A (35–36), except for two slightly higher values (37 and 38 at 119.25 and 309.30 mbsf, respectively; Fig. 42A).

Table 24. Total inorganic carbon, carbonate, total carbon, total organic carbon, nitrogen, and sulfur analyses for Hole 1050A.

Core, section, interval (cm)	Midpoint (mbsf)	TIC (wt%)	$CaCO_3$ (wt%)	TC (wt%)	TOC (wt%)	N (wt%)	S (wt%)
171B-1050A-							
1X-3, 133-138	4.4	8.87	73.91	8.98	0.11		
1X-4, 73-74	5.2	9.13	76.07	9.11	0.00		
2H-3, 133-138	14.5	8.25	68.71	8.32	0.07		
2H-5, 77-78	16.9	8.30	69.16	8.35	0.05		
3H-3, 135-140	24.0	8.09	67.39	8.12	0.03		
3H-5, 78-79	26.4	8.05	67.09	8.16	0.11		
4H-3, 135-140	33.5	7.60	63.30	7.75	0.15		
4H-5, 78-79	35.9	8.46	70.50	8.5	0.04		
5H-3, 135-140	43.0	8.58	71.50	8.67	0.09		
5H-5, 77-78	45.4	8.26	68.84	8.45	0.19		
6H-3, 135-140	52.5	8.01	66.72	8.09	0.08		
6H-5, 77-78	54.9	8.11	67.53	8.22	0.11		
7H-3, 135-140	62.0	8.71	72.52	8.85	0.14		
7H-5, 78-79	64.4	8.73	72.68	8.73	0.00		
8H-3, 136-140	71.5	7.81	65.07	NA	NA	NA	NA
8H-5, 78-79	73.9	7.36	61.30	7.39	0.03		
8H-7, 20-21	76.3	7.61	63.42	7.67	0.06		
9H-3, 132-137	80.5	7.43	61.86	7.97	0.54		
9H-5, 78-79	83.0	7.59	63.21	7.71	0.12		
10H-3, 134-139	90.5	8.55	71.21	8.62	0.07		
10H-5, 85-86	93.0	8.97	74.68	8.91	0.00		
11X-3, 132-135	99.9	8.43	70.22	8.48	0.05		
11X-5, 104-105	102.6	8.89	74.05	8.95	0.06		
12X-1, 78-79	106.0	8.92	74.30	8.97	0.05		
12X-1, 107-109	106.3	8.67	72.20	8.77	0.10		
13X-3, 133-135	119.1	8.86	73.84	8.87	0.01		
13X-5, 81-82	121.6	9.86	82.09	9.32	0.00		
14X-3, 133-137	128.8	8.40	69.95	8.26	0.00		
14X-5, 83-84	131.2	9.33	77.73	9.34	0.01		
15X-3, 131-134	138.3	9.82	81.82	9.91	0.09		
15X-5, 73-74	140.7	9.90	82.43	9.89	0.00		
16X-3, 127-131	147.9	9.07	75.57	9.07	0.00		
16X-5, 70-71	150.3	9.54	79.50	9.57	0.03		
17X-3, 136-139	157.6	6.08	50.62	6.04	0.00		
18X-3, 72-73	166.5	6.31	52.57	6.25	0.00		
18X-3, 131-134	167.1	5.62	46.85	5.63	0.01		
19X-3, 130-133	176.7	5.76	47.95	5.71	0.00		
19X-5, 69-70	179.1	6.24	52.01	6.33	0.09		
20X-1, 127-128	183.3	7.49	62.37	7.67	0.18		
20X-2, 22-23	183.7	6.45	53.75	6.44	0.00		
20X-3, 137-141	186.4	6.84	56.99	6.77	0.00		
20X-5, 92-93	188.9	6.53	54.40	6.59	0.06		
21X-3, 135-138	194.0	7.47	62.24	7.41	0.00		
21X-4, 114-115	195.2	5.99	49.86	5.99	0.00		
21X-5, 72-73	196.3	6.85	57.08	6.79	0.00		
22X-3, 49-50	202.7	8.13	67.73	8.26	0.13		
22X-3, 129-132	203.5	7.04	58.64	7.01	0.00		
23X-2, 125-126	211.6	5.98	49.81	6.18	0.20		
23X-3, 147-150	213.3	7.38	61.45	7.33	0.00		
23X-5, 84-85	215.6	6.87	57.20	7.05	0.18		
24X-3, 141-144	222.8	6.09	50.74	5.99	0.00		
24X-5, 69-70	225.1	6.52	54.32	6.50	0.00		
27X-3, 146-148	246.2	6.89	57.37	6.87	0.00		
28X-4, 50-53	252.3	5.93	49.37	5.83	0.00		
28X-5, 75-77	254.1	7.38	61.43	7.45	0.08		
29X-3, 129-132	261.2	7.51	62.56	7.31	0.00		
29X-5, 114-115	264.0	8.48	70.67	8.38	0.00		
30X-3, 135-138	270.9	6.60	55.00	6.55	0.00		
30X-5, 77-78	273.3	5.60	46.63	5.43	0.00		
31X-3, 135-138	279.3	6.67	55.55	6.67	0.00		
31X-5, 79-80	281.8	6.05	50.38	5.97	0.00		
31X-6, 136-139	283.8	6.11	50.91	6.12	0.01		
32X-1, 71-72	286.4	6.77	56.43	6.65	0.00		
32X-2, 133-136	288.5	8.08	67.34	8.08	0.00		
33X-1, 72-73	289.6	5.77	48.08	5.61	0.00		
33X-3, 62-63	292.5	8.36	69.61	8.30	0.00		
33X-3, 137-140	293.3	8.19	68.19	8.12	0.00		
33X-5, 78-79	295.7	7.17	59.71	7.14	0.00		
34X-3, 79-80	299.1	6.97	58.04	7.21	0.24		
34X-3, 124-127	299.6	6.32	52.62	6.27	0.00		
35X-1, 55-56	305.5	4.18	34.82	4.2	0.02		
35X-2, 47-48	306.9	4.68	39.02	4.74	0.06		
35X-3, 131-134	309.2	3.84	32.00	3.85	0.01		
35X-5, 56-57	311.5	4.20	34.97	4.23	0.03		
35X-6, 13-14	312.5	3.73	31.05	3.68	0.00		
36X-3, 137-140	318.9	4.44	36.99	4.39	0.00		

Notes: TIC = total inorganic carbon; TC = total carbon; TOC = total organic carbon computed by difference (TC – TIC). Negative TOC values are reported as 0.00. wt% = weight percent. NA = not analyzed. Where no values are reported, concentrations are below detection limits.

Table 25. Headspace gas composition from Hole 1050C.

Core, section, interval (cm)	Depth (mbsf)	Gas zone	C_1	C_2	C_2=	C_3	C_3=	$C_1/(C_2+C_3)$
171B-1050C-								
2R-3, 0-5	330.10	Middle IC	23.90	4.20	0.20	1.00		4.43
3R-3, 0-5	339.70	Middle IC	26.30	1.00	0.30	0.20		17.53
4R-4, 0-5	350.80	Deep IC	20.20	1.20				16.83
6R-2, 0-2	367.00	Deep IC	6.69	0.43				15.56
7R-2, 0-2	376.70	Deep IC	14.95	0.56				26.70
8R-2, 0-2	386.40	Deep IC	10.06					
9R-4, 0-2	399.00	Deep IC	13.74	0.22	0.26			28.63
10R-2, 0-1	405.60	Deep IC	20.63	0.17	0.26		0.20	32.75
11R-3, 0-2	411.70	Deep IC	10.51	0.18	0.42			17.52
12R-1, 0-2	413.70	Deep IC	9.92	0.23	0.40			15.75
13R-4, 0-5	427.80	Deep IC	10.71	0.20	1.80			5.36
15R-4, 0-5	447.10	Deep IC	20.74	2.80				7.41
16R-3, 0-2	455.20	Deep IC	15.10	0.40		0.30		21.57
17R-3, 0-5	464.80	Deep IIC	17.40					
18R-4, 0-5	475.90	Deep IIC	32.30	0.20				161.50
19R-2, 0-2	482.50	Deep IIC	21.60					
20R-2, 0-5	492.10	Deep IIC	27.00	0.40				67.50
21R-5, 0-2	506.20	Deep IIIC	16.90					
22R-1, 0-1	509.80	Deep IIIC	16.80		1.00		0.20	14.00
23R-4, 0-2	523.90	Deep IIIC	14.90		0.30			49.67
24R-1, 0-2	529.10	Deep IIIC	12.00		0.40			30.00
25R-3, 0-2	541.70	Deep IIIC	12.10	0.60	0.60			10.08
26R-1, 145-150	549.85	Deep IIIC	12.30	0.90	0.30			10.25
27R-4, 0-1	562.50	Deep IVC	14.60					
28R-4, 0-2	572.10	Deep IVC	20.70	0.50	0.40			23.00
29R-3, 0-2	580.20	Deep IVC	12.50	0.30				41.67
30R-4, 0-2	591.30	Deep IVC	18.50					
31R-3, 0-2	599.40	Deep IVC	7.70					

Notes: In all cases, the injected sample size was 5 cm^3. Concentration of gas is in parts per million by volume. Where no values are reported, concentrations are below detection limits.

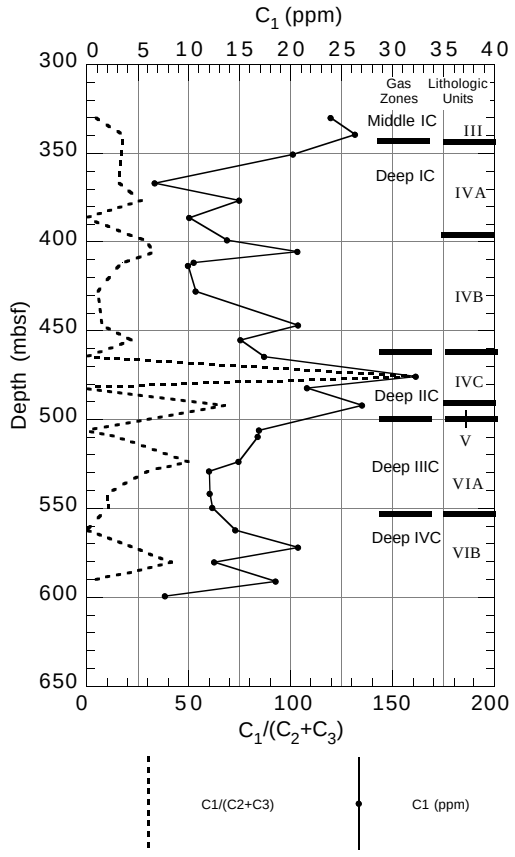

Figure 39. Methane (C_1) content and $C_1/(C_2 + C_3)$ vs. depth in Hole 1050C. Lithologic units are described in the "Lithostratigraphy" section (this chapter).

Pore-water chloride and sodium show a slight increase (Cl^-, 561–577 mM; Na^+, 479–490 mM) with depth from the top of the section to ~120 mbsf, a subsequent decrease (Cl^-, 577–567 mM; Na^+, 490–479 mM) to ~175 mbsf, a second increase (Cl^-, 567–577 mM; Na^+, 479–485 mM) to ~290 mbsf, and a second decrease (Cl^-, 572 mM; Na^+, 477 mM) at 309.30. Chloride and sodium increase slightly with depth until the bottom of Hole 1050C is reached at 600 mbsf (Fig. 42A). In general, the chloride and sodium concentrations recorded in the pore waters at Site 1050 are higher (mean values >2% higher) than those recorded in Hole 1049A. Alkalinity shows a significant increase (3.36–7.32 mM) with depth from the top of the section to ~240 mbsf and a subsequent decrease (7.32–6.28 mM) to the bottom of the hole (Fig. 42C). These alkalinities (mean value = 5.27 mM) are nearly twice as high as those recorded in Hole 1049A (mean value = 2.65 mM). The pH of pore waters at Site 1050 shows less systematic variation with depth than with alkalinity (Fig. 42C), and these pH values are slightly lower (mean value = 7.48) than those recorded in Hole 1049A (mean value = 7.59).

Pore-water calcium increases from a minimum of 11.40 mM (significantly higher than the standard seawater value, 10.55 mM) in the shallowest sample (4.45 mbsf) to a maximum of 26.41 mM at 309.30 mbsf, and decreases with depth to the bottom of Hole 1050C (Fig. 42A). Such variation with depth is significantly greater than that recorded at Hole 1049A. Pore-water magnesium decreases from 53.40 to 42.47 mM at 309.30 mbsf and remains constant to the bottom of Hole 1050C (standard seawater, 54 mM). Pore-water potassium concentrations for Hole 1050A (Fig. 42C) initially increase slightly with depth from 11.4 mM at the top of the section to 12.0 mM at ~50 mbsf, decrease markedly overall with depth to 7.4 mM at 309.30 mbsf, and remain relatively constant to the bottom of Hole 1050C. Two samples (171B-1050A-22X-3, 140–150 cm, and 32X-2, 140–150 cm) are offset from this decreasing trend in the lower part of the section to slightly higher concentrations. These major cation data are consistent with seawater interaction with the upper oceanic crust at basement and/or volcaniclastic sediments within the overlying sediment column.

Pore-water rubidium concentrations in Hole 1050A show a small initial increase with depth from 1.88 µM at the top of the section to 2.02 µM at ~50 mbsf and then show a marked overall decrease with

Table 26. Total inorganic carbon, carbonate, total carbon, total organic carbon, nitrogen, sulfur, and hydrogen analyses for Hole 1050C.

Core, section, interval (cm)	Depth interval (mbsf)	TIC (wt%)	$CaCO_3$ (wt%)	TC (wt%)	TOC (wt%)	N (wt%)	S (wt%)	H (wt%)
171B-1050C-								
2R-1, 67-68	327.77-327.78	4.48	37.33	4.53	0.05	0.01		0.60
2R-3, 139-142	331.49-331.52	3.10	25.78	3.21	0.11			0.78
2R-5, 95-96	334.05-334.06	3.47	28.87	3.54	0.07	0.01		0.73
3R-1, 76-77	337.46-337.47	5.23	43.55	5.30	0.07			0.57
3R-3, 137-140	341.07-341.10	5.40	44.98	5.59	0.19			0.39
3R-5, 67-68	343.34-343.35	5.67	47.27	5.77	0.10			0.50
4R-1, 24-25	346.54-346.55	3.97	33.04	4.05	0.08			0.51
4R-3, 142-145	350.72-350.75	4.29	35.77	4.43	0.14	0.03		0.51
4R-5, 45.5-46	352.76-352.76	4.14	34.49	4.17	0.03			0.45
5R-1, 49-51	356.39-356.41	5.42	45.13	5.45	0.03			0.42
5R-4, 108-112	361.48-361.52	4.99	41.58	4.99	0.00			0.45
5R-5, 48-49	362.19-362.20	4.63	38.54	4.69	0.06			0.50
6R-1, 67-68	366.17-366.18	7.54	62.85	7.55	0.01			0.25
6R-3, 28-29	368.78-368.79	8.22	68.47	8.22	0.00			0.17
6R-3, 136-140	369.86-369.90	8.21	68.39	8.11	0.00			0.23
6R-5, 94-95	372.44-372.45	7.59	63.26	7.59	0.00			0.17
7R-1, 77-78	375.97-375.98	8.62	71.80	8.63	0.01			0.20
7R-4, 46-47	380.16-380.17	6.44	53.63	6.39	0.00			0.36
8R-1, 72.5-73.5	385.63-385.64	5.80	48.33	5.84	0.04			0.52
8R-2, 137-141	387.77-387.81	5.82	48.50	5.86	0.04			0.49
13R-1, 77-78	424.07-424.08	8.56	71.33	8.53	0.00			0.26
13R-3, 83-87	427.13-427.17	7.64	63.65	7.71	0.07			0.32
13R-5, 94-95	430.24-430.25	9.19	76.56	9.20	0.01			0.23
15R-1, 87-88	443.47-443.48	9.84	82.00	9.75	0.00			0.18
15R-3, 139-142	446.99-447.02	7.82	65.13	7.75	0.00	0.01		0.32
15R-5, 63-64	449.23-449.24	10.01	83.38	9.93	0.00			0.15
16R-1, 25-26	452.45-452.46	9.78	81.43	9.66	0.00	0.08		0.16
16R-3, 13-14	455.33-455.34	9.99	83.24	9.98	0.00	0.06		0.15
17R-1, 77-78	462.57-462.58	10.37	86.37	10.32	0.00			0.11
18R-3, 131-134	475.71-475.74	10.83	90.18	10.84	0.01			0.06
19R-1, 25-26	481.25-481.26	11.15	92.89	11.09	0.00			0.04
19R-1, 65-70	481.65-481.70	10.82	90.09	10.87	0.05			0.07
19R-3, 24-25	484.24-484.25	11.16	92.97	11.11	0.00			0.05
21R-1, 34-35	500.54-500.55	9.30	77.45	9.33	0.03			0.19
21R-5, 38-39	506.58-506.59	9.52	79.27	9.56	0.04			0.13
21R-CC, 18-21	510.01-510.04	9.59	79.89	10.81	1.22	0.17	0.48	0.28
22R-1, 36-37	510.16-510.17	8.98	74.81	9.46	0.48	0.10		0.16
22R-2, 910	510.40-510.41	8.03	66.91	8.78	0.75			0.35
23R-2, 141-145	522.31-522.35	9.54	79.45	9.87	0.33	0.09	0.08	0.18
23R-CC, 6-7	529.13-529.14	6.84	56.97	7.01	0.17	0.01		0.45
25R-1, 96-97	539.66-539.67	7.49	62.36	7.63	0.14			0.34
26R-2, 54-55	550.44-550.45	10.76	89.65	10.83	0.07			0.06
27R-1, 79-80	558.79-558.80	4.10	34.12	4.99	0.89	0.04	0.07	0.59
27R-2, 54.5-55	560.05-560.05	3.94	32.84	4.64	0.70		0.07	0.63
27R-CC, 14-15	567.56-567.57	4.83	40.23	5.34	0.51	0.02		0.44
29R-1, 109-110	578.29-578.30	6.16	51.34	6.72	0.56	0.01		0.40
29R-5, 71-72	583.91-583.92	4.78	39.84	5.39	0.61	0.02	0.44	0.51
30R-1, 35-36	587.15-587.16	5.53	46.06	6.21	0.68	0.10		0.41
30R-4, 75-76	592.05-592.06	3.92	32.64	4.85	0.93	0.04	0.28	0.55

Notes: TIC = total inorganic carbon; TC = total carbon; TOC = total organic carbon computed by difference (TC – TIC). Negative TOC values are reported as 0.00. wt% = weight percent. Where no values are reported, concentrations are below detection limits.

depth to 1.02 µM at 309.3 mbsf (Fig. 42D). The pore-water rubidium concentration profile shows remarkable consistency with the potassium profile, thereby confirming the similar geochemical behavior of these two elements in the sediments.

Pore-water strontium concentrations in Hole 1050A show a significant systematic increase with depth from seawater concentrations (86 µM) at the top of the section to almost 500 µM at ~400 mbsf (Fig. 42E). Below this depth, strontium concentrations decrease to ~400 µM at the bottom of the section. Calculated Sr^{2+}/Ca^{2+} (µM/mM) ratios show a similar pattern to the Sr^{2+} concentrations and alkalinity profile (Fig. 42F, E, and C, respectively). These data are consistent with the recrystallization of biogenic calcite in the sediment column at Site 1050.

Pore-water lithium concentrations show an increase with depth from near-seawater values near the top of the section to 275 µM at 288.6 mbsf (Fig. 42E). This increase is significant but small in comparison to increases in lithium concentration (>1000 µM) observed in sediments buried to similar depths on the Ceara Rise. Lithium concentrations decrease with depth below the peak at 288.60 mbsf (Curry et al., 1995).

Dissolved silica concentrations of the interstitial-water samples at Site 1050 show a significant increase with depth to a peak of 1271 µM at 288.6 mbsf (Core 171B-1050A-32X; Fig. 42G) and drop dramatically below that horizon. This peak coincides with the occurrence of chert in this hole and is consistent with the fact that sediments in the upper 300 m (lithologic Units I and II) still contain abundant biogenic (radiolarian) opal (see "Lithostratigraphy" section, this chapter). Pore-water silica concentrations are significantly higher at Site 1050 (mean value = 1059 µM) than in Hole 1049A (mean value = 603 µM).

Pore-water sulfate concentrations at Site 1050 are relatively high (mean value = 25.6 mM) but decrease with depth to values lower than those obtained in Hole 1049A (Fig. 42H). Similarly, pore-water ammonium concentrations are relatively low (mean value = 66 µM), but they are significantly higher than those in Hole 1049A (24.5 µM) and show an overall increase with depth in Hole 1050A (Fig. 42H). These data are consistent with the exceptionally low TOC content of the lithology of the section (see "Organic Geochemistry" section, this chapter).

Pore-water boron concentrations in Hole 1050A show little variation with depth and are near-seawater concentrations (Fig. 42I).

Discussion

The interstitial pore-water chemistry at Site 1050 generally shows greater range and steeper depth gradients than in Hole 1049A. The

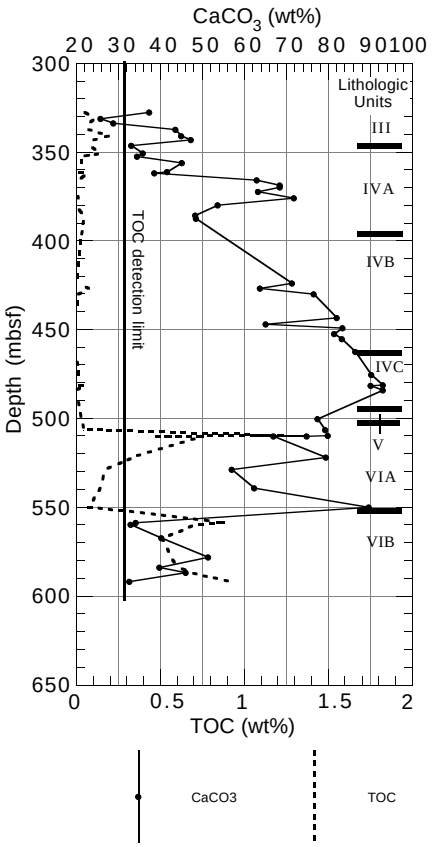

Figure 40. TOC and carbonate contents vs. depth in Hole 1050C. TOC values <0.3 wt% are below the detection limit. Lithologic units are described in the "Lithostratigraphy" section (this chapter).

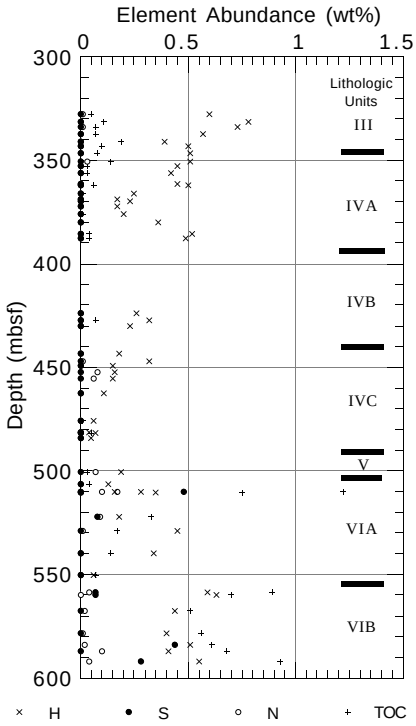

Figure 41. Elemental abundance vs. depth in Hole 1050C. Lithologic units are described in the "Lithostratigraphy" section (this chapter).

subtle chemical gradients in Hole 1049A are interpreted to be consistent with the large distance between the bottom of the hole and the volcanic basement, the shallow core-top and burial depths of the sediments in the hole, and the possibility that the pore-water system at Site 1049 is in communication with adjacent open-ocean waters along the Blake Escarpment (see "Inorganic Geochemistry" section, "Site 1049" chapter, this volume). The most significant difference in these variables between Sites 1049 and 1050 is the greater proximity of Site 1049 to the Blake Escarpment. Therefore, assuming that the lithology of the two sites does not impart a significant control, the data at Site 1050 are consistent with the hypothesis that the pore-water system at Site 1049 is in communication with adjacent open-ocean waters.

PHYSICAL PROPERTIES

Holes 1050A and 1050B

Physical properties in Holes 1050A and 1050B were measured on both whole-round sections and discrete samples from split-core sections. Physical properties data for Hole 1050C follow in a separate subsection of this chapter. Whole-round measurements included determination of GRAPE bulk density, magnetic susceptibility, compressional *P*-wave velocity, and natural gamma radiation, as well as measurements of thermal conductivity. Index properties, compressional *P*-wave velocity, shear strength, and resistivity were measured on discrete samples from split-core sections at a typical frequency of three measurements per core.

MST Measurements

GRAPE and MST *P*-wave velocity data were filtered to remove anomalous values that are artifacts of section-end and void or crack effects. The data sets were filtered to remove values outside the 10% error band of a reference curve, which was calculated from a 10-point running mean of the data. This filtering of the data set significantly improves visual presentation and aids interpretation of the data.

GRAPE bulk density measured on cores from Holes 1050A and 1050B is shown in Figure 43 (also see Tables 28, 29 on CD-ROM, back pocket, this volume). These data, along with magnetic susceptibility and color reflectance, were used to form a Site 1050 composite stratigraphic section (see "Core-Core Integration" section, this chapter).

GRAPE bulk density shows a gradual increase in magnitude between 0 and 150 mbsf in Holes 1050A and 1050B, changing from ~1.5 to 1.7 g/cm^3. Below 150 mbsf, GRAPE bulk density shows considerable fluctuation between values of 1.3 and 1.95 g/cm^3. In the upper 50 m of the sediment column, which corresponds to the siliceous nannofossil ooze of lithologic Subunit IB, bulk density increases gradually from an average of 1.5 to 1.6 g/cm^3. This gradual increase in bulk density continues into lithologic Subunit IC, which consists of siliceous nannofossil ooze and chalk, with bulk density values of 1.7 g/cm^3 at ~150 mbsf. The contact between lithologic Subunits IB and IC cannot be distinguished using GRAPE data because this contact is defined by a color change. Below the occurrence of chert between 140 and 150 mbsf, bulk density decreases in magnitude to 1.3 g/cm^3 at 175 mbsf and then increases to a maximum value of 1.95 g/cm^3 at 215 mbsf. The contact between lithologic Subunit IC and the siliceous nannofossil chalk of Subunit ID is located at the transition at 150 mbsf. The interval between 150 and 305 mbsf, where bulk density values fluctuate about an ~average of 1.8 g/cm^3, corresponds to an increased amount of siliceous material in lithologic Subunit ID. A distinctive decrease in bulk density values occurs at 305 mbsf, which corresponds to the contact between lithologic Subunit ID and the

Table 27. Interstitial-water geochemical data for Site 1050.

Core, section, interval (cm)	Depth (mbsf)	pH	Alkalinity (mM)	Salinity (g/kg)	Cl (mM)	Na (mM)	Mg (mM)	Ca (mM)	SO_4 (mM)	NH_4 (μM)	H_4SiO_4 (μM)	K (mM)	Sr (μM)	Li (μM)	Rb (μM)	B (μM)
171B-1050A-																
1X-3, 145-150	4.45	7.61	3.36	35.0	561	479	53.40	11.40	27.7	22.8	832	11.4	86	34	1.88	491
2H-3, 145-150	13.25	7.55	3.26	35.0	566	483	53.25	11.79	27.8	32.3	844	11.6	94	34	1.91	483
3H-3, 145-150	24.05	7.59	3.56	35.5	564	480	53.29	12.09	27.3	33.1	955	11.7	95	36	1.88	515
4H-3, 145-150	33.55	7.56	3.64	35.0	564	480	53.26	12.36	27.7	28.3	943	11.6	97	37	1.93	459
5H-3, 145-150	43.05	7.45	3.68	35.0	570	484	53.65	12.94	27.8	59.1	1051	12.0	102	43	2.02	475
6H-3, 145-150	52.55	7.52	3.79	35.0	565	481	51.62	13.43	26.9	28.3	1055	12.0	114	46	2.02	459
9H-3, 145-150	80.62	7.48	4.53	35.0	570	485	51.28	14.90	27.1	72.4	1087	11.8	137	64	1.94	275
13X-3, 145-150	119.25	7.56	5.63	37.0	577	490	50.16	17.01	26.2	44.9	1075	10.3	158	102	1.72	515
16X-3, 145-150	148.05	7.58	6.13	36.0	569	483	48.45	18.94	26.3	54.3	1027	10.3	186	124	1.65	619
19X-3, 140-150	176.80	7.18	7.11	36.0	567	479	46.33	21.90	25.2	71.7	1163	9.4	237	172	1.48	1202
22X-3, 140-150	203.60	7.30	7.26	36.0	570	479	45.77	22.78	24.6	86.6	1075	10.2	253	188	1.63	491
26X-2, 140-150	240.60	7.70	7.32	36.0	573	480	43.00	25.71	22.6	103.1	1030	8.5	326	252	1.33	531
29X-3, 140-140	261.30	7.26	6.92	36.0	576	483	42.72	25.88	22.8	103.9	1243	7.9	363	252	1.13	507
32X-2, 140-150	288.60	7.18	6.63	36.0	577	485	40.27	25.84	21.5	129.9	1271	9.2	370	275	1.14	547
35X-3, 140-150	309.30	7.65	6.28	38.0	572	477	42.47	26.41	22.1	114.2	1211	7.4	417	260	1.02	523
171B-1050C-																
2R-2, 140-150	330.00	7.30	5.33	36.0	570	481	40.86	25.54	23	172.5	860	8.02	450	226	1.03	
5R-4, 116-131	361.56	7.57	2.50	35.5	564	473	41.32	24.45	23	181.3	543	7.67	438	212	0.88	
8R-1, 134-150	386.24			35.0	559		39.70	24.06	20.8	212.9	209	7.94	470	216	0.83	
13R-3, 135-150	427.65	7.79	1.33	35.5	572	482	39.09	22.17	20.7	258.7	52	9.97	474	229	1.60	
17R-2, 135-150	464.65				574		40.47	23.05	20.9	209.4	66	8.72	428	221	1.09	
21R-2, 102-115	502.72				568		40.80	23.35	22.1	183.0	88	7.83	444	188	0.82	
23R-3, 135-150	523.75			36.0	576		40.22	22.00	20.8	197.1	93	9.06	403	191	0.98	
26R-2, 135-140	551.25				588		41.68	21.04	22.2	205.9	46	10.1	407	163	1.34	
29R-2, 135-150	580.05	8.46	0.64	35.0	572	490	38.00	20.53	22.4	197.1	28	10.8	395	122	1.20	
31R-2, 135-150	599.25	7.65	1.04		565	483	39.12	20.39	22	142.5	50	8.28	410	117	0.76	

Note: Where no values are reported, data are absent.

diatomaceous nannofossil chalk of Unit II. The contacts between lithologic Subunits IC and ID and Subunit ID and Unit II are also well indicated by changes in the percentage of carbonate (see "Organic Geochemistry" section, this chapter).

MST measurements of magnetic susceptibility in Holes 1050A and 1050B are shown in Figure 44 (also see Tables 30, 31 on CD-ROM, back pocket, this volume). In the upper 175 m of both holes, magnetic susceptibility fluctuations cannot be distinguished from background levels, except for a number of magnetic susceptibility "spikes," which in some instances correspond to ash layers (see "Lithostratigraphy" section, this chapter). Magnetic susceptibility spikes below 200 mbsf, however, are not associated with observed ash layers and may be related to the occurrence of manganese- or pyrite-rich intervals (see "Lithostratigraphy" section, this chapter). Below 175 mbsf, magnetic susceptibility can be measured above background levels and shows minor fluctuations in magnitude.

MST *P*-wave velocity data only from Hole 1050A APC cores are shown in Figure 45 (also see Table 32 on CD-ROM, back pocket, this volume). Despite the apparent scatter in this data set, which may be the result of cracking in the sediment or poor liner/sediment contact, it can be observed that *P*-wave velocity slightly increases with depth from ~1.45 to 1.48 km/s across the depth range 10–57 mbsf.

Natural gamma-radiation counts measured on the MST for Hole 1050A are shown in Figure 46 (also see Table 33 on CD-ROM, back pocket, this volume). Natural gamma-radiation counts fluctuate slightly about background levels of 6 counts per second (cps) in the upper 150 m of the sediment column. Below 150 mbsf, the counts fluctuate between 7 and 10 cps. The highest number of counts occurs in the interval between 210 and 225 mbsf, which corresponds to part of lithologic Subunit ID. The increase in natural gamma counts between 300 and 305 mbsf corresponds to the contact between lithologic Subunit ID and Unit II.

Index Properties

Index properties determined for Hole 1050A are listed in Table 34 and shown in Figure 47. The index properties data show that progressive sediment compaction and fluid expulsion with depth below seafloor are major factors contributing to the physical nature of the sediments. Bulk and dry density data show a steady increase with depth in the upper 140 m of Hole 1050A, ranging from values of 1.58 to 1.7 g/cm^3 and 0.9 to 1.1 g/cm^3, respectively, whereas grain density fluctuates about an average value of 2.58 g/cm^3. At 150 mbsf, bulk, dry, and grain density values show a distinctive decrease in magnitude, which is followed by a steady increase to near maximum values at 215 mbsf. This reduction in bulk, dry, and grain density values corresponds with an interval between 140 to 150 mbsf immediately below a chert layer (see "Lithostratigraphy" section, this chapter). The maximum bulk and dry density values occur between 215 and 300 mbsf, whereas grain density values in this interval appear to be of lower magnitude than those values measured above 150 mbsf. The distinctive changes of grain density with depth, as observed at 150 and 310 mbsf, correspond to the contacts between lithologic units and therefore reflect compositional changes in the sediment column. Bulk and dry density values also decrease in magnitude at 310 mbsf, which corresponds to the change from the siliceous nannofossil chalk of lithologic Subunit ID to the diatomaceous nannofossil chalk of lithologic Unit II (see "Lithostratigraphy" section, this chapter).

Porosity, water content, and void ratio (Fig. 47) show complementary inverse trends with depth to the trends observed for bulk, dry, and grain densities. Of particular interest is the increase in porosity, water content, and void ratio in the diatomaceous nannofossil chalk of lithologic Unit II, compared with lithologic Subunit ID.

Discrete bulk density measurements show good agreement with GRAPE bulk density estimates for Hole 1050A (Fig. 48). Between the seafloor and 105 mbsf, which was drilled primarily with the APC, GRAPE bulk density only slightly underestimates the values obtained by discrete measurements. Between 115 and 225 mbsf, drilled with the XCB, the average GRAPE bulk density values match the discrete bulk density measurements. Below 240 mbsf, the GRAPE bulk density values are significantly lower than the discrete bulk density values, although depth trends are still reproduced in both data sets. GRAPE bulk densities most likely underestimate the true values because of the occurrence of void spaces, tension cracks created by sediment unloading or reduced core diameter, and the presence of slurry between drilling biscuits, which is common in the XCB cores. Figure

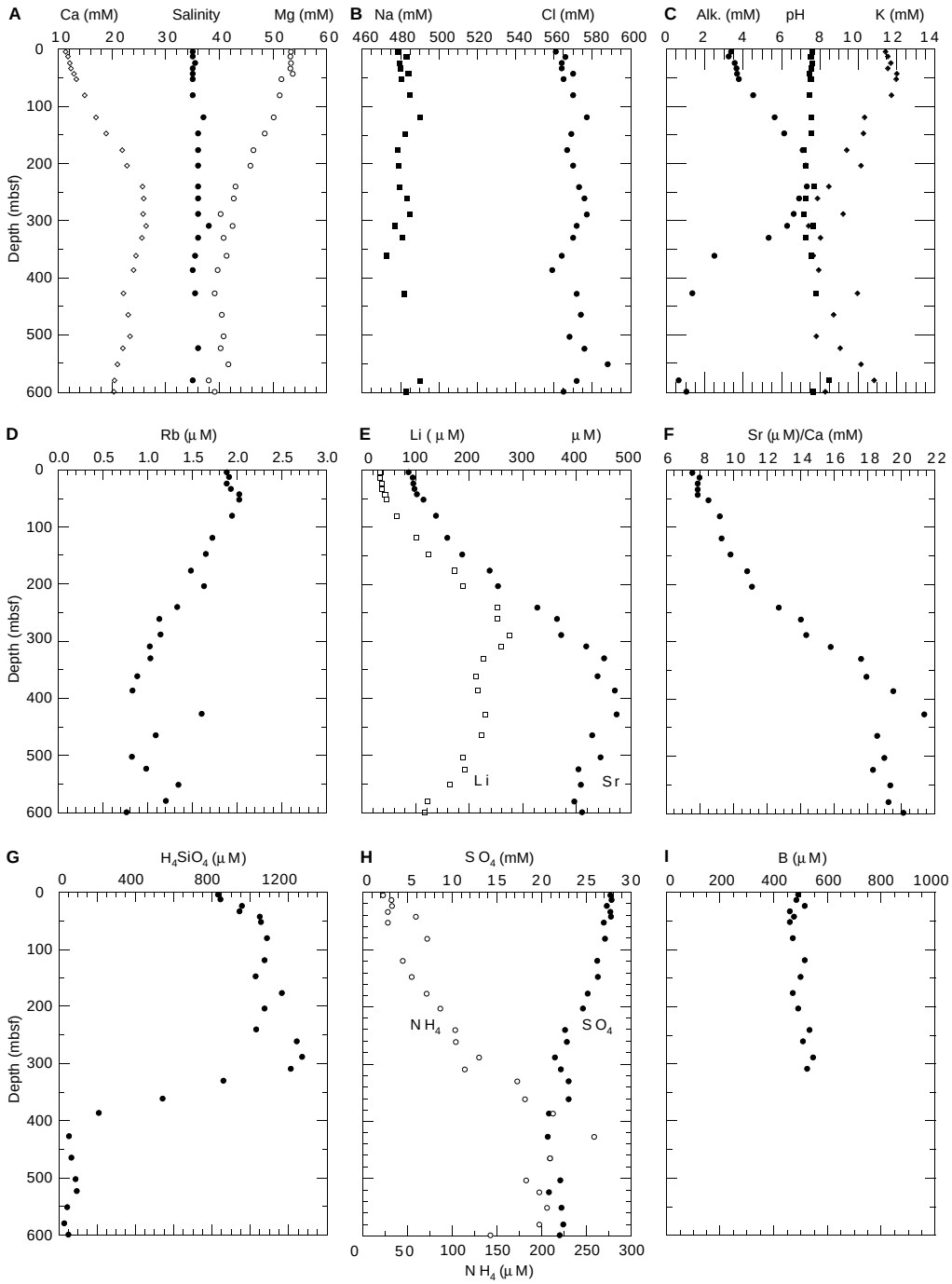

Figure 42. Interstitial-water geochemical data for Holes 1050A and 1050C vs. depth. **A.** Calcium, salinity, and magnesium. **B.** Sodium and chloride. **C.** Alkalinity, pH, and potassium. **D.** Rubidium. **E.** Lithium and strontium. **F.** Strontium/calcium ratio. **G.** Silica. **H.** Sulfate and ammonium. **I.** Boron.

48 shows that GRAPE bulk density may be of value even in sections where drilling techniques may result in an incompletely filled core liner.

P-*wave Velocity*

Discrete measurements of *P*-wave velocity were obtained on split-core sections using the Hamilton Frame velocimeter in Hole 1050A. These data are listed in Table 35 and are illustrated in Figure 49. Comparison of the discrete measurements of *P*-wave velocity with the MST *P*-wave logger (PWL) data shows that the MST PWL significantly underestimates true *P*-wave velocity.

P-wave velocity shows little variability about an average value of 1.56 km/s across the depth range 0–90 mbsf. The contact between lithologic Subunits IB and IC cannot be recognized using velocity data because these units are defined by color. Between 90 and 170

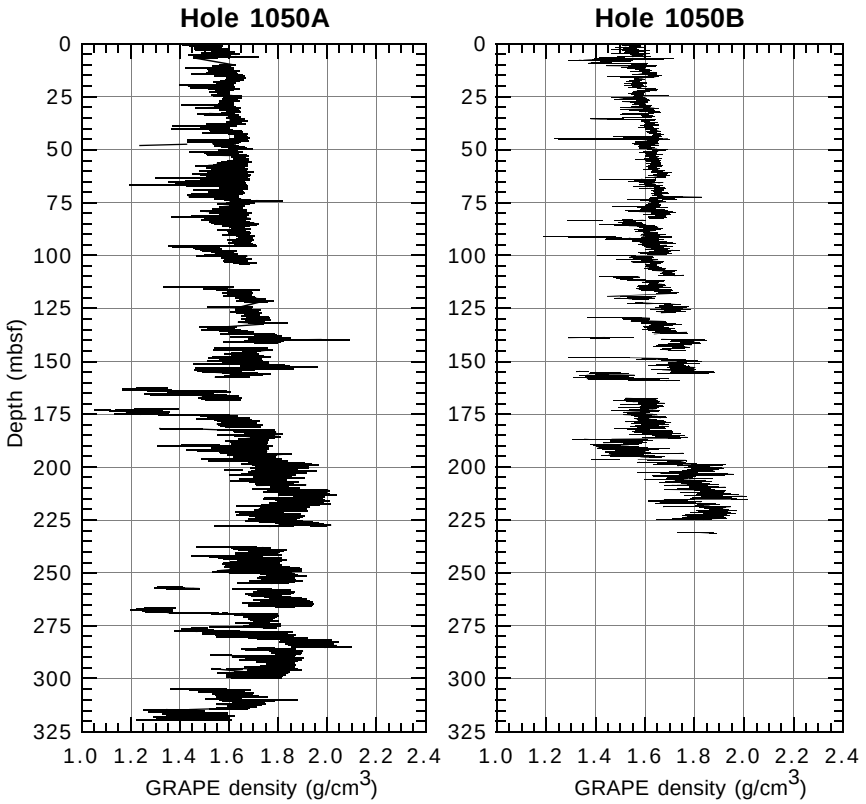

Figure 43. GRAPE bulk density for Holes 1050A and 1050B (see Tables 28, 29 [CD-ROM, back pocket, this volume] for data).

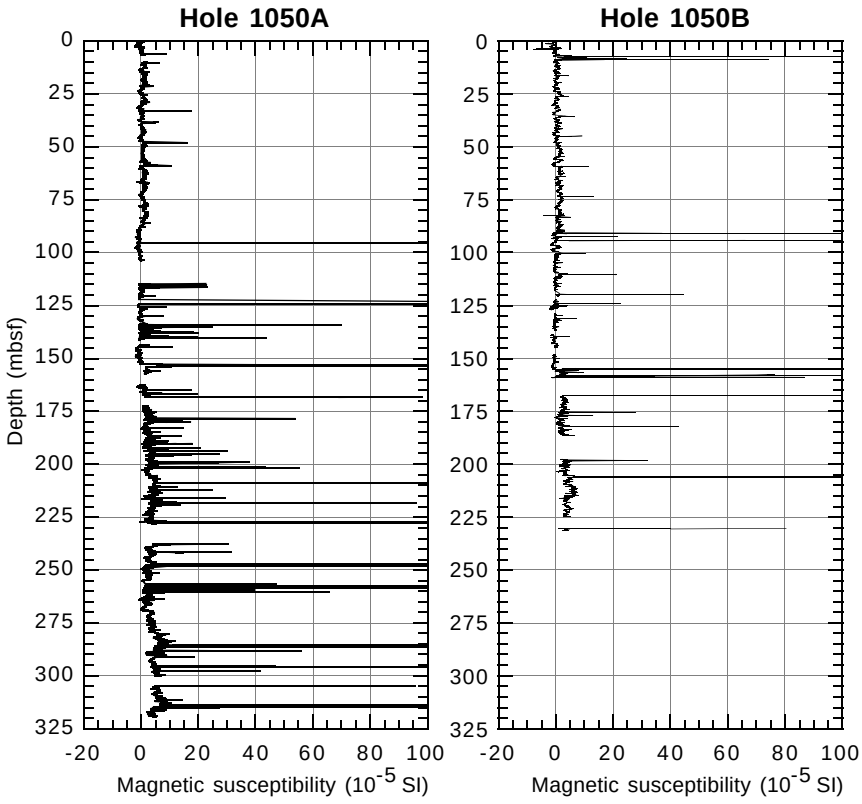

Figure 44. Magnetic susceptibility for Holes 1050A and 1050B (see Tables 30, 31 [CD-ROM, back pocket, this volume] for data).

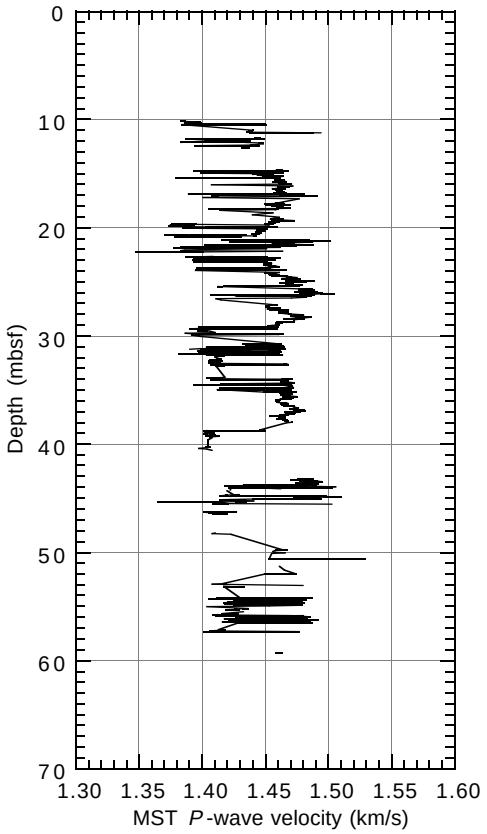

Figure 45. MST *P*-wave velocity for Hole 1050A (see Table 32 [CD-ROM, back pocket, this volume] for data). *P*-wave velocity was measured on APC cores only.

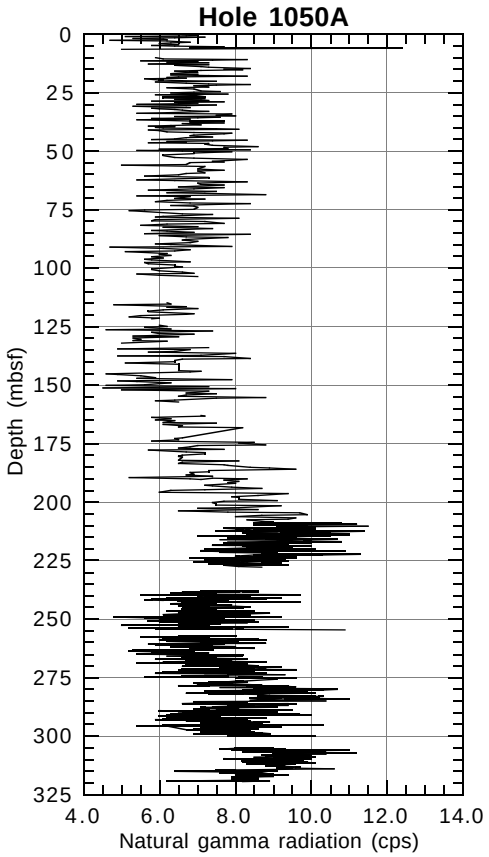

Figure 46. Natural gamma radiation for Hole 1050A (see Table 33 [CD-ROM, back pocket, this volume] for data).

mbsf, *P*-wave velocity increases from ~1.58 to 1.90 km/s, which can be explained by the ooze to chalk transition at 90 mbsf (see "Lithostratigraphy" section, this chapter). Within the interval at 90 to 170 mbsf, *P*-wave velocity increases sharply, whereas bulk density exhibits only a minor increase over the same interval (Fig. 50A). The general trend for all data from Hole 1050A, however, shows a weak correlation with bulk density (Fig. 50B). Between 170 and 300 mbsf, which comprises the siliceous nannofossil chalk of lithologic Subunit ID, *P*-wave velocity fluctuates about an average of 1.95 km/s. Below 305 mbsf, *P*-wave velocity decreases significantly to 1.85 km/s, which, like the changes observed in GRAPE density and index properties, correlates with the change from the siliceous nannofossil chalk of lithologic Subunit ID to the diatomaceous nannofossil chalk of lithologic Unit II.

Undrained Shear Strength

Undrained sediment shear strength was measured on sediments recovered from Hole 1050A using the miniature vane-shear device and, when the sediment became too indurated to insert the vane-shear device, a pocket penetrometer. The shear-strength data are listed in Table 36 and are shown in Figure 51. The majority of measurements were made using the pocket penetrometer, an instrument that does not have the accuracy or reproducibility of the vane-shear device, and this may explain the high degree of scatter in the data set.

Normalized shear strength, the ratio of shear strength (S_u) to effective overburden pressure (P_0'), can be used to assess the stress history of a sediment column. Normalized shear strength ratios (S_u/P_0') determined for Hole 1050A are plotted against depth in Figure 52. A normally consolidated sediment has an S_u/P_0' between 0.2 and 0.22 (Ladd et al., 1977). Sediments above 90 mbsf in Hole 1050A have S_u/P_0' >0.22 and are overconsolidated. Below 90 mbsf in Hole 1050A, S_u/P_0' are <0.2, suggesting that sediments below this depth are underconsolidated. The ooze to chalk transition is also observed at ~90 mbsf in Hole 1050A, and this lithologic transition correlates with the change from overconsolidated to underconsolidated sediment.

Resistivity

The resistivity data from Hole 1050A were measured using the Scripps Institution of Oceanography probe and are listed in Table 37 and shown in Figure 53. Resistivity values show general increase from 0.5 to 0.58 Ωm across the interval 0–90 mbsf. Between 90 and 170 mbsf, resistivity values increase sharply from 0.58 to 0.9 Ωm. Although a relationship between sediment resistivity and porosity was seen in Hole 1049A (see "Physical Properties" section, "Site 1049" chapter, this volume), there is no clear relationship in Hole 1050A (Fig. 54). The abrupt increase in sediment resistivity below 90 mbsf also correlates with the occurrence of the ooze to chalk transition at this depth. The increase in resistivity across this interval is most likely caused by a cementation process, which has reduced sediment permeability, rather than compaction. This lithification process can also account for the increase in *P*-wave velocity below 90 mbsf by decreasing *P*-wave traveltime across grain contacts in the sediment.

Table 34. Discrete index properties measurements for Hole 1050A.

Core, section, interval (cm)	Depth (mbsf)	Water content (total mass wt%)	Water content (solid mass wt%)	Bulk density (g/cm^3)	Grain density (g/cm^3)	Dry density (g/cm^3)	Porosity (%)	Void ratio
171B-1050A-								
1X-1, 68-70	0.68	42.2	72.9	1.57	2.59	0.91	64.8	1.84
1X-2, 75-77	2.25	41.6	71.3	1.59	2.61	0.93	64.5	1.82
1X-3, 75-77	3.75	41.5	70.8	1.59	2.62	0.93	64.4	1.81
1X-4, 75-77	5.25	41.1	69.7	1.60	2.64	0.94	64.3	1.80
2H-1, 75-77	10.85	40.5	68.0	1.60	2.58	0.95	63.1	1.71
2H-2, 75-77	12.35	40.1	67.1	1.61	2.60	0.96	63.0	1.70
2H-3, 75-77	13.85	39.6	65.6	1.62	2.62	0.98	62.7	1.68
2H-4, 75-77	15.35	37.6	60.4	1.64	2.58	1.02	60.3	1.52
2H-5, 75-77	16.85	41.3	70.2	1.59	2.58	0.93	63.9	1.77
2H-6, 75-77	18.35	38.7	63.1	1.62	2.55	0.99	61.1	1.57
2H-7, 75-77	19.85	39.8	66.1	1.62	2.61	0.97	62.7	1.68
3H-1, 75-77	20.35	39.8	66.2	1.61	2.58	0.97	62.5	1.67
3H-2, 75-77	21.85	39.3	64.9	1.61	2.58	0.98	62.0	1.63
3H-3, 75-77	23.35	40.2	67.4	1.60	2.57	0.96	62.8	1.69
3H-4, 75-77	24.85	38.8	63.4	1.62	2.55	0.99	61.2	1.58
3H-5, 75-77	26.35	38.7	63.1	1.62	2.58	1.00	61.4	1.59
3H-6, 75-77	27.85	39.6	65.5	1.61	2.56	0.97	62.0	1.63
3H-7, 75-77	29.35	40.2	67.1	1.60	2.57	0.96	62.8	1.69
4H-1, 75-77	29.85	38.6	63.0	1.63	2.60	1.00	61.5	1.60
4H-2, 75-77	31.35	38.3	62.1	1.64	2.60	1.01	61.2	1.58
4H-3, 75-77	32.85	39.4	64.9	1.61	2.55	0.97	61.8	1.62
4H-4, 75-77	34.35	37.4	59.7	1.65	2.58	1.03	60.1	1.50
4H-5, 75-77	35.85	37.2	59.4	1.65	2.59	1.04	60.0	1.50
4H-6, 75-77	37.35	37.6	60.3	1.65	2.60	1.03	60.5	1.53
5H-1, 75-77	39.35	41.1	69.9	1.59	2.59	0.94	63.9	1.77
5H-2, 75-77	40.85	38.5	62.7	1.63	2.59	1.00	61.4	1.59
5H-3, 75-77	42.35	37.4	59.8	1.66	2.63	1.04	60.6	1.54
5H-4, 75-77	43.85	36.6	57.8	1.67	2.61	1.06	59.6	1.48
5H-5, 75-77	45.35	37.1	58.9	1.66	2.60	1.04	59.9	1.49
5H-6, 75-77	46.85	36.4	57.1	1.67	2.61	1.06	59.3	1.46
6H-1, 75-77	48.85	36.6	57.6	1.67	2.61	1.06	59.5	1.47
6H-2, 75-77	50.35	38.5	62.7	1.63	2.59	1.00	61.3	1.58
6H-3, 75-77	51.85	37.7	60.4	1.64	2.56	1.02	60.2	1.51
6H-4, 75-77	53.35	36.4	57.3	1.66	2.58	1.06	59.1	1.45
6H-5, 75-77	54.85	36.6	57.6	1.67	2.60	1.06	59.4	1.47
6H-6, 75-77	56.35	36.2	56.7	1.68	2.62	1.07	59.2	1.45
7H-1, 75-77	58.35	37.0	58.7	1.65	2.56	1.04	59.5	1.47
7H-2, 75-77	59.85	36.9	58.6	1.65	2.58	1.04	59.6	1.48
7H-3, 75-77	61.35	36.0	56.3	1.68	2.62	1.07	59.0	1.44
7H-4, 75-77	62.85	36.1	56.5	1.67	2.61	1.07	59.0	1.44
7H-5, 75-77	64.35	34.7	53.2	1.69	2.57	1.10	57.1	1.33
7H-6, 75-77	65.85	36.8	58.2	1.65	2.58	1.05	59.4	1.46
8H-1, 75-77	67.85	37.1	59.0	1.66	2.60	1.04	60.0	1.50
8H-2, 75-77	69.35	37.2	59.1	1.65	2.59	1.04	59.9	1.49
8H-3, 75-77	70.85	37.8	60.9	1.63	2.56	1.02	60.3	1.52
8H-4, 75-77	72.35	38.4	62.4	1.62	2.54	1.00	60.8	1.55
8H-5, 75-77	73.85	37.2	59.2	1.65	2.58	1.04	59.9	1.49
8H-6, 75-77	75.35	35.1	54.2	1.69	2.60	1.10	57.9	1.38
9H-1, 30-32	76.90	38.9	63.7	1.61	2.55	0.99	61.4	1.59
9H-2, 75-77	78.42	36.7	58.0	1.66	2.58	1.05	59.4	1.46
9H-3, 75-77	79.92	36.7	58.1	1.66	2.61	1.05	59.6	1.48
9H-4, 75-77	81.42	34.5	52.7	1.73	2.28	1.14	58.4	1.40
9H-5, 44-46	82.61	37.9	60.9	1.63	2.55	1.01	60.3	1.52
9H-6, 75-77	84.42	40.2	67.3	1.60	2.56	0.95	62.7	1.68
9H-7, 75-77	85.92	36.3	57.1	1.67	2.60	1.06	59.2	1.45
10H-1, 75-77	86.85	37.0	58.8	1.65	2.58	1.04	59.7	1.48
10H-2, 75-77	88.35	37.7	60.5	1.63	2.54	1.02	60.0	1.50
10H-3, 75-77	89.85	36.7	57.9	1.65	2.57	1.05	59.2	1.45
10H-4, 75-77	91.35	36.0	56.2	1.66	2.56	1.06	58.4	1.40
10H-5, 75-77	92.85	36.4	57.2	1.66	2.58	1.06	59.0	1.44
10H-6, 75-77	94.35	36.7	58.0	1.65	2.56	1.05	59.2	1.45
11X-1, 36-38	95.96	37.0	58.8	1.64	2.55	1.04	59.5	1.47
11X-2, 80-82	97.90	37.3	59.4	1.64	2.57	1.03	59.8	1.49
11X-3, 72-74	99.32	37.3	59.5	1.65	2.58	1.03	60.0	1.50
11X-4, 74-76	100.84	35.9	55.9	1.67	2.58	1.07	58.5	1.41
11X-5, 79-81	102.39	35.1	54.1	1.69	2.59	1.09	57.8	1.37
11X-6, 64-66	103.74	35.3	54.7	1.68	2.59	1.09	58.0	1.38
12X-1, 75-77	105.95	36.4	57.3	1.67	2.60	1.06	59.2	1.45
13X-1, 75-77	115.55	37.1	59.0	1.65	2.56	1.04	59.6	1.48
13X-2, 77-79	117.07	35.9	56.1	1.68	2.62	1.08	58.9	1.43
13X-3, 74-76	118.54	38.7	63.2	1.63	2.62	1.00	61.8	1.62
13X-4, 75-77	120.05	37.7	60.5	1.65	2.63	1.03	60.8	1.55
13X-5, 79-81	121.59	33.9	51.3	1.70	2.58	1.13	56.4	1.30
14X-1, 75-77	125.15	36.9	58.5	1.66	2.62	1.05	60.0	1.50
14X-2, 77-79	126.67	35.7	55.5	1.68	2.61	1.08	58.6	1.42
14X-3, 75-77	128.15	36.8	58.2	1.66	2.61	1.05	59.7	1.48
14X-4, 77-79	129.67	34.0	51.4	1.70	2.58	1.12	56.5	1.30
14X-5, 75-77	131.15	34.1	51.8	1.70	2.60	1.12	56.8	1.31
15X-1, 77-79	134.77	37.4	59.6	1.65	2.60	1.03	60.2	1.51
15X-2, 75-77	136.25	35.4	54.7	1.68	2.60	1.09	58.1	1.39
15X-3, 76-78	137.76	32.3	47.8	1.74	2.60	1.18	54.9	1.22
15X-4, 74-76	139.24	29.5	41.8	1.80	2.62	1.27	51.6	1.07
15X-5, 75-77	140.75	37.5	60.0	1.66	2.66	1.04	61.0	1.56
16X-1, 71-73	144.31	32.0	47.1	1.75	2.62	1.19	54.7	1.21
16X-2, 76-78	145.86	34.4	52.4	1.70	2.58	1.11	56.9	1.32
16X-3, 75-77	147.35	26.7	36.3	1.84	2.60	1.35	48.0	0.92
16X-4, 75-77	148.85	34.2	52.0	1.71	2.62	1.13	57.1	1.33
16X-5, 72-74	150.32	23.2	30.2	1.93	2.64	1.49	43.8	0.78

Table 34 (continued).

Core, section, interval (cm)	Depth (mbsf)	Water content (total mass wt%)	Water content (solid mass wt%)	Bulk density (g/cm^3)	Grain density (g/cm^3)	Dry density (g/cm^3)	Porosity (%)	Void ratio
16X-6, 74-76	151.84	36.8	58.3	1.66	2.61	1.05	59.8	1.49
17X-1, 79-81	153.99	35.2	54.4	1.67	2.55	1.08	57.5	1.36
17X-2, 76-78	155.46	38.1	61.6	1.62	2.53	1.00	60.3	1.52
17X-3, 75-77	156.95	39.0	64.0	1.61	2.52	0.98	61.2	1.58
18X-1, 91-93	163.71	37.5	60.0	1.62	2.50	1.01	59.4	1.46
18X-2, 75-77	165.05	39.5	65.2	1.59	2.47	0.96	61.2	1.57
18X-3, 74-76	166.54	36.5	57.4	1.65	2.55	1.05	58.9	1.43
18X-4, 75-77	168.05	36.0	56.2	1.65	2.53	1.06	58.1	1.39
19X-1, 69-71	173.09	35.0	54.0	1.67	2.52	1.08	57.0	1.33
19X-2, 68-70	174.58	37.3	59.6	1.63	2.51	1.02	59.3	1.46
19X-3, 80-82	176.20	36.1	56.5	1.64	2.49	1.05	57.9	1.38
19X-4, 54-56	177.44	33.8	51.0	1.70	2.56	1.13	56.1	1.28
19X-5, 72-74	179.12	33.2	49.6	1.68	2.45	1.12	54.3	1.19
19X-6, 75-77	180.65	34.3	52.3	1.66	2.46	1.09	55.7	1.26
20X-1, 77-79	182.77	29.9	42.6	1.77	2.58	1.24	51.8	1.07
20X-2, 78-80	184.28	30.9	44.8	1.75	2.56	1.21	52.8	1.12
20X-3, 72-74	185.72	29.7	42.2	1.77	2.54	1.24	51.2	1.05
20X-4, 75-77	187.25	32.2	47.6	1.72	2.54	1.17	54.2	1.18
20X-5, 92-94	188.92	30.7	44.3	1.76	2.58	1.22	52.8	1.12
20X-6, 75-77	190.25	32.3	47.7	1.72	2.53	1.16	54.1	1.18
21X-1, 85-87	190.45	31.3	45.5	1.72	2.49	1.18	52.5	1.11
21X-2, 68-70	191.78	32.6	48.3	1.72	2.56	1.16	54.7	1.21
21X-3, 75-77	193.35	29.3	41.4	1.78	2.56	1.26	50.8	1.03
21X-4, 73-75	194.83	28.8	40.5	1.79	2.57	1.28	50.4	1.02
21X-5, 67-69	196.27	26.9	36.8	1.82	2.54	1.33	47.7	0.91
21X-6, 43-45	197.53	26.7	36.4	1.83	2.57	1.34	47.7	0.91
22X-1, 74-76	199.94	27.2	37.4	1.82	2.56	1.33	48.3	0.94
22X-2, 79-81	201.49	26.3	35.7	1.84	2.58	1.36	47.3	0.90
22X-3, 47-49	202.67	23.9	31.4	1.90	2.60	1.45	44.3	0.80
22X-4, 68-70	204.38	25.9	34.9	1.84	2.56	1.37	46.6	0.87
22X-5, 74-76	205.94	28.5	39.9	1.78	2.52	1.27	49.5	0.98
22X-6, 73-75	207.43	28.4	39.7	1.79	2.55	1.28	49.7	0.99
23X-1, 80-82	209.60	24.6	32.5	1.86	2.54	1.41	44.7	0.81
23X-3, 81-83	212.61	23.3	30.4	1.90	2.56	1.45	43.2	0.76
23X-5, 80-82	215.60	23.0	29.8	1.93	2.61	1.48	43.2	0.76
23X-7, 70-72	217.90	24.6	32.7	1.88	2.58	1.42	45.2	0.82
24X-1, 67-69	219.07	26.5	36.0	1.84	2.57	1.35	47.4	0.90
24X-3, 65-67	222.05	25.7	34.6	1.84	2.54	1.37	46.1	0.86
24X-5, 67-69	225.07	25.8	34.8	1.83	2.53	1.36	46.3	0.86
27X-1, 80-82	242.50	26.4	35.8	1.63	2.07	1.20	42.0	0.72
27X-3, 78-80	245.48	27.6	38.2	1.81	2.57	1.31	49.0	0.96
28X-1, 69-71	247.99	25.5	34.3	1.87	2.60	1.39	46.5	0.87
27X-5, 81-83	248.51	25.1	33.5	2.12	3.30	1.59	51.9	1.08
28X-3, 82-84	251.12	25.0	33.4	1.87	2.58	1.40	45.7	0.84
29X-1, 62-64	257.52	26.8	36.5	1.82	2.55	1.34	47.6	0.91
29X-3, 55-57	260.45	28.5	39.9	1.79	2.56	1.28	49.9	1.00
29X-5, 113-115	264.03	24.9	33.2	1.89	2.62	1.42	45.9	0.85
30X-1, 62-64	267.12	28.5	39.9	1.79	2.56	1.28	49.9	1.00
30X-3, 73-75	270.23	29.2	41.3	1.77	2.52	1.25	50.4	1.02
30X-5, 74-76	273.24	27.6	38.1	1.80	2.53	1.30	48.5	0.94
31X-3, 65-67	278.61	27.3	37.6	1.83	2.59	1.33	48.8	0.95
31X-5, 73-75	281.69	20.5	25.8	1.98	2.62	1.58	39.8	0.66
31X-7, 78-80	284.74	21.5	27.5	1.96	2.63	1.54	41.3	0.70
32X-1, 69-71	286.39	21.8	27.9	1.95	2.60	1.52	41.5	0.71
33X-1, 98-100	289.88	22.3	28.7	1.94	2.61	1.51	42.2	0.73
33X-2, 79-81	291.19	21.9	28.1	1.96	2.63	1.53	41.9	0.72
33X-3, 80-82	292.70	21.7	27.7	1.95	2.61	1.53	41.3	0.70
33X-4, 80-82	294.20	22.6	29.3	1.94	2.62	1.50	42.8	0.75
33X-5, 77-79	295.67	23.4	30.6	1.92	2.61	1.47	43.8	0.78
34X-1, 84-86	296.14	23.0	29.9	1.92	2.59	1.48	43.1	0.76
33X-6, 81-83	297.21	22.7	29.4	1.93	2.61	1.49	42.8	0.75
34X-2, 82-84	297.62	24.2	31.9	1.89	2.58	1.43	44.6	0.80
34X-3, 78-80	299.08	22.6	29.2	1.93	2.61	1.50	42.7	0.75
35X-1, 71-73	305.61	32.4	47.9	1.71	2.50	1.15	53.9	1.17
35X-2, 63-65	307.03	32.3	47.8	1.70	2.48	1.15	53.7	1.16
35X-3, 73-75	308.63	30.5	43.9	1.74	2.52	1.21	51.9	1.08
35X-5, 63-65	311.53	32.3	47.7	1.71	2.52	1.16	54.0	1.18
35X-6, 68-70	313.08	33.1	49.5	1.70	2.53	1.14	55.1	1.23
36X-1, 68-70	315.18	34.4	52.4	1.67	2.48	1.09	55.9	1.27
36X-2, 47-49	316.47	31.5	45.9	1.73	2.53	1.19	53.1	1.13
36X-3, 46-48	317.96	30.9	44.6	1.74	2.53	1.20	52.4	1.10

Thermal Conductivity

Thermal conductivity data from Hole 1050A are listed in Table 38 and are shown in Figure 55. Thermal conductivity measurements for Hole 1050B display a large degree of scatter, even for cores that were drilled with the APC. The lack of any observable relationship between thermal conductivity and depth suggests that either changes in thermal conductivity are not apparent in the sediments from Sites 1049 and 1050 or that the Thermcon needle probe technique is yielding inconsistent results. If the former is assumed, then an average thermal conductivity of 1.19 ± 0.18 W/(m·K) can be determined for the depth interval 0–150 mbsf in Hole 1050A.

Summary

Physical properties data for Holes 1050A and 1050B indicate that compaction, fluid expulsion, and physicochemical changes related to lithology are the factors controlling sediment properties. The physical properties data are influenced largely by sediment type, and this is particularly apparent at the ooze to chalk transition at 90 mbsf in Hole

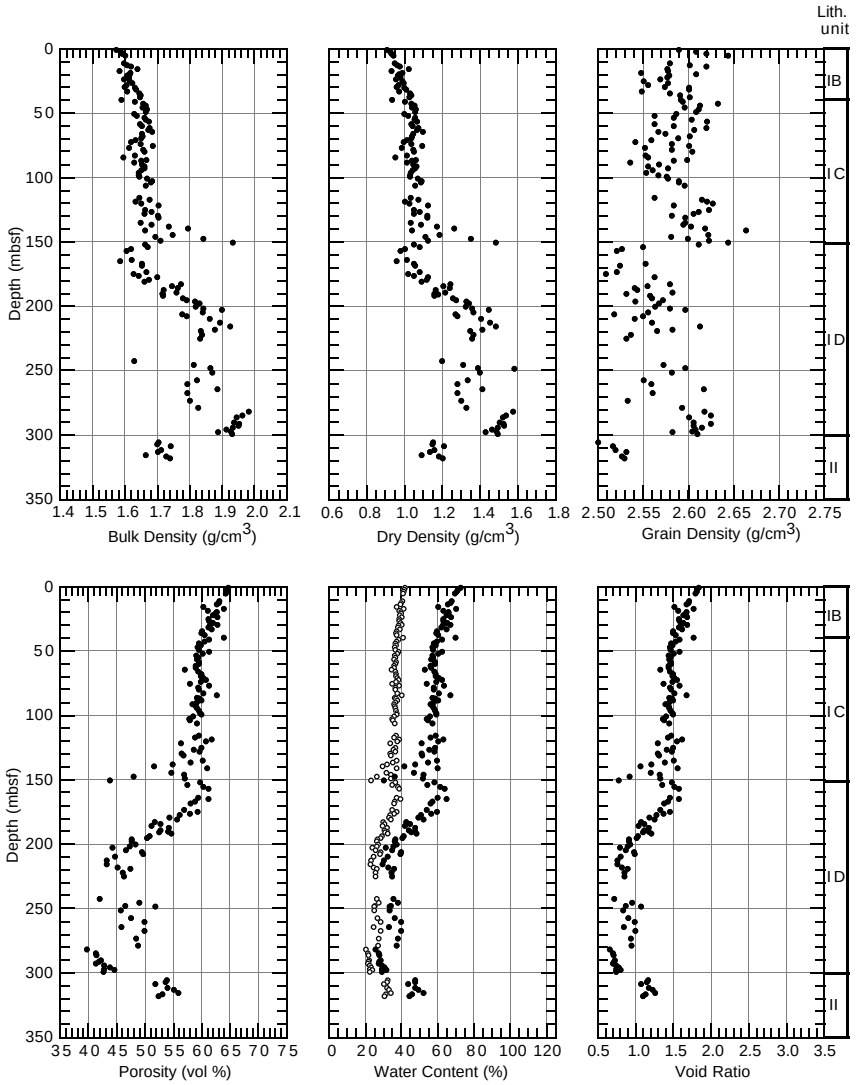

Figure 47. Discrete measurements of bulk density, dry density, grain density, porosity, water content, and void ratio for Hole 1050A. In the water content plot, open circles = values expressed in terms of total mass; solid circles = values expressed in terms of the total mass of solids.

1050A. Cementation and sediment lithification in this interval control *P*-wave velocity and resistivity by decreasing *P*-wave traveltime across grain contacts and by decreasing permeability, respectively. Cementation in this interval does not, however, appear to have significantly increased bulk density or significantly decreased porosity.

Hole 1050C

Physical properties in Hole 1050C were measured on both whole-round sections and discrete samples from split-core sections. Whole-round measurements included the determination of GRAPE bulk density, magnetic susceptibility, and natural gamma radiation. Index properties and *P*-wave velocity were measured on discrete samples from split-core sections at a frequency of one to three measurements per core.

MST Measurements

The GRAPE data were filtered in the same manner as for Holes 1050A and 1050B. GRAPE bulk density (Fig. 56; Table 39 on CD-ROM, back pocket, this volume) shows an increase in magnitude from 1.45 to 1.75 g/cm^3 in the interval between 325 and 370 mbsf and remains relatively constant until 500 mbsf, which corresponds to the boundary between the phosphatic hardground of lithologic Unit V and the nannofossil chalk of lithologic Subunit VIA. Between 500 and 540 mbsf, GRAPE bulk density increases to a constant average value of 1.9 g/cm^3. Below 550 mbsf, GRAPE bulk density drops sharply in the first 10 m of lithologic Subunit VIB to 1.7 g/cm^3 and fluctuates between 1.65 and 2.0 g/cm^3 until the total depth of the hole at 605 mbsf.

MST measurements of magnetic susceptibility are shown in Figure 57 (also see Table 40 on CD-ROM, back pocket, this volume). Above 460 mbsf, magnetic susceptibility can be distinguished from background levels. A magnetic susceptibility "spike" at 330 mbsf occurs within the siliceous nannofossil chalk of lithologic Unit III but has not been correlated with any lithologic change, such as the ash layers identified at Sites 1050, 1051, and 1053. An interval of larger fluctuations in magnetic susceptibility occurs between 443 and 455 mbsf, which corresponds to the basal layers of the clay-rich nannofossil chalk of lithologic Subunit IVB. In the interval between 460 and 480 mbsf, which contains deformed nannofossil chalk of lithologic Subunit IVC, magnetic susceptibility is at background levels. Between 490 and 500 mbsf, magnetic susceptibility attains values up to 345×10^{-5} SI units, the highest value measured during Leg 171B. This maximum corresponds with the phosphatic hardground of lithologic Unit V. Between 500 and 550 mbsf, the magnetic susceptibility record is discontinuous because of coring gaps. Between 550 and 554 mbsf, magnetic susceptibility increases sharply to values as much as

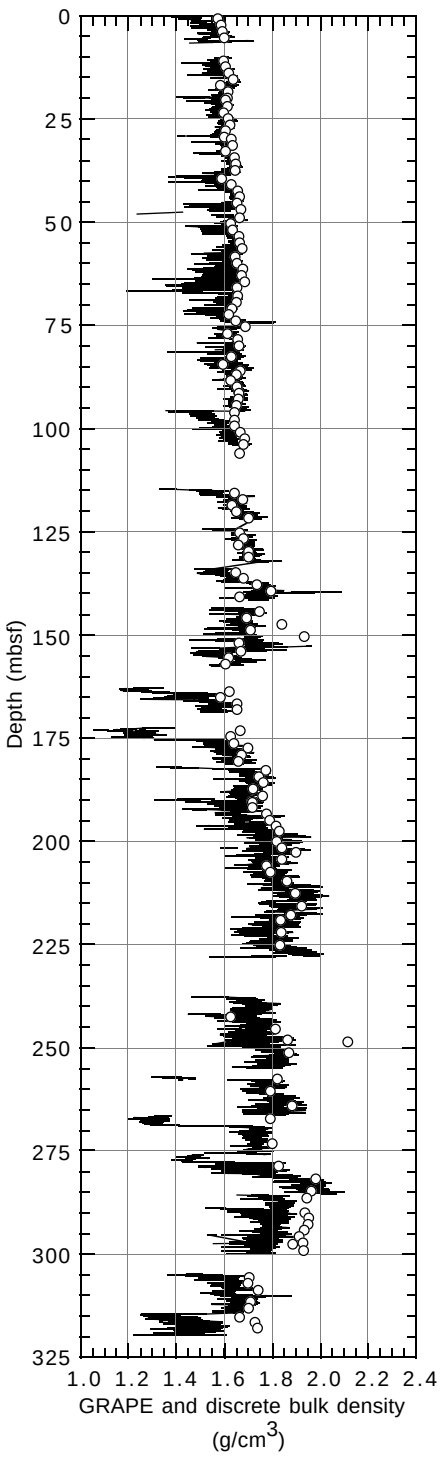

Figure 48. Comparison of GRAPE bulk density (line) with discrete measurements of bulk density (open circles) for Hole 1050A.

38×10^{-5} SI. This increase appears to be associated with extremely contorted bedding in the basal portion of lithologic Subunit VIA, a nannofossil chalk. Magnetic susceptibility fluctuates about an average value of 13×10^{-5} SI between 555 and 605 mbsf, which corresponds to the black shale interval of lithologic Subunit VIB.

Natural gamma-radiation measurements are shown in Figure 58 (also see Table 41 on CD-ROM, back pocket, this volume). Natural gamma radiation is above background levels throughout most of Hole 1050C. Between 325 and 455 mbsf, measurements fluctuate between 7 and 11 cps. Gamma-radiation levels are at background levels between 460 and 480 mbsf, corresponding to the nannofossil chalk of lithologic Subunit IIIB. Between 490 and 605 mbsf, gamma radiation increases steadily from 7 to 14 cps, with the highest levels recorded in the black shale interval of lithologic Subunit VIB.

Index Properties

Index properties data are listed in Table 42 and are illustrated in Figure 59. Between 325 and 340 mbsf, bulk, dry, and grain density values show a distinctive minimum that occurs near the base of the siliceous nannofossil chalk of lithologic Unit III. Below 340 mbsf, bulk and dry densities are relatively constant, with average values of ~2.0 and 1.6 g/cm^3, respectively. Between 340 and 450 mbsf, grain density increases steadily from 2.56 g/cm^3 to a maximum value of 2.73 g/cm^3. Porosity, water content, and void ratio (Fig. 59) show complementary inverse trends with depth to those trends observed for bulk and dry densities. The excursion of high porosity, water content, and void ratio does not have any obvious lithologic association, although it occurs below a sharp magnetic susceptibility spike (Fig. 44) at 339 mbsf and just above a series of thin cherts contained in the siliceous nannofossil chalk of lithologic Unit III.

Except for a few data points, the discrete bulk density measurements do not show good agreement with GRAPE bulk density in Hole 1050C (Fig. 60) because this hole was cored with the RCB. GRAPE bulk densities significantly underestimate true values of bulk density because RCB coring generally results in a much reduced sediment core diameter.

P-*wave Velocity*

Discrete measurements of *P*-wave velocity were obtained on minicores using the Hamilton Frame velocimeter (Table 43; Fig. 61). Transverse *P*-wave velocity fluctuates between 1.8 and 2.6 km/s over the length of Hole 1050C and shows two maxima at 365 and 570 mbsf and two minima at 410 and 570 mbsf. Transverse *P*-wave velocity increases sharply from 1.80 to 2.6 km/s between 330 and 370 mbsf. This interval spans the boundary between lithologic Unit III and Subunit IVA. Two anomalously high values of about 3.1 km/s occur at about 372 mbsf and have no obvious lithologic correlation. Velocity drops almost as quickly within lithologic Subunit IVA and remains relatively constant at an average value of 2.05 km/s between 400 and 470 mbsf until rising within lithologic Subunit IVC to slightly over 2.45 km/s. No velocity data were collected for Core 171B-1050C-21R because it was designated as a "critical interval." Between 500 and 530 mbsf, velocity remains constant at about 2.40 km/s and decreases sharply below 530 mbsf, reaching 1.95 km/s at 570 mbsf. A slight increase in velocity occurs between 570 and 600 mbsf.

Acoustic anisotropy, the ratio of *P*-wave velocity measured perpendicular to the split-core surface (x-direction) to that measured parallel to the core axis (z-direction), is plotted for Hole 1050C in Figure 61. The acoustic anisotropy data show that *P*-wave velocity is faster in the transverse direction (x), than in the longitudinal direction (z). This ratio is highest in the interval between 340 and 365 mbsf, which corresponds to a *P*-wave maximum. A similar, but less well-defined, acoustic anisotropy maximum corresponds with the other maximum in *P*-wave velocity lower in Hole 1050C. The physicochemical cause of the increased acoustic anisotropy and *P*-wave velocity is not clear from preliminary lithologic data. The relatively higher transverse velocity suggests that there may be evidence for pressure solution, recrystallization, and grain growth parallel to bedding planes.

Figure 62 illustrates the general positive relationship between *P*-wave velocity and bulk density. The four bulk density data points

Table 35. Discrete measurements of uncorrected transverse *P*-wave velocity for Site 1050A.

Core, section, interval (cm)	Depth (mbsf)	Transverse *P*-wave velocity (m/s)
171B-1050A-		
1X-1, 74-76	0.74	1558.7
1X-3, 74-76	3.74	1558.2
2H-1, 74-76	10.84	1554.6
2H-3, 74-76	13.84	1579.7
2H-5, 74-76	16.84	1573.9
2H-7, 74-76	19.84	1560.5
3H-1, 74-76	20.34	1555.0
3H-3, 74-76	23.34	1582.9
3H-5, 74-76	26.34	1580.3
3H-7, 74-76	29.34	1554.8
4H-3, 74-76	32.84	1566.6
4H-5, 74-76	35.84	1575.5
4H-1, 74-76	29.84	1563.5
5H-1, 74.1-76.1	39.34	1563.1
5H-3, 74-76	42.34	1568.5
5H-5, 74-76	45.34	1559.9
6H-1, 74-76	48.84	1572.2
6H-3, 74-76	51.84	1577.0
6H-5, 74-76	54.84	1577.7
7H-1, 71.5-73.5	58.32	1575.0
7H-3, 74-76	61.34	1573.7
7H-5, 72.4-74.4	64.32	1585.2
8H-1, 74-76	67.84	1580.5
8H-3, 74-76	70.84	1578.1
8H-5, 74-76	73.84	1595.2
9H-1, 34-36	76.94	1572.0
9H-3, 79-81	79.96	1590.4
9H-5, 40.8-42.8	82.58	1580.2
10H-1, 74-76	86.84	1580.7
10H-3, 74-76	89.84	1583.9
10H-5, 74-76	92.84	1639.4
11X-1, 74-76	96.34	1668.9
11X-1, 36.8-38.8	95.97	1711.5
12X-1, 74-76	105.94	1735.1
13X-1, 74-76	115.54	1667.7
13X-3, 71.7-73.7	118.52	1789.0
13X-5, 78.4-80.4	121.58	1839.9
14X-1, 74.1-76.1	125.14	1686.1
14X-3, 74-76	128.14	1696.4
14X-5, 73.9-75.9	131.14	1706.9
15X-1, 74-76	134.74	1683.3
15X-3, 69.8-71.8	137.70	1789.3
15X-5, 72.8-74.8	140.73	1876.8
16X-1, 74-76	144.34	1675.8
16X-3, 81.5-83.5	147.42	1714.2
16X-5, 71.5-73.5	150.32	1790.7
17X-1, 96.8-98.8	154.17	1788.6
17X-3, 74-76	156.94	1786.4
18X-1, 89.2-91.2	163.69	1822.6
18X-3, 69-71	166.49	1795.9
19X-1, 70-72	173.10	1931.2
19X-3, 80.2-82.2	176.20	1833.5
19X-5, 72.4-74.4	179.12	1860.4
19X-1, 69-71	173.09	1964.9
19X-3, 80-82	176.20	1899.3
19X-5, 72-74	179.12	1945.4
20X-1, 75.9-77.9	182.76	1966.0
20X-3, 72.4-74.4	185.72	1891.0
20X-5, 91.5-93.5	188.92	1906.8
20X-1, 77-79	182.77	2062.2
20X-3, 72-74	185.72	1952.2
20X-5, 92-94	188.92	1975.2
21X-1, 84-86	190.44	1930.5
21X-4, 73-75	194.83	1937.5
21X-2, 68-70	191.78	2017.4
21X-5, 67-69	196.27	1963.9
22X-1, 74-76	199.94	2062.2
22X-3, 47-49	202.67	1973.7
22X-5, 74-76	205.94	1902.7
23X-1, 80-82	209.60	1927.1
23X-3, 81-83	212.61	2059.2
23X-5, 80-82	215.60	1972.7
24X-1, 67-69	219.07	1847.3
24X-3, 65-67	222.05	1935.9
24X-5, 67-69	225.07	1910.6
28X-1, 69.5-71.5	248.00	1963.6
28X-3, 82-84	251.12	2024.6
27X-1, 80-82	242.50	2008.0
27X-3, 78-80	245.48	1935.0
27X-5, 81-83	248.51	1976.3
29X-1, 62-64	257.52	1965.7
29X-3, 55-57	260.45	1942.9
29X-5, 113-115	264.03	2001.2
30X-1, 62-64	267.12	1925.9
30X-3, 73-75	270.23	1934.8
30X-5, 74-76	273.24	1964.1
31X-3, 65-67	278.61	2016.6
31X-5, 73-75	281.69	1981.6
31X-7, 78-80	284.74	2069.2
32X-1, 69-71	286.39	2027.6
33X-1, 98-100	289.88	1970.8
33X-3, 80-82	292.70	2069.7
33X-5, 77-79	295.67	2013.6
34X-1, 84-86	296.14	1979.6
34X-3, 78-80	299.08	1966.2
35X-1, 71-73	305.61	1844.0
35X-3, 73-75	308.63	1857.5
35X-5, 63-65	311.53	1844.6
36X-1, 68-70	315.18	1843.0
36X-3, 46-48	317.96	1874.6

<1.8 g/cm^3 are from the zone of anomalously high porosity identified in the basal portion of the siliceous nannofossil chalk of lithologic Unit II.

Summary

Physical properties data from Hole 1050C identify a high-porosity, low-*P*-wave velocity zone between 325 and 340 mbsf. This zone is directly above a series of thin cherts in siliceous nannofossil chalk and may represent an interval where there is contemporaneous fluid flow. Large magnetic susceptibility values are associated with the phosphatic hardground that occurs between 490 and 500 mbsf.

DOWNHOLE LOGGING

Logging Operations

After Hole 1050C was drilled to a total depth of 606 mbsf, the lower limit of the BHA was placed at 108 mbsf. Hole 1050C was logged with three different tool strings: triple-combo, FMS, and GHMT (see "Downhole Logging" section, "Explanatory Notes" chapter, this volume). The Lamont-Doherty temperature-logging tool was attached at the bottom of the first logging run. A brief 3-min stop was made at the seafloor to allow the temperature tool to equilibrate to ocean-bottom temperatures. Each tool string was lowered to the bottom of the hole and pulled up at a rate between 300 and 600 m/hr to acquire high-resolution log data. All three tool strings reached the total depth drilled. A repeat interval was also run with each logging string to provide data quality control.

The wireline heave compensator was not available for use during logging operations during Leg 171B. Fortunately, sea-state conditions during logging were moderate, with sea swells on the order of 1.5 m, and had no obvious effects on the logging data. Table 44 shows the logging schedule and intervals logged with each tool string in Hole 1050C. The log data are shown in Figures 63 through 68.

REFERENCES

Aubry, M.-P., 1996. Towards an upper Paleocene-lower Eocene high resolution stratigraphy based on calcareous nannofossil stratigraphy. *Israel J. Earth Sci.*, 44:239–253.

Berggren, W.A., Kent, D.V., Swisher, C.C., III, and Aubry, M.-P., 1995. A revised Cenozoic geochronology and chronostratigraphy. *In* Berggren, W.A., Kent, D.V., Aubry, M.-P., and Hardenbol, J. (Eds.), *Geochronology, Time Scales and Global Stratigraphic Correlation.* Spec. Publ.—Soc. Econ. Paleontol. Mineral., 54:129–212.

Blome, C.D., 1992. Radiolarians from Leg 122, Exmouth and Wombat Plateaus, Indian Ocean. *In* von Rad, U., Haq, B.U., et al., *Proc. ODP, Sci. Results*, 122: College Station, TX (Ocean Drilling Program), 633–652.

Curry, W.B., Shackleton, N.J., Richter, C., et al., 1995. *Proc. ODP, Init. Repts.*, 154: College Station, TX (Ocean Drilling Program).

Gradstein, F.M., Agterberg, F.P., Ogg, J.G., Hardenbol, J., van Veen, P., Thierry, J., and Huang, Z., 1995. A Triassic, Jurassic and Cretaceous time scale. *In* Berggren, W.A., Kent, D.V., and Aubry, M.P. (Eds.), *Geochronology, Time Scales and Global Stratigraphic Correlation.* Spec. Publ.—Soc. Econ. Paleontol. Mineral., 54:95–128.

Ladd, D.D., Foott, R., Ishihara, K., Schlosser, F., and Poulos, H.G., 1977. Stress-deformation and strength characteristics: state-of-the-art report. *Proc. 9th Int. Conf. Soil Mechanics Foundation Engineering*, Tokyo, 2:421–482.

Nishimura, A., 1992. Paleocene radiolarian biostratigraphy in the northwest Atlantic at Site 384, Leg 43, of the Deep Sea Drilling Project. *Micropaleontology*, 38:317–362.

Quirein, J.A., Garden, J.S., and Watson, J.T., 1982. Combined natural gamma-ray spectral/litho-density measurements applied to complex lithology. *SPE of AIME, 57th Annual Fall Technical Conf. and Exhibit.*, New Orleans, pap. SPE 11143:1–14.

Riedel, W.R., and Sanfilippo, A., 1978. Stratigraphy and evolution of tropical Cenozoic radiolarians. *Micropaleontology*, 24:61–96.

Ryan, W.B.F., Bolli, H.M., Foss, G.N., Natland, J.H., Hottman, W.E., and Foresman, J.B., 1978. Objectives, principle results, operations, and explanatory notes of Leg 40, South Atlantic. *In* Bolli, H.M., Ryan, W.B.F., et al., *Init. Repts. DSDP*, 40: Washington (U.S. Govt. Printing Office), 5–26.

Tjalsma, R.C., and Lohmann, G.P., 1983. Paleocene-Eocene bathyal and abyssal benthic foraminifera from the Atlantic Ocean. *Micropaleontol. Spec. Publ.*, 4.

Toumarkine, M., and Luterbacher, H., 1985. Paleocene and Eocene planktic foraminifera. *In* Bolli, H.M., Saunders, J.B., and Perch-Nielsen, K. (Eds.), *Plankton Stratigraphy:* Cambridge (Cambridge Univ. Press), 87–154.

van Morkhoven, F.P.C.M., Berggren, W.A., and Edwards, A.S., 1986. Cenozoic cosmopolitan deep-water benthic foraminifera. *Bull. Cent. Rech. Explor.—Prod. Elf-Aquitaine*, Mem. 11.

von Rad, U., and Kreuzer, H., 1987. Composition, K-Ar dates and origin of a mid-Eocene rhyolitic ash layer at Deep Sea Drilling Project Sites 605 and 613, New Jersey Transect, Legs 93 and 95. *In* van Hinte, J.E., Wise, S.W., Jr., et al. *Init. Repts., DSDP*, 93: Washington (U.S. Govt. Printing Office), 977–981.

Wei, W., and Wise, S.W., Jr., 1989. Paleogene calcareous nannofossil magnetobiochronology: results from South Atlantic DSDP Site 516. *Mar. Micropaleontol.*, 14:119–152.

Ms 171BIR-104

NOTE: Core-description forms ("barrel sheets") and core photographs can be found in Section 4, beginning on page 363. Forms containing smear-slide data, thin-section descriptions, and shore-based log processing data can be found on CD-ROM. See Table of Contents for material contained on CD-ROM.

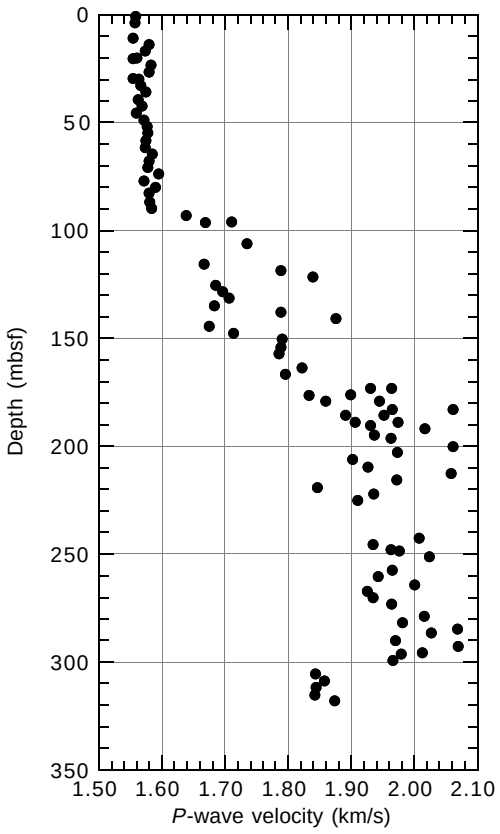

Figure 49. Discrete *P*-wave velocity for Hole 1050A.

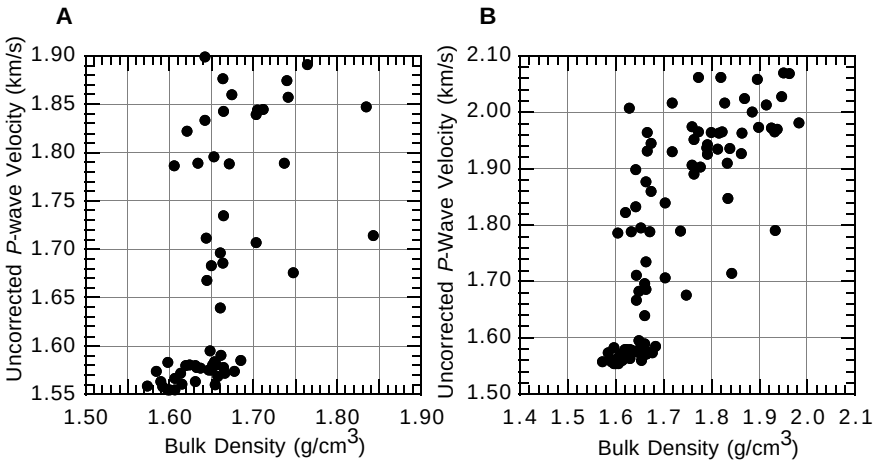

Figure 50. **A.** Comparison of discrete *P*-wave velocity and discrete bulk density for the interval 90–170 mbsf, where the transition to higher *P*-wave velocity with depth is not matched with a corresponding increase in bulk density. **B.** Comparison of all discrete *P*-wave velocity and discrete bulk density data for Hole 1050A. The *P*-wave velocity values are uncorrected for in situ pressure and temperature conditions.

Table 36. Discrete measurements of shear strength for Hole 1050A.

Core, section, interval (cm)	Depth (mbsf)	Peak (kPa)	Residual (kPa)	Penetrometer (kPa)
171B-1050A-				
1X-1, 62.1-63.1	0.62	20.36	11.61	
1X-3, 76.5-77.5	3.77	20.32	11.79	
2H-1, 77-78	10.87	58.80	7.64	
2H-3, 71.5-72.5	13.82			85.8
2H-5, 69.5-70.5	16.80			161.8
2H-7, 71.5-72.5	19.82			112.8
3H-1, 71.5-72.5	20.32			83.4
3H-3, 72.5-73.5	23.33			90.7
3H-5, 71.5-72.5	26.32			218.2
3H-7, 72.5-73.5	29.33			117.7
4H-1, 72.5-73.5	29.83			107.9
4H-3, 71.5-72.5	32.82			122.6
4H-5, 71.5-72.5	35.82			147.1
5H-1, 71.5-72.5	39.32			49.0
5H-3, 71.5-72.5	42.32			112.8
5H-5, 72.5-73.5	45.33			137.3
6H-1, 71.5-72.5	48.82			105.4
6H-3, 71.5-72.5	51.82			98.1
6H-5, 71.5-72.5	54.82			188.8
7H-1, 69-70	58.29			68.6
7H-3, 71.5-72.5	61.32			98.1
7H-5, 66.5-67.5	64.27			110.3
8H-1, 71.5-72.5	67.82			152.0
8H-3, 71.5-72.5	70.82			85.8
8H-5, 71.5-72.5	73.82			134.8
9H-1, 31.5-32.5	76.92			105.4
9H-3, 76.5-77.5	79.94			147.1
9H-5, 37.5-38.5	82.55			120.1
10H-1, 71.5-72.5	86.82			144.7
10H-3, 71.5-72.5	89.82			93.2
10H-5, 71.5-72.5	92.82			61.3
11X-1, 37.5-38.5	95.98			73.6
12X-1, 70.5-71.5	105.91			147.1
13X-1, 70-71	115.50			78.5
13X-3, 70-71	118.50			71.1
13X-5, 67.5-68.5	121.48			103.0
14X-1, 76.5-77.5	125.17			61.3
14X-3, 72-73	128.12			63.7
14X-5, 71.5-72.5	131.12			134.8

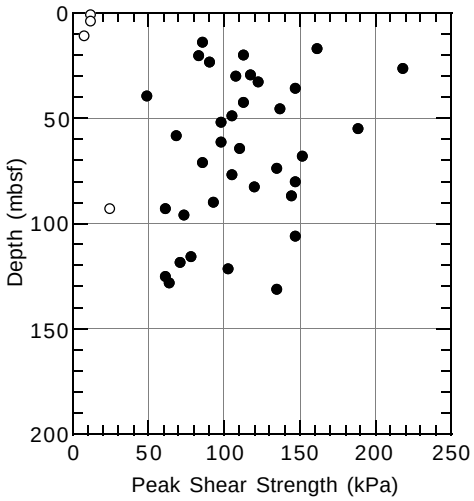

Figure 51. Shear strength for Hole 1050A. The open cricles = vane-shear device measurements; the solid circles = pocket penetrometer measurements.

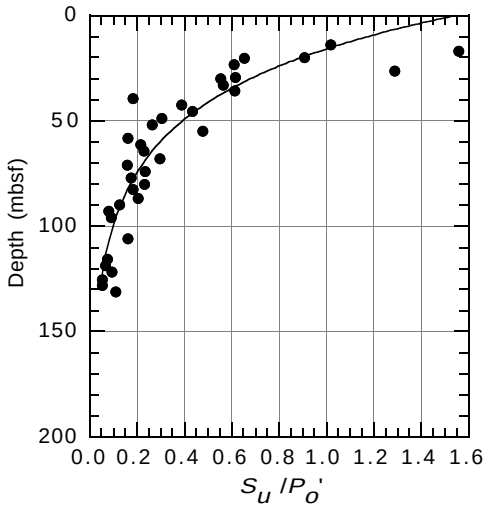

Figure 52. S_u/P_0' for Hole 1050A. The S_u/P_0' are calculated from bulk density and undrained shear strength data (see "Physical Properties" section, this chapter, for further details).

Table 37. Discrete measurements of resistivity for Hole 1050A.

Core, section, interval (cm)	Depth (mbsf)	Longitudinal resistivity (Ωm)	Transverse resistivity (Ωm)
171B-1050A-			
1X-1, 81.5-84.5	0.82	0.539	0.551
1X-3, 68.5-71.5	3.69	0.421	0.453
2H-1, 70.5-73.5	10.81	0.525	0.518
2H-3, 78.5-81.5	13.89	0.526	0.510
2H-5, 75.5-78.5	16.86	0.522	0.537
2H-7, 68.5-71.5	19.79	0.522	0.519
3H-1, 76.5-79.5	20.37	0.468	0.464
3H-3, 77.5-80.5	23.38	0.479	0.461
3H-5, 76.5-79.5	26.37	0.566	0.577
3H-7, 70.5-73.5	29.31	0.553	0.530
4H-1, 76.5-79.5	29.87	0.536	0.523
4H-3, 70-73	32.80	0.547	0.551
4H-5, 78.5-81.5	35.89	0.528	0.528
5H-1, 80.5-83.5	39.41	0.536	0.526
5H-3, 77.5-80.5	42.38	0.649	0.682
5H-5, 77-80	45.37	0.603	0.651
6H-1, 77-80	48.87	0.511	0.522
6H-3, 77-80	51.87	0.579	0.561
6H-5, 77-80	54.87	0.554	0.549
7H-1, 74.5-77.5	58.35	0.621	0.602
7H-3, 77-80	61.37	0.881	0.622
7H-5, 76.5-79.5	64.37	0.780	0.864
8H-1, 76.5-79.5	67.87	0.551	0.554
8H-3, 76.5-79.5	70.87	0.660	0.623
8H-5, 76.5-79.5	73.87	0.652	0.600
9H-1, 36.5-39.5	76.97	0.565	0.532
9H-3, 82.5-85.5	80.00	0.566	0.639
9H-5, 42.5-45.5	82.60	0.584	0.545
10H-1, 76.5-79.5	86.87	0.554	0.501
10H-3, 76.5-79.5	89.87	0.593	0.547
10H-5, 76.5-79.5	92.87	0.574	0.575
12X-1, 68-71	105.88	0.615	0.600
13X-1, 77-80	115.57	0.667	0.631
13X-3, 76.5-79.5	118.57	0.588	0.558
13X-5, 80.5-83.5	121.61	0.735	0.673
14X-1, 79.5-82.5	125.20	0.654	0.659
14X-3, 77.5-80.5	128.18	0.621	0.639
14X-5, 77-80	131.17	0.643	0.642
15X-1, 77.5-80.5	134.78	0.607	0.613
15X-3, 82-85	137.82	0.862	0.750
15X-5, 81.5-84.5	140.82	0.767	0.803
16X-1, 78.5-81.5	144.39	0.826	0.748
16X-3, 83-86	147.43	0.781	0.864
16X-5, 71.5-74.5	150.32	0.824	0.744
17X-1, 95.5-98.5	154.16	0.856	0.819
17X-3, 73-76	156.93	0.809	0.779
18X-1, 87.5-90.5	163.68	0.887	0.898
18X-3, 67.5-70.5	166.48	0.888	0.901

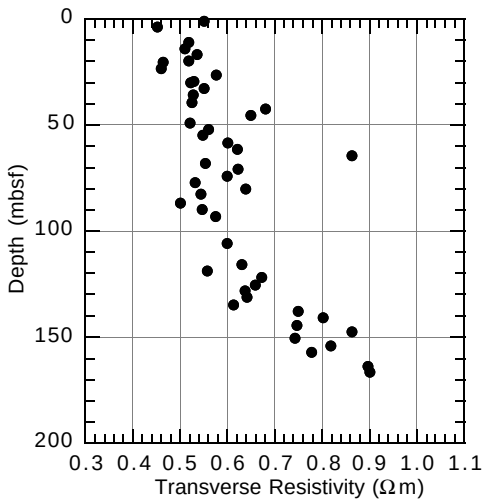

Figure 53. Sediment resistivity for Hole 1050A. Transverse resistivity measurements are considered more reliable than longitudinal measurements because planar unloading cracks that are perpendicular to the core axis bias longitudinal resistivity measurements to higher values.

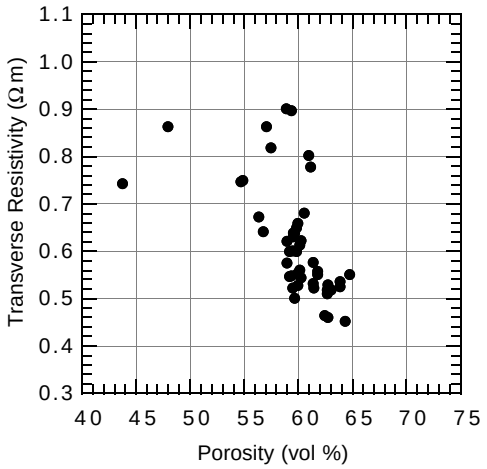

Figure 54. Comparison of transverse resistivity and sediment porosity for Hole 1050A.

Table 38. Discrete measurements of thermal conductivity for Hole 1050A.

Core, section, interval (cm)	Depth (mbsf)	Thermal conductivity (W/[m·K])
171B-1050A-		
1X-1, 75-75	0.75	1.09
1X-3, 75-75	3.75	1.40
2H-1, 75-75	10.85	1.11
2H-3, 75-75	13.85	1.07
2H-5, 75-75	16.85	1.23
3H-1, 75-75	20.35	1.03
3H-3, 75-75	23.35	1.09
3H-5, 75-75	26.35	1.21
4H-1, 75-75	29.85	1.05
4H-3, 75-75	32.85	1.40
4H-5, 75-75	35.85	1.2
5H-1, 75-75	39.35	0.99
5H-5, 75-75	45.35	1.22
6H-1, 75-75	48.85	1.01
6H-3, 75-75	51.85	1.11
6H-5, 75-75	54.85	1.24
7H-1, 75-75	58.35	1.04
7H-3, 75-75	61.35	1.21
7H-5, 75-75	64.35	1.39
8H-1, 75-75	67.85	1.03
8H-3, 75-75	70.85	1.08
8H-5, 75-75	73.85	1.30
9H-1, 75-75	77.35	1.01
9H-3, 75-75	79.92	2.07
9H-5, 75-75	82.92	1.14
10H-1, 75-75	86.85	1.08
10H-3, 75-75	89.85	1.23
10H-5, 75-75	92.85	1.30
11X-1, 75-75	96.35	1.01
11X-3, 75-75	99.35	1.16
11X-5, 75-75	102.35	1.22
13X-1, 75-75	115.55	1.15
13X-3, 75-75	118.55	1.07
14X-1, 75-75	125.15	1.16
14X-3, 75-75	128.15	1.10
14X-5, 75-75	131.15	1.21
15X-1, 75-75	134.75	1.11
15X-3, 75-75	137.75	1.37
15X-5, 75-75	140.75	1.38
16X-1, 75-75	144.35	1.09
16X-3, 75-75	147.35	1.26
16X-5, 75-75	150.35	1.23

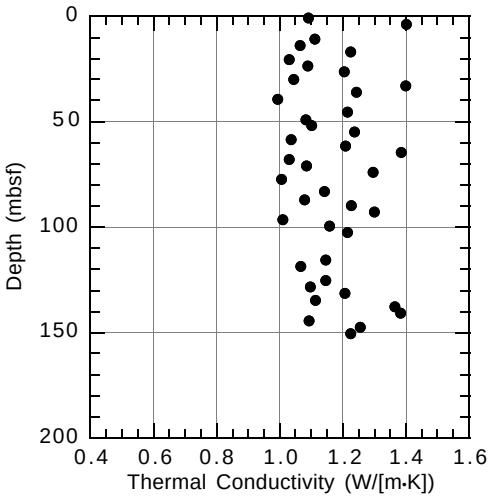

Figure 55. Thermal conductivity for Hole 1050A.

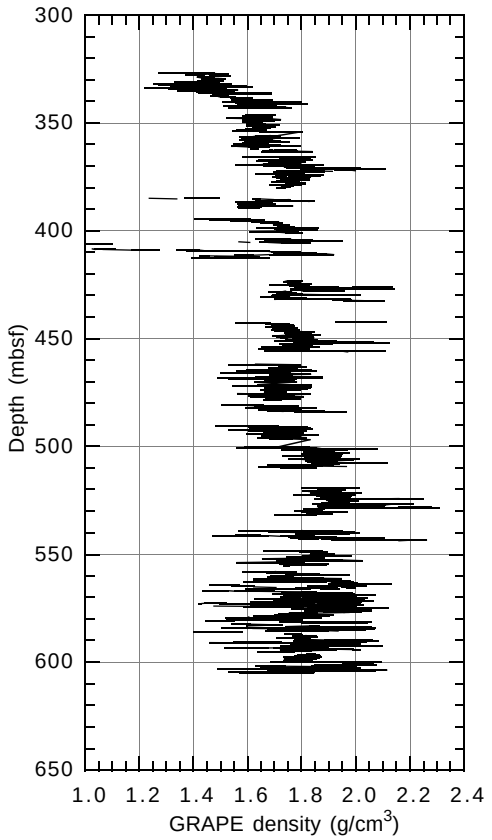

Figure 56. GRAPE bulk density for Hole 1050C (also see Table 39 on CD-ROM, back pocket, this volume).

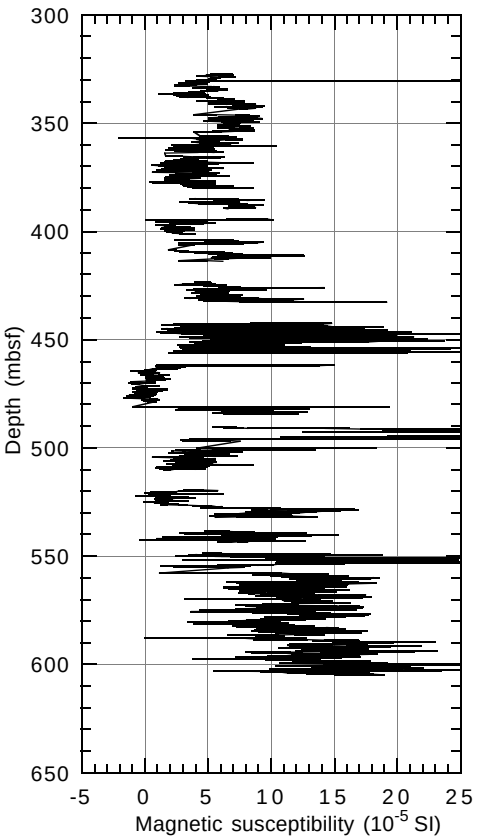

Figure 57. Magnetic susceptibility for Hole 1050C (also see Table 40 on CD-ROM, back pocket, this volume).

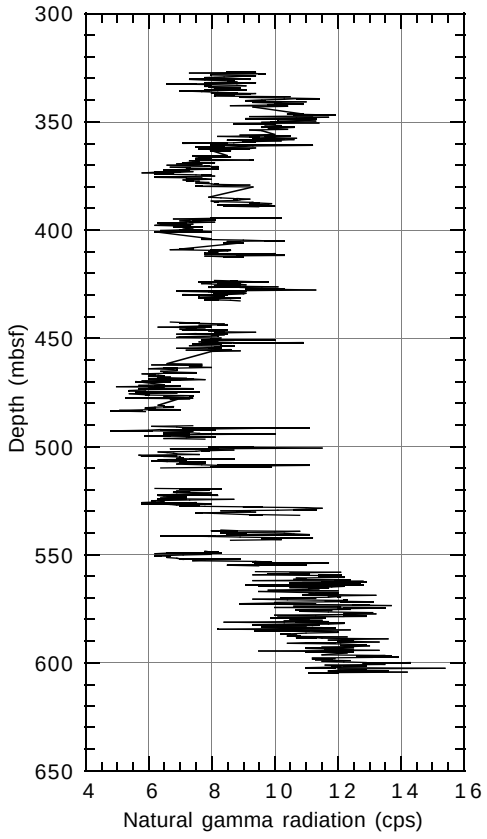

Figure 58. Natural gamma radiation for Hole 1050C (also see Table 41 on CD-ROM, back pocket, this volume).

Table 42. Discrete index properties measurements for Hole 1050C.

Core, section, interval (cm)	Depth (mbsf)	Water content (total mass wt%)	Water content (solid mass wt%)	Bulk density (g/cm^3)	Grain density (g/cm^3)	Dry density (g/cm^3)	Porosity (%)	Void ratio
171B-1050C-								
2R-1, 68-70	327.78	18.7	23.0	2.01	2.58	1.63	36.6	0.58
2R-3, 88-90	330.98	34.4	52.3	1.68	2.52	1.10	56.3	1.29
2R-5, 93-95	334.03	44.6	80.5	1.51	2.46	0.84	66.0	1.94
3R-1, 75-77	337.45	38.5	62.6	1.61	2.51	0.99	60.6	1.54
3R-3, 84-86	340.54	34.3	52.2	1.70	2.60	1.12	57.0	1.33
3R-5, 77-79	343.44	23.3	30.4	1.92	2.63	1.48	43.8	0.78
4R-1, 22-24	346.52	21.1	26.7	1.95	2.58	1.54	40.2	0.67
4R-3, 16-18	349.46	20.8	26.2	1.95	2.56	1.55	39.6	0.66
4R-5, 44-46	352.74	20.5	25.8	1.96	2.55	1.55	39.1	0.64
5R-1, 53-55	356.43	22.1	28.3	1.94	2.60	1.51	41.8	0.72
5R-3, 15-17	359.05	21.7	27.7	1.93	2.54	1.51	40.7	0.69
5R-5, 48-50	362.19	24.4	32.4	1.89	2.61	1.43	45.2	0.82
6R-1, 67-69	366.17	16.4	19.7	2.09	2.63	1.75	33.5	0.51
6R-3, 28-30	368.78	18.5	22.8	2.04	2.64	1.67	37.0	0.59
6R-5, 94-96	372.44	13.3	15.4	2.13	2.55	1.85	27.7	0.38
7R-1, 69-71	375.89	14.4	16.8	2.11	2.56	1.80	29.6	0.42
7R-3, 11-13	378.31	19.9	24.8	2.01	2.65	1.61	39.1	0.64
7R-4, 44-46	380.14	19.2	23.8	2.02	2.64	1.64	38.0	0.61
8R-1, 74-76	385.64	23.2	30.2	1.94	2.65	1.49	43.9	0.78
8R-3, 77-79	388.67	19.0	23.4	2.07	2.71	1.67	38.3	0.62
8R-4, 63-65	389.53	22.3	28.7	1.98	2.71	1.54	43.2	0.76
13R-1, 74-76	424.04	20.5	25.7	2.03	2.71	1.61	40.5	0.68
13R-3, 71-73	427.01	19.3	24.0	2.06	2.72	1.66	38.9	0.64
13R-5, 93-95	430.23	23.3	30.4	2.00	2.82	1.53	45.6	0.84
15R-1, 85-87	443.45	24.0	31.6	1.94	2.71	1.48	45.6	0.84
15R-3, 75-77	446.35	21.7	27.7	2.00	2.71	1.56	42.2	0.73
15R-5, 54-56	449.14	22.1	28.3	2.00	2.73	1.56	43.0	0.76
17R-1, 75-77	462.55	20.5	25.7	2.03	2.71	1.61	40.5	0.68
17R, 103-105	470.48	22.3	28.7	1.99	2.73	1.55	43.4	0.77
18R-1, 31-33	471.71	18.5	22.7	2.08	2.72	1.70	37.7	0.60
18R-3, 37-39	474.77	22.2	28.6	1.98	2.71	1.54	43.0	0.76
18R-5, 21-23	477.61	19.9	24.9	2.04	2.71	1.64	39.8	0.66
19R-1, 132-134	482.32	23.8	31.3	1.95	2.73	1.49	45.5	0.83
21R-2, 47-49	502.17	16.1	19.2	2.16	2.74	1.81	33.9	0.51
21R5, 101-103	507.21	16.4	19.7	2.14	2.71	1.78	34.3	0.52
22R-1, 40-42	510.20	17.0	20.5	2.12	2.71	1.76	35.2	0.54
23R-1, 88-90	520.28	13.5	15.6	2.22	2.72	1.92	29.3	0.41
23R-7, 60-62	529.00	15.5	18.4	2.17	2.74	1.84	32.9	0.49
24R-1, 43-45	529.53	16.2	19.4	2.14	2.72	1.80	34.0	0.51
24R-3, 12-14	531.58	14.3	16.7	2.20	2.72	1.89	30.7	0.44
25R-1, 93-95	539.63	17.3	20.9	2.11	2.72	1.75	35.7	0.56
25R-3, 70-72	542.40	16.5	19.7	2.16	2.76	1.80	34.8	0.53
26R-1, 10-12	548.50	17.2	20.8	2.13	2.74	1.76	35.7	0.56
26R-3, 130-132	552.70	23.4	30.5	1.97	2.75	1.51	45.0	0.82
26R-4, 146-148	554.36	17.5	21.3	2.11	2.73	1.74	36.2	0.57
27R-1, 77-79	558.77	19.7	24.5	2.04	2.70	1.64	39.2	0.65
27R-5, 81-83	546.81	19.1	23.6	2.07	2.72	1.67	38.6	0.63
28R-1, 73-75	568.33	22.3	28.7	1.99	2.73	1.55	43.4	0.77
28R-4, 44-46	572.54	18.7	23.0	2.08	2.72	1.69	38.0	0.61
29R-5, 69-71	583.89	18.3	22.4	2.08	2.71	1.70	37.1	0.59
30R-4, 71-73	592.01	19.2	23.7	2.06	2.72	1.67	38.6	0.63
30R-CC, 13-15	595.74	20.0	25.0	2.04	2.71	1.63	39.8	0.66

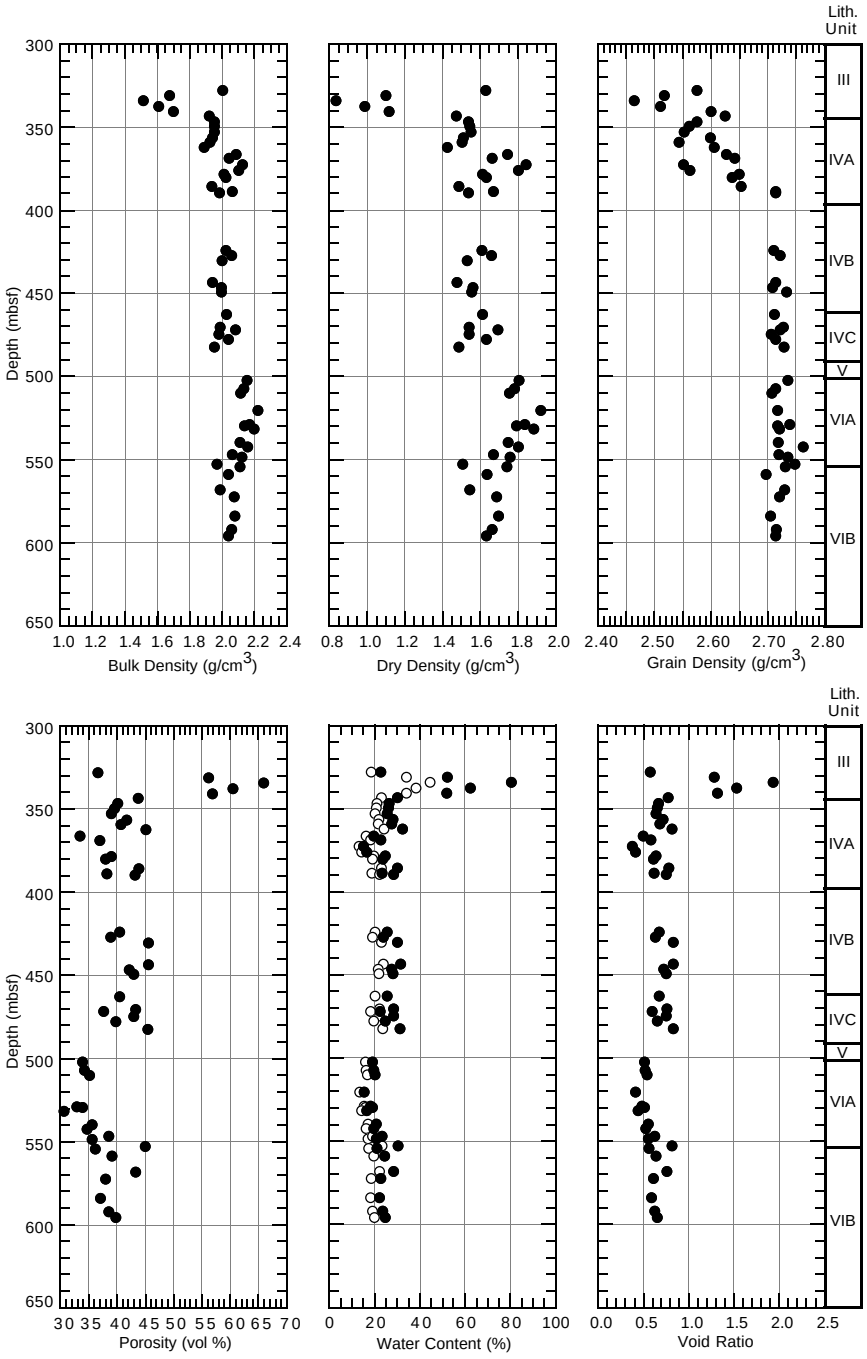

Figure 59. Discrete measurements of bulk density, dry density, grain density, porosity, water content, and void ratio for Hole 1050C. Lithologic units (see "Lithostratigraphy" section, this chapter) are included for comparative purposes. In the water content plot, open circles = values expressed in terms of total mass; solid circles = values expressed in terms of the total mass of solids.

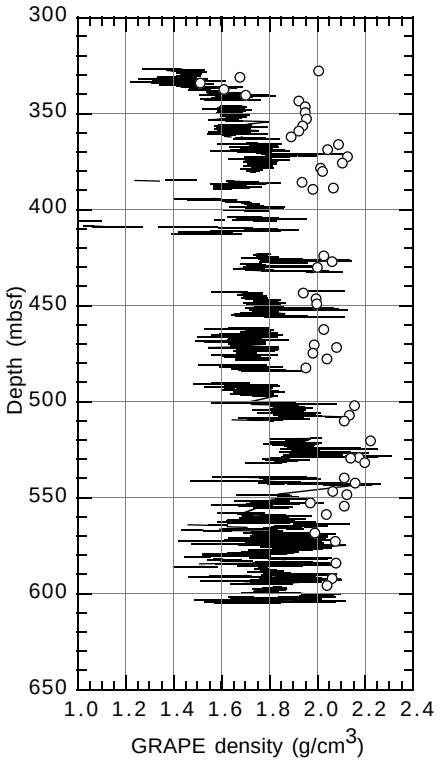

Figure 60. Comparison of GRAPE bulk density (line) with discrete measurements of bulk density (open circles) for Hole 1050C.

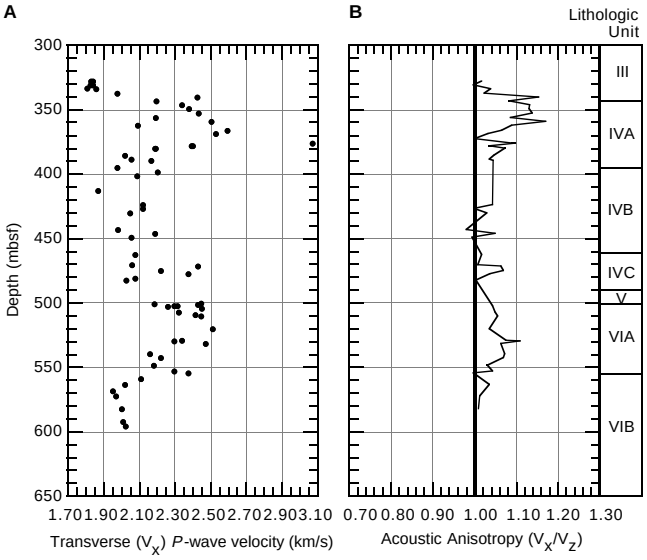

Figure 61. **A.** Discrete transverse *P*-wave velocity measured perpendicular to the split-core surface (x-direction) for Hole 1050C. **B.** Acoustic anisotropy (x-direction/z-direction) for Hole 1050C. The z-direction is oriented parallel to the core axis. Lithologic units (see "Lithostratigraphy" section, this chapter) are included for comparative purposes.

Table 43. Discrete measurements of uncorrected *P*-wave velocity for Hole 1050C.

Core, section, interval (cm)	Depth (mbsf)	Transverse *P*-wave velocity (km/s)	Longitudinal *P*-wave velocity (km/s)	Acoustic anisotropy (x/z)
171B-1050C-				
2R-1 69-71	327.79	1.832	1.801	1.017
2R-1 75-77	327.85	1.842		
2R-3 60.2-62.2	330.70	1.830		
2R-3 89-91	330.99	1.842	1.847	0.997
2R-5 51.8-53.8	333.62	1.812		
2R-5 94-96	334.04	1.860	1.790	1.039
3R-1 76-78	337.46	1.980	1.935	1.023
3R-3 85-87	340.55	2.425	2.100	1.155
3R-5 79-81	343.46	2.200	2.029	1.084
4R-1 22-24	346.52	2.340	2.067	1.132
4R-3 16-18	349.46	2.380	2.104	1.131
4R-5 44-46	352.74	2.436	2.138	1.139
5R-1 53-55	356.43	2.195	2.022	1.086
5R-3 15-17	359.05	2.507	2.140	1.171
5R-5 48-50	362.19	2.095	1.924	1.089
6R-1 67-69	366.17	2.594	2.437	1.065
6R-3 28-30	368.78	2.531	2.450	1.033
6R-5 94-96	372.44	3.185	3.185	1.000
7R-1 69-71	375.89	3.073	2.817	1.091
7R-1 69-71	375.89	3.072	2.795	1.099
7R-3 11-13	378.31	2.402	2.311	1.040
7R-3 11-13	378.31	2.395	2.314	1.035
7R-4 44-46	380.14	2.193	2.041	1.075
7R-4 44-46	380.14	2.190	2.041	1.073
8R-1 75-77	385.65	2.021	1.932	1.046
8R-3 78-80	388.68	2.057	1.987	1.035
8R-4 64-66	389.54	2.168	2.074	1.045
9R-1 75-77	395.25	1.978		
9R-3 75-77	398.25	2.204		
9R-5 75-77	401.25	2.092		
11R-CC 8.1-10.1	412.93	1.871		
13R-1 75-77	424.05	2.124	2.035	1.044
13R-3 72-74	427.02	2.120	2.121	1.000
13R-5 94-96	430.24	2.050	1.990	1.030
15R-1 86-88	443.46	1.985	2.025	0.980
15R-3 76-78	446.36	2.189	2.085	1.050
15R-5 55-57	449.15	2.058	2.069	0.995
17R-1 76-78	462.56	2.080	2.044	1.018
17R-7 104-106	470.49	2.064	2.045	1.009
18R-1 31-33	471.71	2.430	2.284	1.064
18R-3 37-39	474.77	2.223	2.079	1.069
18R-5 21-23	477.61	2.376	2.289	1.038
19R-1 8-10	481.08	2.080		
19R-1 132-134	482.32	2.029	2.022	1.004
21R-1 24.1-26.1	500.44	2.448		
21R-1 65.1-67.1	500.85	2.188		
21R-1 125.1-127.1	501.45	2.431		
21R-2 47-49	502.17	2.314	2.218	1.043
21R-2 64.2-66.2	502.34	2.300		
21R-2 130.2-132.2	503.00	2.261		
21R-3 96.2-98.2	504.16	2.453		
21R-5 101-103	507.21	2.322	2.213	1.050
21R-7 81.2-83.2	509.11	2.416		
22R-1 40-42	510.20	2.447	2.319	1.055
23R-1 88-90	520.28	2.511	2.423	1.036
23R-7 60-62	529.00	2.342	2.176	1.077
24R-1 43-45	529.53	2.298	2.071	1.110
24R-3 12-14	531.58	2.473	2.326	1.063
25R-1 94-96	539.64	2.163	2.018	1.072
25R-3 71-73	542.41	2.221	2.077	1.069
26R-1 11-13	548.51	2.184	2.118	1.031
26R-3 131-133	552.71	2.297	2.199	1.044
26R-4 147-149	554.37	2.375	2.380	0.998
27R-1 78-80	558.78	2.111		
27R-4 82-84	563.32	2.023	1.953	1.036
28R-1 75-77	568.35	1.955		
28R-4 45-47	572.55	1.973	1.948	1.013
29R-4 70-72	582.40	2.005	1.985	1.010
30R-4 72-74	592.02	2.013		
30R-CC 14-16	595.75	2.027		

Note: Where no values are reported, data are absent.

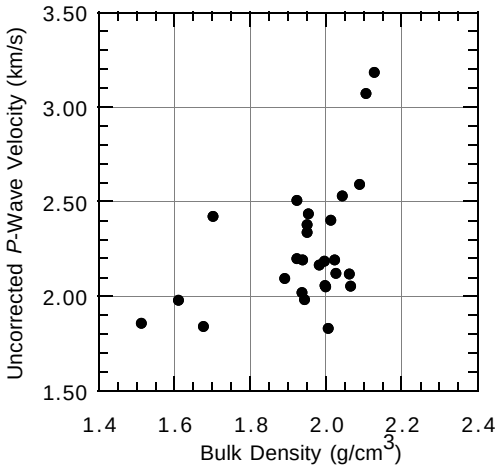

Figure 62. Comparison of discrete transverse *P*-wave velocity and discrete bulk density for Hole 1050C. The *P*-wave velocity values are uncorrected for in situ pressure and temperature conditions.

Table 44. The time schedule for logging operations in Hole 1050C, including a list of the tools used during each logging run.

Time	Operations
12 February 1997	
03:00	Triple combo assembled and prepared for logging.
04:20	Run in hole with triple combo.
05:23	Stop at mudline to equilibrate TLT.
05:27	Run down to bottom of hole (606 mbsf).
05:53	Stop at bottom of hole to equilibrate TLT.
05:56	Begin logging first upward pass (597-0 mbsf) at 1800 ft/hr.
06:53	Enter pipe (105 mbsf).
07:06	Drop back down into hole and log repeat section (262-144 mbsf).
08:30	Triple combo pulled out of pipe, disassembled, and removed from rig floor.
09:00	FMS-SDT assembled and prepared for logging.
09:25	Run in hole with FMS-SDT.
10:34	Begin logging first upward pass (599.3-97 mbsf) at 900 ft/hr.
12:10	Finish first pass.
12:32	Drop back down to bottom and log repeat interval (598.3-261 mbsf).
13:47	Finish logging interval.
13:57	Enter pipe.
14:46	FMS-SDT pulled out of pipe, disassembled, and removed from rig floor.
15:00	GHMT assembled and prepared for logging.
15:15	Run in hole with GHMT.
16:30	Exit pipe and run down to bottom of hole (597.1 mbsf).
16:57	Begin logging first upward pass (597.1-97 mbsf) at 900 ft/hr.
18:38	Enter pipe.
18:40	Drop back down into hole for repeat interval.
18:48	Start repeat section (260-213.5 mbsf).
19:07	GHMT pulled out of pipe, disassembled, and removed from rig floor.
20:30	Rig-down finished.

Notes: Drillers total depth = 2914 mbrf (606 mbsf). Water depth = 2308 mbrf.

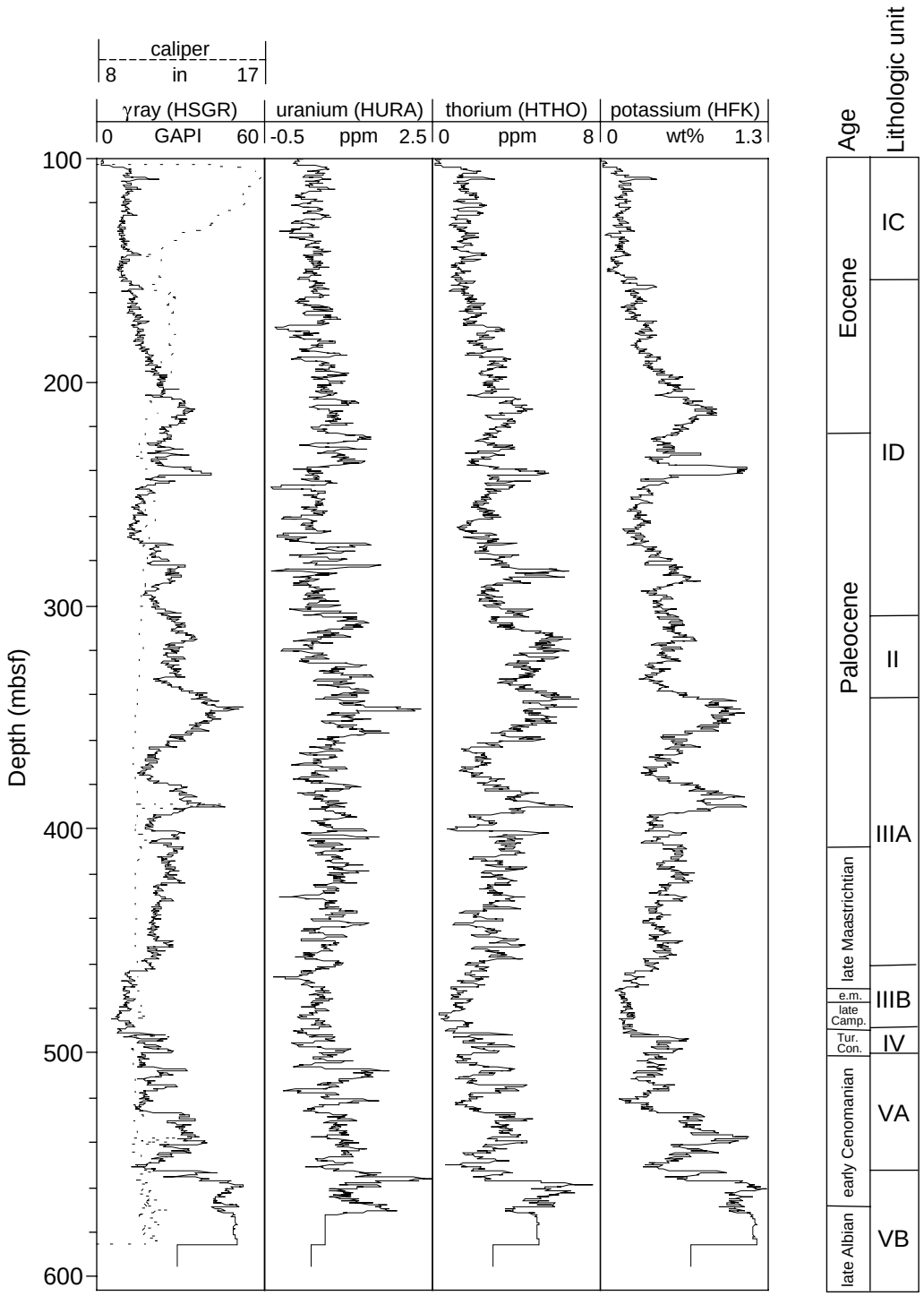

Figure 63. Spectral natural gamma-ray results, using the NGT tool on the triple-combo tool string for the interval 100–606 mbsf, and a lithologic summary column for Site 1050 (see “Lithostratigraphy” section, this chapter).

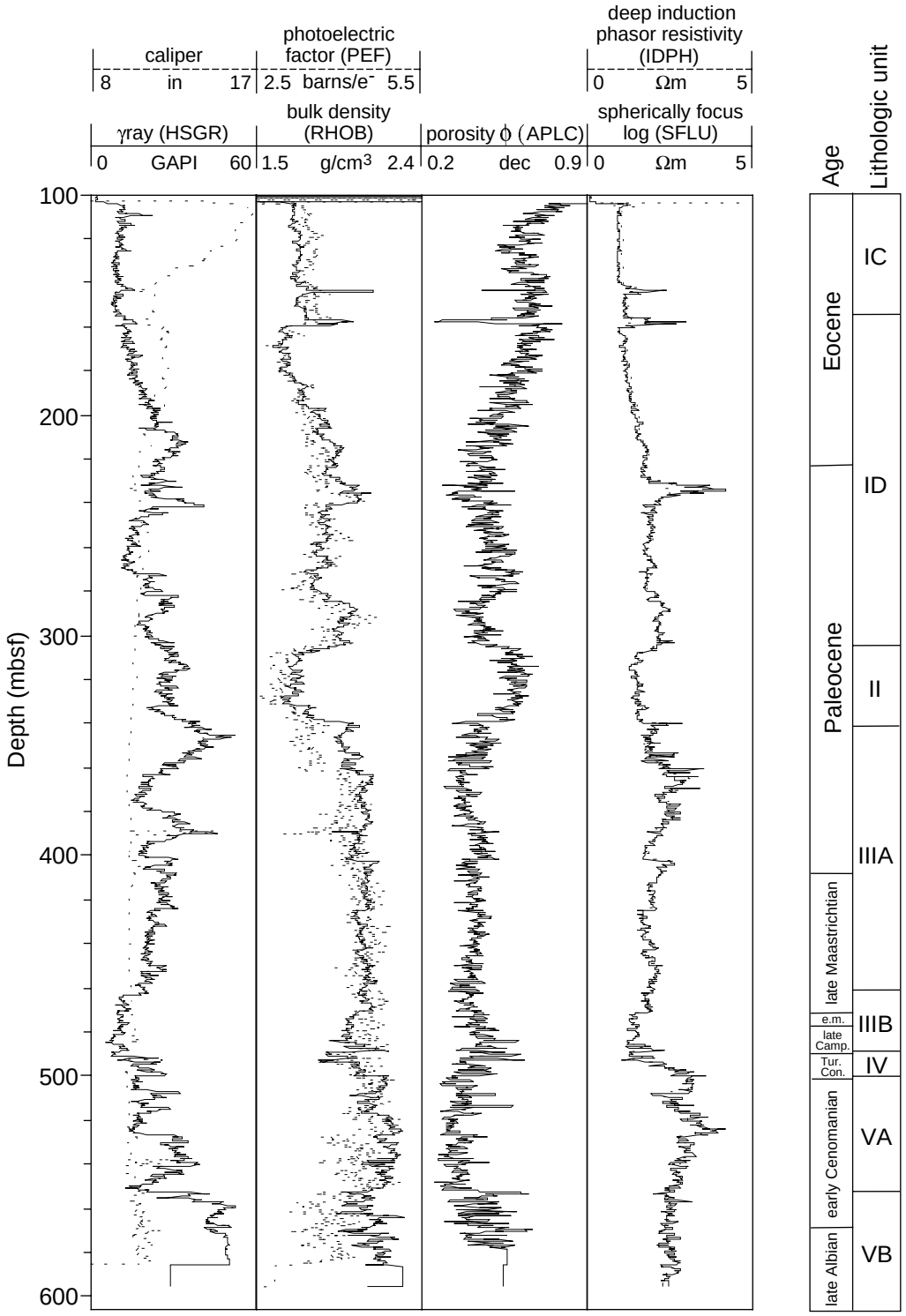

Figure 64. Summary of key geophysical logs acquired with the triple-combo tool string. From left to right, the tracks are the natural gamma ray and caliper, bulk density (RHOB) and photoelectric effect (PEF), porosity (APLC), and shallow (SFLU) and deep resistivity (IDPH).

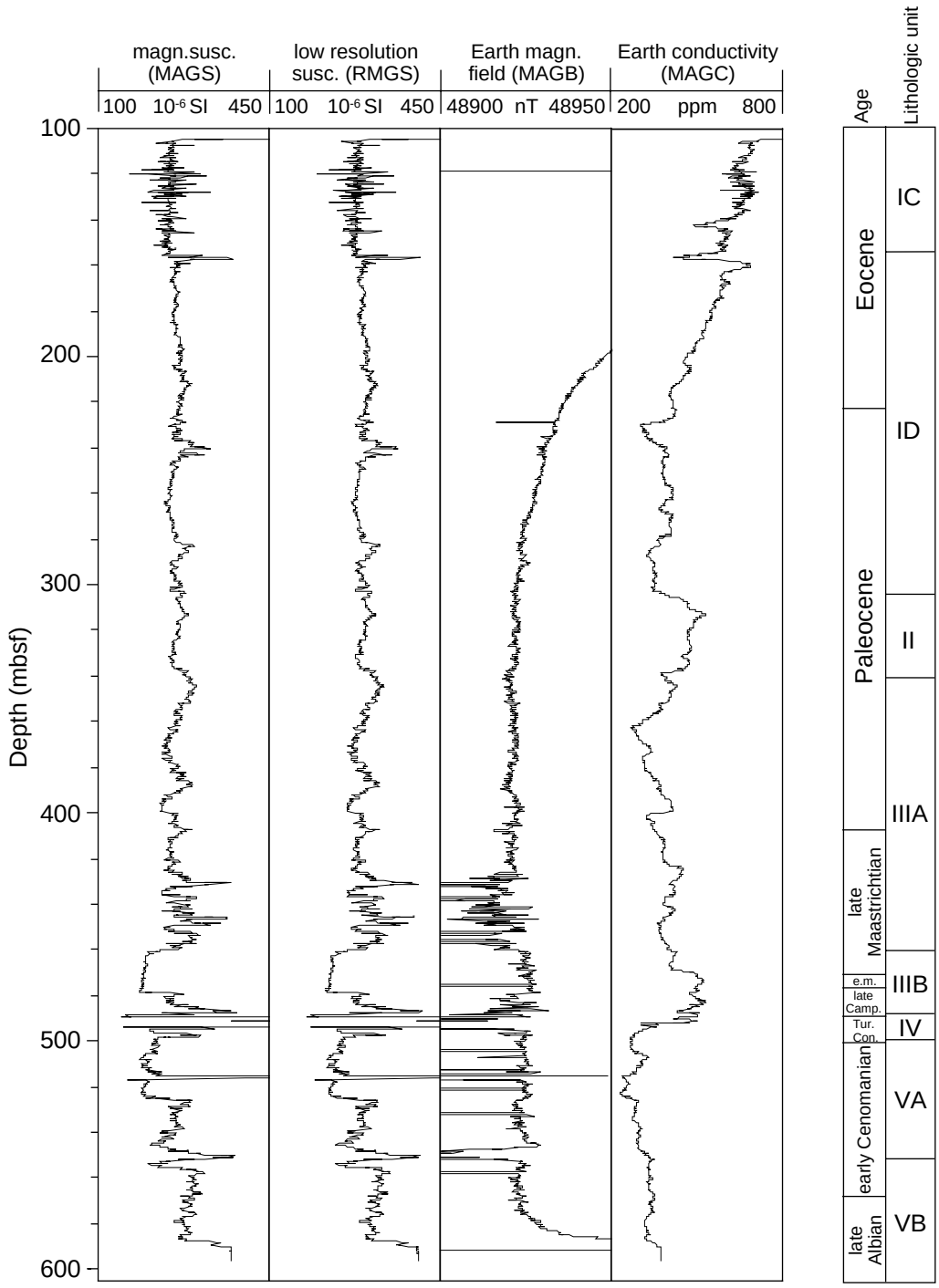

Figure 65. Selected downhole logs from the GHMT tool string for the interval 100–606 mbsf in Hole 1050C. From left to right, the tracks are magnetic susceptibility (MAGS), low-resolution susceptibility (RMSG), Earth's magnetic field (MAGB), and Earth's conductivity (MAGC). The logging units are discussed in the "Downhole Logging" section (this chapter); the lithologic units and ages are discussed in the "Lithostratigraphy" section (this chapter).

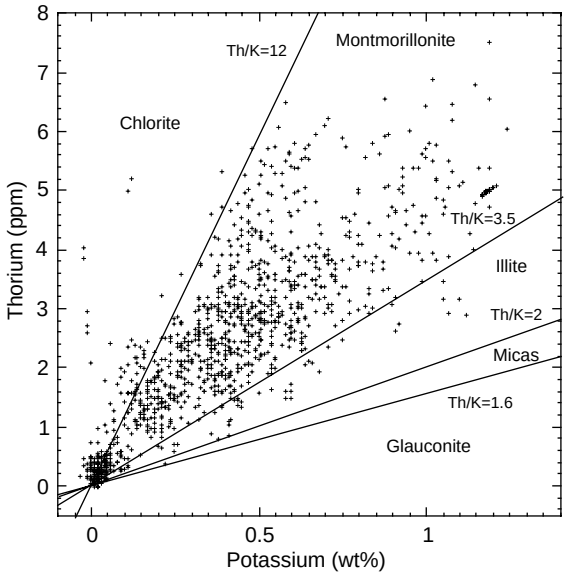

Figure 66. Identification of clay minerals as a function of thorium and potassium concentrations in Hole 1050C, as recorded by the NGT. Graph modified after Quirein et al. (1982).

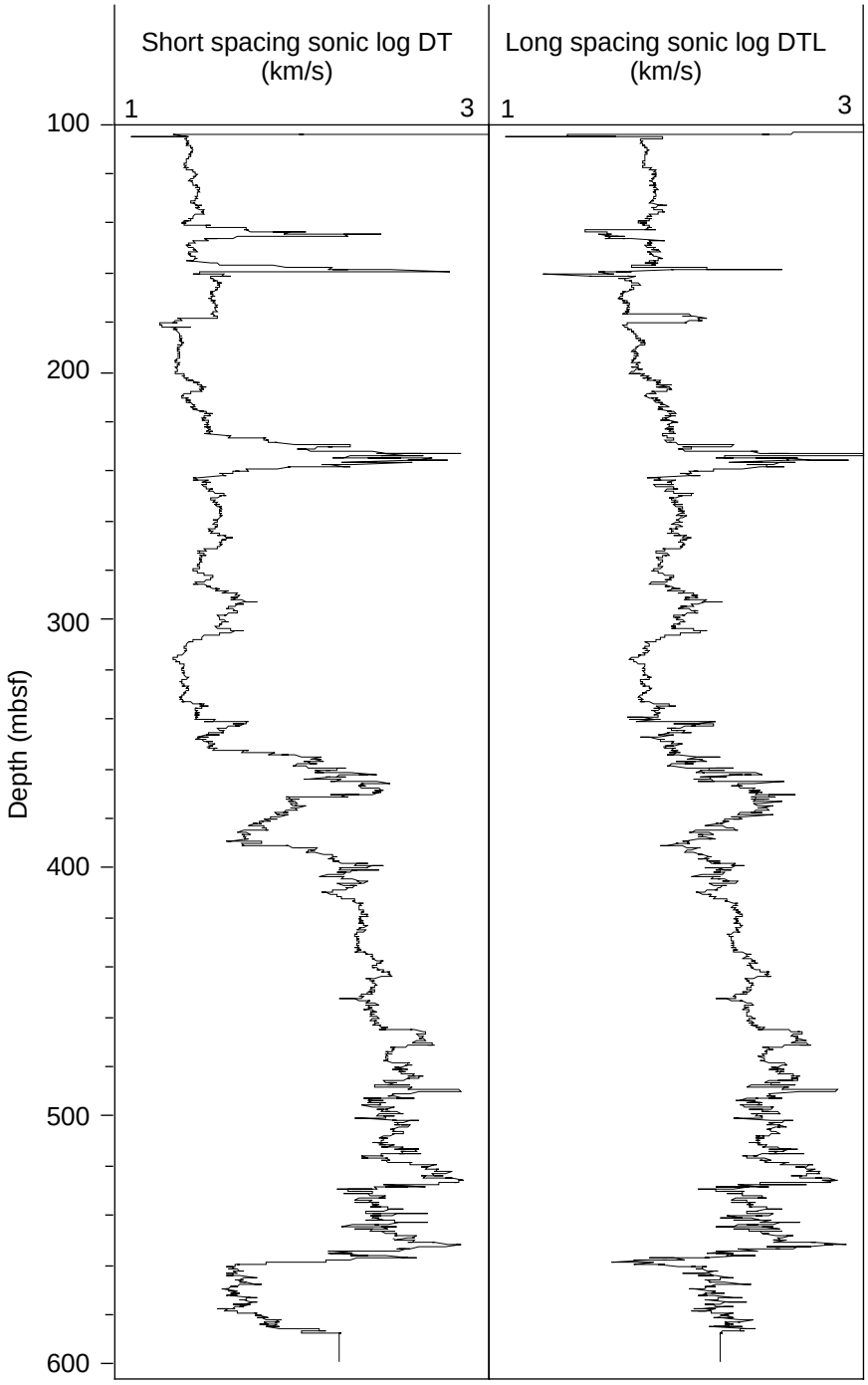

Figure 67. Comparison of short-spacing (DT) and long-spacing (DTL) sonic logs for Hole 1050C.

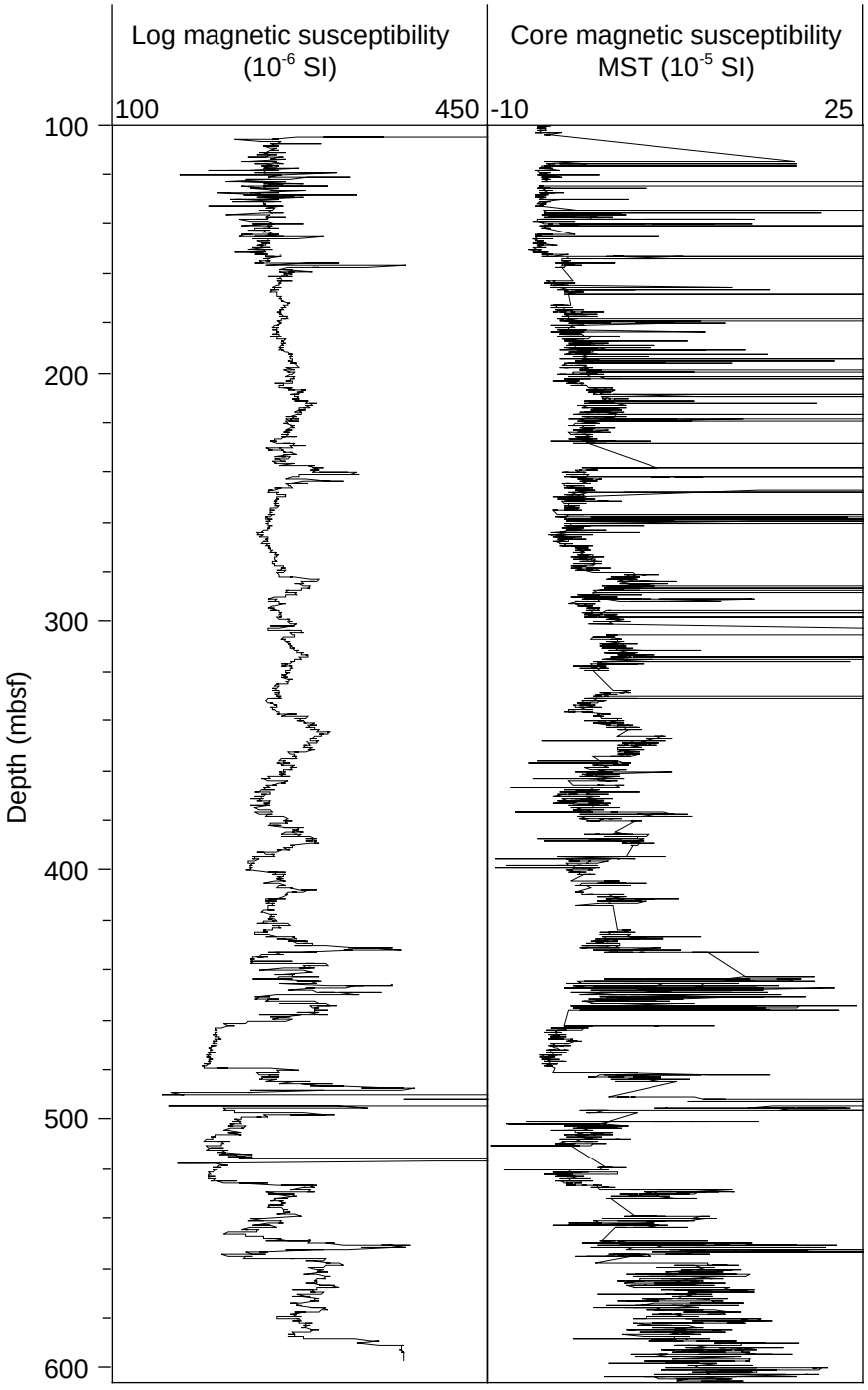

Figure 68. Comparison of log magnetic susceptibility data and discrete core measurements (MST; see "Physical Properties" section, this chapter). The differences between the data sets are real and reflect changes in the internal tool temperature as the tool warms in the borehole, an effect that can be corrected after processing.